



## Danksagung

Ich danke Herrn o.Univ.Prof.Dipl.-Ing.Dr. Uwe B. Sleytr für die Möglichkeit mein Doktoratsstudium an seinem Department für Nanobiotechnologie durchzuführen, die faszinierende Welt der S-Schichten kennen zu lernen, für sein Engagement und seine menschliche Unterstützung.

Besonders bedanken möchte ich mich bei meinem Betreuer Ao.Univ.Prof.Dipl.-Ing.Dr. Dietmar Pum für die Finanzierung, fachlichen Betreuung meiner Dissertation und die Möglichkeit bei den beiden Spanienaufenthalten in der Arbeitsgruppe von Dr. Prof. José mein Methodenspektrum zu erweitern. Ich danke ihm dafür, dass er jederzeit ein offenes Ohr hatte, seine Hilfsbereitschaft sowie sein klares und schnelles Denken und Handeln. Ich bin ihm über die Freiheit meinen eigenen Weg zu finden und somit eigenständiges Denken und Arbeiten zu lernen sehr dankbar. Weiters möchte ich ihm für seine unendliche Menschlichkeit danken die es mir unter anderem auch ermöglichte nach meinem Verkehrsunfall meine begonnene Arbeit fortzusetzen.

Prof. Dr. José Luis Toca-Herrera danke ich für die herzliche Aufnahme und die Möglichkeit in seiner Arbeitsgruppe in San Sebastián in Spanien zu arbeiten. Seine unermüdliche Geduld mit meiner Ungeduld, seine permanente Hilfsbereitschaft, seine fachliche Betreuung und die vielen gemeinsamen Diskussionen haben sehr viel zum Gelingen dieser Arbeit beigetragen. Für die nette Zeit und die Hilfsbereitschaft in San Sebastián möchte ich Dr. Susana Moreno-Flores, Marco Möller und allen Kollegen am Institut CiCbiomagune danken.

Den KollegInnen am Department danke ich für die freundliche Aufnahme, das angenehme und freundschaftliche Arbeitsklima, die zahlreichen Diskussionen und die vielen hilfreichen Tipps.

Besonders danken möchte ich an dieser Stelle Dr. Kerstin Steiner, Mag. Jacqueline Friedmann, Univ. Ass. Dr. Seta Küpcü, Dr. Kristof Zarschler und Andrea Scheberl. Sie fanden immer Zeit für fachliche Diskussionen und unterstützten mich unermüdlich mit ihrem praktischen und theoretischen Wissen im Bereich der Nanobiotechnologie.

Weiters möchte ich mich bei allen Professoren u. Kollegen für die Unterstützung und Hilfsbereitschaft in der Zeit nach dem Unfall danken.

Meinen Eltern danke ich für die Unterstützung jeder Art und den Optimismus welchen sie mir in den letzten Jahren entgegenbrachten.

## Abstract

This work describes the construction and characterisation of fluorescent S-layer fusion proteins used as building blocks for the fabrication of nanostructured monomolecular biocoatings on silica particles with defined fluorescence properties. The S-layer protein SgsE of *Geobacillus stearothermophilus* NRS 2004/3a was fused with the pH-dependant cyan, green and yellow variant of the green fluorescent protein (GFP) and the red fluorescent protein mRFP1. These fluorescent S-layer fusion proteins, acting as scaffold and optical sensing element simultaneously, were able to reassemble in solution and on silica particles forming 2D nanostructures with p2 lattice symmetry ( $a=11 \pm 0.5$  nm,  $b=14 \pm 0.4$  nm,  $\gamma=80 \pm 1^\circ$ ). The pH-dependant fluorescence behaviour was studied with fluorimetry, confocal microscopy and flow cytometry. These fluorescent S-layer fusion proteins can be used as pH-sensor. 50% of the fluorescence intensity decreases at their calculated  $pK_a$  values (pH6 . pH5). The fluorescence intensity of the GFP variants vanished completely between pH4 and pH3 whereas the chromophore of the red protein mRFP1 was only slightly affected in acidic conditions. At the isoelectric point of the S-layer coated silica particles (pH4.6  $\pm$ 0.2) an increase in particle aggregation was detected by flow cytometry.

The cyan and yellow fluorescent proteins were chosen to create a bi-fluorescent S-layer tandem fusion protein with the possibility for resonance energy transfer (FRET). A transfer efficiency of 20% and a molecular distance between the donor (ECFP) and acceptor (YFP) chromophores of around 6.2 nm could be shown. This bi-fluorescent ECFP-SgsE-YFP tandem fusion protein was able to reassemble on solid surfaces. The remarkable combination of fluorescence and self-assembly and the design of bi-functional S-layer tandem fusion protein matrices makes them to a promising tool in nanobiotechnology.

## Kurzfassung

Diese Arbeit beschreibt die Herstellung und Charakterisierung von fluoreszierenden S-Schicht Fusionsproteinen als Bausteine für die Entwicklung von nano-strukturierten monokristallinen Proteinbeschichtungen auf Siliziumpartikel mit kontrollierten Fluoreszenzeigenschaften. Das S-Schichtprotein SgsE vom *Geobacillus stearothermophilus* NRS 2004/3a wurde mit den pH-Wert abhängigen cyanen, grünen und gelben Fluoreszenzproteinen (Varianten des grünen Fluoreszenzproteins GFP) und dem roten Fluoreszenzprotein mRFP1 fusioniert. Diese fluoreszierenden S-Schicht Fusionsproteine, die gleichzeitig als Matrix und optische Sensoren dienen, re-assemblieren in Lösung und auf Siliziumpartikel indem sie 2D Nanostrukturen mit p2 Gittersymmetrie ausbilden ( $a=11 \pm 0.5$  nm,  $b=14 \pm 0.4$  nm,  $\gamma=80 \pm 1^\circ$ ). Fluorimetrie, konfokal Mikroskopie und Durchflussszytometrie wurden für die Messung der pH-Wert Abhängigkeit herangezogen. Die fluoreszierenden S-Schicht Fusionsproteine können als pH-Sensor verwendet werden wobei am berechneten pKa Wert (pH6 . pH5) die Fluoreszenzintensität um 50 % sinkt. Die GFP Varianten zeigen zwischen pH4 und pH3 keine Fluoreszenz, während der Chromophor vom mRFP1 in sauren Bedingungen nur wenig beeinträchtigt wird. Am isoelektrischen Punkt der beschichteten Partikel (pH4.6  $\pm$ 0.2) konnte man eine Zunahme der Partikelaggregation im Durchflussszytometer beobachten.

Das cyane und gelbe Fluoreszenzprotein wurden herangezogen, um so ein bi-fluoreszierendes S-Schicht Tandemfusionsprotein mit der Möglichkeit zum Resonanz- Energietransfer herzustellen. Eine Transfereffizienz von 20% und ein molekularer Abstand zwischen Donor (cyan) und Akzeptor (gelb) Chromophor von ca. 6.2 nm wurden nachgewiesen. Dieses Tandemprotein re-assemblierte auf festen Trägern. Die außerordentliche Kombination von Fluoreszenz und Selbst-Assemblierung von bi-funktionellen S-Schicht Tandemfusionsproteinen macht sie zu einem vielversprechenden Werkzeug in der Nanobiotechnologie.

# Table of contents

<b>Summary</b> .....	<b>7</b>
<b>General Introduction</b> .....	<b>9</b>
<b>Nanobiotechnology and Self-assembly</b> .....	<b>9</b>
<b>S-layer proteins</b> .....	<b>10</b>
S-layer technology .....	11
Recombinant S-layer fusion protein technology .....	13
Application potential of biofunctional S-layer matrices .....	14
The S-layer protein SgsE of <i>Geobacillus stearothermophilus</i> NRS 2004/3a. ....	15
<b>Fluorescent proteins</b> .....	<b>17</b>
The pH-dependence of the GFP variants .....	19
<b>Luminescence</b> .....	<b>21</b>
Fluorescence probes .....	24
Fluorescence resonance energy transfer (FRET) .....	25
<b>Methods</b> .....	<b>28</b>
AFM . Atomic force microscopy .....	28
TEM . Transmission electron microscopy .....	29
Zeta-potential measurements .....	31
Fluorescence methods .....	32
Fluorimetry .....	32
Steady state fluorescence .....	32
Time-resolved fluorescence .....	33
Fluorescence microscopy .....	34
Epi-fluorescence microscopy .....	34
Confocal microscopy .....	35
Flow cytometry .....	36
<b>References</b> .....	<b>38</b>
<b>Publications</b> .....	<b>43</b>
First author papers .....	43
Co-author papers .....	43
Posters, Proceeding .....	44
<b>Curriculum Vitae</b> .....	<b>45</b>

### Appendix 1

Paper: *Absorption, Steady-State Fluorescence, Fluorescence Lifetime, and 2D Self-Assembly Properties of Engineered Fluorescent S-Layer Fusion Proteins of Geobacillus stearothermophilus NRS 2004/3a*, Birgit Kainz, Kerstin Steiner, Marco Möller, Dietmar Pum, Christina Schäffer, Uwe B. Sleytr, José L. Toca-Herrera, in: *Biomacromolecules* 2010 (11) 207-214

### Appendix 2

Paper: *Fluorescent S-Layer Protein Colloids*, Birgit Kainz, Kerstin Steiner, Uwe B. Sleytr, Dietmar Pum, José L. Toca-Herrera, in: *Soft Matter* DOI:10.1039/C0SM00008F

### Appendix 3

Manuscript: *Study of the fluorescent energy transfer in the bi-fluorescent S-layer tandem fusion protein ECFP-SgsE-YFP*, Birgit Kainz, Kerstin Steiner, Uwe B. Sleytr, Dietmar Pum, José L. Toca-Herrera

### Appendix 4

Paper: *Recombinant Glycans on an S-Layer Self-Assembly Protein: A New Dimension for Nanopatterned Biomaterials*, Kerstin Steiner, Angelika Harnreich, Birgit Kainz, Paul Hitchen, Anne Dell, Paul Messner, Christina Schäffer, in: *Small* 2008 (4) 1728-1740

### Appendix 5

Paper: *Genetic Engineering of the S-Layer Protein SbpA of Lysinibacillus sphaericus CCM 2177 for the Generation of Functionalized Nanoarrays*, Helga Badelt-Lichtblau, Birgit Kainz, Christine Völlenkle, Eva-Maria Egelseer, Uwe B. Sleytr, Dietmar Pum, Nicola Ilk, in: *Bioconjugate Chem.* 2009 (20) 895-903

### Appendix 6

Paper: *Optical oxygen sensor based on Pt(II)porphyrin dye immobilized on S-layer protein matrices*, Sylvia R. Scheicher, Birgit Kainz, Stefan Köstler, Michael Suppan, Alessandro Bizzarri, Dietmar Pum, Uwe B. Sleytr, Volker Ribitsch, in: *Biosensors and Bioelectronics* 2009 (25) 797-802

### Appendix 7

Paper: *Cell surface display of chimeric glycoproteins via the S-layer of Paenibacillus alvei*, Kristof Zarschler, Bettina Janesch, Birgit Kainz, Robin, Ristl, Paul Messner, Christina Schäffer, in: *Carbohydrate Research* (in press)

## Summary

The key issue in optical biosensor technology is the design and making of multifunctional, nanostructured artificial biosurfaces with specific physical properties. This work focuses on the design of nanostructured fluorescent surfaces on silica particles by using genetically functionalised fluorescent S-layer fusion proteins (crystalline bacterial cell surface layer proteins), which act as scaffold and as sensing element simultaneously. Therefore, the intrinsic self assembling capability of the S-layer protein SgsE from *Geobacillus stearothermophilus* NRS 2004/3a with p2 symmetry is combined with the pH-dependent green fluorescent protein (GFP) variants ECFP (cyan), EGFP (green), YFP (yellow) and the red fluorescent protein mRFP1 in a 1:1 stoichiometry. With these fluorescent fusion proteins novel pH-sensitive S-layer biocolloids were designed. Furthermore, a fluorescence resonance energy transfer system (RET) with molecular precision on silica particles is described by using for the first time a bi-functional tandem S-layer fusion protein ECFP-SgsE-YFP where the cyan fluorescent protein ECFP is acting as donor and the yellow fluorescent protein YFP as acceptor fluorophore.

A truncated form of the S-layer protein SgsE was used to incorporate N- and/or C-terminal fused pH-dependent fluorescent proteins [green fluorescent protein (GFP) variants used as fusion partners: green EGFP variant: F64L, S65T; cyan ECFP variant: F64L, S65T, Y66W, N146I, M153T, V163A; yellow YFP 10C variant: S65G, V68L, S72A, T203Y; red mRFP1] termed SgsE-ECFP, SgsE-EGFP, SgsE-YFP, SgsE-mRFP1. Molecular cloning procedures, heterologous expression in *E. coli* host cells, isolations and purifications were performed by means of S-layer technology. Spectral characteristics of the fluorescent fusion proteins in different pH environments (from pH 8 to pH 3) were compared with hexahistidine tagged reference fluorescent proteins (His<sub>6</sub>-ECFP, His<sub>6</sub>-EGFP, His<sub>6</sub>-YFP, His<sub>6</sub>-mRFP1). Absorption measurements were carried out to determine the isosbestic point and the absorption maximum of the fusion proteins. Fluorescence measurements with the four fluorescent S-layer fusion proteins in solution were carried out using steady state and time correlated single photon counting (TCSPC) fluorimetry. Confocal microscopy and flow cytometry were used to monitor the spectral behaviour of the fluorescent S-layer biocolloids (S-layer coated silica particles) under different pH conditions and to determine the resonance energy transfer efficiency within the

assembled bi-fluorescent tandem fusion protein ECFP-SgsE-YFP. Structural investigations were carried out with transmission electron (TEM) and atomic force microscopy (AFM). Zeta-potential measurements were performed to follow the particle coating, to understand their colloidal behaviour and to determine the isoelectric point.

With fluorescence measurements in different pH environments it was found, that 50% of the fluorescence vanished between pH 5 and 6 (at calculated pK<sub>a</sub> values) when the chromophores are changing from their fluorescent anionic state to their neutral state. In addition, the free energy was calculated from obtained pK<sub>a</sub> values. The fluorescence intensity of the different GFP-mutants EGFP, ECFP and YFP strongly decreased in acidic conditions vanishing completely between pH 4 and 3 when the chromophores are changing to their cationic state. The chromophore of the red protein mRFP1 was minimally affected in acidic condition leading to 40 % loss of intensity at pH 3. The fluorescent S-layer fusion proteins in solution and assembled on silica particles behaved in the same way as their His-tagged reference fluorescent proteins. Structure investigations of self-assembly products in solution with TEM (differently sized flat sheets and double-layered self assembly products) and reassembled on silica particles with AFM revealed, that the p2 lattice symmetry ( $a=11 \pm 0.5$  nm,  $b=14 \pm 0.4$  nm,  $\gamma=80 \pm 1^\circ$ ) of the SgsE-protein is not affected by the fused fluorescent protein-moieties. At the isoelectric point of the fluorescent S-layer biocolloids (pH 4.6 +/-0.2) an increase in particle aggregation was detected with flow cytometry.

The bi-fluorescent ECFP-SgsE-YFP tandem fusion protein still retained the unique self-assembly ability on solid surfaces and fluorescence behavior of both fused fluorescent proteins. Around  $20 \pm 6$  % energy transfer efficiency between the cyan ECFP donor and yellow YFP acceptor moieties could be detected. The molecular distance between the two chromophores within the bi-fluorescent S-layer fusion was calculated to be around  $6.2 \pm 1.5$  nm. Thus, it was possible to gain structural information about location and distance of the fused moieties between the N and the C-terminus of the S-layer protein.

The remarkable combination of fluorescence and the self-assembly ability of S-layer fusion proteins as well as the possibility to design bi-functional S-layer tandem fusion protein matrices makes them to a promising tool to build novel multi-functional highly ordered nanopatterned architectures for different applications in nanobiotechnology.

# General Introduction

## Nanobiotechnology and Self-assembly

Nanobiotechnology deals with the understanding and control of biological materials (proteins, lipids, nucleic acids, polysaccharides) in the nanometer scale (1 . 100 nm). It can be described as a converging science including elements of biology, (bio)chemistry and (bio)physics to aim for novel functional materials for biosensing, bioelectronics and medical devices. In the last past years a lot of work was done in developing, characterizing, engineering nanoscale devices with functional components in a controlled fashion [1]. Self-assembly biosystems are playing an important role for the formation of higher-ordered structures with nanoscale periodicity in (i) bulk media (solution) or (ii) at interfaces. These nanopatterned biomaterials serve as template for nanoscopic metallic or semiconductor particles or as scaffold to present bioaffinity or biofunctional units in high-density and defined molecular orientation for molecular and cellular biology, biomedicine, biophysics and materials science. Biosensors are analytical devices, with a well organized sensitive functional biological matrix, which converts a biological response into an electrical signal.

Self-assembly is the spontaneous organization of molecular units into ordered structures that lowers the free energy of the system by non-covalent interactions like hydrophobic-hydrophobic interactions, van der Waals forces, hydrogen bonding and molecular stacking. Biomolecules such as proteins, oligonucleotides, polysaccharide and lipids have this intrinsic ability to form self-assembly products exhibiting spherical, rod-like, or sheet-like shapes associated with a specific function (virus capsids, cytoskeleton components, extracellular surface layer proteins). Lipid like systems (spontaneous forming of micelles and bilayers) or engineered protein-layers are well known scaffolds of bottom-up approaches in controlled fabrication of nanostructured functional devices [2]. In this context, a remarkable example is the unique self assembly system of S-layer (fusion) proteins (crystalline monomolecular cell surface layer proteins) that builds two-dimensional superlattices in the nanoscale which can be used as a structural basis for a biomolecular construction kit involving all major species of biological molecules [3].

## **S-layer proteins**

S-layers are very fascinating regular crystalline monomolecular nano-arrays of protein or glycoprotein subunits located at the outermost cell surface of all major phylogenetic groups of bacteria and archaea species [4-6] [3, 7, 8]. With high resolution electron microscopy studies (freeze-etching and negative staining) it was found that these cell surface proteins generally are covering the entire cell surface with two-dimensional highly porous arrays of most identical (glyco)protein subunits (ranging from 40 to 200 kD) (see Figure 1). [5, 9] These regular macromolecular high anisotropic nano-lattices are mostly showing oblique (p1, p2), square (p4), or hexagonal (p3, p6) lattice symmetry with center-to-center spacings between adjacent morphological (glyco)protein units varying from 3 to 30 nm. Their pores (30 . 70% porosity) are in the range of approximately 2 . 8 nm and are also of identical size and morphology. The thickness of the S-layer surface is about 5 . 10 nm [10-12]. S-layer proteins from Bacillaceae are linked via specific binding domains (lectin-type) on their N-terminus (SLH-domain, SLH-motif) to a heteropolysaccharide containing cell wall polymer (secondary cell wall polymers) which is covalently linked to the peptidoglycan matrix of the cell wall [13, 14]. The S-layer subunits are linked among each other by non-covalent interactions. Sleytr and co-workers found, that the outer face of the S-layer matrix is charge-neutral and less corrugated than the inner net negatively or positively charged face [5]. These supramolecular regular protein nanostructures on bacterial cell envelopes are involved in i) cell adhesion and surface recognition, ii) forming protective coats, iii) building molecular sieves as well as molecule and ion traps, iv) scaffolding for enzymes and v) being a virulence factor in pathogenic organisms [8, 15-17].

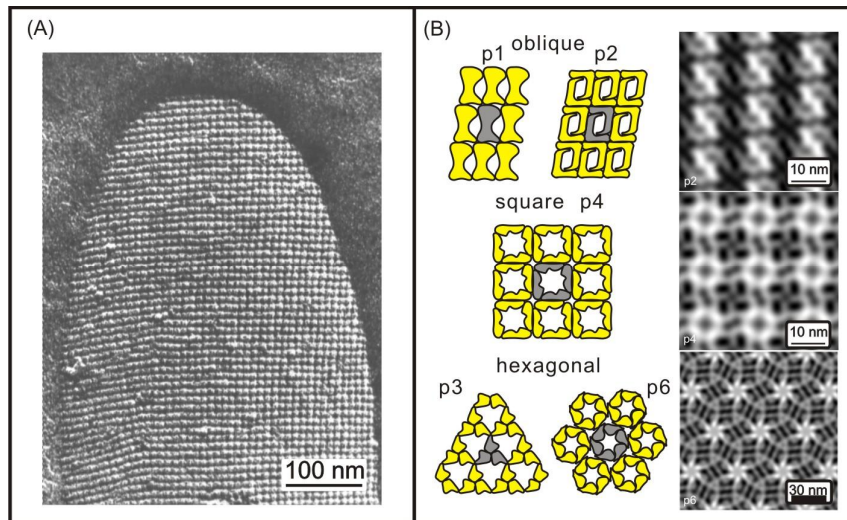


Figure 1: (A) Electron micrograph of a freeze etched and metal shadowed preparation of an intact cell of *Lysinibacillus sphaericus* CCM 2177 with a square (p4) S-layer lattice symmetry. (B) Schematic drawing of different S-layer lattice types and corresponding computer image reconstructions obtained from Transmission Electron microscopy of negatively stained preparations (protein is white, pores are dark). One morphological unit consist of one, two, three, four or six identical (glyco)protein subunits forming regular arrays with oblique (p1, p2), square (p4) or hexagonal (p3, p6) symmetry. [3]

## S-layer technology

One of the most fascinating properties of S-layers is the fact, that isolated and purified (glyco)protein subunits still maintain their unique intrinsic ability to reassemble into the same regular isoporous two-dimensional nano-arrays as those originally found *in vivo* on the cell surface. For this purpose, different disruption and isolation methods using chaotropic agents (e.g. urea, guanidine hydrochloride) have been developed to release the S-layers from the bacterial cell envelope and disintegrate them into their subunits. After removing the chaotropic agent and providing defined recrystallisation conditions (e.g. ionic strength, ion composition, temperature, pH value) the subunits immediately reassemble into their specific two dimensional supramolecular lattices. This reassembling process occurs (i) in suspension forming differently shaped self-assembly products, (ii) on the air-water interface, (iii) on lipid-membrans including liposomes, (iv) on different kinds of solid supports and colloidal systems (for example silica wafer and glass, beads, nanocapsules), (v) on polyelectrolyte layers and (vi) on different chemically modified surfaces (see Figure 2). Self assembly formation in solution is an entropy driven process leading to differently sized mono or double layered free floating flat sheets or

tube-like structures [18]. The kinetic of the reassembling process of the S-layer protein SbpA from *Lysinibacillus sphaericus* CCM 2177 (p4 lattice symmetry) was investigated with atomic force microscopy (AFM) (see Figure 3) [19-21]. First subunits adsorb on the surface, forming nucleation points at which the domains are growing only laterally until the front lines of these patches meet each other. This leads to the formation of closed monocrystalline nanopatterned biofunctional surface coatings. During several reassembling studies on solid supports it was found that S-layers are adsorbed on the surfaces via hydrophobic interactions, hydrogen bonds and ionic bonds involving divalent cations or direct interactions with polar groups [3, 20]. It could be shown that these intermolecular interactions between the surface and the S-layer lattices are not so strong than the intramolecular bonds holding the subunits together. Thus, the ultrastructure of reassembled S-layers is only determined by the tertiary structure of the S-layer protein species. At the moment little is known about the tertiary structure of S-layer proteins. Molecular modelling, in particular molecular dynamic simulations have been used to calculate a 3-D structure prediction of the S-layer protein SbsB from *Geobacillus stearothermophilus* PV72/p2 [22]. Crystallisation studies helped to gain structural information about different parts of a specifically truncated form of the S-layer protein SbsC from *Geobacillus stearothermophilus* ATCC 12980 [23]. Different site specific mutation experiments (for example insertion of cysteine groups at specific positions) were carried out to get information about the topology and the location of individual amino acid residues or to investigate assembly-inhibiting and assembly-tolerant sites of the S-layer protein SbsB [24].

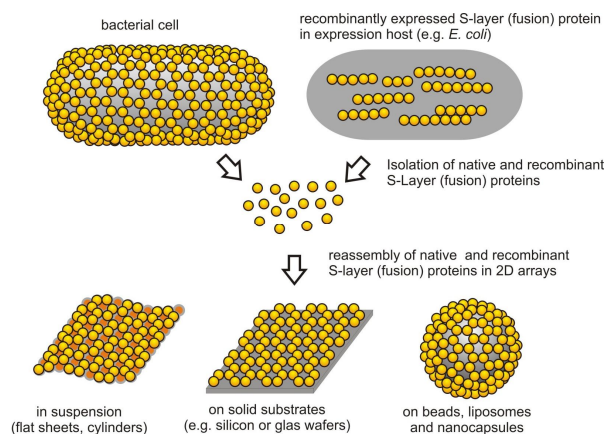


Figure 2: Schematic drawing of the fabrication and reassembly procedure of native or recombinant S-layer (fusion) proteins. After isolation and disintegration, the native or recombinant proteins reassemble either in suspension, on solid supports and on different kinds of colloidal systems like liposomes, beads or nanocapsules.

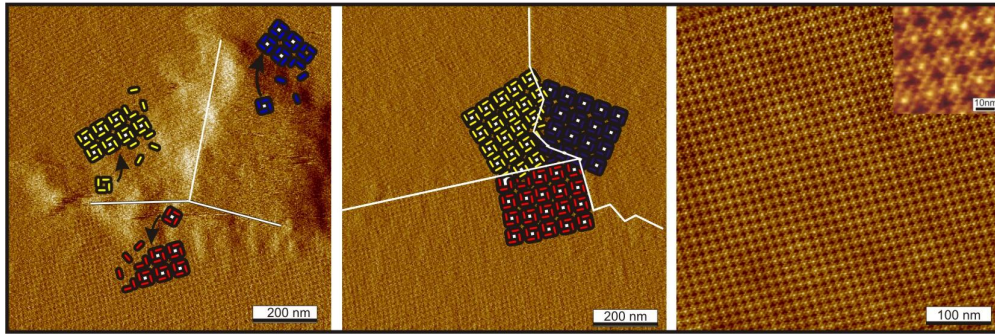


Figure 3: AFM images of the reassembling process of the S-layer protein SbpA from *Lysinibacillus sphaericus* CCM 2177 (p4 lattice symmetry) on silicon wafer [19].

### Recombinant S-layer fusion protein technology

Another amazing feature is the recombinant S-layer technology and therefore their use for genetic engineering to design functional S-layer fusion proteins expressed heterologously in host cells (e.g. *Escherichia coli*, *Bacillus subtilis* or yeast [25]). In several works it was shown that incorporated functional moieties on the N- or/and C-terminus of the used S-layer protein do not interfere with the intrinsic self-assembly property of the S-layer system, while simultaneously fully retaining their specific biological properties (e.g. enzyme activity, fluorescence). Most important, the arrangement of the fused moiety on each S-layer unit cell is repeated with the periodicity of the protein lattices as shown in Figure 4 [26]. Examples for biofunctional S-layer fusionproteins include i) streptavidin S-layer proteins for binding of biotinylated molecules and particles [27-29], ii) different coloured variants of the green fluorescent protein GFP and the red fluorescent protein mRFP1 for imaging, pH-investigations and cell uptake experiments [30, 31], iii) antibodies and allergens for vaccine development [32-34], iv) enzymes [35, 36] and v) tags like Strep-tag, His<sub>6</sub>-tag or cysteines for binding of specific molecules or generating of ordered nanoparticle (gold, quantum dots) arrays [37, 38]. The 1:1 stoichiometry of S-layer protein to fused protein makes them to a useful tool as biofunctional patterning element in (nano)biotechnology (e.g. diagnostics vaccine development, biomimetics or controlled biomineralization) [10, 39].

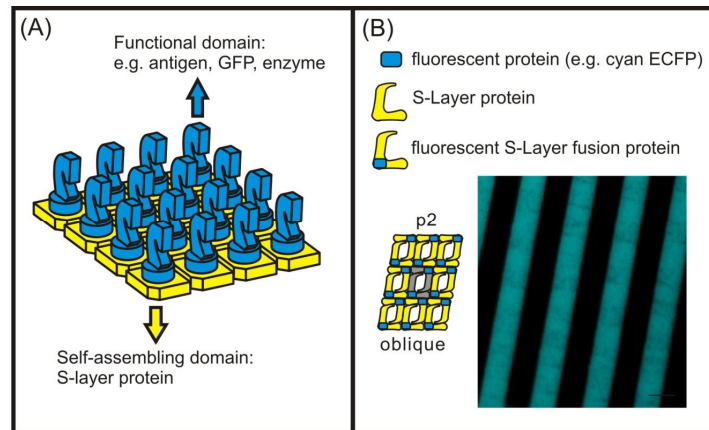


Figure 4: S-Layer fusion protein nanoarrays. (A) Schematic drawing of the S-Layer self-assembling domain and the well oriented genetically fused functional domain in an S-Layer fusion protein array. (B) Example for a cyan fluorescent S-Layer fusion protein SgsE-ECFP assembled on a glass with p2 lattice symmetry.

## Application potential of biofunctional S-layer matrices

The fabrication of S-layer based biosensors can be carried out by (i) immobilization of functional macromolecules (e.g. glucoseoxidase, fluorophores, etc.) onto S-layer matrices by activating the carboxyl-groups of the assembled S-layers using EDC/NHS technology, (ii) using the amino-groups for covalent conjugation of isothiocyanat-activated molecules, (iii) adsorption of, for example, preformed nanoparticles or semiconductor nanocrystals, or (iii) applying novel functional S-layer fusion proteins [26]. S-layer matrices on fiber-optics were exploited to immobilize glucose-oxidase for fabrication of a glucose biosensor and to label it with an oxygen-sensitive porphyrine fluorescent dye to build an oxygen biosensor [40]. Another approach was to design a pH-biosensor on silica-particles or liposomes by using different colored fluorescent S-layer fusion proteins by incorporating different coloured mutants of the green fluorescent proteins (GFP) to the S-layer protein SgsE and SbpA for cell uptake investigations or *in vitro* and *in vivo* cell pH measurements [30, 31]. Novel biocatalysts Enzyme based on enzyme S-layer fusion proteins (SgsE-rmlA, SbpA-larimnarinase) could be shown on liposomes and in microplates [35, 36]. Biofunctional S-layer surfaces are presently applied in a wide area of (nano)biotechnology as a building block for diagnostics, vaccine development, biomimetics, biomineralization and for many biophysical investigations as listed in Table 1 [10, 39, 41].

Table 1: Areas of application potential of S-layer (fusion) proteins where highly defined uniform biofunctional surfaces are required

Isoporous ultrafiltration membranes (SUM), Biosperation	[42, 43]
Biomineralization	[44, 45]
Microfluidics (micromolding in capillares), Biochips	[28, 46]
Biotemplating of preformed nanoparticles (gold nanoparticles, quantum dots) for molecular electronic devices, nonlinear optics and catalysts	[38, 47-51]
Biosensors for <i>in vivo</i> and <i>in vitro</i> applications (glucose sensor, optical oxygen sensor, pH-sensor)	[40, 52, 53]
Drug targeting and delivery systems (functionalisation of liposomes, emulsomes and nanocapsules)	[30, 54, 55]
Stabilization of functional lipid membranes	[56]
Immunogenic and immunomodulation structures (e.g. antiallergic vaccines)	[32-34, 57, 58]
Novel biocatalysts (S-layer enzyme fusion proteins and immobilized enzymes)	[35, 36]
High density affinity coatings (functional nano-arrays) for downstream-processing and blood purification	[26, 29, 38, 59]
Biophysics applications (diagnostic systems and label free detection systems)	
Sensing layers for surface Plasmon resonance spectroscopy (SPR), surface acoustic wave, quartz crystal microbalance with dissipation (QCM-D), atomic force microscopy studies (AFM), assembling studies onto different substrates (polyelectrolytes, $\delta$ )	[20, 21, 28, 60, 61]
S-layer neoglycoproteins, glycoprotein investigations	[62, 63]

### The S-layer protein SgsE of *Geobacillus stearothermophilus* NRS 2004/3a.

SgsE is a 903 amino acid containing glycoprotein from *Geobacillus stearothermophilus* NRS 2004/3a (Gen Bank accession number AF328862) including a 30-amino acid signal peptide (SLH-motif) at the N-terminus [64-66]. This S-layer protein forms lattices with oblique (p2) lattice symmetry on cell envelopes as displayed in Figure 5 ( $a=11.6\text{nm}$ ,  $b=9.4\text{nm}$ ,  $\sim 78^\circ$ ). Isolated SgsE subunits build five types of mono- and double-layered self-assembly products, depending on the salt concentration and duration of dialyses to remove the chaotropic agent [64, 65]. Self-assembly products are showing differently sized flat sheets and cylinders as shown in Figure 5c. It was found out, that the formation of double-layered self-assembly products being an entropy-driven process where constituent monolayers are associated with their net-negatively charged inner faces [65]. The back-to-back orientation reflects *the in vivo* situation. Only small cylinders are composed of a monolayer. Genetically engineered and recombinantly produced (fusion)proteins as well as truncated forms show the same reassembling behaviour [36].

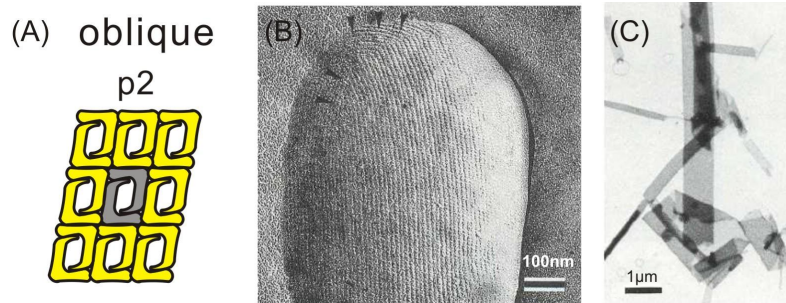


Figure 5: The S-layer protein SgsE is showing p2 lattice symmetry (A) on the cell envelope of a freeze-etched and Pt/C-shadowed cell of *Geococcus stearothermophilus* NRS 2004/3a, arrows showing lattice distortion on the cell poles (B). Image (C) shows different sized flat sheets and tube-like negatively stained self-assembly products. [65]

Up to now, the S-layer protein SgsE has been used as a matrix for templating CdS in a nanometer-scale and to build up novel functional architectures like enzyme fusion proteins (novel biocatalysts) and fluorescent fusion proteins as described before (see Figure 6) [31, 36, 51]. Further, this SgsE S-layer protein was used to create neoglycoproteins in *Escherichia coli* for the design of new biomaterials with a nanopatterned matrix for the periodic display of glycans [62].

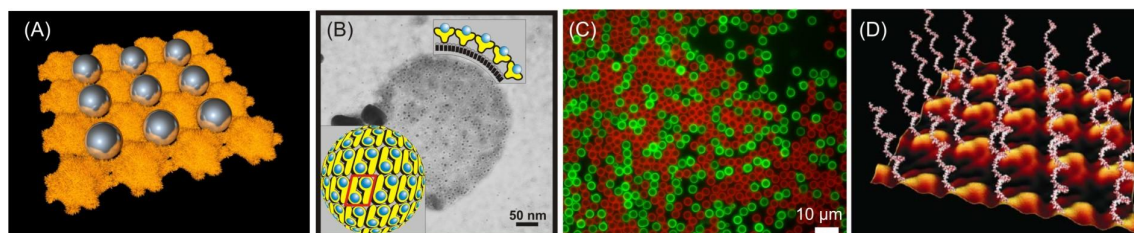


Figure 6: Application potential for SgsE (fusion) proteins. (A) biotemplating of nanocrystals onto SgsE lattices (image Markus Gossmann), (B) SgsE-rmlA biocatalyst on liposomes [36], (C) fluorescent SgsE fusion protein coated silica particles (green SgsE-EGFP, red SgsE-mRFP1) [in press], (D) schematic drawing of the first neoglycoprotein [62].

## Fluorescent proteins

Green fluorescent protein (GFP) from the jellyfish species *Aequorea Victoria* and its differently coloured variants as well as the differently coloured modifications derived from the red fluorescent protein DsRed from the sea anemone *Discosoma striata* have become one of the most useful tools in modern biotechnology [67]. They are now well established as bioimaging markers (gene expression, protein localisation and folding), for numerous biological studies (gene expression, protein targeting, cell uptake investigations, drug delivery), as biosensors (pH sensitivity, redox potential, metal/halide concentrations) and for protein-protein interactions in resonance energy transfer (FRET) based techniques [67-69]. They are detectable by spectroscopic methods, flow cytometry and fluorescence microscopy. The discovery and development of the green fluorescent protein GFP was awarded with the Chemistry Nobel Prize in 2008 to Osamu Shimomura, Marty Chalfie and Roger Tsien.

The main tertiary structure of the 238 amino acid containing wild-type GFP molecule (27 kDa) consists of an 11-stranded  $\beta$ -barrel (approximately 4 nm long and 3 nm in diameter [70]) and single  $\alpha$ -helix running up the axis in the center of the barrel (see Figure 7a) [71]. The chromophore is located in the hydrophobic core of the barrel along the  $\alpha$ -helix. A hydrogen-bonding-network shields the chromophore from the surrounding bulk solvent [72]. The chromophore maturation starts subsequently after the protein is folded within the hexapeptide sequence Ser65-Tyr66-Gly67 through an autocatalytic cyclization reaction followed by dehydration and a final oxidation step with atmospheric oxygen as displayed in Figure 8 [67, 73]. There are no external cofactors involved in the chromophore-formation. It was found out, that the amino acids Arg96 and Glu222 in the proximity of the chromophore are playing an important role during the maturation process [72, 74]. The tertiary structure of the red fluorescent protein DsRed is a tetrameric homologous of GFP with a more elliptically  $\beta$ -barrel (a monomer is shown in Figure 7b). The chromophore has a more extensive conjugated  $\pi$ -system (see Figure 8) which is formed by an additional oxidation step in comparison to the GFP chromophore [75, 76]. It took 33 mutations to DsRed to create a monomeric red fluorescent protein mRFP1 with its excitation at 584 nm and emission at 607 nm [77]. Further modifications of mRFP1 has led to creation of the mFruits series (for example mBanana, mOrange, mCherry, etc.) with enhanced fluorescent properties (photostability, quantum yield, brightness) [78-80].

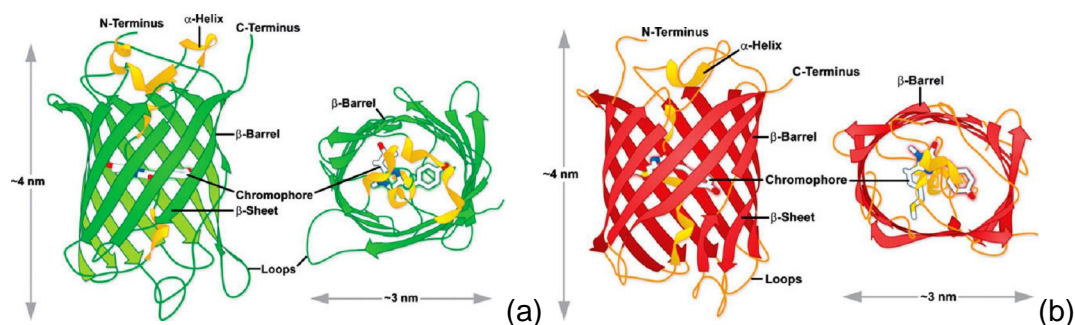


Figure 7: Architecture of the  $\beta$ -barrel and location of the chromophore of a) GFP and b) mCherry a mutant of mRFP. The symmetry of the mRFP  $\beta$ -barrel is more elliptical in comparison to the  $\beta$ -barrel of GFP. (images from ref. [80])

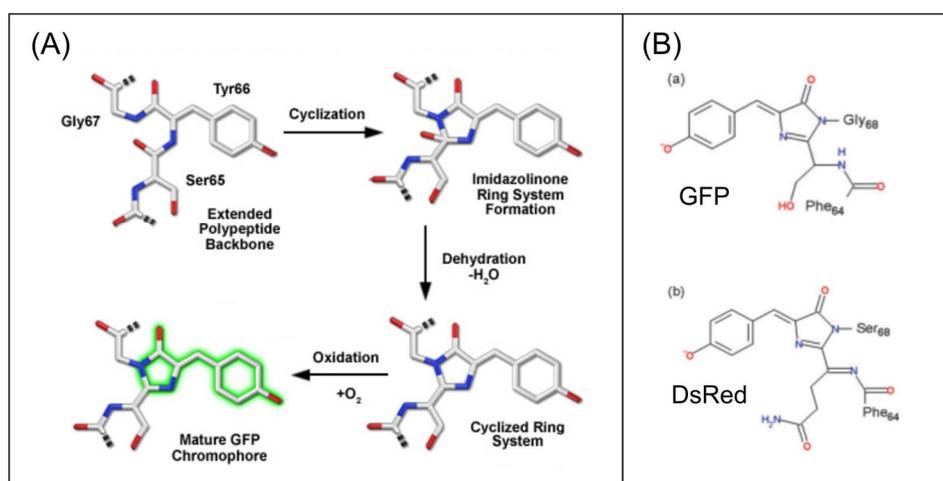


Figure 8: (A) Chromophore formation: (1) folding, (2) cyclisation: nucleophilic attack of the carboxyl carbon of Ser65 to the amino nitrogen atom of Gly67, (3) dehydration and imidazolin-5-one heterocyclic ring formation, (4) oxidation of the Tyr66 alpha-beta carbon bond by molecular oxygen to form a highly conjugated  $\pi$ -electron resonance system. (image from zeiss homepage and [80]) (B) Chemical structures of the chromophores in (a) GFP and (b) DsRed with the extended  $\pi$ -system caused by a second oxidation step. (image from ref. [81])

In the meantime, numerous mutations in the chromophore forming site revealed GFP variants with differently spectral characteristics spanning nearly the entire visible spectra [72]. It is also known that the surrounding residues can affect the spectral properties. F64L (replacement of phenylalanine for leucine at position 64) improved the efficiency of protein maturation at 37°C and the expression in different host cells [67]. Variants carrying this mutation are termed  $\%E+$  for enhanced [82].

Depending on their emission maxima fluorescent proteins can be divided into (i) blue BFPs; 440-470 nm, (ii) green GFPs; 501-520 nm (phenolate anion), (iii) yellow YFPs; 521-550 nm (stacked  $\pi$ -system), (iv) cyan CFPs; 471-500, (v) orange OFPs;

551-575 nm, (vi) red RFPs; 576-610 nm and (vii) far-red (FREPs); 611-660 nm fluorescent proteins [67, 73]. Examples of GFP variants and their excitation and emission spectra are shown in Figure 9.

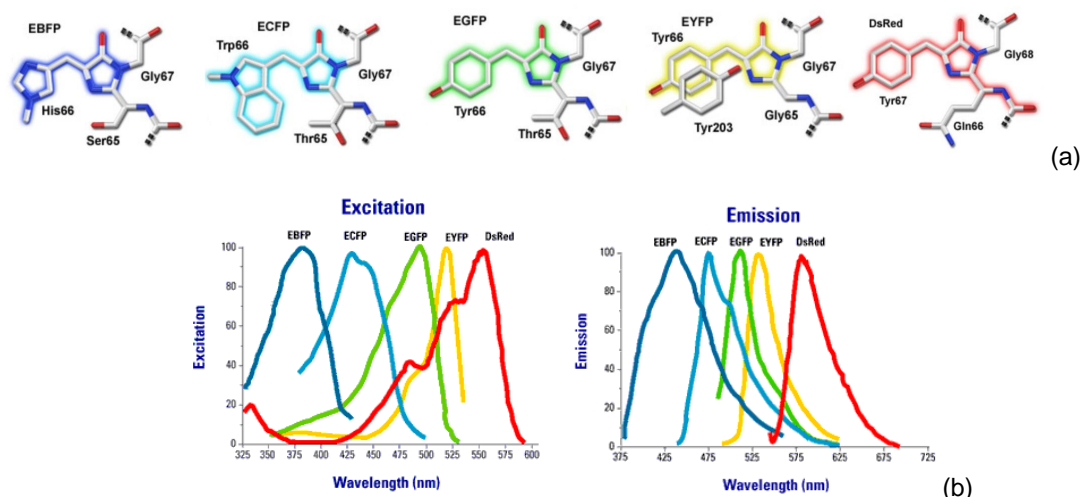


Figure 9: a) Chromophore structures of common fluorescent proteins, the conjugated ring structure of each chromophore is colored to its emission spectrum (blue amino-groups and red hydroxyl-groups) (image modified from ref [73]). b) Excitation and Emission spectra of commonly used fluorescent proteins.

GFP proteins have a number of amazing properties for using them *in vivo* and *in vitro* investigations. They can be expressed in a variety of cells, they don't need cofactors to become fluorescent, they can be fused to proteins to create colourful fusion proteins and they can be targeted to specific organelles to act as cellular reporter and differently colored mutants can be used as FRET-pairs for protein-protein interaction studies.

## The pH-dependence of the GFP variants

In recent years a significant amount of research has been carried out on the spectral properties of green fluorescent protein variants [74, 83, 84]. There is substantial interest in understanding the structural and spectral response of the embedded chromophore to changes in pH [69, 83, 85, 86]. GFP mutants are showing differently pH dependent reversible fluorescence properties. Thus, making them to useful physiological pH-indicators within the intracellular compartments (cytoplasm, alkaline organelles, mitochondria, cytosol and the Golgi) [87, 88].

EGFP (S65T, F64L) is the brightest and most photostable GFP protein and is sensitive to pH because of the connection between the S65 side chain and E222 which are both protonated at  $\text{pH} < 6$ . ECFP is carrying the substitution Y66W leading to a broad bimodal absorption spectrum at 433 and 445 nm and an equally broad bimodal fluorescence emission spectrum with maxima at 475 and 503 nm [89]. The change in fluorescence of ECFP with pH is reported to be smaller than that of EGFP or EYFP. YFP has a stacked  $\pi$ -orbital system, caused by T203 mutation, stabilizing the excited state of the chromophore and leading to a red-shifted emission wavelength at 528 nm. EYFP is very sensitive to acidic pH, losing 50 % of its fluorescence at pH 6.5 and can be used to develop biosensors for measuring cytoplasmic pH [88]. Other substitutions in the surrounding  $\beta$ -barrels of the GFP variants improved mostly the brightness and photostability of the proteins.

It is known that the chromophore in GFP is very well shielded by the rigid  $\beta$ -can and therefore insensitive to fluorescence quenchers. But it was found out that the protonation of the tyrosin residue at position 66 (Y66) is associated with structural rearrangements leading to the reversible pH sensitivity [84]. The hydroxyl group of Y66, pointing towards to the surface of the  $\beta$ -can (perpendicular to the cylinder axis), is able to communicate with the bulk proton concentration leading to conformational thermal fluctuations of the  $\beta$ -sheet [90, 91]. Mutations on the amino acid position 147, 149, 164, 165-168 and 220, located in three adjacent  $\beta$ -strands just above the Y66 hydroxyl group influence this conformational fluctuations and thereby the dependence of GFP fluorescence on bulk pH [90]. At low pH values the chromophore is in his protonated cationic non-fluorescent state, whereas the anionic and neutral states at higher pH values are fluorescent (see Figure 10) [68]. Members of the YFP class also showed a photochromic switching behaviour. Conformational rearrangement of the  $\beta$ -barrel and the amino acids surrounding the embedded chromophore is responsible for external proton transfer and possibly cis/trans isomerization as non-radiative pathways [92].

A further advantage of GFPs is that they are more resistant to photobleaching than fluorescein-based dyes.

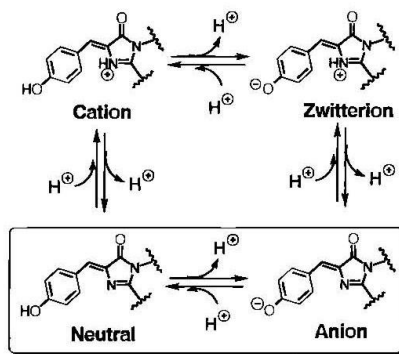


Figure 10: The possible charge states in the GFP variants (S65T) and YFP. The neutral and anionic state of the tyrosin residue of position 66 (Y66) are the fluorescent states (image from ref. [83]), (right image from ref. [68])

## Luminescence

When light interacts with matter a physical process called luminescence (fluorescence and phosphorescence) can occur by emission of ultraviolet, visible or infrared photons [93]. Luminescence spectroscopic techniques are a growing area in biophysics, biochemistry, biotechnology and biomedicine for cellular imaging, genetic analysis or single-molecule detection.

The Jablonski Diagram in Figure 11 is used to describe the processes of absorption and emission of light by a fluorophore. Fluorophores are small aromatic or conjugated molecules with delocalized electrons. The absorption of light  $A(\lambda)$  at a wavelength  $\lambda$  is a very fast process ( $10^{-15}$  s), described by the Beer-Lambert Law

$$A(\lambda) = \log \frac{I^0}{I_\lambda} = \varepsilon(\lambda)cl \quad (\text{Equation 1})$$

where  $I^0$  and  $I$  are the light intensities before and after interaction with the molecules,  $\varepsilon$  is the molar absorption coefficient ( $\text{Lmol}^{-1}\text{cm}^{-1}$ ),  $c$  is the concentration ( $\text{mol}^{-1}$ ) of absorbing molecules and  $l$  is the absorption path length (thickness of the absorbing medium in cm).

After absorption of photons several processes occur (see Figure 11) [93, 94]:

- i. A fluorophore is excited from its vibrational energy level 0 in the singlet electronic ground state ( $S_0$ ) to some vibrational energy level (0, 1, 2  $\tilde{\nu}$ ) of a higher singlet electronic state  $S_1$  or  $S_2$ .

- ii. Subsequently, the electrons are relaxing to the lowest vibrational level 0 of  $S_1$ . This non-radiative process is called internal conversion ( $10^{-13}$  .  $10^{-11}$  seconds) and takes place within the vibrational levels of the electronic states and between two electronic states of the same spin multiplicity (from  $S_2$  to  $S_1$ ).
- iii. Deactivation from the thermodynamically equilibrated excited state  $S_1$  (0) to some vibrational levels of the ground state  $S_0$  is a very fast process (generally  $10^{-8}$  .  $10^{-9}$  seconds) and the energy can be released as (i) a photon called fluorescence emission, (ii) as thermal energy (non-radiative deactivation), or (iii) used for other processes such as energy transfer and collisional quenching.
- iv. The relaxation to the lowest vibrational level (0) of  $S_1$  is again non-radiative.
- v. Molecules in the  $S_1$  state can also undergo conversion to the first triplet electronic state  $T_1$ . This process is called intersystem crossing and occurs between  $10^{-7}$  and  $10^{-9}$  seconds.
- vi. Emission from the lowest vibrational energy level of  $T_1$  is called phosphorescence and is shifted to longer wavelength (low energy).

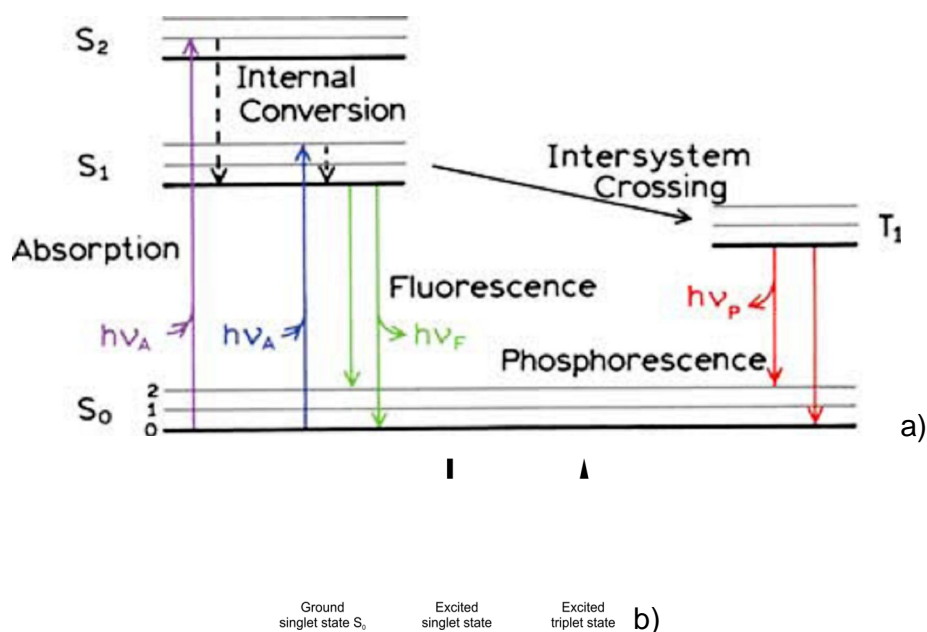


Figure 11: a) Jablonski energy-level diagram: Illustration of the processes after photon absorption.  $S_0$  is the electronic ground state,  $S_1$  and  $S_2$  excited electronic singlet states,  $T_1$  excited triplet state, vibration energy levels are associated (0,1,2) with each electronic state (image from ref. [94]). b) Three different states of electron. In the singlet ground state the electron spins are paired (no splitting of electronic energy levels occurs), in the singlet excited state the spin of the promoted electron is still paired but in the excited triplet state the spins become unpaired and parallel. The excited triplet state is less energetic than the excited singlet state [95].

The fluorescence emission spectrum is located at higher wavelengths than the absorption spectrum because of the energy loss in the excited state caused by vibrational relaxation. The Stoke shift (expressed in wavenumbers  $\nu$ ) is described as the distance between the absorption maximum (A) and the fluorescence emission maximum (F) of a fluorophore, described as

$$\Delta\nu = \nu_A - \nu_F \quad \text{Equation 2}$$

Fluorescence lifetime ( $\tau_s$ ) is defined as time during which the electrons of the fluorophore stay in the excited state before returning back to the ground state  $S_0$  [93]. The lifetime of the excited state  $S_1$  is given by the inverse sum of the total rate of deactivation processes

$$\tau_s = \frac{1}{k_r^S + k_{nr}^S}, \quad k_{nr}^S = k_{ic}^S + k_{isc}^S \quad \text{Equation 3}$$

where  $k_r$  is the radiativ rate constant (fluorescence) of the process,  $k_{nr}$  is the rate constant for the overall non-radiative processes ( $k_{ic}$  for internal conversion  $S_1 \rightarrow S_0$  and  $k_{isc}$  for intersystem crossing) (see Figure 11). The fluorescence lifetime is one of the most important characteristics of a fluorescent molecule because it defines the time window of observation of dynamic phenomena like energy transfer or quenching reactions [93].

The fluorescence quantum yield  $\Phi_F$  of a fluorophore is the ratio of the number of emitted photons to the number of absorbed photons and is describing the second important characteristic of a fluorophore

$$\Phi_F = \frac{k_r^S}{k_r^S + k_{nr}^S} = k_r^S \tau_s \quad \text{Equation 4}$$

The three most common environmental factors influencing the fluorescence properties are (i) solvent polarity, (ii) proximity and concentrations of quenching species, (iii) pH of the aqueous medium. Structurally, pH sensitivity is due to a reconfiguration of the fluorophore's  $\pi$ -system that occurs upon protonation.

## Fluorescence probes

Fluorophores are mostly aromatic and heterocyclic compounds carrying carboxyl, sulfonate or nitro groups. Their emission spectra are dependent upon the degree of conjugation (extent of the delocalised  $\pi$ -electron system) leading to spectra with longer wavelengths and an increase in the fluorescence quantum yield. Fluorescence probes can be divided into intrinsic and extrinsic probes. Intrinsic fluorophores are naturally occurring molecules including aromatic amino acids (tryptophan, tyrosin, phenylalanine), NADH, flavins, porphyrins, modified nucleic acids (Y base in some tRNAs) and chlorophyll. Extrinsic fluorophores are molecules to target a wide variety of biological macromolecules. Thousands of fluorophores are now available for covalent and non-covalent labelling of target systems. Most of the extrinsic fluorophores are carrying reactive groups (e.g. active ester, carboxylate, isothiocyanate, hydrazine, carbodiimide, maleimide,  $\alpha$ ) for covalently attaching them to specific (incorporated) functional groups of proteins (e.g. amino groups, carboxyl groups, thiol,  $\alpha$ ) [93, 94]. Examples of common fluorophores are xanthene (fluorescein, rhodamine, Oregon green, Texas red), cyanine, naphthalene (dansyl), coumarine, pyrene, tetrapyrrole (DAPI, bilirubin, lucifer), oxazine, lanthanide (europium or terbium ions), metal-ligand complexes (ruthenium, osmium, iridium) or fluorescent semiconductor nanocrystals (quantum dots) (examples see Figure 12). For imaging biological systems, researchers have developed a diverse set of fluorescent proteins derived from GFP (Figure 12).

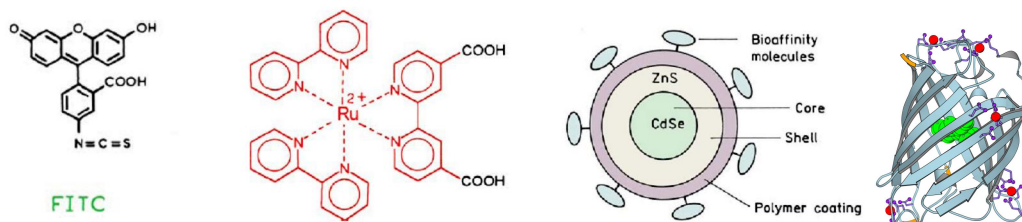


Figure 12: Different kinds of common fluorophores from left to right: fluoresceinisothiocyanate, metal-ligand complex, schematical drawing of a core-shell quantum dot and structure of the green fluorescent protein GFP.

## Fluorescence resonance energy transfer (FRET)

Förster (or fluorescence) energy transfer is based on the distance-dependent transfer of energy from a donor fluorophore (D) to an acceptor (A) fluorophore. When the donor fluorophore (D) is in his excited state it can transfer his excited-state energy radiationless to an adjacent acceptor fluorophore (A). This process is a long-range dipole-dipole interaction that occurs when two fluorophores are located within the Förster radius (80-100 Å) [94]. Thus, the energy transfer is strongly dependend on (i) the extent of spectral overlap of the donor-emission spectrum and the acceptor-excitation spectrum (shown in Figure 13a), (ii) the quantum yield of the donor, (iii) the relative orientation of the donor and acceptor transition dipoles and (iv) the distance (r) between the donor and acceptor molecules. The relative molecular distance (r) dependent energy transfer efficiency between the donor (D) and the acceptor (A) is given by

$$E = \frac{1}{\left[1 + \left(\frac{r}{r_0}\right)^6\right]} \quad \text{Equation 5}$$

with  $r_0$  as the (Förster) distance at which 50% energy transfer takes place (between 20 . 60 Å), expressed as

$$R_0 = \left[ \kappa^2 \times J(\lambda) \times n^{-4} \times Q_D \right]^{1/6} \times 9.7 \times 100 \quad \text{Equation 6}$$

where  $\kappa^2$  is the relative orientation of the transition dipoles of the fluorophores,  $J(\lambda)$  is the integral of the region of overlap between the donor emission and acceptor absorbance spectra,  $n$  is the refractive index of the surrounding medium, and  $Q_D$  is the quantum yield of the donor [94, 95].

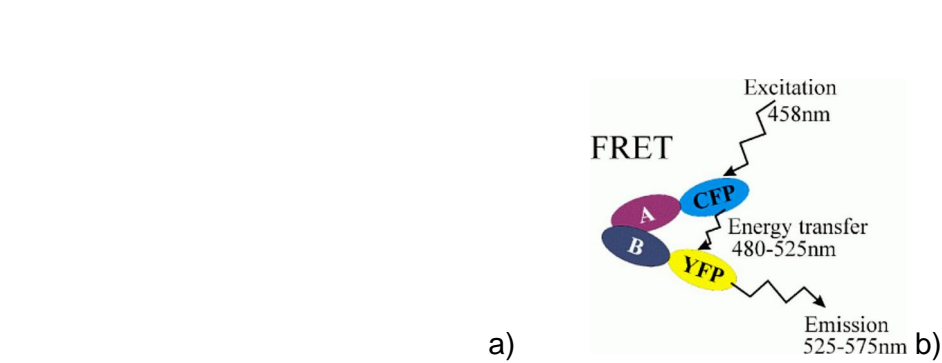


Figure 13: a) Spectral overlap between the emission spectrum of the donor and the excitation spectrum of the acceptor. b) Example for an energy transfer system with two fluorescent proteins where energy is transferred from the excited cyan CFP protein to the yellow YFP protein.

When resonance energy transfer occurs, the donor emission decreases while acceptor emission increases. The transfer efficiency and further the relative molecular distance between the two fluorophores (Equation 7) can be calculated by the extent of donor quenching according to following Equation 7 [99]:

$$E = 1 - \frac{I_{DA}}{I_D} \quad \text{Equation 7}$$

where E is the energy transfer efficiency,  $I_{DA}$  is the fluorescence intensity of the donor in presence of the acceptor and  $I_D$  is the fluorescence intensity of the donor in absence of the acceptor.

Many fluorescent proteins share overlapping spectra and some have been proven useful for FRET-based intracellular biosensors [100, 101]. Recently a lot of work was done in designing and applying fluorescent proteins with different emission and excitation wavelengths for (intracellular) FRET-based investigations [102-104]. The often used FRET pair within the GFP family is the cyan CFP (donor) and the yellow YFP (acceptor) proteins (Figure 13b) [67, 105].

FRET based approaches are playing an increasing role as spectroscopic ruler in the nanometer-scale for (intracellular) protein-protein or cell component interactions, DNA deformations and optical imaging [106, 107]. Examples for FRET-based biosensors are DNA-Hairpin setups or energy transfer between donor and acceptor attached to different sites in the same biosensor+proteins for the design of label-free

*in vivo* and *in vitro* systems. The energy transfer efficiency between donor and acceptor can be monitored using steady-state and time-resolved spectrofluorimetry or confocal microscopy [99, 108] and flow cytometry [106, 109].

## Methods

### AFM – Atomic force microscopy

The atomic force microscope (AFM) is widely used for biological applications in biophysics and nanobiotechnology being a very powerful tool for imaging, measuring and manipulating matter (in aqueous solution) at the nanoscale [95, 110]. The AFM belongs to the family of scanning probe microscopes, using a flexible cantilever to measure the force between the tip and the sample during scanning the surface topography of the sample. When the tip is approached onto the sample, several forces affect the tip-sample interaction. These forces include mechanical contact force, van der Waals forces, capillary forces, chemical bonding and electrostatic forces, etc. The up and down deflection of the cantilever (according to Hooke's law) during tracking the surface is measured using a laser spot reflected from the top surface of the cantilever into an array of photodiodes. The topography of the sample is displayed on the desktop as shown in Figure 15. A feedback mechanism is used to adjust the tip-to-sample distance to maintain a constant force between the tip and the sample to avoid damage of the surface through collision of the tip with the surface. The sample is fixed on a piezoelectric scanner that can move the sample in the z direction for maintaining a constant force and the x and y directions for scanning the sample.

In general, two main imaging modes are applied (i) static contact mode where the tip deflection is used as feedback signal and (ii) dynamic mode where the cantilever is oscillating on the surface of the sample.

- (i) contact mode: The tip is in contact with the sample (1nN to 100 pN). With this mode the highest resolution can be observed. In the height mode the topology of the sample is measured with constant force. The force between the tip and the surface is kept constant by an electronic feedback loop. In the deflection mode the cantilever deflection is kept constant by the feedback loop contracting or expansion of the piezoscanner.
- (ii) tapping mode: The cantilever (driven by a piezoelectric actuator) is oscillating at its resonance frequency on the surface of the sample and the tip touches briefly the surface at the bottom of each swing (intermittent). Depending on the topology

of the sample (sample to tip distance) during scanning, the amplitude of the oscillation changes. The feedback loop keeps the amplitude of cantilever oscillation at a constant level determining the height information of the sample.

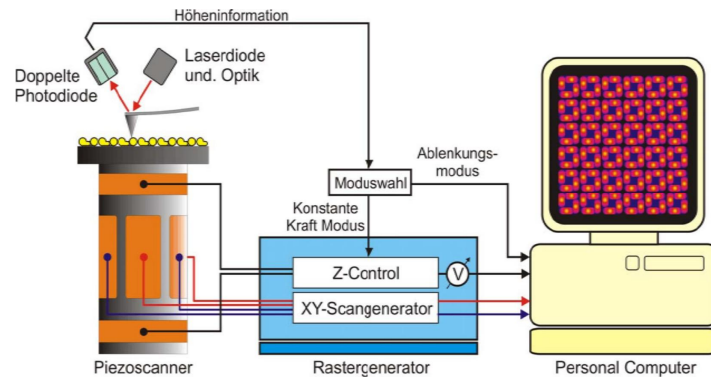


Figure 15: Image of an Atomic force microscope (AFM) setup (image from Dietmar Pum).

The vertical resolution (minimum in height differences) is determined by following parameters: (i) radius of the tip, (ii) spring constant of the cantilever, (iii) sensitivity of the cantilever deflection detection, (iv) softness of the material (v) mechanical and electrical noise. The lateral resolution is dependent on the radius of the tip.

In comparison with TEM, AFM does not need an external contrast. AFM can also work in aqueous environment which is crucial to investigate biological matter. In particular, AFM has already been used for (i) imaging surface topologies in the nanometer scale, (ii) single molecules detection, (iii) force spectroscopy (force-distant curves) [111, 112] and (iv) investigations on living cells [110]. Cantilevers can be modified with particles [113] or other ligands (e.g. antibodies, streptavidine, etc.) [114, 115].

## TEM – Transmission electron microscopy

The image in the TEM is formed by the interaction of electrons with the sample. The contrast is given by electrons passing through the sample and those electrons which are not affected by the sample.

The optical path in a transmission electron microscope is similar to a light microscope (see Figure 14a). The radiation source is a cathode (e.g. tungsten filament or lanthanum hexaboride  $\text{LaB}_6$  source) heated by an electric current for emitting electrons into the vacuum. A negatively charged Wehnelt cylinder and a grounded

anode (e.g. 80 kV) accelerate and attract the electrons in the electric field. Electromagnetic lenses (quadrupole or hexapole lens) are focussing the electrons leaving the radiation source through the hole forming an electronic beam. First the electronic beam is focused through two condenser lenses on the specimen. Scattered electrons are then gated by the aperture in the objective lens to generate an intermediate image. This image is magnified through multi-stage projective lenses. The magnified image (ratio of the distance between the object and the objective lens) can be regarded onto a fluorescence screen or detected by a CCD-camera.

The contrast in the image is caused by the mass-thickness-contrast. In more detail, the amount of scattered electrons is dependent of the thickness of the specimen and the scatter angle is dependant on the mass number (atomic number).

Samples for TEM investigations are adsorbed onto carbon coated EM-grids (different materials and mesh). A common method to visualise biological samples like single proteins is negative staining to get high-contrast images. Biological molecules are not very electron dense and do not interact strongly with the electron beam so they have to be negatively stained by embedding them in materials like uranyl acetat or heavy metals. In the electron image these samples appears as light region surrounded by a dark background originating from the stains (see Figure 14b). Another method is electron cryo-microscopy. For this purpose the sample is rapidly cooled and regarded at liquid nitrogen temperatures. This method improves the preservation of the native structure ob biological samples.

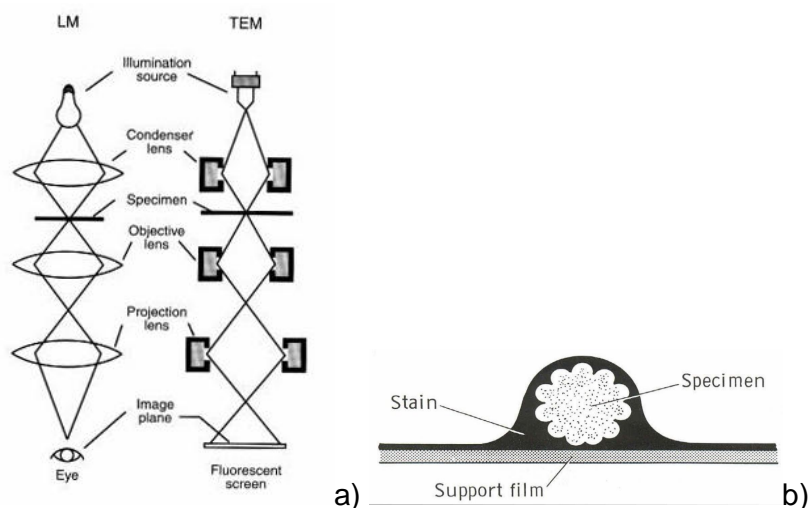


Figure 14: a) Schematic drawing of a light microscope (left) and a transmission electron microscope (right), b) negatively stained specimen.

## Zeta-potential measurements

The stability of colloids in suspension can be affected by the charge on and near their surface. The surface charge of particles affects the distribution of the surrounding ions leading to an increased concentration of ions of opposite charge close to the particle's surface as shown in Figure 16. Thus, an electrical double layer exists around each particle having an inner region (Stern layer) where the ions are strongly bound and an outer (diffuse) region where they are less associated. If the particle moves under Brownian motion, the ions of this diffuse layer move with it. The zeta potential is the potential of the slipping plane (surface of hydrodynamic shear). The charge at this plane is very sensitive to the concentration and type of ions in solution and is strongly affected by the pH value. The magnitude of the zeta potential gives an indication of the potential stability of a colloidal system. If the particles in suspension have the same zeta potential (positive or negative) they repel each other, if they have low zeta-potential values, they attract each other by forming aggregates. At the isoelectric point, the pH value where the zeta-potential is zero, the colloidal system is less stable leading to aggregation. Zeta-potential measurements are often used to determine the stability of colloidal systems.

Zeta potential is obtained from the electrophoretic mobility. By applying an electric field across the dispersion, the charged dispersed particles migrate toward the electrode of opposite charge with a velocity proportional to the magnitude of the zeta potential. This electrophoretic mobility ( $U_e$ ) leads to a frequency shift or phase shift of an incident laser beam which is converted to the zeta potential ( $\zeta$ ) described by the Henry's equation,

$$U_e = \frac{\epsilon \zeta}{6\pi\eta} f(ka) \quad \text{Equation 8}$$

taking into account the viscosity ( $\eta$ ) and the dielectric constant ( $\epsilon$ ) of the medium and the Henry's factor  $f(ka)$  with the ratio between the particle radius ( $a$ ) and the thickness of the double layer ( $1/k$ ). The Henry factor is one [ $f(ka)=1$ ] when the particle radius is smaller than the thickness of the double layer [ $a < (1/k)$  Hückel limit] and 1.5 when the particle radius is bigger than the double layer thickness [ $a > (1/k)$  Smoluchowsky limit] [116, 117].

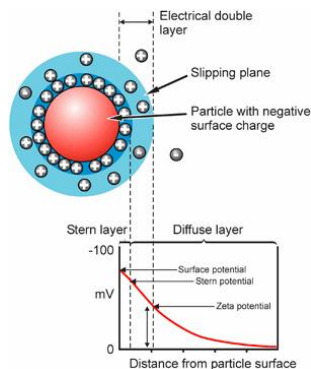


Figure 16: Schematic representation of zeta potential (image from www.malvern.com)

## Fluorescence methods

### Fluorimetry

#### Steady state fluorescence

Steady-state measurements are performed using a spectrofluorimeter by recording emission spectra or intensities during continuous illumination of the sample with light. Under these conditions the concentration of fluorophores in the excited state ( $A^*$ ) remain constant (see Figure 17). The steady state measurement is an average of the time-resolved intensity decay of the fluorophore and is therefore proportional to the lifetime.

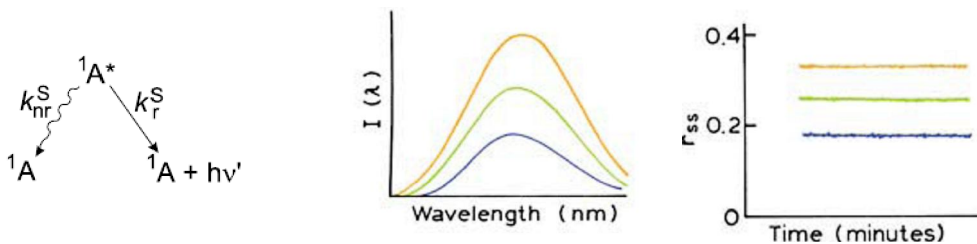


Figure 17 : Steady-state fluorescence spectroscopy: Deactivation energy non-radiativ ( $k_{nr}^S$ ) and fluorescence (radiativ  $k_r^S$ ), emission spectra showing different intensities ( $I$ ), fluorescence steady state ( $r_{ss}$ ) measurement during continuous illumination of the sample with light (image from ref. [93, 94]).

## Time-resolved fluorescence

Time-resolved measurements can be carried out by exposing the sample either to a pulse of light (pulse fluorimetry, see Figure 18) or to a modulate light at variable frequency (phase-modulation fluorimetry) [93, 94]. In pulse fluorimetry the time-dependent intensity is determined from the slope in a plot where the log of the intensity [ $\ln I(t)$ ] is displayed against the time ( $t$ ), as shown in Figure 18.

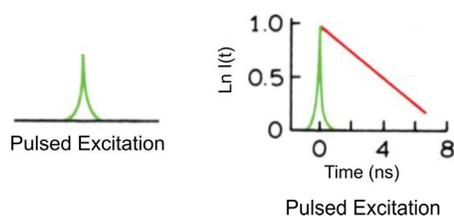


Figure 18: Pulse fluorimetry to measure lifetime, Red slope =  $-1/\tau$ . (image modified from ref. [94]).

When an excited fluorophore is showing a single exponential lifetime ( $\tau$ ), the intensity ( $I$ ) decay is described as

$$I(t) = I_0 \exp(-t/\tau) \quad \text{Equation 9}$$

where  $I_0$  is the intensity at  $t=0$ . For a multiexponential decay with  $n$  components the following equation 10 is used being  $\alpha$  the amplitudes [93].

$$I(t) = \sum_{i=1}^n \alpha_i \exp(-t/\tau_i) \quad \text{Equation 10}$$

The relation between steady state intensity ( $I_{SS}$ ) and lifetime ( $\tau$ ) is given by Equation 11 [94].

$$I_{SS} = \int_0^{\infty} I_0 e^{-t/\tau} dt = I_0 \tau \quad \text{Equation 11}$$

Most of the time-domain measurements are performed using time-correlated single-photon counting (TCSPC). This technique is based on single photon detection per laser pulse (typically 1 photon per 100 excitation pulses). For this application pulsed-

laser diodes (LDs) or light-emitting diodes (LEDs) are used [94, 118]. The time between the excitation pulse and the observed photon is measured and the waveform from the individual time measurements is reconstructed in a histogram (Figure 19). The measured intensity decay is a convolution with the lamp function. The deconvoluted fluorescence decay  $I(t)$  is described as

$$I(t) = F(t) \otimes R(t) \quad \text{Equation 12}$$

whereas  $F(t)$  is the time-resolved fluorescence decay and  $R(t)$  the system response function ( -pulse response) [93].

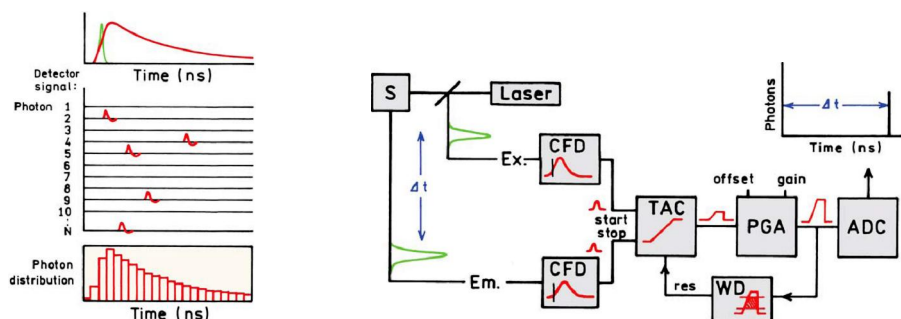


Figure 19: General principle of TCSPC (right) and electronic schematic (images from [94] [118]).

## Fluorescence microscopy

### Epi-fluorescence microscopy

An Epi-fluorescence microscope is an optical microscope equipped with a light source (e.g. xenon arc lamp or mercury vapor lamp) and fluorescence filter block setup composed of a wavelength dependant excitation filter with its corresponding dichroic mirror and emission filter. Depending on the spectral characteristics (excitation, emission) of the used fluorophores, there are many fluorescent filter blocks available. In life-sciences, inverted microscopes are state of the art where the light is coming from below. The light is passing through the excitation filter where it is reflected from the dichroic mirror to the objective lens and focused to the sample where all parts of the sample in the optical path are excited at the same time (see Figure 20). Fluorescence emitted from the sample is collected to the same objective that is used for the excitation and detected by the common arrangement of tube lens and photodecator or camera and ocular. This setup, where the excitation light

passes through the same objective than the fluorescence emission light is called epi-fluorescence microscopy. The obtained image is including a large out-of-focus background part depending on the thickness of the sample.

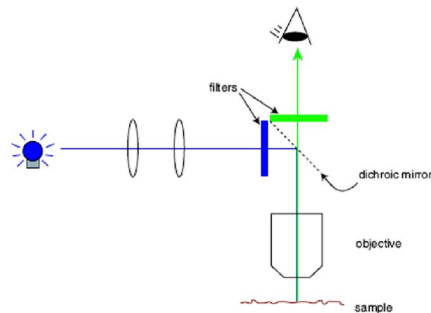


Figure 20: Setup and light path of an epi-fluorescence microscope (image from ref [119]).

## Confocal microscopy

Confocal microscopy is used to increase the optical resolution of microscopic images to get sharp images of thick specimens [119]. This microscopy technique uses point illumination with different laser lines (available in a wide range of wavelengths) and a spatial pinhole in an optically conjugate plane in front of the detector to eliminate out-of-focus light (Figure 21a). The laser is scanning point-by-point across the sample (parallel scanning lines). In that way only one point is excited and the fluorescence emission very close to the focal plane can be detected through the optics (lenses, mirrors, objective). The sharp image of the point of interest is generated with a sensitive photodetector when light from the focus-plane is passing through the pinhole and light from out-of-focus fluorescence is blocked. It allows surface profiling of the sample and building three-dimensional (3D) reconstructions by scanning thin slices (planes) along the vertical axis (z-direction, sample depth direction, cross section).

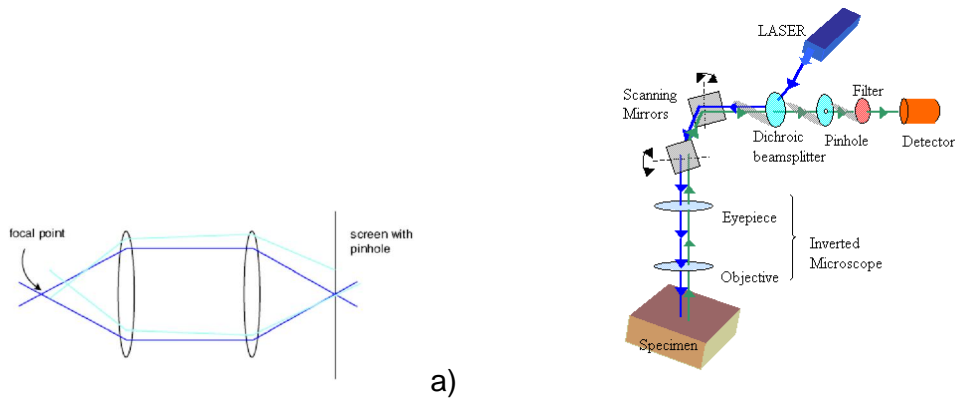


Figure 21: Setup of a confocal microscope. A) pinhole aperture: Light from the focal point is going through the pinhole whereas light from out-of-the focal point is blocked. b) The fluorescent specimen is excited by laser light (dichroic mirror, mirrors, objective), and the fluorescence emission is focused to the pinhole after passing through the same mirrors than used for excitation. The light going through the pinhole is measured by the detector. (Images from ref. [119])

## Flow cytometry

Flow cytometry uses the principles of light scattering and fluorescence to measure the physical and chemical properties of cells and particles in the range of 0.5 to 40  $\mu\text{m}$ . A flow cytometer is generally composed of 4 components (a) fluidics for hydrodynamically focusing of the sample in a sheath flow (see Figure 22a) for measuring single particles or cells, (b) optics with lasers, filters and mirrors (c) detectors to detect scattered light and the fluorescence emission and (d) electronics to generate and process electrical pulses (voltage pulses) (setup see Figure 22b). When a particle or cell is passing through a laser beam at the interrogation point following effects occur (i) it scatters light where the forward scatter (FSC) (transmitted light) is proportional to the surface size and the side scatter (SSC), measured perpendicular to the incident light, is proportional to the roughness (granularity) or internal complexity of cells and (ii) when the particle or cell is fluorescent the fluorophore is excited and the emission is measured through lenses and filter setups perpendicular to the incident light in the same way as the SSC see Figure 22b.

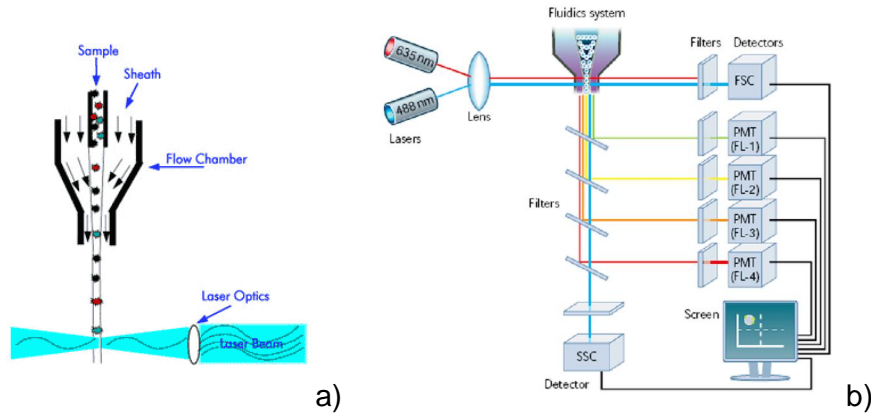


Figure 22: a) Schematically drawing of the hydro-dynamic focussing setup, b) Overview of a flow cytometer set-up with the laser optics, filter and detector systems.

Collected data of mostly 10.000 events are displayed in forward-scatter to side-scatter (FSC vs. SSC) histogram-plots where different sized and shaped populations can be gated as shown in Figure 23. Fluorescence signals are usually presented in signal (fluorescence channel) to counts (events or number of particles or cells) plots.

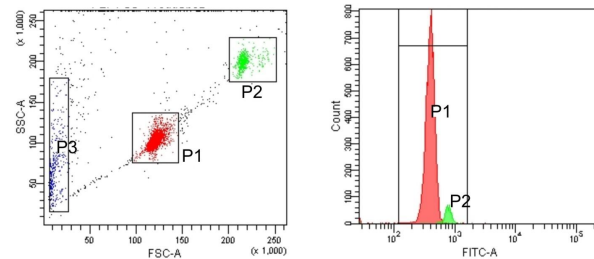


Figure 23: Example for data analysis of 10.000 measured fluorescent particles, a) Histogram plot with gated populations (main red population P1, aggregated green population P2 with higher FSC and SSC values), b) fluorescence signal intensity in the FITC channel of the gated populations.

## References

1. Papapostolou, D. and S. Howorka, *Engineering and exploiting protein assemblies in synthetic biology*. Mol Biosyst, 2009. **5**(7): p. 723-32.
2. Niemeyer, C.M. and C.A. Mirkin, *NanoBiotechnology: Concepts, Methods and Perspectives*. 2004, Weinheim, Germany: Wiley-VCH.
3. Sleytr, U.B., et al., *Crystalline bacterial cell surface layers (S-layers): from supramolecular cell structure to biomimetics and nanotechnology*. Angew. Chem. Int. Ed., 1999. **38**: p. 1034-1054.
4. Sleytr, U.B. and P. Messner, *Crystalline surface layers on bacteria*. Annu Rev Microbiol, 1983. **37**: p. 311-39.
5. Sleytr, U.B., *Regular arrays of macromolecules on bacterial cell walls: structure, chemistry, assembly, and function*. Int Rev Cytol, 1978. **53**: p. 1-62.
6. Sleytr, U.B., *Heterologous reattachment of regular arrays of glycoproteins on bacterial surfaces*. Nature, 1975. **257**(5525): p. 400-2.
7. Sára, M., et al., *Isolation of two physiologically induced variant strains of Bacillus stearothermophilus NRS 2004/3a and characterization of their S-layer lattices*. J Bacteriol, 1994. **176**(3): p. 848-60.
8. Sleytr, U.B. and T.J. Beveridge, *Bacterial S-layers*. Trends Microbiol, 1999. **7**(6): p. 253-60.
9. Sleytr, U.B. and A.M. Glauert, *Analysis of regular arrays of subunits on bacterial surfaces: evidence for a dynamic process of assembly*. J. Ultrastruct. Res., 1975. **50**: p. 103-116.
10. Egelseer, E.M., et al., *S-Layers, Nanobiotechnological Applications*, in *The Encyclopedia of Industrial Biotechnology: Bioprocess, Bioseparation, and Cell Technology* M.C. Flickinger, Editor. in press, John Wiley & Sons, Inc.: Hoboken, USA.
11. Sára, M. and U.B. Sleytr, *Production and characteristics of ultrafiltration membranes with uniform pores from two-dimensional arrays of proteins*. J. Membr. Sci., 1987. **33**: p. 27-49.
12. Sára, M. and U.B. Sleytr, *Membrane Biotechnology: Two-dimensional Protein Crystals for Ultrafiltration Purposes*, in *Biotechnology*, H.J. Rehm, Editor. 1988, VCH: Weinheim. p. 615-636.
13. Sára, M., *Conserved anchoring mechanisms between crystalline cell surface S-layer proteins and secondary cell wall polymers in Gram-positive bacteria?* Trends Microbiol, 2001. **9**(2): p. 47-49.
14. Schäffer, C. and P. Messner, *The structure of secondary cell wall polymers: how Gram-positive bacteria stick their cell walls together*. Microbiology, 2005. **151**(Pt 3): p. 643-51.
15. Sleytr, U.B. and M. Sára, *Bacterial and archaeal S-layer proteins: structure-function relationships and their biotechnological applications*. Trends Biotechnol, 1997. **15**(1): p. 20-6.
16. Sleytr, U.B., et al., *Crystalline bacterial cell surface proteins*. Biotechnology Intelligence Unit. 1996, Austin, Texas, U.S.A.: R. G. Landes Company and Academic Press, Inc. 230.
17. Sára, M. and U.B. Sleytr, *S-Layer proteins*. J Bacteriol, 2000. **182**(4): p. 859-68.
18. Sleytr, U.B. and P. Messner, *Self-assembly of crystalline bacterial cell surface layers (S-layers)*, in *Electron Microscopy of Subcellular Dynamics*, H. Plattner, Editor. 1989, CRC Press: Boca Raton, Florida. p. 13-31.
19. Györvary, E.S., et al., *Self-assembly and recrystallization of bacterial S-layer proteins at silicon supports imaged in real time by atomic force microscopy*. J Microsc, 2003. **212**(Pt 3): p. 300-6.
20. Lopez, A.E., et al., *Surface dependence of protein nanocrystal formation*. Small, 2010. **6**(3): p. 396-403.
21. Martin-Molina, A., et al., *Structure, surface interactions, and compressibility of bacterial S-layers through scanning force microscopy and the surface force apparatus*. Biophys J, 2006. **90**(5): p. 1821-9.
22. Horejs, C., et al., *Structure prediction of an S-layer protein by the mean force method*. J Chem Phys, 2008. **128**(6): p. 065106.
23. Pavkov, T., et al., *The Structure and Binding Behavior of the Bacterial Cell Surface Layer Protein SbsC*. Structure, 2008. **16**(8): p. 1226-37.
24. Kinns, H. and S. Howorka, *The surface location of individual residues in a bacterial S-layer protein*. J Mol Biol, 2008. **377**(2): p. 589-604.
25. Blecha, A., et al., *Expression and cytosolic assembly of the S-layer fusion protein mSbsC-EGFP in eukaryotic cells*. Microb Cell Fact, 2005. **4**: p. 28.
26. Ilk, N., et al., *Surfaces functionalized with self-assembling S-layer fusion proteins for nanobiotechnological applications*. Colloids and Surfaces, 2008. **321**: p. 163-167.

27. Huber, C., et al., *S-layer-streptavidin fusion proteins and S-layer-specific heteropolysaccharides as part of a biomolecular construction kit for application in nanobiotechnology*. *Microelectron Eng*, 2006. **83**: p. 1589-1593.
28. Huber, C., et al., *Heterotetramers formed by an S-layer-streptavidin fusion protein and core-streptavidin as nanoarrayed template for biochip development*. *Small*, 2006. **2**: p. 142-150.
29. Moll, D., et al., *S-layer-streptavidin fusion proteins as template for nanopatterned molecular arrays*. *Proc Natl Acad Sci U S A*, 2002. **99**(23): p. 14646-51.
30. Ilk, N., et al., *A functional chimaeric S-layer-enhanced green fluorescent protein to follow the uptake of S-layer-coated liposomes into eukaryotic cells*. *Biochem J*, 2004. **379**(Pt 2): p. 441-8.
31. Kainz, B., et al., *Absorption, Steady-State Fluorescence, Fluorescence Lifetime, and 2D Self-Assembly Properties of Engineered Fluorescent S-Layer Fusion Proteins of Geobacillus stearothermophilus NRS 2004/3a*. *Biomacromolecules*, 2010. **11**: p. 207-214.
32. Breitwieser, A., et al., *A recombinant bacterial cell surface (S-layer)-major birch pollen allergen-fusion protein (rSbsC/Bet v1) maintains the ability to self-assemble into regularly structured monomolecular lattices and the functionality of the allergen*. *Protein Eng*, 2002. **15**(3): p. 243-9.
33. Ilk, N., et al., *Molecular characterization of the S-layer gene, sbpA, of Bacillus sphaericus CCM 2177 and production of a functional S-layer fusion protein with the ability to recrystallize in a defined orientation while presenting the fused allergen*. *Appl Environ Microbiol*, 2002. **68**(7): p. 3251-60.
34. Völlenkne, C., et al., *Construction of a functional S-layer fusion protein comprising an immunoglobulin G-binding domain for development of specific adsorbents for extracorporeal blood purification*. *Appl Environ Microbiol*, 2004. **70**(3): p. 1514-21.
35. Tschiggerl, H., et al., *Exploitation of the S-layer self-assembly system for site directed immobilization of enzymes demonstrated for an extremophilic laminarinase from Pyrococcus furiosus*. *J Biotechnol*, 2008. **133**(3): p. 403-11.
36. Schäffer, C., et al., *Novel biocatalysts based on S-layer self-assembly of Geobacillus stearothermophilus NRS 2004/3a: a nanobiotechnological approach*. *Small*, 2007. **3**(9): p. 1549-59.
37. Howorka, S., et al., *Surface-accessible residues in the monomeric and assembled forms of a bacterial surface layer protein*. *J Biol Chem*, 2000. **275**(48): p. 37876-86.
38. Badelt-Lichtblau, H., et al., *Genetic Engineering of the S-Layer Protein SbpA of Lysinibacillus sphaericus CCM 2177 for the Generation of Functionalized Nanoarrays (dagger)*. *Bioconjug Chem*, 2009.
39. Sleytr, U.B., et al., *S-layers as a Basic Building Block in a Molecular Construction Kit*. *FEBS J*, 2007. **274**: p. 323-334.
40. Scheicher, S.R., et al., *Optical oxygen sensors based on Pt(II) porphyrin dye immobilized on S-layer protein matrices*. *Biosens Bioelectron*, 2009.
41. Sleytr, U.B., et al., *S-Layers as a Tool Kit for Nanobiotechnological Applications*. *FEMS Microbiol Lett*, 2007. **267**: p. 131-144.
42. Sleytr, U.B. and M. Sára, *Structure with membrane having continuous pores*. 1988: U.S. Pat. 4,752,395
43. Weigert, S. and M. Sára, *Ultrafiltration membranes prepared from crystalline bacterial cell surface layers as model systems for studying the influence of surface properties on protein adsorption*. *J Membrane Sci*, 1996. **121**: p. 185-196.
44. Göbel, C., et al., *S-layer templated bioinspired synthesis of silica*. *Colloids Surf B Biointerfaces*, 2010 **75**(2): p. 565-72.
45. Liu, J., et al., *Generation of oxide nanopatterns by combining self-assembly of S-layer proteins and area-selective atomic layer deposition*. *J Am Chem Soc*, 2008. **130**(50): p. 16908-13.
46. Györvary, E., et al., *Biomimetic nanostructure fabrication: Non-lithographic lateral patterning and self-assembly of functional bacterial S-layers at silicon supports*. *Nano Lett*, 2003. **3**: p. 315-319.
47. Györvary, E., et al., *Formation of nanoparticle arrays on S-layer protein lattices*. *J Nanosci Nanotech* 2004. **4**: p. 115-120.
48. Dieluweit, S., D. Pum, and U.B. Sleytr, *Formation of a gold superlattice on an S-layer with square lattice symmetry*. *Supramol Sci*, 1998. **5**: p. 15-19
49. Dieluweit, S., et al., *Monodisperse gold nanoparticles formed on bacterial crystalline surface layers (S-layers) by electroless deposition*. *Mater Sci Eng C*, 2005. **25**: p. 727-732.

50. Mark, S.S., et al., *Bionanofabrication of metallic and semiconductor nanoparticle arrays using S-layer protein lattices with different lateral spacings and geometries*. Langmuir, 2006. **22**(8): p. 3763-74.
51. Shenton, W., et al., *Biocrystal templating of CdS superlattices using self-assembled bacterial S-layers*. Nature, 1997. **389**: p. 585-587.
52. Neubauer, A., D. Pum, and U.B. Sleytr, *An amperometric glucose sensor based on isoporous crystalline protein membranes as immobilization matrix*. Analytic Letters, 1993. **26**: p. 1347-1360.
53. Neubauer, A., D. Pum, and U.B. Sleytr, *Fibre-optic glucose biosensor using enzyme membranes with 2-D crystalline structure*. Biosensors & Bioelectronics, 1996. **11**: p. 317-325.
54. Mader, C., et al., *S-layer-coated liposomes as a versatile system for entrapping and binding target molecules*. Biochim Biophys Acta, 2000. **1463**(1): p. 142-50.
55. Moya, S.E. and J.L. Toca-Herrera, *From hollow shells to artificial cells: biointerface engineering on polyelectrolyte capsules*. J Nanosci Nanotechnol, 2006. **6**(8): p. 2329-37.
56. Kepplinger, C., et al., *Intact lipid vesicles reversibly tethered to a bacterial S-layer protein lattice*. Soft Matter, 2009. **5**: p. 325-333.
57. Breitwieser, A., et al., *2-D protein crystals as an immobilization matrix for producing reaction zones in dipstick-style immunoassays*. Biotechniques, 1996. **21**(5): p. 918-25.
58. Bohle, B., et al., *A novel approach to specific allergy treatment: the recombinant fusion protein of a bacterial cell surface (S-layer) protein and the major birch pollen allergen Bet v 1 (rSbsC-Bet v 1) combines reduced allergenicity with immunomodulating capacity*. J Immunol, 2004. **172**(11): p. 6642-8.
59. Weber, V., et al., *Development of affinity microparticles for extracorporeal blood purification based on crystalline bacterial cell surface proteins*. Ther Apher, 2001. **5**(5): p. 433-8.
60. Tang, J., et al., *Fabrication of highly ordered gold nanoparticle arrays templated by crystalline lattices of bacterial s-layer protein*. Chemphyschem, 2008. **9**(16): p. 2317-20.
61. Delcea, M., et al., *Mapping bacterial surface layers affinity to polyelectrolytes through the building of hybrid macromolecular structures*. J Nanosci Nanotechnol, 2007. **7**(12): p. 4260-6.
62. Steiner, K., et al., *Recombinant Glycans on an S-Layer Self-Assembly Protein: A New Dimension for Nanopatterned Biomaterials*. Small, 2008. **4**(10): p. 1728-1740.
63. Steiner, K., et al., *Functional characterization of the initiation enzyme of S-layer glycoprotein glycan biosynthesis in Geobacillus stearothermophilus NRS 2004/3a*. J Bacteriol, 2007. **189**(7): p. 2590-8.
64. Sleytr, U.B. and R. Plohberger, *The dynamic process of assembly of two-dimensional arrays of macromolecules on bacterial cell walls*, in *Electron Microscopy at Molecular Dimensions*, W. Baumeister and W. Vogell, Editors. 1980, Springer-Verlag: Berlin, Heidelberg, New York. p. 36-47.
65. Messner, P., D. Pum, and U.B. Sleytr, *Characterization of the ultrastructure and the self-assembly of the surface layer of Bacillus stearothermophilus strain NRS 2004/3a*. J Ultrastruct Mol Struct Res, 1986. **97**(1-3): p. 73-88.
66. Schäffer, C., et al., *The surface layer (S-layer) glycoprotein of Geobacillus stearothermophilus NRS 2004/3a. Analysis of its glycosylation*. J Biol Chem, 2002. **277**(8): p. 6230-9.
67. Tsien, R.Y., *The green fluorescent protein*. Annu Rev Biochem, 1998. **67**: p. 509-44.
68. Haupts, U., et al., *Dynamics of fluorescence fluctuations in green fluorescent protein observed by fluorescence correlation spectroscopy*. Proc Natl Acad Sci U S A, 1998. **95**(23): p. 13573-8.
69. Tsien, R.Y., A. Miyawaki, and J. Llopis, *Fluorescent protein sensors for measuring the pH of a biological sample*, U.S. Patent, Editor. 2003, The Regents of the University of California, Oakland, CA (US).
70. Patnaik, S.S., S. Trohalaki, and R. Pachter, *Molecular modeling of green fluorescent protein: structural effects of chromophore deprotonation*. Biopolymers, 2004. **75**(6): p. 441-52.
71. Zimmer, M., *Green fluorescent protein (GFP): Application, structure, and related photophysical behavior*. Chemical Reviews, 2002. **102**(3): p. 759-782.
72. Craggs, T.D., *Green fluorescent protein: structure, folding and chromophore maturation*. Chem Soc Rev, 2009. **38**(10): p. 2865-75.
73. Sample, V., R.H. Newman, and J. Zhang, *The structure and function of fluorescent proteins*. Chem Soc Rev, 2009. **38**(10): p. 2852-64.
74. Remington, S.J., *Fluorescent proteins: maturation, photochemistry and photophysics*. Curr Opin Struct Biol, 2006. **16**(6): p. 714-21.
75. Gross, L.A., et al., *The structure of the chromophore within DsRed, a red fluorescent protein from coral*. Proceedings of the National Academy of Sciences of the United States of America, 2000. **97**(22): p. 11990-11995.

76. Wall, M.A., M. Socolich, and R. Ranganathan, *The structural basis for red fluorescence in the tetrameric GFP homolog DsRed*. Nat Struct Biol, 2000. **7**(12): p. 1133-8.
77. Campell, R.E., et al., *A monomeric red fluorescent protein*. PNAS, 2002. **99**(12): p. 7877-7882.
78. Shaner, N.C., et al., *Improved monomeric red, orange and yellow fluorescent proteins derived from *Discosoma* sp. red fluorescent protein*. Nature Biotechnology, 2004. **22**(12): p. 1567-1572.
79. Zimmer, M., *GFP: from jellyfish to the Nobel prize and beyond*. Chem Soc Rev, 2009. **38**(10): p. 2823-32.
80. Day, R.N. and M.W. Davidson, *The fluorescent protein palette: tools for cellular imaging*. Chem Soc Rev, 2009. **38**(10): p. 2887-921.
81. Seward, H.E. and C.R. Bagshaw, *The photochemistry of fluorescent proteins: implications for their biological applications*. Chem Soc Rev, 2009. **38**(10): p. 2842-51.
82. Zacharias, D.A. and R.Y. Tsien, *Molecular biology and mutation of green fluorescent protein*. Methods Biochem Anal, 2006. **47**: p. 83-120.
83. Elsliger, M.A., et al., *Structural and spectral response of green fluorescent protein variants to changes in pH*. Biochemistry, 1999. **38**(17): p. 5296-301.
84. McAnaney, T.B., et al., *Protonation, photobleaching, and photoactivation of yellow fluorescent protein (YFP 10C): a unifying mechanism*. Biochemistry, 2005. **44**(14): p. 5510-24.
85. Hanson, G.T., et al., *Green fluorescent protein variants as ratiometric dual emission pH sensors. 1. Structural characterization and preliminary application*. Biochemistry, 2002. **41**(52): p. 15477-88.
86. McAnaney, T.B., et al., *Green fluorescent protein variants as ratiometric dual emission pH sensors. 3. Temperature dependence of proton transfer*. Biochemistry, 2005. **44**(24): p. 8701-11.
87. Kneen, M., et al., *Green fluorescent protein as a noninvasive intracellular pH indicator*. Biophys J, 1998. **74**(3): p. 1591-9.
88. Llopis, J., et al., *Measurement of cytosolic, mitochondrial, and Golgi pH in single living cells with green fluorescent proteins*. Proc Natl Acad Sci U S A, 1998. **95**(12): p. 6803-8.
89. Heim, R., D.C. Prasher, and R.Y. Tsien, *Wavelength mutations and posttranslational autoxidation of green fluorescent protein*. Proceedings of the National Academy of Sciences of the United States of America, 1994. **91**(26): p. 12501-12504.
90. Miesenbock, G., D.A. De Angelis, and J.E. Rothman, *Visualizing secretion and synaptic transmission with pH-sensitive green fluorescent proteins*. Nature, 1998. **394**(6689): p. 192-5.
91. Akke, M., et al., *Pervasive conformational fluctuations on microsecond time scales in a fibronectin type III domain*. Nat Struct Biol, 1998. **5**(1): p. 55-9.
92. Heikal, A.A., S.T. Hess, and W.W. Webb, *Multiphoton molecular spectroscopy and excited-state dynamics of enhanced green fluorescent protein (EGFP): acid-base specificity*. Chemical Physics, 2001. **274**: p. 37-55.
93. Valeur, B., *Molecular Fluorescence: Principles and Applications*. Wiley-VCH Verlag GmbH, 2001.
94. Lakowicz, J.R., *Principles of Fluorescence Spectroscopy*. Springer, 2006. **Third Edition**.
95. Serdyuk, I.N., N.R. Zaccai, and J. Zaccai, *Methods in Molecular Biophysics: Structure, Dynamics, Function*. 2007: Cambridge University Press.
96. Lequeux, N. and B. Dubertret, *Quantum Dots in Nanobiotechnology*. NanoBiotechnology, 2005. **1**(3): p. 279-280.
97. Singhal, A., et al., *Biomedical Applications of Semiconductor Quantum Dots*. Michael Strosio Mitra, Dutta ed. Biological Nanostructures and Applications of Nanostructures in Biology: Electrical, Mechanical, and Optical Properties, ed. B. He. Vol. 2. 2004: Kluwer academic publishers. 37-50.
98. Strosio, M.A., et al., *Integration and Tagging Biological Structures with Nanoscale Semiconductor Quantum Dot Structures*. Michael Strosio, Mitra Dutta ed. Biological Nanostructures and Applications of Nanostructures in Biology: Electrical, Mechanical, and Optical Properties, ed. B. He. Vol. 2. 2004: Kluwer academic publishers. 1-36.
99. Gordon, G.W., et al., *Quantitative fluorescence resonance energy transfer measurements using fluorescence microscopy*. Biophys J, 1998. **74**(5): p. 2702-13.
100. Allen, M.D. and J. Zhang, *Subcellular dynamics of protein kinase A activity visualized by FRET-based reporters*. Biochem Biophys Res Commun, 2006. **348**(2): p. 716-21.
101. Ai, H.W., et al., *Fluorescent protein FRET pairs for ratiometric imaging of dual biosensors*. Nat Methods, 2008. **5**(5): p. 401-3.
102. Ibraheem, A. and R.E. Campbell, *Designs and applications of fluorescent protein-based biosensors*. Curr Opin Chem Biol, 2010. **14**(1): p. 30-6.

103. Pollok, B.A. and R. Heim, *Using GFP in FRET-based applications*. Trends Cell Biol, 1999. **9**(2): p. 57-60.
104. Patterson, G.H., D.W. Piston, and B.G. Barisas, *Forster distances between green fluorescent protein pairs*. Anal Biochem, 2000. **284**(2): p. 438-40.
105. Rizzo, M.A., et al., *An improved cyan fluorescent protein variant useful for FRET*. Nat Biotechnol, 2004. **22**(4): p. 445-9.
106. Nguyen, A.W. and P.S. Daugherty, *Evolutionary optimization of fluorescent proteins for intracellular FRET*. Nat Biotechnol, 2005. **23**(3): p. 355-60.
107. Galperin, E., V.V. Verkhusha, and A. Sorkin, *Three-chromophore FRET microscopy to analyze multiprotein interactions in living cells*. Nat Methods, 2004. **1**(3): p. 209-17.
108. Wallrabe, H. and A. Periasamy, *Imaging protein molecules using FRET and FLIM microscopy*. Curr Opin Biotechnol, 2005. **16**(1): p. 19-27.
109. He, L., et al., *Flow cytometric measurement of fluorescence (Forster) resonance energy transfer from cyan fluorescent protein to yellow fluorescent protein using single-laser excitation at 458 nm*. Cytometry A, 2003. **53**(1): p. 39-54.
110. Moreno-Flores, S., et al., *Stress relaxation microscopy: imaging local stress in cells*. J Biomech, 2010. **43**(2): p. 349-54.
111. Williams, P.M., et al., *Hidden complexity in the mechanical properties of titin*. Nature, 2003. **422**(6930): p. 446-9.
112. Best, R.B., et al., *A simple method for probing the mechanical unfolding pathway of proteins in detail*. Proc Natl Acad Sci U S A, 2002. **99**(19): p. 12143-8.
113. Moreno-Flores, S., et al., *Physical attachment of fluorescent protein particles to atomic force microscopy probes in aqueous media: Implications for surface pH, fluorescence, and mechanical properties studies*. Microsc Res Tech, 2009. DOI:10.1002: p. jemt 2081.
114. Zhu, R., et al., *Topography and recognition imaging of protein-patterned surfaces generated by AFM nanolithography*. Chemphyschem, 2009. **10**(9-10): p. 1478-81.
115. Tang, J., et al., *Detection of metal binding sites on functional S-layer nanoarrays using single molecule force spectroscopy*. J Struct Biol, 2009. **168**(1): p. 217-22.
116. Adamson, A.W., *Physical Chemistry of surfaces*. 1990: Wiley, New York, 1990.
117. Hunter, R.J., *Zeta potential in colloid science: Principles and Applications*. 1981: London, Academic press.
118. Becker, W., *Advanced Time-Correlated Single Photon Counting Techniques*, ed. S.S.i.C. Physics. Vol. 1. 2005: Springer, Berlin.
119. Semwogerere, D. and E.R. Weeks, *Confocal Microscopy*. Encyclopedia of Biomaterials and Biomedical Engineering, 2005: p. 1 - 10.

## Publications

### First author papers

%Absorption, Steady-State Fluorescence, Fluorescence Lifetime, and 2D Self-Assembly Properties of Engineered Fluorescent S-Layer Fusion Proteins of *Geobacillus stearothermophilus* NRS 2004/3a†, Birgit Kainz, Kerstin Steiner, Marco Möller, Dietmar Pum, Christina Schäffer, Uwe B. Sleytr, José L. Toca-Herrera, in: *Biomacromolecules* 2010 (11) 207-214

%Fluorescent S-Layer Protein Colloids†, Birgit Kainz, Kerstin Steiner, Uwe B. Sleytr, Dietmar Pum, José L. Toca-Herrera, in: *Soft Matter* DOI (in press)

Manuskript: %Study of the fluorescent energy transfer in the bi-fluorescent S-layer tandem fusion protein ECFP-SgsE-YFP†, Birgit Kainz, Kerstin Steiner, Uwe B. Sleytr, Dietmar Pum, José L. Toca-Herrera

### Co-author papers

%Recombinant Glycans on an S-Layer Self-Assembly Protein: A New Dimension for Nanopatterned Biomaterials†, Kerstin Steiner, Angelika Harnreich, Birgit Kainz, Paul Hitchen, Anne Dell, Paul Messner, Christina Schäffer, in: *Small* 2008 (4) 1728-1740

%Genetic Engineering of the S-Layer Protein SbpA of *Lysinibacillus sphaericus* CCM 2177 for the Generation of Functionalized Nanoarrays†, Helga Badelt-Lichtblau, Birgit Kainz, Christine Völlenkle, Eva-Maria Egelseer, Uwe B. Sleytr, Dietmar Pum, Nicola Ilk, in: *Bioconjugate Chem.* 2009 (20) 895-903

%Optical oxygen sensor based on Pt(II)porphyrin dye immobilized on S-layer protein matrices†, Sylvia R. Scheicher, Birgit Kainz, Stefan Köstler, Michael Suppan, Alessandro Bizzarri, Dietmar Pum, Uwe B. Sleytr, Volker Ribitsch, in: *Biosensors and Bioelectronics* 2009 (25) 797-802

%Cell surface display of chimeric glycoproteins via the S-layer of *Paenibacillus alvei*†, Kristof Zarschler, Bettina Janesch, Birgit Kainz, Robin, Ristl, Paul Messner, Christina Schäffer, in: *Carbohydrate Research* (in press)

## Posters, Proceeding

### Posters

%Optochemical Oxygen Sensing using Pt(II)-porphyrin dye immobilised on S-layer matrices+, Sylvia Scheicher, Birgit Kainz, Stefan Köstler, Christian Konrad, Michael Suppan, Alessandro Bizzarri, Dietmar Pum and Volker Ribitsch, in: 10<sup>th</sup> Conference on Methods and Applications of Fluorescence, Salzburg 9<sup>th</sup> - 12<sup>th</sup> September 2007

%Layer-by-layer assembly of crystalline S-layer proteins and polyelectrolytes+, S. Scheicher, S. Köstler, B. Kainz, O. Werzer, G. Jakopic, D. Pum, R. Resel, K. Stana-Kleinschek, U.B. Sleytr, V. Ribitsch, in: 1<sup>st</sup> Joint Austrian and Slovenian Polymer Meeting, Graz, 26<sup>th</sup> - 28<sup>th</sup> March 2008

%Optochemical Oxygen Sensing based on S-layer matrices+, Sylvia Scheicher, Birgit Kainz, Stefan Köstler, Christian Konrad, Michael Suppan, Alessandro Bizzarri, Dietmar Pum, Volker Ribitsch, in: Eurotrode IX, Dublin, 30<sup>th</sup> March - 2<sup>nd</sup> April 2008

%Application of S-layer proteins as matrices for Optochemical Sensors+, Sylvia Scheicher, Stefan Köstler, Birgit Kainz, Michael Suppan, Dietmar Pum, Uwe B Sleytr, Volker Ribitsch, in: Lab-on-a-Chip World Congress, Barcelona, 7<sup>th</sup> - 8<sup>th</sup> May 2008

%Optochemical Sensors based on nanostructured S-Layer Proteins+, Sylvia Scheicher, Birgit Kainz, Frank Reil, Dietmar Pum, Uwe B. Sleytr, Alfred Leitner, Volker Ribitsch, Stefan Köstler, in: Nanosens, Vienna, Austria, 2008

%Fluorescent S-Layer Biocolloids+, Birgit Kainz, Kerstin Steiner, Seta Küpcü, Uwe B. Sleytr, José Luis Toca-Herrera, Dietmar Pum, in: NanoMeasure 2010 Krakau, Poland 3<sup>th</sup> - 4<sup>th</sup> June 2010

%Nanostructured fluorescent S-layer coatings on silica particles+, Birgit Kainz, Seta Küpcü, Kerstin Steiner, Uwe B. Sleytr, José Luis Toca-Herrera, Dietmar Pum, in: NanoBio 2010 Zürich, Switzerland, 24<sup>th</sup> - 27<sup>th</sup> August 2010

### Proceeding

%Optical Sensors Based on S-layer proteins+, Scheicher Sylvia, Kainz Birgit, Köstler Stefan, Konrad Christian, Suppan Michael, Bizzarri Alessandro, Pum Dietmar, Sleytr Uwe B., Ribitsch Volker, in: Proceedings of IEEE Sensors 2007. Atlanta: 600-603., 2007

# CURRICULUM VITAE

Dipl.-Ing. Birgit Kainz

## PERSONAL DATA

Birth: 2<sup>nd</sup> April 1977, 8160 Weiz, Austria  
Gender: female  
Nationality: Austria

## EDUCATION

1996 final examination (Matura) in Weiz, Höhere Bundeslehranstalt für wirtschaftliche Berufe (HLW), Austria

1996 . 1998 Studies of Medicine at Karl-Franzens-University Graz, Austria

1998 Changing to studies of Technical Chemistry at University of Technology (TU) Graz, Austria

Field of study: Biotechnology, Bio- and Food Chemistry

2004 Diploma thesis on *Untersuchung zur Stabilität der Anthocyane in Fragaria ananassa* at the Institute of Food Technology, University of Technology Graz in cooperation with the company Agrana Fruit (former: Steirerobst)

10/2004 Graduation (Dipl.-Ing.) in Technical Chemistry (MSc. equivalent)

since 06/2006 PhD (Dr.nat.techn.) thesis at the Department of NanoBiotechnology, University of Natural Resources and Applied Life Sciences (BOKU), Vienna, Austria: *Optochemical sensors based on fluorescent S-layer fusion proteins*

11/12 2008 and 05/07 2009: CiCbiomaGUNE, Biosurface Unit, San Sebastián (Spain) in the group of Prof. José Luis Toca-Herrera.

## WORKING EXPERIENCE

1998 . 2004 Scientist at Agrana Fruit (former: Steirerobst), Gleisdorf, Austria: Development of antiseptic strawberries, Colour stabilisation in fruit preparations, Food chemistry

2005 . 2006 Scientist at Roche Diagnostics GmbH, Graz, Austria: Subcutaneous glucose biosensor development, Polymer chemistry

2007, 2008 Tutor of students in the lab course *Ultrastrukturforschung* at the Department of NanoBiotechnology, BOKU, Vienna

2008 Advisor of the master thesis *Characterization of Fluorescent S-Layer Fusion Proteins* at the Department of NanoBiotechnology, BOKU, Vienna

# Appendix

## Appendix 1

Paper: *Absorption, Steady-State Fluorescence, Fluorescence Lifetime, and 2D Self-Assembly Properties of Engineered Fluorescent S-Layer Fusion Proteins of Geobacillus stearothermophilus NRS 2004/3a*, Birgit Kainz, Kerstin Steiner, Marco Möller, Dietmar Pum, Christina Schäffer, Uwe B. Sleytr, José L. Toca-Herrera, in: *Biomacromolecules* 2010 (11) 207-214

Additional Information

## Appendix 2

Paper: *Fluorescent S-Layer Protein Colloids*, Birgit Kainz, Kerstin Steiner, Uwe B. Sleytr, Dietmar Pum, José L. Toca-Herrera, in: *Soft Matter* DOI:10.1039/C0SM00008F

## Appendix 3

Manuskript: *Study of the fluorescent energy transfer in the bi-fluorescent S-layer tandem fusion protein ECFP-SgsE-YFP*, Birgit Kainz, Kerstin Steiner, Uwe B. Sleytr, Dietmar Pum, José L. Toca-Herrera

Additional Information

## Appendix 4

Paper: *Recombinant Glycans on an S-Layer Self-Assembly Protein: A New Dimension for Nanopatterned Biomaterials*, Kerstin Steiner, Angelika Harnreich, Birgit Kainz, Paul Hitchen, Anne Dell, Paul Messner, Christina Schäffer, in: *Small* 2008 (4) 1728-1740

## Appendix 5

Paper: *Genetic Engineering of the S-Layer Protein SbpA of *Lysinibacillus sphaericus* CCM 2177 for the Generation of Functionalized Nanoarrays*, Helga Badelt-Lichtblau, Birgit Kainz, Christine Völlenkle, Eva-Maria Egelseer, Uwe B. Sleytr, Dietmar Pum, Nicola Ilk, in: *Bioconjugate Chem.* 2009 (20) 895-903

## Appendix 6

Paper: *Optical oxygen sensor based on Pt(II)porphyrin dye immobilized on S-layer protein matrices*, Sylvia R. Scheicher, Birgit Kainz, Stefan Köstler, Michael Suppan, Alessandro Bizzarri, Dietmar Pum, Uwe B. Sleytr, Volker Ribitsch, in: *Biosensors and Bioelectronics* 2009 (25) 797-802

## Appendix 7

Paper: *Cell surface display of chimeric glycoproteins via the S-layer of *Paenibacillus alvei**, Kristof Zarschler, Bettina Janesch, Birgit Kainz, Robin Ristl, Paul Messner, Christina Schäffer, in: *Carbohydrate Research* (in press)

# Absorption, Steady-State Fluorescence, Fluorescence Lifetime, and 2D Self-Assembly Properties of Engineered Fluorescent S-Layer Fusion Proteins of *Geobacillus stearothermophilus* NRS 2004/3a

Birgit Kainz,<sup>†</sup> Kerstin Steiner,<sup>†,‡</sup> Marco Möller,<sup>§</sup> Dietmar Pum,<sup>†</sup> Christina Schäffer,<sup>†</sup> Uwe B. Sleytr,<sup>†</sup> and José L. Toca-Herrera<sup>\*,§</sup>

Department for NanoBiotechnology, University of Natural Resources and Applied Life Sciences, Muthgasse 11, A-1190 Vienna, Austria, and CIC biomaGUNE, Biosurfaces Unit, Paseo Miramón 182, 20009 San Sebastián, Spain

Received September 19, 2009; Revised Manuscript Received November 11, 2009

S-layer fusion protein technology was used to design four different fluorescent fusion proteins with three different GFP mutants and the red fluorescent protein mRFP1. Their absorption spectra, steady-state fluorescence, and fluorescence lifetime were investigated as a function of pH. It was found that fluorescence intensities and lifetime of the GFP mutant S-layer fusion proteins decreased about 50% between pH 6 and pH 5. The spectral properties of the red S-layer fusion protein were minimally affected by pH variations. These results were compared with His-tagged reference fluorescent proteins, demonstrating that the S-layer protein did not change the general spectral properties of the whole fusion protein. In addition, the  $pK_a$  values of the fluorescent S-layer fusion proteins were calculated. Finally, it was shown that the S-layer fusion proteins were able to self-assemble forming 2D nanostructures of oblique p2 symmetry with lattice parameters of about  $a = 11$  nm,  $b = 14$  nm, and  $\gamma = 80^\circ$ . The fluorescence tag did not hinder the natural self-assembly process of the S-layer protein. The combination of the fluorescence properties and the self-assembly ability of the engineered fusion proteins make them a promising tool to generate biomimetic surfaces for future applications in nanobiotechnology at a wide range of pH.

## Introduction

The green fluorescent protein (GFP) from the jellyfish species *Aequorea victoria* and its different colored mutants have become the standard as bioimaging markers for numerous biological studies such as gene expression, protein targeting, and biosensors due to their robust fluorescence properties and pH sensitivity.<sup>1,2</sup> The importance of the GFP protein was acknowledged with the Chemistry Nobel Prize in 2008 to Osamu Shimomura, Marty Chalfie, and Roger Tsien. A red-shifted fluorescent protein is the monomeric red fluorescent protein mRFP1, which is a monomeric mutant of the tetrameric red fluorescent protein dsRed from *Discosoma coral*.<sup>3,4</sup> This red fluorescent protein has nearly the same structure as its GFP homologue, but the chromophore has a more extensively conjugated  $\pi$ -system. In recent years a significant amount of research has been carried out on the spectral properties of GFP and its mutants.<sup>5–7</sup> There is substantial interest in understanding the complex photophysics and photochemistry of the embedded chromophore at changing pH values.<sup>5,8,9</sup> Techniques such as fluorescence spectroscopy provide critical data on the nature and lifetimes of photogenerated species.<sup>10</sup> The main structure of the 238 amino acid contained in the GFP molecule consists of an 11-stranded  $\beta$ -barrel (approximately 4 nm long and 3 nm in diameter<sup>11</sup>) and an  $\alpha$ -helix running up the axis in the center of the cylinder. The chromophore is produced in vivo and localized in the

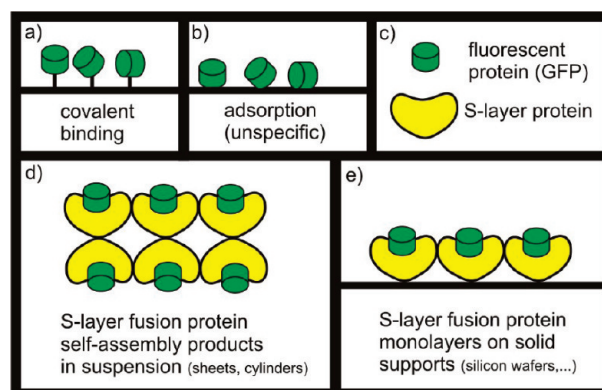


**Figure 1.** Comparison of different methods for fluorescence labeling with a fluorescent protein: (a) covalent conjugation of the fluorescent protein to activated groups, (b) unspecific physical adsorption, (c) creation of a fluorescent S-layer fusion protein build up of an S-layer protein and a fluorescent protein, (d) double layer self-assembly products (sheets, cylinders) of the fluorescent S-layer fusion proteins in suspension, and (e) S-layer assembling technique on solid supports (glass slides, silicon waver, liposomes, polyelectrolytes, thiols, etc.) to create monolayers with orientated fluorescence labeling.

middle of the  $\beta$ -barrel where it is attached to the  $\alpha$ -helix. The chromophore is a *p*-hydroxybenzylideneimidazolinone formed from residues 65–67 in the presence of atmospheric oxygen<sup>1</sup> and does not need external cofactors.<sup>12</sup> Depending on the chromophore structure, different GFP variants can be divided into seven classes of which class 2 phenolate anion (EGFP), class 4 phenolate anion with stacked  $\pi$ -electron system (yellow fluorescent proteins), and class 5 with indole in the chromophore (cyan fluorescent proteins) were used in this study.

\* To whom correspondence should be addressed. Tel.: +34 943 005313. E-mail: jltocaherrera@cicbiomagune.es.

<sup>†</sup> University of Natural Resources and Applied Life Sciences.

<sup>‡</sup> Current address: Biomolecular Science Research Complex, University of St Andrews, North Haugh, KY169ST St Andrews, Scotland.

<sup>§</sup> CIC biomaGUNE.

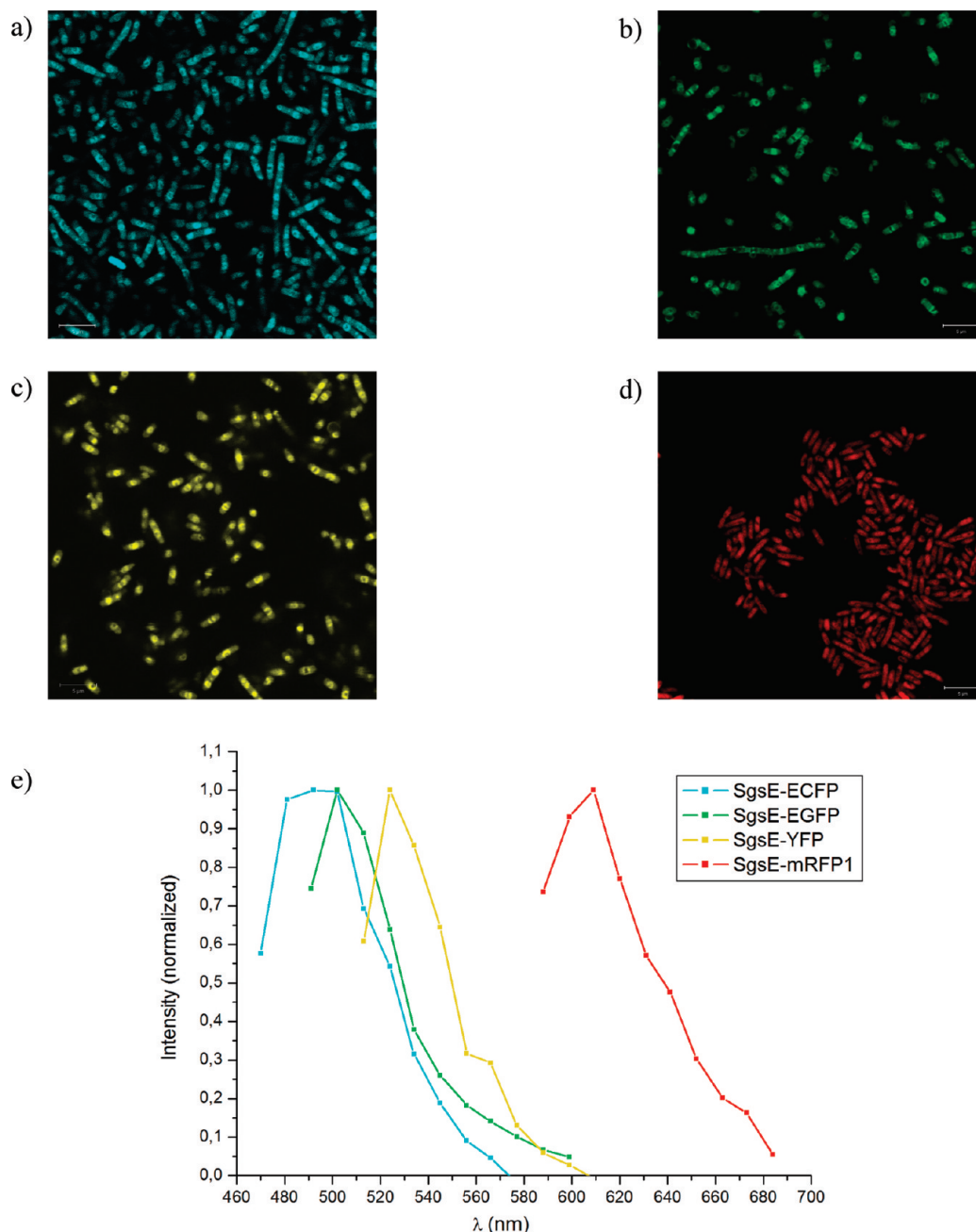


**Figure 2.** Confocal fluorescence micrograph of *E. coli* BL21 Star (DE3) biomass samples 4 h after induction of expression: (a) SgsE-ECFP, (b) SgsE-EGFP, (c) SgsE-YFP, (d) SgsE-mRFP1, and (e) wavelength-scan of the expressed fluorescence S-layer fusion proteins located in inclusion bodies (sampling interval: 10 nm). Solution: PBS-buffer; Scale bar 5 μm.

One of the most remarkable features of the prokaryotic cell envelopes is the presence of monomolecular arrays of protein or glycoprotein subunits referred to as S-layers.<sup>13</sup> The S-layers are recognized as one of the most commonly observed bacterial cell surface structures. They have been identified so far in hundreds of different species belonging to all major phylogenetic groups of bacteria and represent an almost universal feature of archaea.<sup>14,15</sup> High resolution electron microscopy and atomic force microscopy studies revealed that S-layer lattices can have oblique (p1, p2), square (p4), or hexagonal (p3, p6) symmetry with a center-to-center spacing of the morphological units of approximately 3–35 nm. The S-layers of prokaryotic organisms represent unique self-assembly systems, which can be used as a patterning element for a biomolecular construction kit involving all major species of biological molecules.<sup>16–18</sup> The broad application potential of S-layer proteins in nanobiotechnology

is based on their unique capability to recrystallize into 2D lattices on surfaces of a wide variety of materials. Another important property of bacterial proteins is their versatility with regards to fusion with other biomolecules. Previous studies showed that several functional domains (streptavidin, enzymes, antibodies, allergens, tags like Strep-tag and His<sub>6</sub>-tag, or amino acids like cysteine) could be incorporated into S-layer proteins at the N- or C-terminal positions, combining in a unique way the biological activity of the functional domain of interest with the intrinsic self-assembly capacity of the S-layer protein. Most important, the arrangement of functional domains on each S-layer unit cell is repeated with the periodicity of the protein lattice arrays.<sup>19</sup>

Proteins are often labeled with fluorescent tags to detect their location and sometimes their conformational changes both in vitro and in vivo. Typically, fluorescence labeling is done by

purifying the proteins and, then, covalently conjugating organic fluorophores to their activated groups or just by unspecific adsorption of the fluorophores as schematically shown in Figure 1. The stoichiometry and locations of dye attachment are difficult to control. An alternative way is to concatenate the gene for a fluorescent protein and an S-layer protein to create fluorescent S-layer fusion proteins (see Figure 1c). The successful cloning, expression and emission properties of such a fluorescent S-layer fusion protein with EGFP as a fluorescence tag (rSbpA<sub>31–1068</sub>/EGFP) were reported in previous papers.<sup>20,21</sup>

In this study, the 903 amino acid containing S-layer protein SgsE from *Geobacillus stearothermophilus* NRS 2004/3a (GenBank accession number AF328862)<sup>22–24</sup> was used to build up novel functional fluorescent architectures for different fluorescent applications in the future. The three main objectives of this work were the building of fluorescent S-layer fusion proteins by tagging the S-layer protein SgsE for the first time with different colored GFP mutants, the investigation of their fluorescence properties, and the determination of the lattice parameters of the self-assembled S-layer fusion proteins. The nucleotide sequences encoding the green fluorescent protein EGFP, the cyan fluorescent protein ECFP, and the yellow shifted YFP 10C variant as well as the monomeric red fluorescent protein mRFP1 were fused with their N-terminus to the C-terminus (3'-end) of the sequence encoding the 130 amino acid N-terminal truncated form of SgsE (rSgsE<sub>131–903</sub>). Different N-terminal truncated forms of this S-layer protein and their self-assembly properties and their use for creating fusion proteins with enzymatic activity were reported in a previous paper.<sup>25</sup>

The steady-state spectra and fluorescence lifetimes of the S-layer fusion proteins were compared with their His<sub>6</sub>-tagged reference fluorescent proteins. The nanostructure of the self-assembled S-layer fusion proteins was investigated with the transmission electron microscope (TEM). These studies show that the newly engineered S-layer fusion proteins have the potential to build periodic biomimetic nanostructures of controlled fluorescent properties.

## Experimental Section

Unless otherwise stated, all solvents and reagents were purchased from Sigma-Aldrich (Vienna). Buffer solutions were prepared with Milli-Q water (resistivity: 18.2 MΩ cm<sup>-1</sup>).

**Construction of Plasmids.** All experiments in this work were carried out with the N-terminal truncated rSgsE<sub>131–903</sub> (C-SgsE)<sup>25</sup> of SgsE, referred in the following as SgsE, incorporating C-terminal fluorescent proteins. Green fluorescent protein mutants EGFP (F64L, S65T), ECFP (F64L, S65T, Y66W, N146I, M153T, V163A), and YFP 10C (S65G, V68L, S72A, T203Y) as well as mRFP1 were used as fusion partners. Molecular cloning procedures were performed as previously published.<sup>25</sup> The cloning of pET28a-C<sub>SgsE</sub> and pET28a-C<sub>SgsE</sub>(Kpn) were described previously.<sup>25</sup> For the construction of SgsE fusion proteins with C-terminal fused fluorescent proteins, the fluorescent fusion partners were PCR (polymerase chain reaction)-amplified using the primer pairs EGFP\_for(*KpnI*)/EGFP\_rev(*XhoI*) for EGFP, YFP, and ECFP and mRFP1\_for(*KpnI*)/mRFP1\_rev(*XhoI*) for mRFP1, digested with *KpnI*/*XhoI* and inserted into the *KpnI*/*XhoI* linearized plasmid pET28a-C<sub>SgsE</sub>(Kpn). To obtain fluorescent proteins with N-terminal His<sub>6</sub>-tag, as a positive control for the determination of fluorescence, EGFP, YFP, ECFP, and mRFP1 were amplified by PCR using the primer pairs EGFP\_for(*NdeI*)/EGFP\_rev(*XhoI*) and mRFP1\_for(*NdeI*)/mRFP1\_rev(*XhoI*) and ligated into pET28a(+) (Invitrogen, Lofer Austria) via the *NdeI*/*XhoI* sites. Strains and plasmids used in this study are shown in the Supporting Information. PCR was carried out using Super Yield *Pwo* polymerase (Roche, Vienna, Austria). Restriction enzymes and T4 DNA ligase were purchased from Invitrogen (Lofer,

Austria). *Escherichia coli* DH5α (Invitrogen, Lofer, Austria) was used for plasmid propagation and all other cloning and expression experiments were performed using *E. coli* BL21 Star (DE3). Protein expression and purification were monitored by SDS-PAGE (see Supporting Information) and fluorescence measurements. SDS-PAGE and visualization of the protein bands with Coomassie Blue R-250 were carried out as described elsewhere.<sup>25</sup> Cells were grown at 37 °C in Luria-Bertani (LB) medium supplemented with kanamycin (50 μg/mL). Protein expression was induced with 1 mM IPTG (Fermentas, St. Leon-Rot, Germany), and cultivation was continued at 37 °C for additional 4 h in the dark. Isolation of the fusion proteins (SgsE-EGFP, SgsE-EGFP, SgsE-YFP, SgsE-mRFP1) and FPLC purification (Superdex 200 prep grade XK16 FPLC-column, 1.6 × 60 cm, GE-Healthcare) were carried out as recently described.<sup>25</sup> Soluble His<sub>6</sub>-tagged fluorescent proteins (EGFP, EGFP, YFP, mRFP1) were purified by Ni<sup>2+</sup> affinity chromatography (HisTrap HP prepacked column, GE-Healthcare) as described elsewhere.<sup>26</sup> The proteins were dialyzed (cutoff 12–16 kDa, Biomol) against 2 mM EDTA. After centrifugation protein concentrations were determined with a NanoDrop spectrophotometer (ND-1000, Peqlab Biotechnology, Germany) at 280 nm. The protein solutions were diluted to 1 mg/mL with Milli-Q water and stored at 4 °C in the dark.

**Self-Assembly of Fluorescent SgsE-Fusion Proteins in Aqueous Solution.** To obtain self-assembly products of the different recombinant fluorescent S-layer proteins in solution, 5 mL of the monomer solutions were dialyzed (cutoff 12–16 kDa, Biomol) against HBSS solution (Hanks' balanced salt solution containing calcium and magnesium, pH 7.4) for 18 h at 4 °C followed by 2 h against multiply exchanged Milli-Q water. Self-assembly product suspensions were stored at 4 °C in the dark.

**TEM.** Images of S-layer lattices were obtained using a JEOL JEM-2100F (Model EM-20014) transmission electron microscope (TEM). Hydrophilized carbon-coated pioloform supported 300-mesh copper grids were incubated with the carbon-coated side on the drop of each S-protein self-assembly suspension for 1 h. The adsorbed S-layer proteins were chemically fixed with 0.5% glutaraldehyde in 0.1 M K-dihydrogen phosphate buffer (pH 7.2) for 10 min and after three washing steps with Milli-Q-water negatively stained with 1.0% uranyl acetate for less than 1 min. Dry samples were used for electron microscopy studies. The S-layer lattice parameters (base vector lengths and base angle) were determined using a homemade software based on Fourier analysis.

**Confocal Laser Scanning Microscopy.** Confocal fluorescence images of the heterologous expressed fluorescent S-layer fusion proteins in *E. coli* BL21 Star (DE3) cells were taken using a Zeiss LSM510 Meta (Zeiss, Jena, Germany) microscope with an argon/2 laser (458, 477, 488, 514 nm) and a DPSS 561-10 laser (561 nm). The *E. coli* BL21 Star (DE3) cells were washed twice with 150 mM PBS buffer solution (pH 7.4). SgsE-EGFP was imaged with the 488 nm laser line and a BP505-530 emission filter, SgsE-YFP with the 514 nm laser line and a BP520-555IR emission filter, SgsE-EGFP with the 458 nm laser line and a LP475 emission filter, and SgsE-mRFP1 with the 561 nm laser line and a LP575 emission filter.

**Spectroscopy.** The investigated samples consisted of fluorescent proteins immersed in McIlvaine CP buffers (10 mM citric acid/20 mM sodium phosphate). The pH values ranged from pH 3 to 8. Absorption spectra were measured with a NanoDrop ND-1000 Spectrophotometer (3 μL test volume).

Steady-state fluorescence spectra were recorded using a FluoroLog-3 (Model FL3-22) steady-state spectrofluorimeter (Horiba Jobin Yvon) with integration time of 0.1 s, entrance slit, intermediate slit, and exit slit of 5 nm for excitation and emission monochromators. The protein concentration was 0.4 μM. Measurements were carried out within 2 min at room temperature in quartz cuvettes with a path length of 10 mm and a minimum test volume of 2 mL. Spectra were recorded with FluorEssence and analyzed using Origin7 software. Excitation spectra were corrected with the spectrum of the Xe-lamp (Sample/Reference).

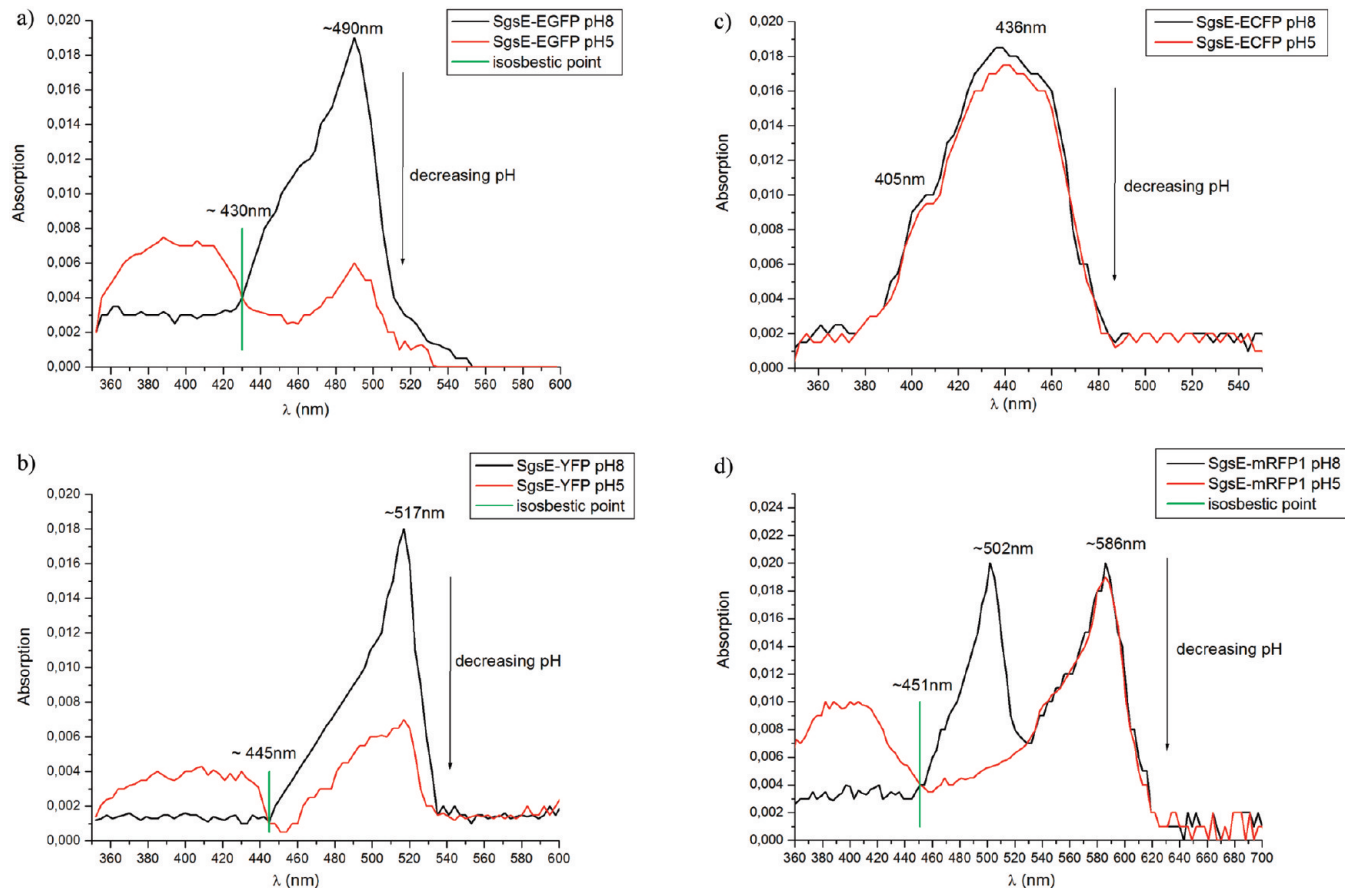


**Figure 3.** Absorption spectra of (a) SgsE-EGFP, (b) SgsE-YFP, (c) SgsE-ECFP, and (d) SgsE-mRFP1 in phosphate citrate buffer at pH 8 and 5. The absorption decreased at lower pH. The isosbestic point could be estimated from the intersection of both pH spectra (green vertical line).

At least three spectra of each protein were recorded until the final relative error was lower by approximately 5%.

Fluorescence decay data were acquired using the TCSPC (time-correlated single-photon-counting) Triple Illuminator accessory for the FluoroLog-3 steady-state spectrofluorimeter (Data Station v2.2 software, 10000 counts, TAC range: 50 ns, repetition rate: 1 MHz, coaxial delay 65 ns). NanoLEDs from Horiba Jobin Yvon were used as pulsed diode excitation source. NanoLED-460 (peak wavelength 463 nm, max. rep. rate 1 MHz, pulse duration 1.4 ns) was used for EGFP, YFP, and mRFP1; NanoLED-370 (peak wavelength 376 nm, max. rep. rate 1 MHz, pulse duration 1.2 ns) was used for ECFP. For the measurement of the prompt trace, a 0.01% dilution of Ludox AS40 colloidal silica (Sigma-Aldrich) was taken as scatter sample. The time-resolved fluorescence decays  $F(t)$  were fitted with three exponentials after deconvolution ( $\otimes$ ) with the system response function  $R(t)$  (full-width half-maximum, fwhm =  $1.251 \pm 0.033$  ns), by using the decay analysis software DAS6 v6.1.

The deconvoluted fluorescence decay  $I(t)$  is described as a sum of exponentials with time constants ( $\tau_i$ ) and amplitudes ( $\alpha_i$ ; see eq 1). The average fluorescence lifetimes ( $\langle\tau\rangle_{fl}$ ) are calculated as described in eq 2.<sup>27–29</sup>

$$I(t) = F(t) \otimes R(t) = \sum_{i=1}^n \alpha_i \exp(-t/\tau_i) \quad (1)$$

$$\langle\tau\rangle_{fl} = \frac{\sum_{i=1}^n \alpha_i \tau_i}{\sum_{i=1}^n \alpha_i} \quad (2)$$

The complete fitting procedure is shown in the Table 4 of the Supporting Information including the values of the standard deviation.

## Results and Discussion

The His<sub>6</sub>-tagged fluorescent proteins and the S-layer fusion proteins were heterologously expressed in *E. coli* BL21 (DE3) Star. Figure 2 shows that the four different fluorescent fusion proteins were accumulated in inclusion bodies in the cytoplasm of the *E. coli* host cells. The protein emission spectra were recorded with a confocal microscope using the wavelength-scan function (Figure 2e). The obtained emission spectra of the four proteins were similar to the results reported by Zimmer and Tsien.<sup>4,12</sup>

After protein extraction and purification, the absorption, emission, and excitation spectra of the fusion protein were measured between pH 8 and pH 3. Figure 3 shows the absorption spectra of the four different S-layer fluorescent proteins. It can be seen that at high pH values (pH 8) the main absorption band of the anionic state of SgsE-EGFP had its maximum around 490 nm (Figure 3a). At pH 5 the 490 nm absorption was reduced while the absorption band of the neutral state around 390 nm increased and an isosbestic point at ~430 nm appeared, in agreement with Haupts et al.<sup>2</sup> The same behavior could be observed with the yellow S-layer fusion protein SgsE-YFP (Figure 3b), in which the 517 nm absorption peak maximum at pH 8 decreased in acidic bulk conditions while the neutral state absorption band appeared at around 410 nm with an isosbestic point at ~445 nm. SgsE-ECFP absorption spectra were less pH sensitive than the green and yellow fusion proteins. Figure 3c shows that the shape of the spectra of the cyan fluorescent protein was nearly identical for pH 8 and pH 5. Thus, neither a neutral state absorption peak at pH 5 nor an

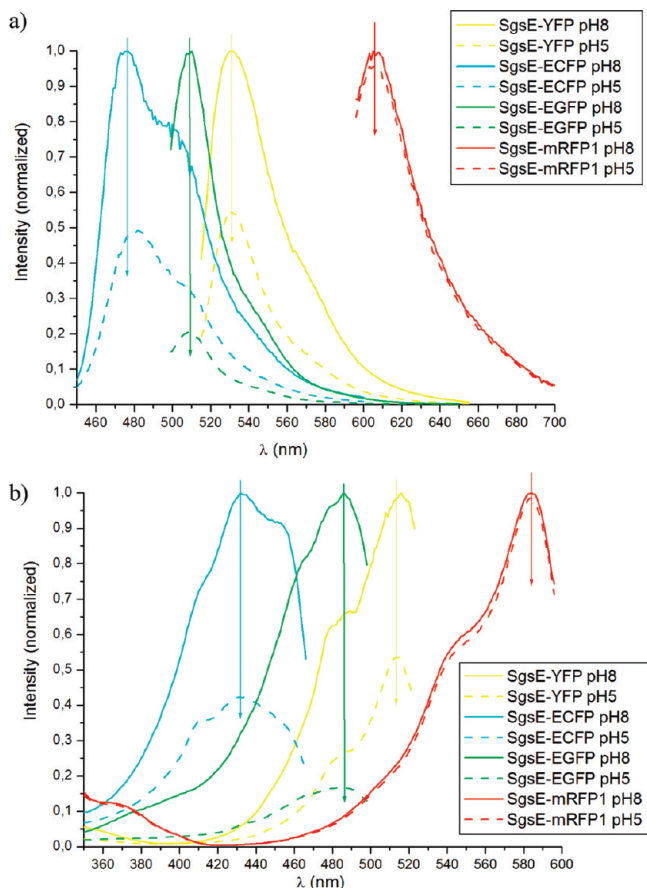


**Figure 4.** (a) Emission spectra (excitation at absorption maxima see Figure 3) and (b) excitation spectra of SgsE-ECFP ( $\lambda_{\text{ex}}$  435 nm,  $\lambda_{\text{em}}$  476 nm), SgsE-EGFP ( $\lambda_{\text{ex}}$  488 nm,  $\lambda_{\text{em}}$  510 nm), SgsE-YFP ( $\lambda_{\text{ex}}$  514 nm,  $\lambda_{\text{em}}$  527 nm), and SgsE-mRFP1 ( $\lambda_{\text{ex}}$  585 nm,  $\lambda_{\text{em}}$  607 nm) at pH 8 and pH 5 (dotted lines). The fluorescence intensities decreased at lower pH (as the arrow indicates).

isosbestic point could be detected. Figure 3d displays the absorption spectra of SgsE-mRFP1 protein at pH 8 and pH 5. In this case, an additional adsorption band could be observed at around 502 nm at pH 8. This peak was not associated with excitation of fluorescence.<sup>4</sup> At pH 5, the situation was different; while the anionic peak at 586 nm remained the same; a neutral peak appeared at around 390 nm. In addition, the isosbestic point could be observed at  $\sim$ 451 nm.

The emission and excitation spectra of the fusion proteins at pH 8 and pH 5 are presented in Figure 4. It can be observed that the excitation and emission maxima were 488 and 509 nm for SgsE-EGFP, 435 and 476 nm for SgsE-ECFP, 514 and 527 nm for SgsE-YFP, and 585 and 607 nm for SgsE-mRFP1, respectively. These values were the same as the values obtained for the His<sub>6</sub>-tagged reference proteins (see Supporting Information) and coincided with the spectra reported for different GFP proteins.<sup>1</sup> Furthermore, it can be seen that the excitation maxima coincided with the absorption maxima. Figure 4 (dotted lines) also shows how the fluorescence intensities diminished when the pH varied from pH 8 to pH 5. The main difference between the S-protein GFP mutants and the SgsE-mRFP1 fluorescence spectra was the pH resistance of the red fluorescent protein.

The influence of the pH on the fluorescent properties of the S-layer fusion proteins was investigated in detail. This is shown in Figure 5. On one hand, it can be seen that the fluorescence intensity decreases at acidic pH. Remarkably, the red fluorescence proteins SgsE-mRFP1 and the reference His<sub>6</sub>-mRFP1 were

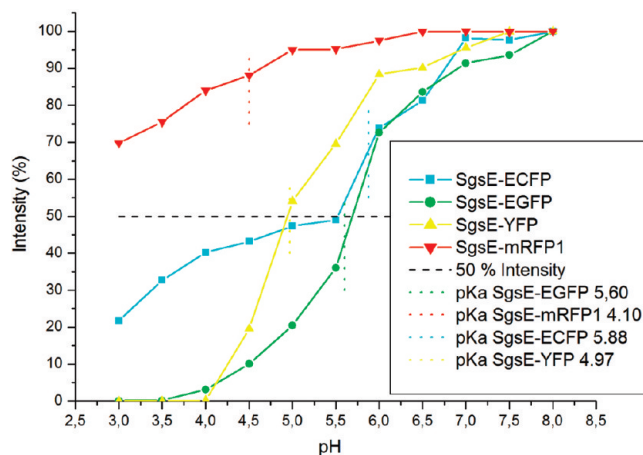


**Figure 5.** Fluorescence emission intensities as a function of pH values of SgsE-ECFP, SgsE-EGFP, SgsE-YFP, and SgsE-mRFP1. The variation of pH ranged from pH 8 to pH 3. Between pH 6 and 5, the intensities of SgsE-ECFP, SgsE-EGFP, and SgsE-YFP decreased about 50%. The  $pK_a$  (vertical colored lines) values of the four fluorescent S-layer fusion proteins were estimated; these values are indicated in the inset. Note that the absorption maxima shown in Figure 3 have been taken as excitation wavelength for emission spectra.

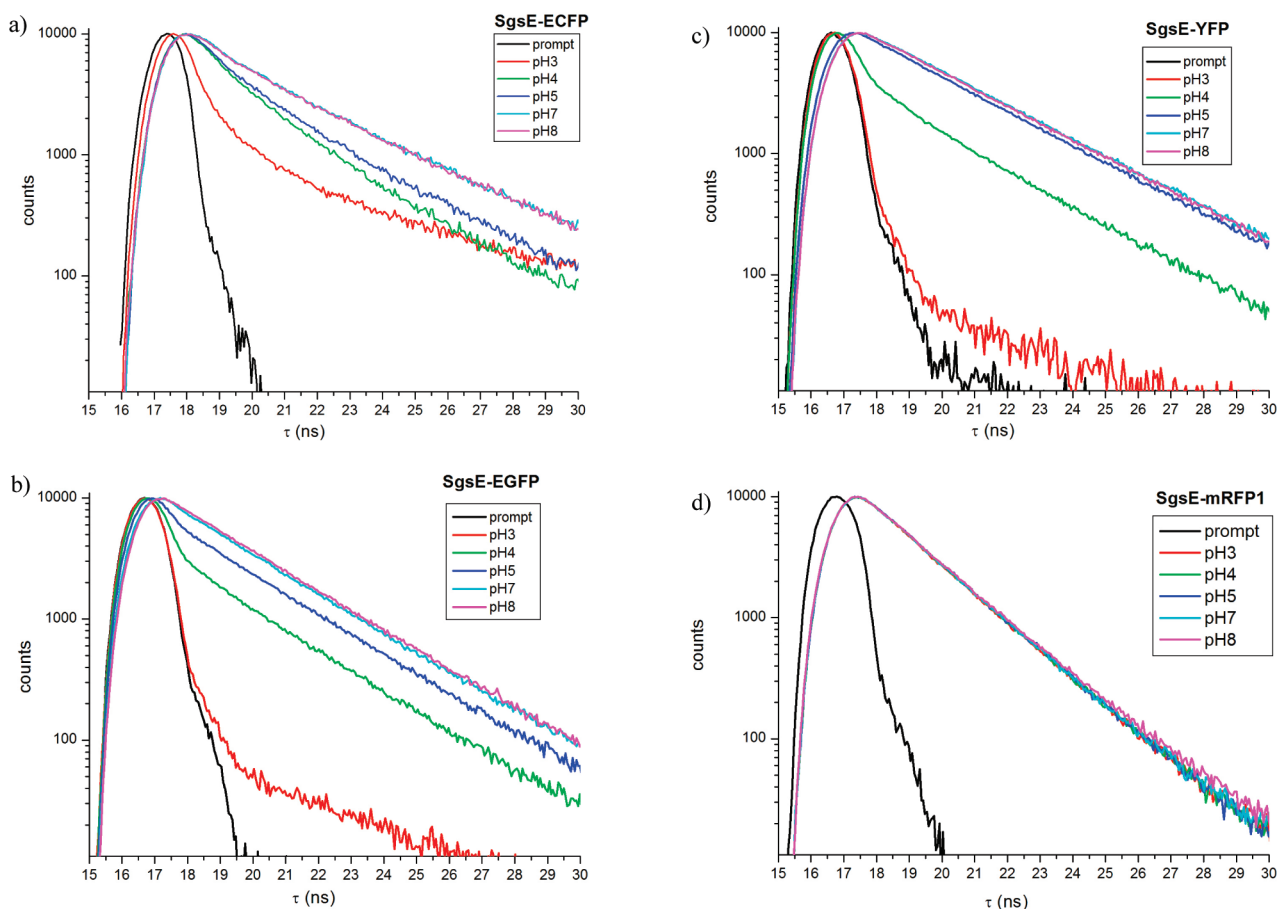
not as strongly affected by pH changes. On the other hand, the different GFP mutants ECFP, EGFP, and YFP lost at least 50% of intensity at pH 5, vanishing completely at pH 3. Within these pH ranges, however, the three proteins behaved in a different way, with ECFP being the most stable one. A detailed quantification of the percentage fluorescence lost is provided in Table 1. Furthermore, the behavior of the fusion proteins was compared with the behavior of the reference proteins. It should be mentioned that the reference proteins had a similar behavior, showing few differences. From the fluorescence intensities shown in Figure 5, the  $pK_a$  values of the different proteins could be estimated using the following equation:  $F = x + y/(1 + 10^z)$ , where  $F$  is the intensity,  $z$  is  $(pK_a - \text{pH})$ , and  $x$  and  $y$  are related to the offset and the dynamic range of the data.<sup>2</sup> The details of the fitting procedure can be found in the Supporting Information. In addition, from the equilibrium constant  $K_a$ , the standard free reaction energies from the fluorescent S-layer fusion proteins could be calculated using the equation  $\Delta G^0 = -RT \ln K_a$ , where  $pK_a = -\log K_a$ . The estimated  $pK_a$  and  $\Delta G^0$  values were  $pK_a = 5.6$  and  $\Delta G^0 = 29.28$  kJ/mol for SgsE-EGFP,  $pK_a = 5.88$  and  $\Delta G^0 = 30.75$  kJ/mol for SgsE-ECFP,  $pK_a = 4.97$  and  $\Delta G^0 = 25.99$  kJ/mol for SgsE-YFP, and  $pK_a$  value is 4.01 and  $\Delta G^0 = 21.44$  kJ/mol for SgsE-mRFP1. The  $pK_a$  values for the fusion proteins were similar to those described in the literature. For example, the  $pK_a$  for EGFP<sup>2</sup> is around 5.8 and 4.5 for mRFP1.<sup>4</sup>

To complete the characterization of the spectral properties of the fluorescent proteins, lifetime decay experiments were carried out using time-correlated single photon counting spectroscopy (TCSPC). Figure 6 displays the fluorescence lifetime decay of the four different colored fluorescent S-layer fusion proteins as a function of pH. The measurements showed that the red S-layer fusion protein was slightly affected by variations in environmental pH values below pH 5 in comparison to the other fluorescent fusion proteins. For example, the fluorescence lifetime for the red fusion protein was around 1.83 ns at pH 8, while this value decreased to 1.32 ns at pH 3. These values, as well as the lifetime decays of the other fluorescent proteins, are listed in Table 2. A different behavior could be observed for the green, yellow, and cyan fluorescent proteins. The lifetime

**Table 1.** Fluorescence Intensity as a Function of pH of Fluorescent S-Layer Fusion Proteins and His<sub>6</sub>-Tagged Fluorescent Proteins (reference)<sup>a</sup>

pH	intensity (%)							
	SgsE-ECFP	His <sub>6</sub> -ECFP	SgsE-EGFP	His <sub>6</sub> -EGFP	SgsE-YFP	His <sub>6</sub> -YFP	SgsE-mRFP1	His <sub>6</sub> -mRFP1
8.0	100	100	100	100	100	100	100	98.6
7.5	97.6		93.6		99.9		99.8	
7.0	98.2	91.5	91.4	99.7	95.6	98.4	100	100
6.5	81.3		83.6		90.2		99.9	
6.0	73.9	79.6	72.6	90.2	88.4	96.0	97.5	98.1
5.5	49.0		36.0		69.6		95.2	
5.0	47.3	51.5	20.5	30.5	54.1	51.6	95.0	92.4
4.5	43.2		10.1		19.6		88.1	
4.0	40.2	47.2	3.1	0.34	0.2	0.16	84.0	76.9
3.5	32.7		0.2		0		75.5	
3.0	21.8	26.7	0.1	0	0	0	69.8	65.9

<sup>a</sup> Note that the intensity is expressed in % (highest value at pH 8).

**Figure 6.** Fluorescence lifetime decays as a function of pH of (a) SgsE-ECFP, (b) SgsE-EGFP, (c) SgsE-YFP, and (d) SgsE-mRFP1, which was the only case where the lifetime decay was not strongly affected by pH. The black curve represents the prompt trace. Calculated fluorescence lifetime decay values of all fluorescent proteins investigated in this work are listed in Table 2.**Table 2.** Summary of Fluorescence Lifetime Data as a Function of pH for Fluorescent S-Layer Fusion Proteins and Fluorescent Reference His<sub>6</sub>-Tagged Proteins

pH	$\tau_{fl}$ (ns)							
	SgsE-ECFP	His <sub>6</sub> -ECFP	SgsE-EGFP	His <sub>6</sub> -EGFP	SgsE-YFP	His <sub>6</sub> -YFP	SgsE-mRFP1	His <sub>6</sub> -mRFP1
8.0	2.31	2.25	2.61	2.68	3.02	3.08	1.83	1.76
7.0	1.95	2.21	2.05	2.68	3.11	3.10	1.75	1.73
5.0	1.16	1.33	1.67	2.66	2.91	2.24	1.70	1.74
4.0	0.65	0.96	1.07	2.67	1.40	1.49	1.34	1.62
3.0	0.65	0.05	0.16	0.08	0.12	0.12	1.32	1.31

decays for these proteins decreased by at least 50% at pH 4, and became much lower than 1 ns at pH 3. Table 2 also shows that the S-layer fusion proteins and the reference proteins have a similar spectral behavior. Therefore, it can be assumed that

S-layer lattices are suitable carriers of functional fluorescent proteins. At this point, it should be mentioned that steady-state measurements (Table 1) and lifetime decay measurements (Table 2) followed similar trends: between pH 5 and pH 4 about 50%

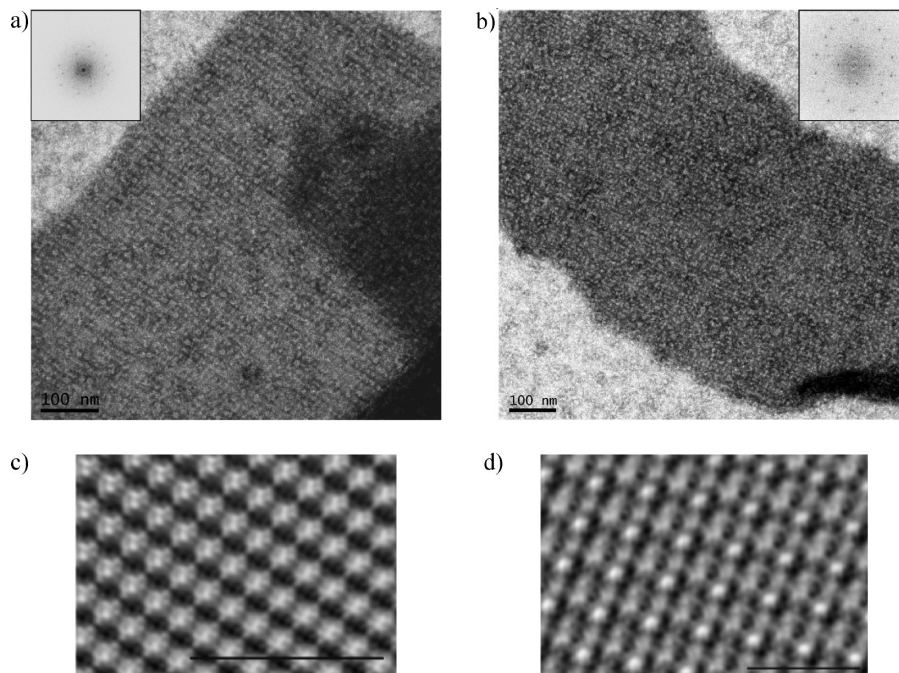


**Figure 7.** Electron microscopy images (TEM) of self-assembly products of (a) SgsE truncated and (c) SgsE-EGFP after negative-staining. The insets are the Fourier transforms of the p2 nanostructures. The filtered image reconstructions of the truncated SgsE S-layer self-assembly product and SgsE-EGFP are shown in (b) and (d), respectively. Note that the scale bar in (c) is 70 nm and in (d) is 40 nm.

of the fluorescence intensity and lifetime was lost, with the exception of the red fluorescent protein. These results demonstrated that the S-layer protein SgsE does not affect the fluorescence decay of the fused fluorescent protein tag, implying that fluorescent S-layer fusion proteins are suitable candidates for future applications in nanobiotechnology at a wide range of pH. For example, the steady-state spectra and lifetime decay values for the ECFP fusion protein and the yellow fusion protein SgsE-YFP indicated that the engineered proteins are suitable partners for resonance energy transfer (FRET) investigations.

**Characterization of the S-Layer Material and Self-Assembly Experiments Self-Assembly and Image Reconstruction.** In previous work<sup>22–24</sup> it has been shown that isolated S-layer subunits from the wildtype strain can reassemble into distinct types of cylindrical and sheet-like self-assembly products. The negatively stained preparations revealed that the four engineered fluorescent fusion proteins as well as the SgsE reference protein reassembled mostly into double-layered self-assembly products in solution. Generally, they showed different types of cylindrical and sheet-like self-assembly products while some of the larger sheets also tended to convolve to rolls or fold otherwise to different shapes of an oblique (p2) lattice symmetry. The self-assembly products of SgsE-mRFP1 occurred mostly in very long and small cylinders (see Supporting Information). Figure 7 shows the electron microscopy micrographs of the truncated SgsE protein and the fluorescent fusion protein SgsE-EGFP. On one hand, Figure 7a refers to the self-assembly product of SgsE. In this figure the regular p2 nanostructure could be observed. The inset in Figure 7a shows the Fourier transform of the SgsE-nanostructure, while Figure 7c is a filtered picture reconstruction of Figure 7a. Fourier analysis provided the following lattice parameters  $a = 10.5$  nm,  $b = 13.1$  nm, angle =  $78.7^\circ$ . On the other hand, Figure 7b shows the self-assembly product of the SgsE-EGFP fusion protein. In this case, a p2 nanostructure could also be observed. As before, the inset in Figure 7b shows the Fourier analysis while the computer image reconstruction of the SgsE-EGFP nanostructure

**Table 3.** Lattice Parameters of the Self-Assembly Products of Fluorescent S-Layer Fusion Proteins Investigated by Transmission Electron Microscopy<sup>a</sup>

	a-vec (nm)	b-vec (nm)	angle ( $^\circ$ )
SgsE WT <sup>24</sup>	9.4	11.6	78
SgsE truncated	10.5 ( $\pm 0.1$ )	13.1 ( $\pm 0.1$ )	78.7 ( $\pm 0.8$ )
SgsE-ECFP	11.7 ( $\pm 0.4$ )	13.9 ( $\pm 1.0$ )	80.1 ( $\pm 1.7$ )
SgsE-EGFP	11.9 ( $\pm 0.6$ )	14.7 ( $\pm 0.6$ )	81.2 ( $\pm 1.1$ )
SgsE-YFP	11.2 ( $\pm 0.3$ )	14.2 ( $\pm 0.1$ )	79.8 ( $\pm 2.4$ )
SgsE-mRFP1	11.4 ( $\pm 0.4$ )	14.3 ( $\pm 0.3$ )	79.0 ( $\pm 1.6$ )

<sup>a</sup> The error is indicated inside the brackets.

is shown in Figure 7d. In this case, the lattice parameters were  $a = 11.9$  nm,  $b = 14.7$  nm, angle =  $81.2^\circ$ . These results showed that the lattice parameters were larger due to the fusion tag although the spatial symmetry (p2) is preserved. This was a general feature for the fusion proteins presented in this work (see Table 3). However, it has to be pointed out that the fusion tag did not hinder the self-assembly process that leads to nanocrystal formation, being exposed to the surface of the double-layer assembly products.

## Conclusion

Four different fluorescent fusion proteins have been successfully genetically engineered, heterologously expressed in *E. coli* BL21 Star (DE3), isolated and purified, combining S-layer proteins with three different GFP mutants and the red fluorescent protein mRFP1. Absorption spectra, steady state and lifetime fluorescence measurements showed that the fluorescent S-layer fusion proteins and the His<sub>6</sub>-tag fluorescent proteins (reference) had a similar behavior in different pH environments. The isosbestic points of the different fluorescent S-layer fusion proteins could be determined from the absorption spectra. While the fluorescence intensity of the different GFP mutants, EGFP, ECFP, and YFP, strongly decreased at pH 3, the intensity of the red fluorescent protein dropped only by 40%. In addition, the pK<sub>a</sub> values of the four fusion proteins were estimated. It

was found that the fluorescence lifetime was reduced when the pH decreased. These measurements permitted the identification of FRET-partners based on S-layer fusion proteins. The fluorescent S-layer fusion proteins retained their self-assembly properties, building a p2 lattice nanostructure, although the fluorescent tag enlarged slightly the original lattice parameters of the truncated S-layer protein SgsE.

These results indicate that the assembling and the fluorescence properties of the newly designed fluorescent S-layer fusion proteins can be used for building nanopatterned biofunctional surfaces for future applications in nanobiotechnology in a wide range of pH, such as pH indicators both in vivo and in vitro or as fluorescent markers for drug delivery systems. Co-crystallization of SgsE-ECFP (donor) and SgsE-YFP (acceptor) on solid supports with molecular precision can be used for fluorescence resonance energy transfer (FRET) investigations. The coating of colloidal particles with these fluorescent S-layer fusion proteins could be used as pH biosensors. Finally, after determining which proteins are suitable as FRET partners, the challenge will be to engineer a tandem fluorescent S-layer fusion protein with the donor and acceptor dye on both the N- and the C-terminal ends of the S-layer protein.

**Acknowledgment.** This work was supported by the Austrian NanoInitiative under the project SLAYSENS within the project cluster ISOTEC and by the U.S. Air Force Office of Scientific Research (AFOSR) Projects FA9550-07-0313 and FA9550-09-1-0342. Rene Novotny is acknowledged for cloning of the red fusion protein. J.L.T.-H. is an I3 research professor and, therefore, thanks the I3 programme of the Spanish Government. Dr. Kathryn Melzak is acknowledged for reading the manuscript. This work was partially financed by the Spanish Ministry of Education and Science (Project CTQ-2007-66541) and the EU-programme Marie Curie Host Fellowships for the Transfer of Knowledge (MTKD-CT-2005-030040). Dr. Susana Moreno Flores is acknowledged for technical assistance in TEM measurements and helpful discussions.

**Supporting Information Available.** Data about (i) used strains, plasmids, and oligonucleotides, (ii) SDS/PAGE electrophoresis and (iii) fluorescence emission spectra, (iv) fitting procedure for the estimation of the lifetime fluorescence decay, (v) transmission electron microscopy micrographs, and (vi) fitting procedure for the estimation of the  $pK_a$  values. This material is available free of charge via the Internet at <http://pubs.acs.org>.

## References and Notes

- (1) Tsien, R. Y. *Annu. Rev. Biochem.* **1998**, *67*, 509–44.
- (2) Haupts, U.; Maiti, S.; Schwille, P.; Webb, W. W. *Proc. Natl. Acad. Sci. U.S.A.* **1998**, *95* (23), 13573–8.
- (3) Shaner, N. C.; Campbell, R. E.; Steinbach, P. A.; Giepmans, B. N. G.; Palmer, A. E.; Tsien, R. Y. *Nat. Biotechnol.* **2004**, *22* (12), 1567–1572.
- (4) Campell, R. E.; Tour, O.; Palmer, A. E.; Steinbach, P. A.; Baird, G. S.; Zacharias, D. A.; Tsien, R. Y. *Proc. Natl. Acad. Sci. U.S.A.* **2002**, *99* (12), 7877–7882.
- (5) Elsliger, M. A.; Wachter, R. M.; Hanson, G. T.; Kallio, K.; Remington, S. J. *Biochemistry* **1999**, *38* (17), 5296–301.
- (6) Remington, S. J. *Curr. Opin. Struct. Biol.* **2006**, *16* (6), 714–21.
- (7) McAnaney, T. B.; Zeng, W.; Doe, C. F.; Bhanji, N.; Wakelin, S.; Pearson, D. S.; Abbyad, P.; Shi, X.; Boxer, S. G.; Bagshaw, C. R. *Biochemistry* **2005**, *44* (14), 5510–24.
- (8) Hanson, G. T.; McAnaney, T. B.; Park, E. S.; Rendell, M. E.; Yarbrough, D. K.; Chu, S.; Xi, L.; Boxer, S. G.; Montrose, M. H.; Remington, S. J. *Biochemistry* **2002**, *41* (52), 15477–88.
- (9) McAnaney, T. B.; Shi, X.; Abbyad, P.; Jung, H.; Remington, S. J.; Boxer, S. G. *Biochemistry* **2005**, *44* (24), 8701–11.
- (10) Lakowicz, J. R. *Principles of Fluorescence Spectroscopy*, 3rd ed.; Springer: New York, 2006.
- (11) Patnaik, S. S.; Trohalaki, S.; Pachter, R. *Biopolymers* **2004**, *75* (6), 441–52.
- (12) Zimmer, M. *Chem. Rev.* **2002**, *102* (3), 759–782.
- (13) Sleytr, U. B. *Int. Rev. Cytol.* **1978**, *53*, 1–62.
- (14) Sleytr, U. B.; Beveridge, T. J. *Trends Microbiol.* **1999**, *7* (6), 253–60.
- (15) Sleytr, U. B.; Messner, P.; Pum, D.; Sára, M. *Angew. Chem., Int. Ed.* **1999**, *38*, 1034–1054.
- (16) Sleytr, U. B.; Egelseer, E. M.; Ilk, N.; Pum, D.; Schuster, B. *FEBS J.* **2007**, *274*, 323–334.
- (17) Sleytr, U. B.; Huber, C.; Ilk, N.; Pum, D.; Schuster, B.; Egelseer, E. M. *FEMS Microbiol. Lett.* **2007**, *267*, 131–144.
- (18) Egelseer, E. M.; Ilk, N.; Pum, D.; Messner, P.; Schäffer, C.; Schuster, B.; Sleytr, U. B. In *The Encyclopedia of Industrial Biotechnology: Bioprocess, Bioseparation, and Cell Technology*; Flickinger, M. C., Ed.; John Wiley & Sons, Inc.: Hoboken, NJ, 2009, in press.
- (19) Ilk, N.; Egelseer, E. M.; Ferner-Ortner, J.; Kuepcue, S.; Pum, D.; Schuster, B.; Sleytr, U. B. *Colloids Surf.* **2008**, *321*, 163–167.
- (20) Toca-Herrera, J. L.; Kupcu, S.; Diederichs, V.; Moncayo, G.; Pum, D.; Sleytr, U. B. *Biomacromolecules* **2006**, *7* (12), 3298–301.
- (21) Ilk, N.; Küpcü, S.; Moncayo, G.; Klimt, S.; Ecker, R. C.; Hofer-Warbinek, R.; Egelseer, E. M.; Sleytr, U. B.; Sára, M. *Biochem. J.* **2004**, *379* (Pt 2), 441–8.
- (22) Sleytr, U. B.; Plohberger, R. The dynamic process of assembly of two-dimensional arrays of macromolecules on bacterial cell walls. In *Electron Microscopy at Molecular Dimensions*; Baumeister, W., Vogell, W., Eds.; Springer-Verlag: Berlin, Heidelberg, NY, 1980; pp36–47.
- (23) Sára, M.; Pum, D.; Küpcü, S.; Messner, P.; Sleytr, U. B. *J. Bacteriol.* **1994**, *176* (3), 848–60.
- (24) Messner, P.; Pum, D.; Sleytr, U. B. *J. Ultrastruct. Mol. Struct. Res.* **1986**, *97* (1–3), 73–88.
- (25) Schäffer, C.; Novotny, R.; Küpcü, S.; Zayni, S.; Scheberl, A.; Friedmann, J.; Sleytr, U. B.; Messner, P. *Small* **2007**, *3* (9), 1549–59.
- (26) Steiner, K.; Harnreich, A.; Kainz, B.; Hitchen, P.; Dell, A.; Messner, P.; Schäffer, C. *Small* **2008**, *4* (10), 1728–1740.
- (27) Valeur, B. *Molecular Fluorescence: Principles and Applications*; Wiley-VCH Verlag GmbH: New York, 2001.
- (28) Hess, S. T.; Sheets, E. D.; Wagenknecht-Wiesner, A.; Heikal, A. A. *Biophys. J.* **2003**, *85*, 2566–2580.
- (29) Liu, Y.; Kim, H.-R.; Heikal, A. A. *J. Phys. Chem. B* **2006**, *110* (47), 24138–24146.

BM901071B

## Additional information

*Absorption, steady-state fluorescence, fluorescence lifetime and 2D self-assembly properties of engineered fluorescent S-Layer fusion proteins of Geobacillus stearothermophilus NRS 2004/3a by Birgit Kainz et al.*

**Table 1:** Strains and plasmids used in this study

Strain or plasmid	Description	Source
<i>Geobacillus stearothermo-philus</i> NRS 2004/3a	Wild-type covered by an S-layer	N. R. Smith collection
<i>E. coli</i> DH5α	F <sup>+</sup> φ80 <i>lacZ</i> M15 ( <i>lacZYA-argF</i> ) U169 <i>deoR recA1 endA1 hsdR17 (rk, mk<sup>+</sup>) phoA supE44 thi-1 gyrA96 relA1 λ</i>	Invitrogen
<i>E. coli</i> BL21 Star (DE3)	F <sup>+</sup> <i>ompT hsdSB (rB mB) gal dcm rne131</i>	Invitrogen
pET28a(+)	<i>E. coli</i> expression vector, IPTG inducible, Km <sup>r</sup>	Novagen
pET28a-C_SgsE(C)	pET-28a(+)/C_SgsE <sub>131-903</sub> ; pET-28a(+) containing <i>sgsE</i> from <i>G. stearothermophilus</i> NRS 2004/3a, devoid of aa 1-100 of the mature S-layer protein;	Schäffer et al., 2007
pET28a-C_SgsE-xFP	pET28a-C_SgsE containing eGFP, eYFP, eCFP, mRFP fused to the C-	This study
x...eGFP, eYFP, eCFP, mRFP	terminus of the S-layer protein; Km <sup>r</sup>	
pET28a-His <sub>6</sub> -xFP	pET-28a(+) containing eGFP; eYFP, eCFP, mRFP N-terminal	This study
x...eGFP, eYFP, eCFP, mRFP	hexahistidine-tag; Km <sup>r</sup>	

**Table 2:** Oligonucleotide primers used for PCR amplification of different forms of SgsE

Primer	Nucleotide sequence (5'→3') <sup>a</sup>
SgsE_rev (Xho)	AATCACTCGAGGGATACATGTGCGGTACAAGAAAGC
A_SgsE_for (Nco)	AATCACCAATCGCGGACGTGGCGACGGTCCG
EGFP_for(KpnI)	AATCAGGTACCgGTGAGCAAGGGCGAGGAG
EGFP_rev(XhoI)	AATCACTCGAGTTACTTGACAGCTCGTCCATG
EGFP_for(NdeI)	AATCACCAATATGCTGAGCAAGGGCGAGGAG
mRFP_for(KpnI)	AATCAGGTACCcCTCCTCCGAGGACGTCATC
mRFP_rev(XhoI)	AATCACTCGAGCTACCCTTGGCGCCGGTG
mRFP_for(NdeI)	AATCACCAATATGCTCCTCCTCCGAGGACGTCATC

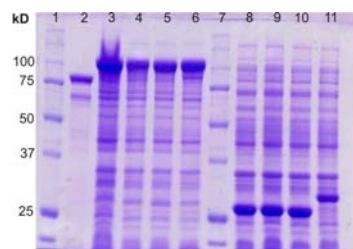
<sup>a</sup> Artificial restriction sites are underlined; lowercase letters indicate changes in the chromosomal DNA sequence. The triples corresponding to the initiation and termination codons in the primer sequence are shown in boxes.

**Table 3:** Characteristic parameters of chimeric fluorescent S-layer fusion proteins and fluorescent proteins

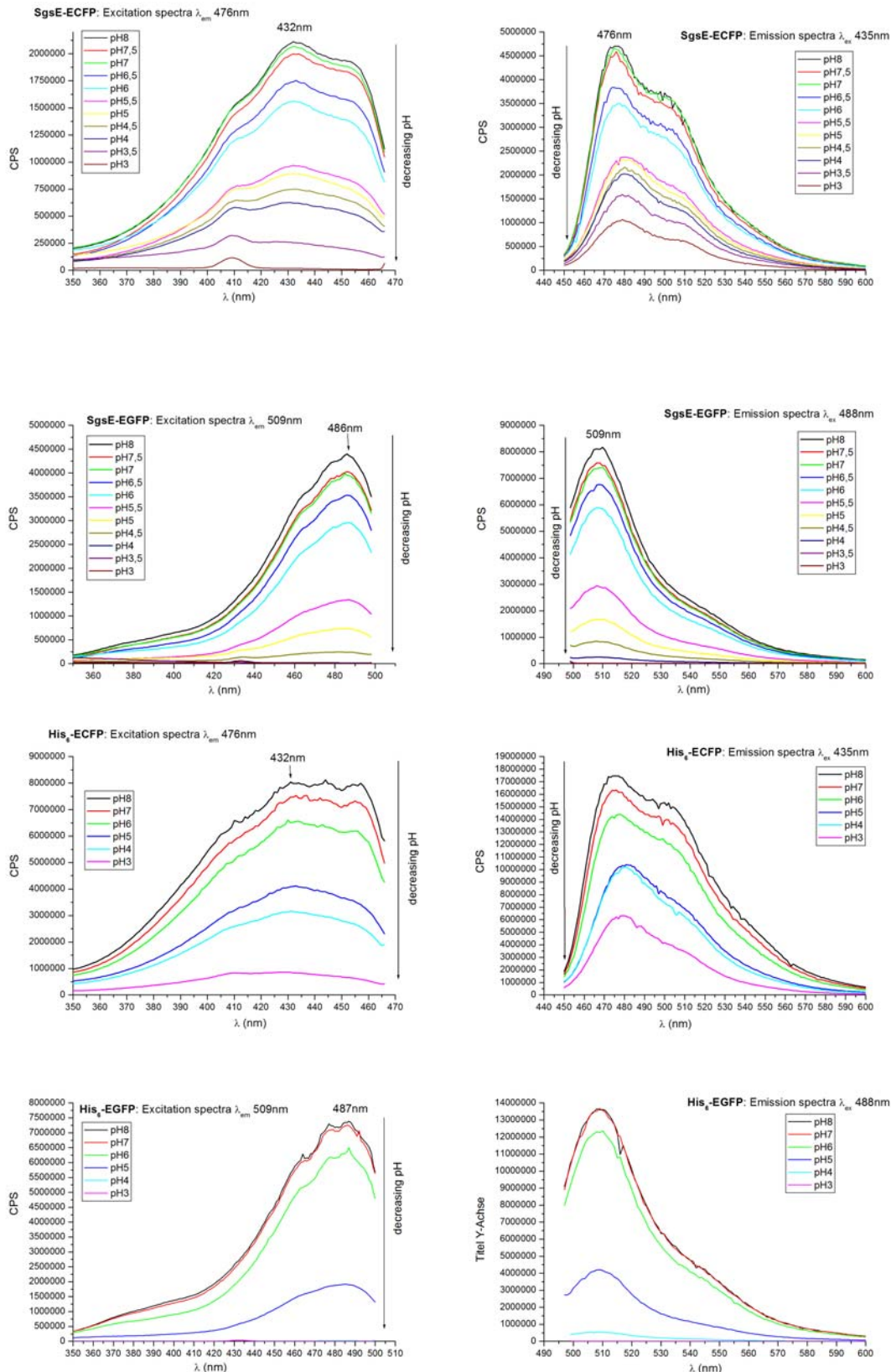
Protein	Mw (kDa)	pI	$\epsilon_{280nm}$ (L/mol*cm)	$\lambda_{ex}$ (nm)	$\lambda_{em}$ (nm)
C_SgsE truncated	82.795	5.556	36410		
SgsE-EGFP	109.783	5.523	56420	485	509
SgsE-mRFP1	108.194	5.546	67560	585	607
SgsE-YFP	109.833	5.523	57700	514	527
SgsE-ECFP	109.747	5.523	60830	433	477
His <sub>6</sub> -EGFP	29.105	6.136	20010	510	509
His <sub>6</sub> -mRFP1	27.587	6.335	31150	585	607
His <sub>6</sub> -YFP	29.155	6.136	21290	527	527
His <sub>6</sub> -ECFP	29.069	6.136	24420	433	477

**Figure 1:** SDS/PAGE pattern of the expressed fusion proteins

Lanes: 1,7 Standard All Blue (Bio-RAD), 2 SgsE (Mw 82.795 kD), 3 SgsE-ECFP (Mw 109.747 kD), 4 SgsE-EGFP (Mw 109.783 kD). 5 SgsE-YFP (Mw 109.833 kD), 6 SgsE-mRFP1 (Mw 108.194 kD), 8 His<sub>6</sub>-ECFP (29.069 kD), 9 His<sub>6</sub>-EGFP (29.105 kD), His<sub>6</sub>-YFP (29.155 kD), His<sub>6</sub>-mRFP1 (Mw 27.587 kD)



**Figure 2:** Fluorescence emission spectra of the fluorescence fusion proteins and His<sub>6</sub>-tagged fluorescence proteins in CP buffer (10mM citric acid/20mM sodium phosphate) at various pH values. The fluorescence is similar for both proteins.



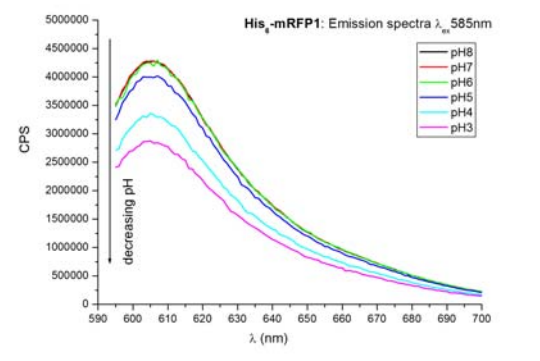
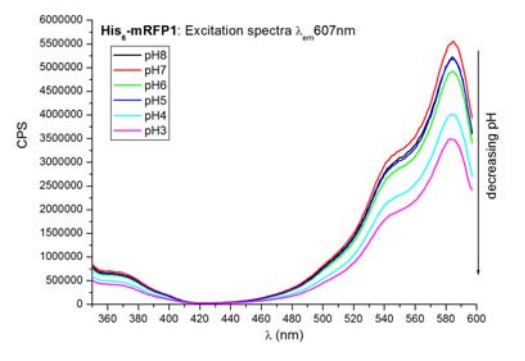
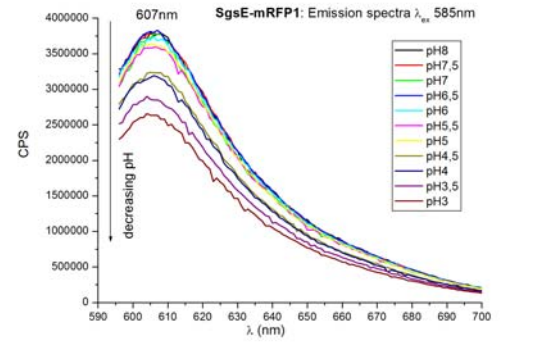
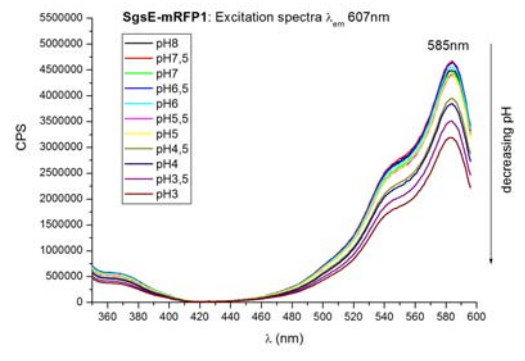
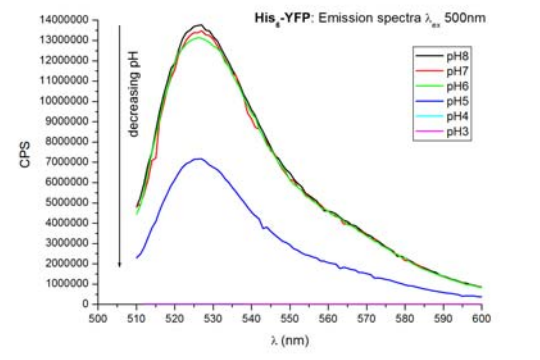
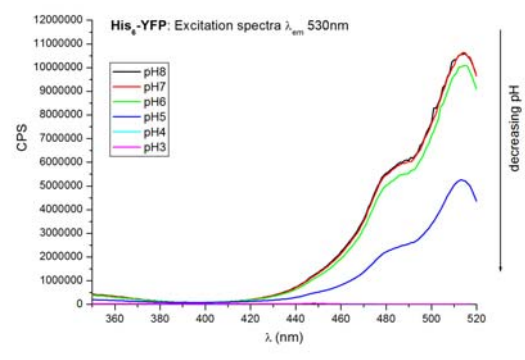
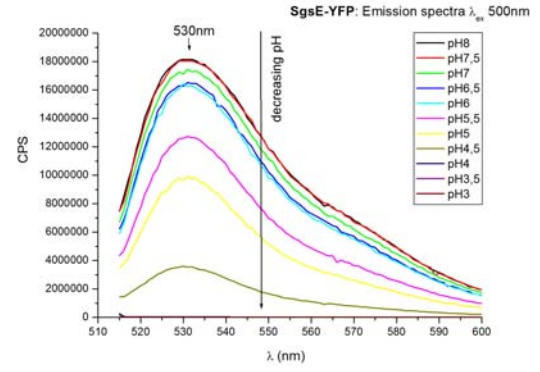
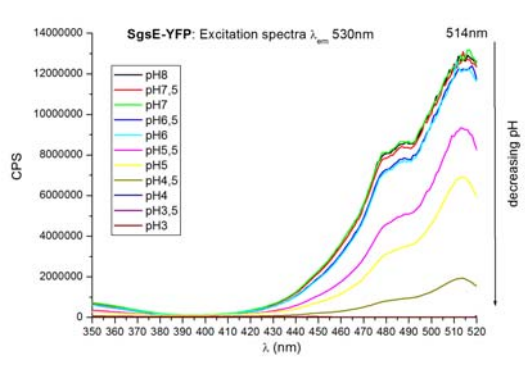
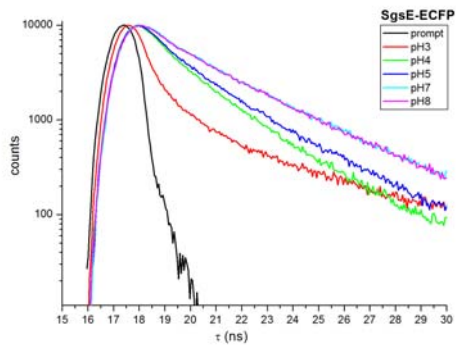
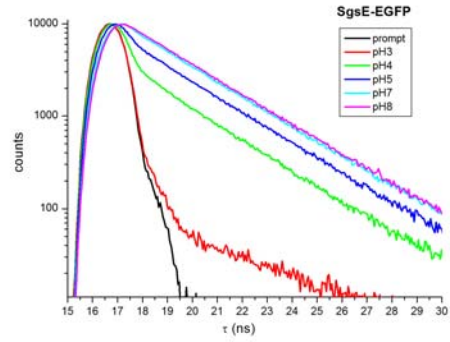


**Figure 3:** Counts versus lifetime of the following fluorescent fusion proteins: a) SgsE-ECFP, b) SgsE-EGFP and c) SgsE-YFP

a)



b)



c)

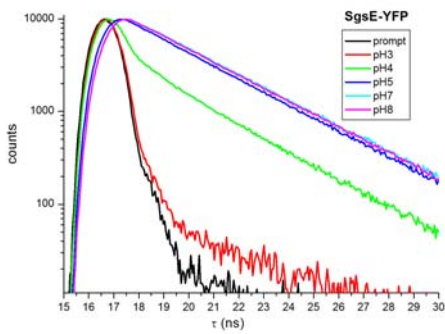


**Table 4:** Lifetime of the bacterial fluorescent fusion proteins and the His<sub>6</sub>-tagged fluorescent proteins.

**C SgsE-eGFP**

	$\tau 1$ (sec)	sDev	$\tau 2$ (sec)	sDev	$\tau 3$ (sec)	sDev	rel.Ampl1	sDev	rel.Ampl2	sDev	rel.Ampl3	sDev	ChiS	$\tau$ (fl)
pH8	1,25E-09	9,42E-12	1,12E-08	3,70E-09	2,80E-09	9,04E-12	12,99	2,57E-04	0,2	4,80E-06	86,8	1,32E-04	1,04	<b>2,61E-09</b>
pH7	1,56E-09	1,44E-10	2,75E-09	9,89E-12	3,46E-11	8,44E-12	7,78	3,21E-04	69,81	1,66E-04	22,41	9,83E-03	0,73	<b>2,05E-09</b>
pH5	1,59E-09	1,61E-10	2,73E-09	1,27E-11	4,99E-11	6,52E-12	7,66	2,85E-04	56,04	1,47E-04	36,3	5,31E-03	0,74	<b>1,67E-09</b>
pH4	1,54E-09	1,65E-10	6,12E-11	4,65E-12	2,72E-09	1,82E-11	7,85	2,18E-04	58,35	3,80E-03	33,79	1,04E-04	0,73	<b>1,07E-09</b>
pH3	1,09E-10	2,10E-11	1,08E-10	1,12E-11	3,87E-09	6,98E-11	-1725,61	0,46	1823,44	0,47	2,17	7,48E-06	0,74	<b>1,63E-10</b>

**his6-eGFP**

	$\tau 1$ (sec)	sDev	$\tau 2$ (sec)	sDev	$\tau 3$ (sec)	sDev	rel.Ampl1	sDev	rel.Ampl2	sDev	rel.Ampl3	sDev	ChiS	$\tau$ (fl)
pH8	2,15E-09	1,00E-10	3,34E-09	2,84E-10	4,38E-09	1,90E-10	43,73	3,89E-04	69,73	4,81E-04	-13,46	1,93E-04	0,75	<b>2,68E-09</b>
pH7	2,28E-09	5,76E-11	6,27E-09	1,15E-09	3,16E-09	4,31E-11	49,54	3,68E-04	-1,48	3,05E-05	51,93	3,07E-04	0,70	<b>2,68E-09</b>
pH5	2,28E-09	1,80E-10	2,35E-09	1,26E-10	2,31E-09	7,98E-11	11306,98	3,41E-01	6937,97	1,82E-01	-18145	5,24E-01	0,72	<b>2,66E-09</b>
pH4	2,27E-09	3,41E-11	4,46E-09	1,41E-09	3,51E-09	7,38E-11	55,86	3,70E-04	-15,54	2,10E-04	59,68	4,85E-04	0,73	<b>2,67E-09</b>
pH3	4,31E-11	6,78E-12	6,25E-10	6,07E-11	6,48E-09	4,91E-10	97,81	6,73E-03	1,75	1,59E-04	0,44	3,10E-06	1,27	<b>8,16E-11</b>

**C SgsE-eYFP**

	$\tau 1$ (sec)	sDev	$\tau 2$ (sec)	sDev	$\tau 3$ (sec)	sDev	rel.Ampl1	sDev	rel.Ampl2	sDev	rel.Ampl3	sDev	ChiS	$\tau$ (fl)
pH8	3,03E-09	1,61E-10	6,69E-09	1,38E-09	6,69E-09	4,57E-10	97,97	1,40E-04	44397,89	7,85E-01	-44395,9	7,85E-01	0,88	<b>3,02E-09</b>
pH7	1,33E-10	2,65E-11	3,09E-09	5,36E-12	1,40E-08	1,27E-09	-2,19	9,48E-04	102,66	7,74E-05	-0,47	3,49E-06	0,81	<b>3,11E-09</b>
pH5	2,90E-10	6,01E-11	2,87E-09	1,60E-10	2,88E-09	8,10E-11	4,14	6,09E-04	-871,51	1,76E-02	967,38	1,75E-02	0,94	<b>2,91E-09</b>
pH4	1,05E-09	8,39E-11	6,97E-11	6,17E-12	2,87E-09	1,23E-11	8,57	2,73E-04	47,02	3,57E-03	44,41	7,54E-05	0,93	<b>1,40E-09</b>
pH3	9,41E-11	1,64E-11	9,35E-11	1,25E-11	3,97E-09	1,73E-10	-5155,74	1,54	5254,34	1,55	1,4	7,13E-06	1,27	<b>1,20E-10</b>

**his6-eYFP**

	$\tau 1$ (sec)	sDev	$\tau 2$ (sec)	sDev	$\tau 3$ (sec)	sDev	rel.Ampl1	sDev	rel.Ampl2	sDev	rel.Ampl3	sDev	ChiS	$\tau$ (fl)
pH8	1,54E-09	9,06E-11	3,15E-09	1,30E-11	1,70E-08	1,47E-09	0,00	2,49E-04	1,01E+02	1,40E-04	-0,53	2,67E-06	1,06	<b>3,08E-09</b>
pH7	5,43E-10	1,95E-11	3,16E-09	7,35E-12	1,69E-08	1,30E-09	-0,77	6,03E-02	101,32	8,77E-05	-0,55	2,67E-06	1,12	<b>3,10E-09</b>
pH5	1,34E-09	8,77E-12	3,02E-09	9,22E-12	1,89E-11	5,11E-12	4,14	3,21E-04	72,45	1,33E-04	23,41	4,31E-02	1,04	<b>2,24E-09</b>
pH4	1,37E-09	8,84E-12	3,02E-09	8,98E-12	1,22E-11	2,17E-12	2,84	3,19E-04	47,85	1,35E-04	49,31	2,18E-01	1,03	<b>1,49E-09</b>
pH3	5,30E-11	4,12E-12	1,52E-09	8,71E-10	3,17E-09	1,48E-10	98,88	-4,72E-04	7,20E-01	6,18E-05	1,84	2,05E-05	0,96	<b>1,22E-10</b>

**C SgsE-eCFP**

	$\tau 1$ (sec)	sDev	$\tau 2$ (sec)	sDev	$\tau 3$ (sec)	sDev	rel.Ampl1	sDev	rel.Ampl2	sDev	rel.Ampl3	sDev	ChiS	$\tau$ (fl)
pH8	1,52E-09	7,10E-11	7,08E-11	1,50E-11	3,69E-09	1,53E-11	17,25	2,15E-04	27,67	3,08E-03	55,08	7,58E-05	1,02	<b>2,31E-09</b>
pH7	1,48E-09	8,61E-11	7,62E-11	7,74E-12	3,65E-09	1,73E-11	13,76	1,97E-04	39,18	2,81E-03	47,06	6,65E-05	1,06	<b>1,95E-09</b>
pH5	1,46E-09	8,36E-11	7,94E-11	7,15E-12	3,06E-09	3,03E-11	19,9	1,85E-04	53,08	2,58E-03	27,02	6,87E-05	1,08	<b>1,16E-09</b>
pH4	1,05E-09	9,84E-11	5,54E-11	6,59E-12	2,51E-09	2,17E-11	9,04	2,21E-04	70,39	4,67E-03	20,57	6,49E-05	1,02	<b>6,51E-10</b>
pH3	1,22E-09	9,32E-11	6,87E-11	6,28E-12	2,66E-09	2,77E-11	11,58	1,83E-04	71,02	3,21E-03	17,41	5,97E-05	0,85	<b>6,53E-10</b>

**his6-eCFP**

	$\tau 1$ (sec)	sDev	$\tau 2$ (sec)	sDev	$\tau 3$ (sec)	sDev	rel.Ampl1	sDev	rel.Ampl2	sDev	rel.Ampl3	sDev	ChiS	$\tau$ (fl)
pH8	1,52E-09	9,06E-11	3,65E-09	1,53E-11	6,51E-11	1,28E-11	14,83	2,12E-04	5,51E+01	7,58E-05	30,1	3,45E-03	1,01	<b>2,25E-09</b>
pH7	1,50E-09	7,57E-11	3,64E-09	1,51E-11	6,61E-11	1,16E-11	16,16	2,12E-04	53,38	7,39E-05	30,46	3,39E-03	0,96	<b>2,21E-09</b>
pH5	1,46E-09	5,82E-11	7,30E-11	1,27E-11	3,18E-09	2,30E-11	25,41	1,90E-04	45,55	2,89E-03	29,04	6,73E-05	0,87	<b>1,33E-09</b>
pH4	1,23E-09	7,68E-11	8,21E-11	6,72E-12	2,58E-09	2,20E-11	16,2	2,22E-04	56,14	2,56E-03	27,65	7,85E-05	0,92	<b>9,59E-10</b>
pH3	4,21E-11	4,16E-12	4,40E-10	4,81E-11	1,64E-09	1,19E-10	97,71	8,56E-03	1,97E+00	3,63E-04	3,20E-01	1,75E-05	0,56	<b>5,51E-11</b>

**SgsE-mRFP1**

	$\tau 1$ (sec)	sDev	$\tau 2$ (sec)	sDev	$\tau 3$ (sec)	sDev	rel.Ampl1	sDev	rel.Ampl2	sDev	rel.Ampl3	sDev	ChiS	$\tau$ (fl)
pH8	5,75E-10	1,88E-10	5,71E-10	1,56E-10	1,59E-09	8,89E-11	5488,33	5,98E-01	-5490,01	5,99E-01	101,68	1,86E-03	1,19	<b>1,83E-09</b>
pH7	4,47E-10	1,77E-10	4,42E-10	2,40E-10	1,39E-09	4,28E-11	1368,48	4,48E-01	-1399,06	4,49E-01	130,58	1,72E-03	1,21	<b>1,75E-09</b>
pH5	4,71E-10	1,53E-10	3,60E-10	1,13E-10	1,35E-09	3,50E-11	15,02	1,95E-02	-49,46	2,07E-02	134,44	1,76E-03	1,23	<b>1,70E-09</b>
pH4	4,83E-10	7,57E-11	8,61E-10	1,49E-10	8,62E-10	8,73E-11	18,66	1,25E-02	-36263,83	2,22E+00	36345,17	2,21E+00	1,39	<b>1,34E-09</b>
pH3	4,22E-10	2,09E-10	4,14E-10	1,64E-10	1,32E-09	3,72E-11	0	3,78E-03	-0,01	7,27E-04	100,01	1,43E-04	1,23	<b>1,32E-09</b>

**his<sub>6</sub>-mRFP1**

	$\tau 1$ (sec)	sDev	$\tau 2$ (sec)	sDev	$\tau 3$ (sec)	sDev	rel.Ampl1	sDev	rel.Ampl2	sDev	rel.Ampl3	sDev	ChiS	$\tau$ (fl)
pH8	4,60E-10	2,11E-10	4,59E-10	2,63E-11	1,39E-09	5,64E-11	10537,48	3,68E+00	-1,06E+04	3,68E+00	1,31E+02	2,14E-03	1,17	<b>1,76E-09</b>
pH3	4,84E-10	1,74E-10	4,84E-10	1,47E-10	1,43E-09	5,98E-11	29894,91	5,39E+00	-2,99E+04	9,56E-02	1,19E+02	1,84E-03	1,36	<b>1,73E-09</b>
pH5	4,94E-10	2,04E-10	4,96E-10	1,39E-10	1,36E-09	4,62E-11	-5873,18	1,55E+00	5839,81	1,55E+00	133,37	2,34E-03	1,04	<b>1,74E-09</b>
pH4	2,32E-10	4,88E-11	1,04E-09	1,62E-10	1,05E-09	6,65E-11	-20,21	6,14E-03	-17737,53	8,82E-01	17857,74	8,79E-01	1,25	<b>1,62E-09</b>
pH7	7,41E-10	1,49E-10	7,36E-10	9,43E-11	7,54E-10	6,20E-11	-257802,5	2,54E+01	187141	1,89E+01	70761,51	6,60E+00	1,38	<b>1,31E-09</b>

**Figure 5:** Electron microscopy micrographs: a) SgsE-YFP, b) SgsE-ECFP, c) SgsE-mRFP1

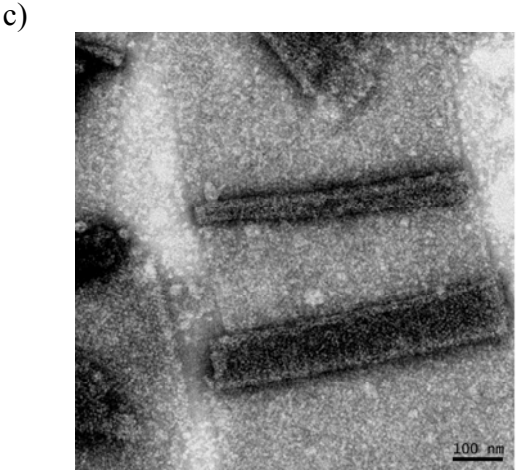
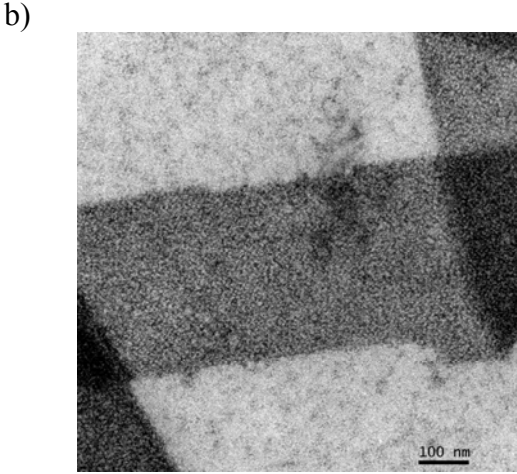
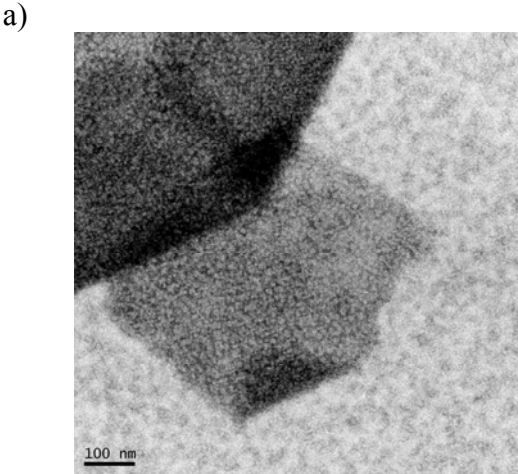
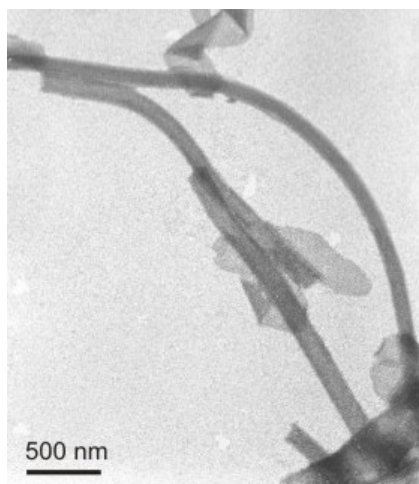
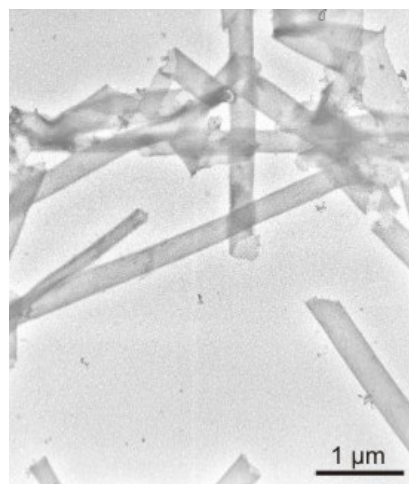


**Figure 6:** Electron microscopy micrographs self assemblies a) SgsE-mRFP1, b) SgsE-ECFP, c) SgsE-EGFP, d) SgsE-YFP

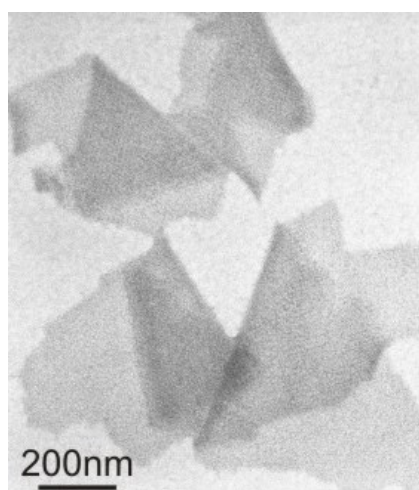
a)



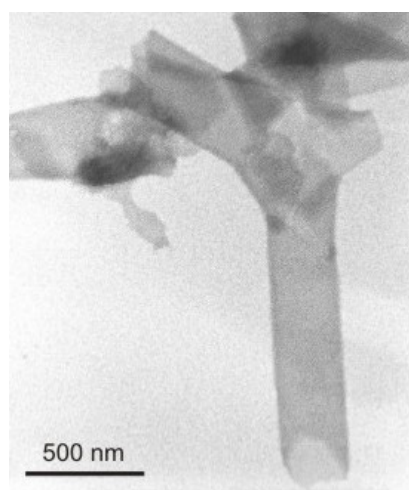
b)



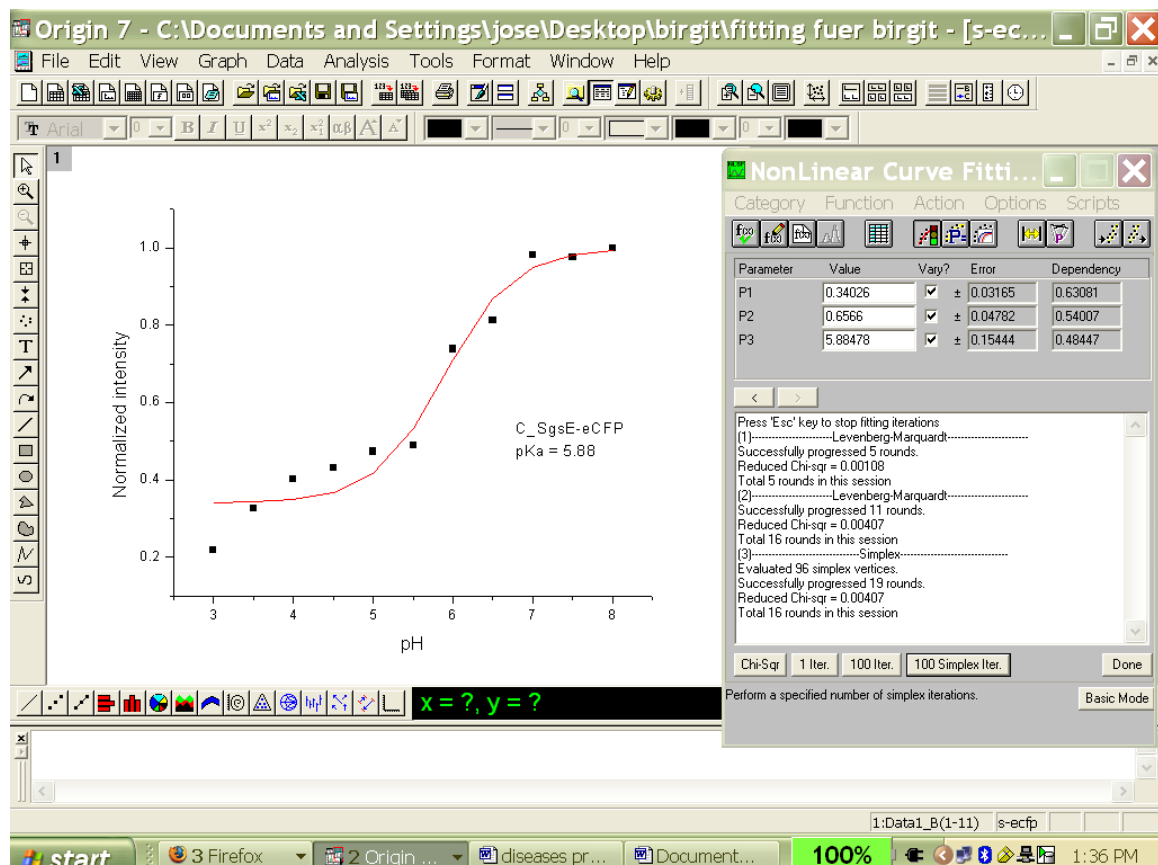
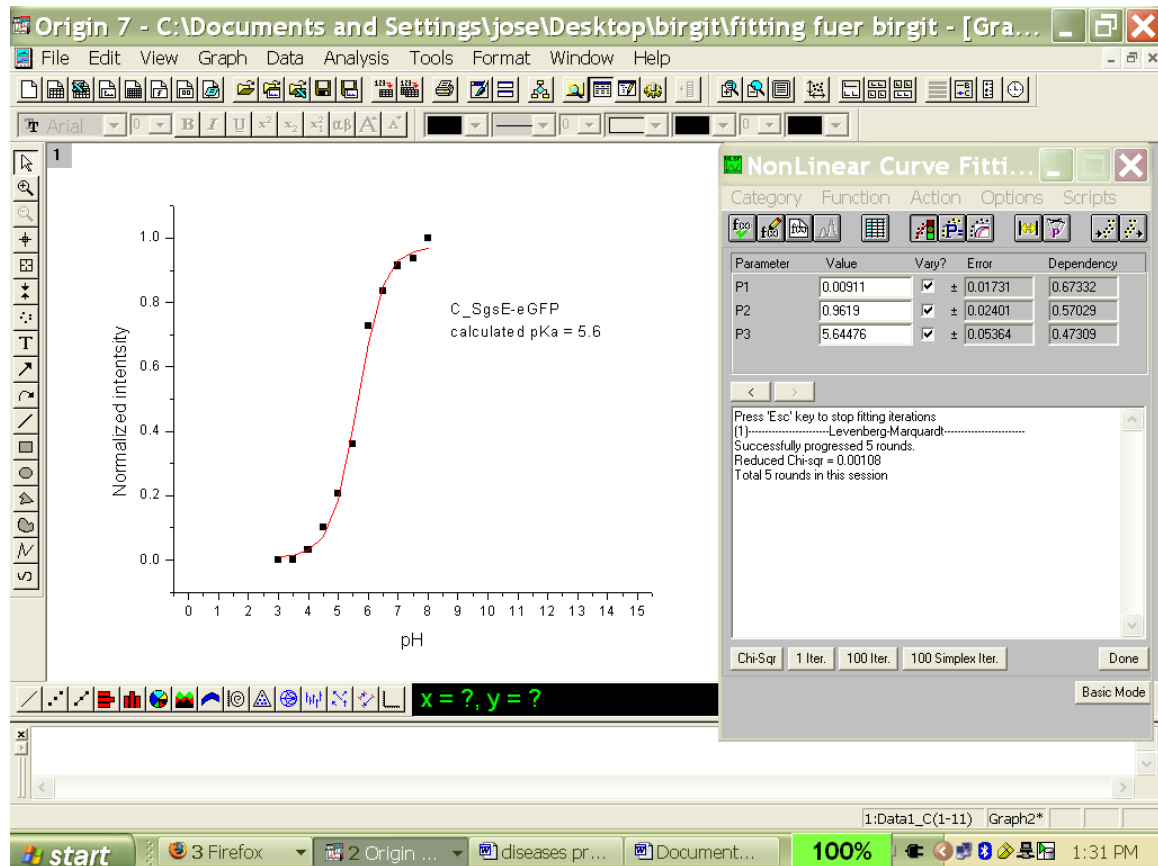
c)

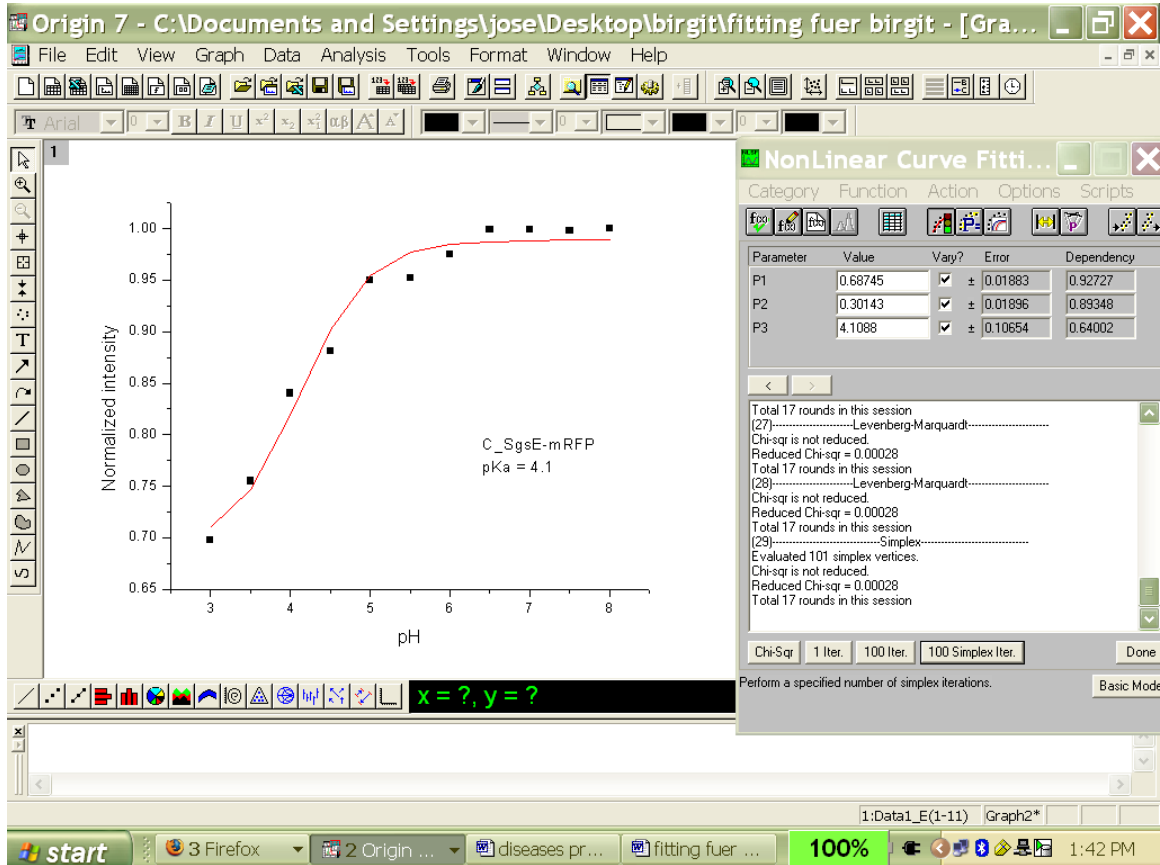
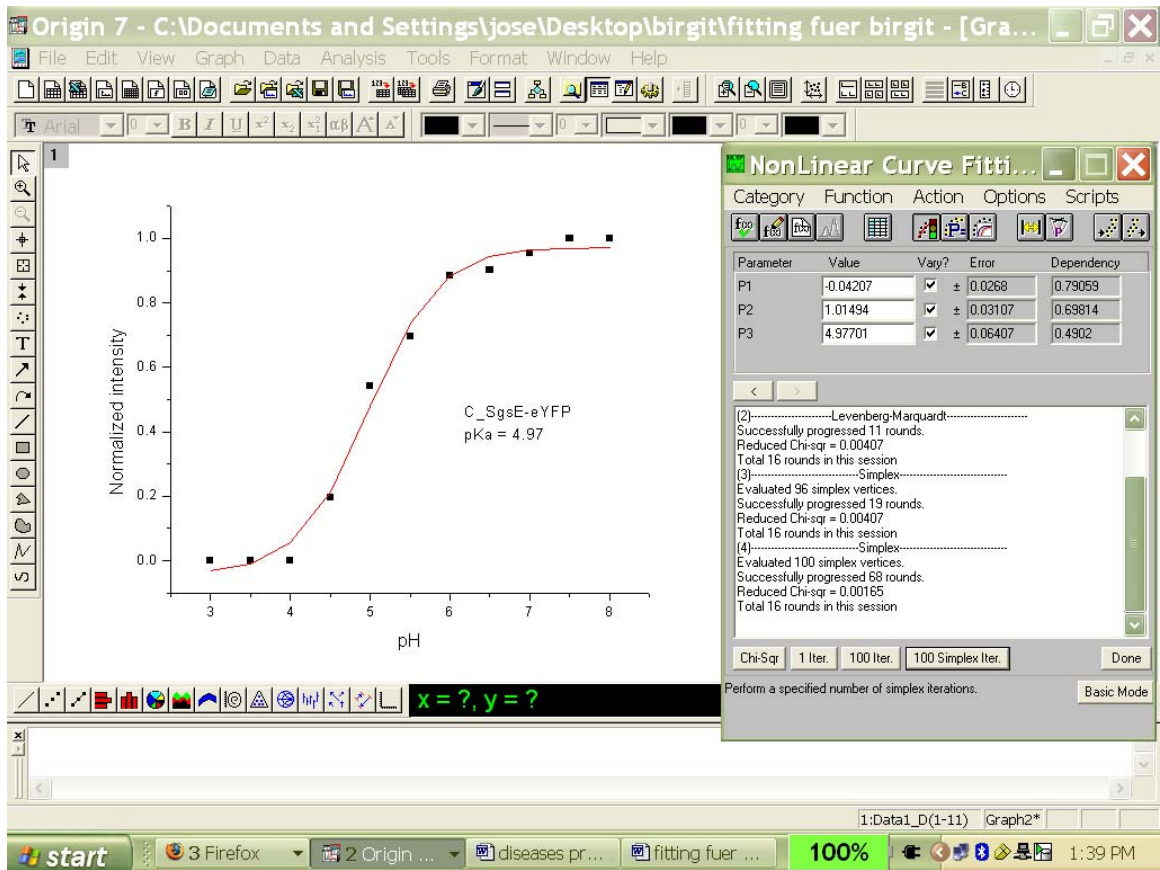


d)



**Figure 7:** Estimation of the pKa values of the fluorescence fusion proteins (see details in text). The following equation  $F = x + y / (1 + 10^z)$  was introduced in the fitting procedure of Origin 7.





# Fluorescent S-Layer Protein Colloids

5 **Birgit Kainz,\*<sup>1</sup> Kerstin Steiner,<sup>1,2</sup> Uwe B. Sleytr,<sup>1</sup> Dietmar Pum<sup>1</sup> and José Luis Toca-Herrera\*<sup>3</sup>**

10 <sup>1</sup> Department for NanoBiotechnology, University of Natural Resources and Applied Life Sciences (BOKU), 1190 Vienna (Austria)

<sup>2</sup> Biomolecular Science Research Complex, University of St Andrews, North Haugh, KY169ST St Andrews (Scotland)

15 <sup>3</sup> CICbiomaGUNE, Biosurfaces Unit, Paseo Miramón 182, 20009 San Sebastián (Spain)

20 Corresponding author:  
Jose L. Toca-Herrera, E-mail: [jltocaherrera@cicbiomagune.es](mailto:jltocaherrera@cicbiomagune.es)

Co-corresponding author:  
Birgit Kainz, E-mail: [birgit.kainz@boku.ac.at](mailto:birgit.kainz@boku.ac.at)

25

30 Keywords: fluorescence, S-layer fusion proteins, biocolloids, pH-biosensor

Four different coloured pH dependent biocolloids have been designed with fluorescent S-layer fusion proteins. The intrinsic self assembling capability of the S-layer protein  
35 SgsE on silicon dioxide particles leading to crystalline p2 lattice symmetry was combined with the fluorescent properties of fused cyan ECFP, green EGFP, yellow YFP and red mRFP1. Confocal microscopy was used to monitor the pH dependence of the fluorescent S-layer coating. Electrophoretic measurements were carried out to understand the colloidal behaviour of the S-layer protein coated particles. It was found  
40 with flow cytometry that the stable SgsE-ECFP, SgsE-EGFP, SgsE-YFP and SgsE-mRFP bioparticle suspensions lost 50 % of the fluorescence emission at the pKa of the chromophores. These novel fluorescent S-layer biocolloids can be used as pH sensor and might have an important role in surface pH determination.

## Introduction

Biofunctional fluorescent particles and capsules are playing an increasing role in biophysics and biomedicine. They are highly useful for biosensing and bioimaging in cell and drug delivery studies.<sup>[1]</sup> An interesting biointerface engineering technique is the layer-by-layer deposition of fluorescently labelled oppositely charged polyelectrolytes onto colloidal particles or capsules.<sup>[2-5]</sup> In another method proteins are attached to sensor surfaces and subsequently labelled with organic fluorophores by covalently conjugating them to specifically activated groups of the proteins or just by unspecific adsorption.

Fluorescent labelled liposomes are often used for drug delivery systems.<sup>[6]</sup> A key issue in biosensor technology is the design and making of multifunctional, nanostructured biomimetic surfaces with specific physical properties. This work describes a new approach for making pH-dependent fluorescent biocolloids by using ECFP, EGFP, YFP and mRFP S-layer fusion proteins (crystalline bacterial surface layer proteins) as scaffold and sensing element simultaneously.<sup>[7,8]</sup> S-layers are one of the most common cell envelopes in bacteria and archaea.<sup>[9,10]</sup> Isolated S-layer subunits have the intrinsic ability to self-assemble forming molecular protein arrays similar to those originally found in the bacteria and archaea. They can be recrystallised on different type of substrates, such as silicon,<sup>[11]</sup> disulfides,<sup>[12]</sup> liposomes<sup>[13]</sup> or polymers<sup>[14]</sup>. Therefore the S-protein layers can be used as scaffold to immobilise other biomolecules, leading to the so called S-layer fusion proteins. In the last years recombinant S-layer fusion proteins incorporating enzymes, fluorescent proteins and allergens have been already designed for a broad range of applications in nanobiotechnology and biomimetics.<sup>[15-22]</sup> These S-layer proteins combine the functionality of the genetically fused moieties with their intrinsic self-assembly properties to build well-defined 2D-lattices. They can be used as nanopatterning element for creating novel surface materials at the nanoscale.<sup>[7,23-25]</sup> In general, for fluorescence setups, S-layers are labelled with dyes in a covalent way after activating the carboxyl groups or by genetically inserted cysteine groups.<sup>[26,27]</sup> In previous works, an EGFP S-layer fusion protein was used to functionalise liposomes, polyelectrolyte hollow capsules and microstructured surfaces.<sup>[16, 28-30]</sup> The big advantage of genetically engineered fluorescent S-layer fusion proteins is the 1:1 stoichiometry of fluorescent protein to S-layer protein as shown in Figure 1a. These proteins can be expressed, purified and reassembled without further labelling steps. In a previous work

we described the design of the four different coloured S-layer fluorescent fusion proteins SgsE-ECFP (cyan), SgsE-EGFP (green), SgsE-YFP (yellow) and SgsE-mRFP (red).<sup>[8]</sup>

The different green fluorescent protein (GFP) variants ECFP, EGFP and YFP as well as the monomeric red fluorescent protein mRFP are widely used for genetic protein targeting and cell biology studies. For these proteins, fluorescence quenching is a well-known effect that occurs when the chromophores change from their anionic to their cationic; a fact also observed with the fluorescent S-layer fusion proteins in solution.<sup>[8,31,32]</sup>

10 In this work, we have focused on the design of novel pH sensitive S-layer biocolloids. For this purpose the four different fluorescent S-layer fusion proteins<sup>1</sup> SgsE-ECFP, SgsE-EGFP, SgsE-YFP and SgsE-mRFP, were recrystallised on silicon dioxide microparticles.<sup>[8,33]</sup> Atomic force microscopy has been used to study the nanostructure of the self- assembled protein layers. Zeta potential measurements were performed to follow the particle coating and to understand the colloidal behaviour of the S-layer bioparticles. Confocal microscopy and flow cytometry measurements were carried out to study the fluorescence behavior under different pH conditions. In addition the pKa value of the fused chromophore has been determined.

## 20 **Experimental**

### **Materials and sample preparations**

The engineering of the fluorescent S-layer fusion proteins SgsE-ECFP, SgsE-EGFP, SgsE-YFP and SgsE-mRFP<sup>1</sup> incorporating the N-terminal truncation rSgsE<sub>131-903</sub> and C-terminal fluorescent proteins was described in a previous work.<sup>[8]</sup> Expression of the four fluorescent S-layer fusion proteins in *E. coli* BL21 Star (DE3), isolation from the inclusion bodies, FPLC-purification (Superdex 200 prep grade XK16, GE-Healthcare) and dialysing against Milli-Q water to obtain monomer solutions have been carried out as described previously.<sup>[8, 22]</sup> Protein concentrations were determined with NanoDrop spectrophotometer (ND-1000, Peqlab Biotechnology, Germany) at 280 nm. Finally, the proteins were diluted to 1.0 mg/ml with Milli-Q water and the monomer solutions were stored at 4°C in the dark. Silicon dioxide microparticles of 3 and 1 µm-diameter

---

<sup>1</sup> The S-layer protein used was SgsE of *Geobacillus stearothermophilus* NRS 2004/3a with oblique (p2) lattice symmetry.

were purchased from Fluka (Austria); 8  $\mu\text{m}$ -diameter  $\text{SiO}_2$ -microparticles were purchased from Microparticles (Berlin).

The coating of the  $\text{SiO}_2$ -microparticles was carried out in HBSS (Hank's buffered saline solution) containing 0.1 mg/ml the S-layer (fusion) proteins (SgsE, SgsE-EGFP, SgsE-YFP, SgsE-ECFP, SgsE-mRFP1). The reassembling process was carried out under rotation on a Test Type Rotator for 4 h at room temperature. The excess of non-assembled proteins in solution was removed by repeated centrifugation (Eppendorf bench centrifuge, 13.000g, room temperature, 15 sec) and washing steps with Milli-Q water. Fluorescent S-layer biocolloids were stored in Milli-Q water at 4°C in the dark.

10 Fluorescence measurements were carried out by immersing the fluorescent S-layer biocolloids in McIlvaine CP (10mM citric acid/20mM sodium phosphate) buffer solutions ranging from pH 8 to pH 3 in pH 0.5 steps.

#### **Atomic force microscopy**

15 AFM measurements were carried out in contact mode with a Nanoscope IIIa multimode (Veeco Instruments, Santa Barbara, CA) with a J-scanner (nominal scan size 130  $\mu\text{m}$  x 130  $\mu\text{m}$ ). Silicon nitride cantilevers with a nominal spring constant of about 0.06  $\text{Nm}^{-1}$  (NP-S, NanoProbes, Digital Instruments, Santa Barbara, CA) were used. Samples were measured in 100 mM NaCl-solution to avoid electrostatic interactions between tip and

20 sample. The imaging scan rate was approximately 4 Hz and the applied force during scanning was minimized to prevent the tip from modifying the sample. Lattice parameters were determined using Crisp 2.1 software (Calidris, Sweden).

#### **Confocal microscopy**

25 Confocal laser scanning microscopy studies of the S-layer coated 8  $\mu\text{m}$  sized  $\text{SiO}_2$ -particles were performed using a Zeiss LSM510 Meta (Zeiss, Jena, Germany) microscope with an Argon/2 laser (458-nm, 488-nm, 514-nm), a DPSS 561-10 laser (561-nm) and an additional TCSPC SPC-130 module (time-correlated single photon counting modul, bh Becker&Hickel GmbH, Berlin Germany) with an external 405-nm

30 laser, a DCC-100 Detector control module for FLIM measurements (fluorescence lifetime imaging microscopy) and SPCImage 2.8 data software. Measurements were carried out in Nunc-chambers (VWR, Vienna) at pH 8, pH 5 and pH 3. The fluorescence of the samples was recovered by centrifugation the particles in pH 3 solution and incubating them again in pH 8 solution. SgsE-EGFP proteins were imaged

with the 488-nm laser line using a BP505-530 emission filter, SgsE-YFP proteins with the 514-nm laser line and a BP520-555IR emission filter, SgsE-ECFP proteins with the 458-nm laser line and a LP475 emission filter and SgsE-mRFP1 with the 561-nm laser line and a LP575 emission filter. Images and wavelength scan data were taken using the  
5 ZEN software (Zeiss, Jena, Germany) and analyzed with Zeiss LSM Image Browser software. FLIM measurements were carried out at pH 8 with DCC standard software and SPCImage 2.8 data analysis software (bh Becker&Hickel GmbH, Berlin Germany).

### **Flow cytometry**

10 Flow cytometry measurements were performed on a CantoII Flow cytometer (BD Biosciences). Ten thousand events of 3  $\mu\text{m}$ -diameter fluorescent SgsE biocolloids were measured in pH-solutions ranging from pH 8 to pH 3. A violet 405-nm diode laser was used for excitation of SgsE-ECFP and the emission was detected through an AmpCyan 450/50-nm emission filter. Excitation of SgsE-EGFP, SgsE-YFP and SgsE-mRFP were  
15 performed with the blue 488-nm diode laser whereas the fluorescence of SgsE-EGFP and SgsE-YFP were detected through a FITC 530/30-nm emission filter and the SgsE-mRFP emission through a PE 585/42-nm filter. Data analysis was performed using BD FACSDiva 6.0 software (BD Biosciences).

### **20 IEP determination**

Electrophoretic mobility measurements of 1  $\mu\text{m}$ -diameter fluorescent S-layer biocolloids were carried out using a Malvern Zetasizer Nano ZS with an MPT-2 Autotitrator (Malvern Instruments, UK). Experiments were started in 1 mM KCl/HCl solution at pH 8 and titrations were carried out with HCl (0.01 M, 0.1 M) until pH 3 (pH  
25 steps 0.5). The electrophoretic mobility was converted into zeta potential using the Smoluchowski equation.<sup>[34]</sup>

30

35

## Results and Discussion

Fluorescent SgsE biocolloids were made by coating silica particles with SgsE-ECFP, SgsE-EGFP, SgsE-YFP and SgsE-mRFP fluorescent S-layer fusion proteins. As an example, yellow SgsE-YFP biocolloids are shown in Figure 1b and Figure 1c. The intrinsic self-assembly capability and the nanostructure of the fluorescent SgsE fusion proteins were investigated by atomic force microscopy (AFM). The deflection AFM image (Figure 1b) revealed the formation of protein crystal monolayers with oblique p2 lattice symmetry on an 8  $\mu\text{m}$  diameter  $\text{SiO}_2$ -particle. All four fluorescent S-layer fusion proteins reassembled in patches of different size covering the entire particle, being the lattice parameters  $a=11.2 (\pm 0.5)$  nm,  $b=8.8 (\pm 0.4)$  nm and  $\gamma=79.1 (\pm 1)^\circ$ . These values are similar to those obtained for self-assemblies in solution, investigated with electron microscopy in a previous work.<sup>[8]</sup> These results indicate that silicon dioxide particles are a good template to fabricate functional biomimetics colloids since the nanostructure of the S-layer protein and the function of the incorporated fluorescent tag are preserved.

The S-layer coating was also monitored with zeta potential measurements as a function of pH (Figure 2). In this way, the isoelectric point (IEP) of the bare silica particles (black squares) and the S-layer biocolloids was determined. It can be observed that the IEP of the fusion proteins varies between 4.5 and 4.8, while the IEP for the reference SgsE is slightly higher (5.1). Bare silica particles presented an IEP of 3.3. These values are shown in Table 1. The zeta potential values of the S-layer coated particles indicate that they are more positive than the uncoated silicon dioxide particles. The electrophoretic behaviour of the S-layer biocolloids as a function of pH was used to generate stable fluorescent colloid suspensions (discussed later with flow cytometry studies).

The changes in fluorescence emission behaviour of the fluorescent S-layer protein coated particles as a function of pH were monitored by confocal microscopy (Figure 3). SgsE-ECFP, SgsE-EGFP, SgsE-YFP and SgsE-mRFP1 biocolloids were mixed in pH 8, pH 5 and pH 3 phosphate citrate buffer solutions. The measurements indicate that in alkaline conditions (pH 8), the anionic state of the chromophores led to highest emission intensities (Figure 3a), obtaining a colourful colloidal suspension.<sup>[31]</sup> The distinction between green SgsE-EGFP and yellow SgsE-YFP was not clear because YFP was also detected by the green filter (after excitation with 488-nm). At pH 5, the

chromophores of the three GFP-mutants (SgsE-ECFP, SgsE-EGFP and SgsE-YFP) changed to their neutral state, inducing a decrease in the fluorescence emission that vanished completely in acidic conditions (pH 3). On the contrary, it could be observed that the fluorescence emission of the red SgsE-mRFP1 biocolloids was only slightly affected by pH variation. Fluorescence reversibility was tested by increasing the pH from 3 to 8 (last picture of Figure 3a). The chromophores changed again from the non-fluorescent protonated state to the fluorescent anionic state. Thus the S-layer fusion proteins seem to be stable under pH variations.

Furthermore, the fluorescent emission as a function of pH 8, pH 5 and pH 3 was verified with the wavelength-scan function of the confocal microscope (Figure 3b). The maxima of the emission spectra were 490 nm for SgsE-ECFP after excitation at 458 nm, 510 nm for SgsE-EGFP after excitation at 488 nm, 530 nm for SgsE-YFP after excitation at 514 nm, and 610 nm for SgsE-mRFP1 after excitation at 561 nm. The shape and the values of the emission spectra were similar to previously reported results for the fusion proteins in solution.<sup>[8,31]</sup> The arrows in Figure 3b indicate the loss of fluorescence emission intensity when pH is decreased from 8 to 3. It can be observed that at pH 5 SgsE-ECFP biocolloids lost around 55 %, SgsE-EGFP and SgsE-YFP biocolloids about 75 % and SgsE-mRFP1 biocolloids around 30 % of their initial intensities, measured at pH 8. Finally, at pH 3 only SgsE-mRFP1 biocolloids emitted fluorescence. The fluorescence emission studies were complemented with fluorescence lifetime experiments of the S-layer biocolloids at pH 8. The obtained results were the same to those reported for the fusion proteins in solution.<sup>[8]</sup> SgsE-YFP biocolloids presented the longest lifetime with 3 ns whereas SgsE-mRFP1 biocolloids had the shortest one (1.6 ns). The fluorescence lifetime values of SgsE-ECFP and SgsE-EGFP biocolloids were 2.3 ns and 2.6 ns respectively. The fluorescence lifetime of the fused fluorescent proteins are not affected by the supporting reassembled S-layer lattice, demonstrating that these proteins are a very stable nanostructured coating material.

The fluorescence and the colloidal properties of the S-layer coated silicon dioxide particles were studied simultaneously with flow cytometry (Figure 4). Figure 4a and Figure 4c show the forward scatter (FSC) versus the side scatter (SSC) plots for the SgsE-YFP biocolloids at pH 8 and pH 4.5 respectively<sup>2</sup>. The collected counts displayed in the dot plots of Figure 4a and Figure 4c indicate that two major populations could be differentiated according to their light scattering properties. The main population

---

<sup>2</sup> FSC is related to the size of the colloid while SSC takes into account the surface structure.

consisted of monodispersed particles (red population), while colloid aggregation was also observed (green population), being larger at pH 4.5 than at pH 8. This fact can be explained by the isoelectric point (IEP) obtained with electrophoretic measurements (see Figure 2), which showed that the biocolloids were almost uncharged between pH 4.5 and pH 4.8. In a more quantitative way, at pH 8 about 90 % of the collected counts represented monodispersed SgsE-YFP biocolloids<sup>3</sup> and only about 2 % were aggregates, whereas at pH 4.5 the amount of aggregated biocolloids increased to more than 10 %. The other fluorescent SgsE biocolloids behaved in the same way (data not shown). Quantitative information of the fluorescence emission of the monodispersed biocolloids versus pH were obtained from the histogram plots (Figure 4b and Figure 4d). In this type of plots the number of particles (counts) versus intensity are displayed. It can be observed that the biocolloids emitted more fluorescence at pH 8 (Figure 4b) than at pH 4.5 (Figure 4d). The mean values of the fluorescence emission intensity of the four coloured SgsE biocolloids between pH 8 and pH 3, obtained from the histogram plots, are presented in Figure 5. A quick look in Figure 5 reveals that the fluorescence intensity of the red biocolloids is more stable under pH variation than the colloids coated with the three different GFP variants (EGFP, ECFP, YFP). In particular, the fluorescence emission of SgsE-EGFP and SgsE-YFP biocolloids vanished at pH 4, whereas the fluorescence of the SgsE-ECFP biocolloids is more stable at acidic pH. Furthermore the dependence of the fluorescence intensity on pH can be used to obtain the the  $pK_a$  values<sup>4</sup> of the chromophore. These values were calculated with the equation  $F=x+y/(1+10^z)$ , where F was the intensity, z was ( $pK_a - pH$ ) and x and y related to the offset and the dynamic range of the data.<sup>[35]</sup> The obtained  $pK_a$  values, around  $6.0\pm 0.3$ , are in agreement with a decrease of about 50 % of the fluorescence emission intensity recorded in the studied pH range (see Table 2). In addition, the reaction standard free energy could be determined using the equation  $\Delta G^0 = -RT\ln K_a$  where  $pK_a = -\log K_a$  (see Table 2). These measurements confirmed the behavior of the fluorescent S-layer colloids observed by confocal microscopy.

30

---

<sup>3</sup> To the best of our knowledge the colloidal coloured suspensions lasted at least for a year. The suspensions are kept at four degree Celsius in the dark.

<sup>4</sup> At this value the chromophore changes from the anionic to the neutral state and the fluorescence intensity diminishes approximately by 50%.

A recent work carried out by Zhang et al., reports the influence of surface charge on the fluorescent properties of SNARF proteins.<sup>[36]</sup> Thus, a negative surface charge acting as local “proton” sink (or attractor) can induce a shift in the pH response of the fluorescent dye, if the dye is close enough to the charged surface (e.g. a few nanometers). This phenomena has also been observed after exposing albumin fluorescent particles, attached to atomic force microscopy cantilevers, to different charge surfaces.<sup>[37]</sup>

In our case, the silicon dioxide particles are negatively charged. A comparison between the  $pK_a$  value for protein solutions reported Kainz et al.<sup>[8]</sup> and the values obtained for the S-layer fluorescent colloids (Table 2), shows a  $pK_a$ -shift only for SgsE-YFP and SgsE-mRFP<sup>5</sup>.

This result indicates that both dyes are very close to the negative silicon dioxide surface. Furthermore, the result might imply that the fluorescent dye is integrated in the three dimensional folding of the recrystallised S-layer fusion protein; a fact supported by the atomic force microscopy images.

Finally, it should be pointed out that this important effect must be studied in detail in the near future, since it can deliver structural information about the tertiary structure of the recrystallized S-layer fusion proteins that is still unknown.

## Conclusion

Four different monodispersed homogenous fluorescent S-layer biocolloids were produced combining the intrinsic self assembling capability of the S-layer protein SgsE on silicon dioxide particles, and the controlled pH dependent fluorescence properties of fused cyan ECFP, green EGFP, yellow YFP and red mRFP1 fluorescent proteins. The S-layer fluorescent fusion proteins recrystallised on bare silicon dioxide particles forming lattices with p2 symmetry. The fluorescent S-layer biocolloids lost 50 % of the initial fluorescence emission at their chromophore  $pK_a$  value (between pH 4.5 and pH 5). The determination of the IEPs of the fluorescent SgsE biocolloids was used to elucidate the behavior of the colored colloidal suspensions. These novel fluorescent S-layer biocolloids represent a strong tool for engineering pH-biosensor setups and

---

<sup>5</sup> The  $pK_a$  value for SgsE-YFP and for SgsE-mRFP in solution are 5 and 4.1 respectively

surface pH determination. They can also be used as markers for controlled cellular uptake studies.

5

## 10 Acknowledgements

This work was supported by the Austrian NanoInitiative under the project SLAYSENS within the project cluster ISOTEC and by the U.S. Air Force Office of Scientific Research (AFOSR) Projects FA9550-07-0313 and FA9550-09-1-0342. This work was partially financed by the financed by the Spanish Ministry of Education and Science (Project CTQ-2007-66541). The authors thank S. Küpcü, J. Friedmann, I. Llanera, S. Moreno-Flores, C. Schäffer, P. Messner and A. Scheberl for technical support and scientific discussions.

20

## References

- [1] M. Semmling, O. Kreft, A. Munoz Javier, G. B. Sukhorukov, J. Kas, W. J. Parak, *Small*, 2008, **4**, 1763-1768.
- [2] F. Caruso, *Advanced Materials* 2001, **13**, 11-22.
- 25 [3] X. Li, Q. Hu, L. Yue, J. Shen, *Chemistry* 2006, **12**, 5770-5778.
- [4] W. Yang, D. Trau, R. Renneberg, N. T. Yu, F. Caruso, *J. Coll. Interf. Sci.*, 2001, **234**, 356-362.
- [5] P. Pescador, I. Katakis, J. L. Toca-Herrera, and E. Donath, *Langmuir*, 2008, **24**, 14108-14114.
- 30 [6] G. Nordlund, R. Lonneborg, P. Brzezinski, *Langmuir*, 2009, **25**, 4601-4606.
- [7] U. B. Sleytr, C. Huber, N. Ilk, D. Pum, B. Schuster, E. M. Egelseer, *FEMS Microbiol. Lett.*, 2007, **267**, 131-144.
- [8] B. Kainz, K. Steiner, M. Möller, D. Pum, C. Schäffer, U. B. Sleytr, J. L. Toca-Herrera, *Biomacromolecules*, 2010, **11**, 207-214.
- 35 [9] U. B. Sleytr, P. Messner, D. Pum, M. Sára, *Angew. Chem. Int. Ed.*, 1999, **38**, 1034-1054.
- [10] M. Sára, D. Pum, S. Küpcü, P. Messner, U. B. Sleytr, *J. Bacteriol.*, 1994, **176**, 7182-7189.
- [11] J. L. Toca-Herrera, S. Moreno-Flores, J. Friedmann, D. Pum, U. B. Sleytr, *Microsc. Res. Techniq.*, 2004, **65**, 226-234
- 40 [12] S. Moreno-Flores, A. Kasry, H.-J. Butt, Ch. Vavilala, M. Schmittl, D. Pum, U. B. Sleytr, and J. L. Toca-Herrera, *Ang. Chem. Int. Ed.*, 2008, **47**, 4707-4710
- [13] S. Küpcü, M. Sára, U. B. Sleytr, *Biochim. Biophys. Acta* 1995, **1235**, 263-269.
- [14] M. Delcea, R. Krastev, Th. Gutberlet, D. Pum, U. B. Sleytr, J. L. Toca-Herrera, *Soft Matter*, 2008, **4**, 1414-1421.
- 45 [15] C. Huber, J. Liu, E. M. Egelseer, D. Moll, W. Knoll, U. B. Sleytr, M. Sára., *Small*, 2006, **2**, 142-150.

- [16] N. Ilk, S. Küpcü, G. Moncayo, S. Klimt, R. C. Ecker, R. Hofer-Warbinek, E. M. Egelseer, U. B. Sleytr, M. Sára, *Biochem. J.*, 2004, **379**, 441-448.
- [17] N. Ilk, C. Völlenklee, E. M. Egelseer, A. Breitwieser, U. B. Sleytr, M. Sára, *Appl. Environ. Microbiol.*, 2002, **68**, 3251-3260.
- 5 [18] D. Moll, C. Huber, B. Schlegel, D. Pum, U. B. Sleytr, M. Sára, *Proc. Natl. Acad. Sci. USA*, 2002, **99**, 14646-14651.
- [19] C. Völlenklee, S. Weigert, N. Ilk, E. Egelseer, V. Weber, F. Loth, D. Falkenhagen, U. B. Sleytr, M. Sára, *Appl. Environ. Microbiol.*, 2004, **70**, 1514-1521.
- 10 [20] H. Tschiggerl, A. Breitwieser, G. de Roo, T. Verwoerd, C. Schäffer, U. B. Sleytr, *J. Biotechnol.*, 2008, **133**, 403-411.
- [21] H. Tschiggerl, J. L. Casey, K. Parisi, M. Foley, U. B. Sleytr, *Bioconjug. Chem.*, 2008, **19**, 860-865.
- [22] C. Schäffer, R. Novotny, S. Küpcü, S. Zayni, A. Scheberl, J. Friedmann, U. B. Sleytr, P. Messner, *Small*, 2007, **3**, 1549-1559.
- 15 [23] U. B. Sleytr, *Int. Rev. Cytol.* 1978, **53**, 1-62.
- [24] U. B. Sleytr, T. J. Beveridge, *Trends Microbiol.*, 1999, **7**, 253-260.
- [25] U. B. Sleytr, E. M. Egelseer, N. Ilk, D. Pum, B. Schuster, *FEBS J.*, 2007, **274**, 323-334.
- 20 [26] S. R. Scheicher, B. Kainz, S. Kostler, M. Suppan, A. Bizzarri, D. Pum, U. B. Sleytr, V. Ribitsch, *Biosens. Bioelectron.*, 2009, **25**, 797-802.
- [27] H. Badelt-Lichtblau, B. Kainz, C. Völlenklee, E. M. Egelseer, U. B. Sleytr, D. Pum, N. Ilk, *Bioconjug. Chem.*, 2009, **20**, 895-903.
- [28] J. L. Toca-Herrera, R. Krastev, V. Bosio, S. Küpcü, D. Pum, A. Fery, M. Sára, U. B. Sleytr, *Small*, 2005, **1**, 339-348.
- 25 [29] S. E. Moya, J. L. Toca-Herrera, *J. Nanosci. Nanotechnol.*, 2006, **6**, 2329-2337.
- [30] V. Saravia, S. Küpcü, M. Nolte, C. Huber, D. Pum, A. Fery, U. B. Sleytr, J. L. Toca-Herrera, *J. Biotechnol.*, 2007, **130**, 247-252.
- [31] R. Y. Tsien, *Annu. Rev. Biochem.*, 1998, **67**, 509-544.
- 30 [32] N. C. Shaner, R. E. Campbell, P. A. Steinbach, B. N. G. Giepmanns, A. E. Palmer, R. Y. Tsien, *Nat. Biotechnol.*, 2004, **22**, 1567-1572
- [33] P. Messner, D. Pum, U. B. Sleytr, *J. Ultrastruct. Mol. Struct. Res.* 1986, **97**, 73-88.
- [34] A. W. Adamson, *Physical Chemistry of Surfaces*, Wiley, New York, 1990, p.220
- 35 [35] U. Haupts, S. Maiti, P. Schwille, W. W. Webb, *Proc. Natl. Acad. Sci. U S A* 1998, **95**, 13573-13578.
- [36] F. Zhang, Z. Ali, F. Amin, A. Feltz, M. Oheim, W. J. Parak, *ChemPhysChem* 2010, **11**, 730-735.
- 40 [37] S. Moreno-Flores, R. Georgieva, Y. Xiong, K. Melzak, H. Bäumler, J. L. Toca-Herrera, *Microsc. Res. Tech.* 2010, DOI: 10.1002/jemt.20816

**Table 1.** Isoelectric point (IEP) for bare silica particles and S-layer biocolloids.

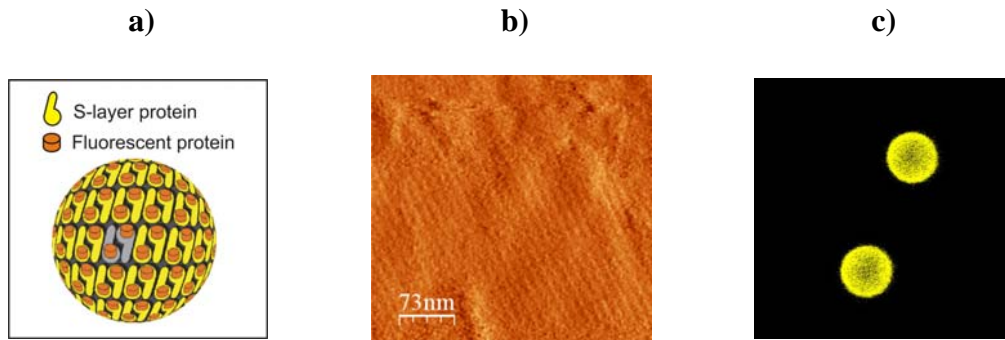
5

<b>Colloid type</b>	<b>IEP</b>
Silica particles	3.3
SgsE	5.1
SgsE-ECFP	4.6
SgsE-EGFP	4.8
SgsE-YFP	4.5
SgsE-mRFP1	4.6

5 **Table 2.**  $pK_a$  and  $\Delta G^0$  values obtained after fitting the fluorescent data depicted in Figure 5. The 50 % decrease in fluorescence was determined directly from the fluorescence vs. pH curves.

<b>Fluorescent SgsE Biocolloids</b>	<b>50 % Intensity lose (from Figure 5)</b>	<b><math>pK_a</math> (fitted values)</b>	<b><math>\Delta G^0</math> (kJ/mol)</b>
SgsE-ECFP	5,7	5.7	29.8
SgsE-EGFP	6.0	5.9	31.1
SgsE-YFP	6.0	5.9	31.1
SgsE-mRFP1	6.3	6.2	32.4

**Figure 1.** Fluorescent S-layer biocolloids. **a)** Schematic representation of a fluorescent S-layer fusion protein biocolloid. The marked grey area shows one unit cell consisting of two monomeric proteins (p2 lattice symmetry). **b)** AFM deflection image of the surface of an 8  $\mu\text{m}$ -diameter SgsE-YFP biocolloid (in liquid). **c)** Confocal micrograph of 8  $\mu\text{m}$ -sized SgsE-YFP biocolloids in pH 8 solution.



10

**Figure 2.** Zeta potential as a function of pH for SgsE-ECFP, SgsE-EGFP, SgsE-YFP and SgsE-mRFP1 coated SiO<sub>2</sub>-microparticles (1 μm-diameter). The isoelectric point of the bare silica particles and the S-layer biocolloids was determined at the cross point when the zeta potential becomes zero (see Table 1 for more details).

5

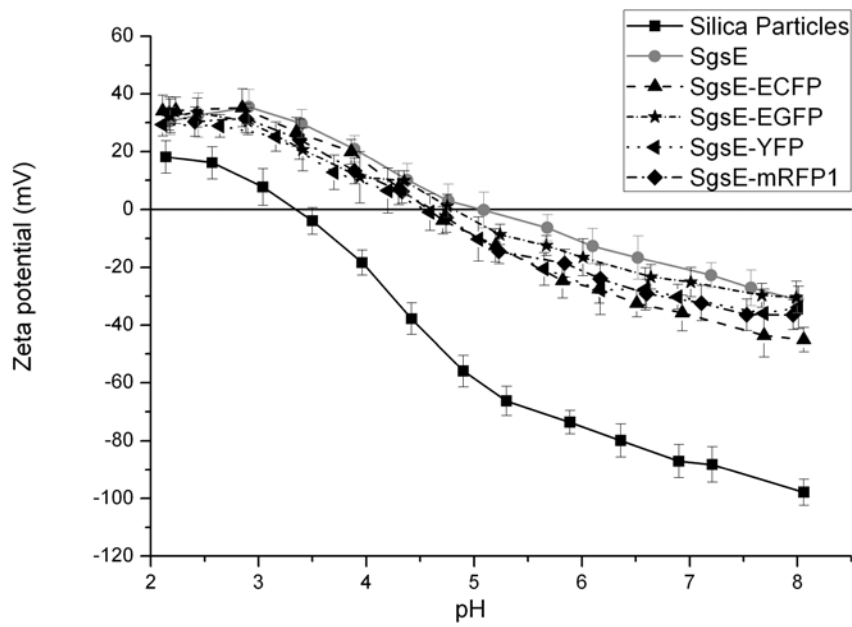


**Figure 3.** Confocal microscopy of 8  $\mu\text{m}$ -diameter fluorescent S-layer biocolloids. **a)** The images show cyan, green, yellow and red S-layer biocolloids in pH 8, pH 5 and pH 3 solutions (scale bar: 20 $\mu\text{m}$ ). The fourth picture illustrates the fluorescence recovery from pH 3 to pH 8. **b)** Wavelength scan: Fluorescence emission behavior of the cyan SgsE-ECFP, green SgsE-EGFP, yellow SgsE-YFP and red SgsE-mRFP1 biocolloids in pH 8, pH 5 and pH 3 solutions. The arrows indicate the fluorescence decrease in acidic pH-solutions.

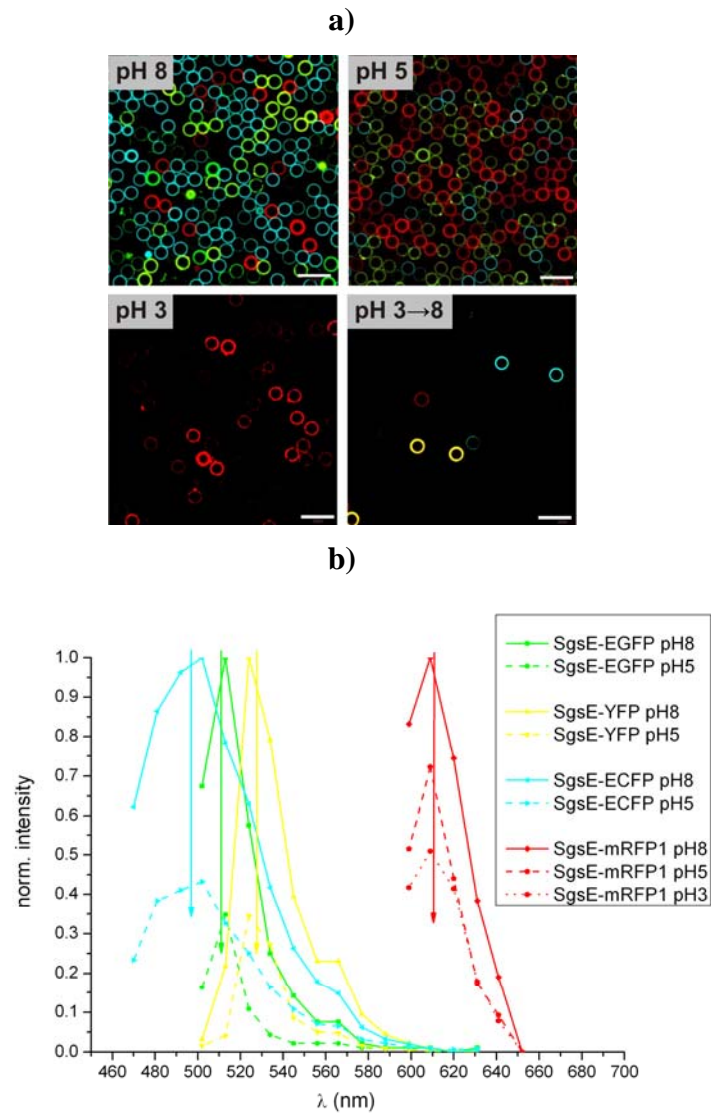
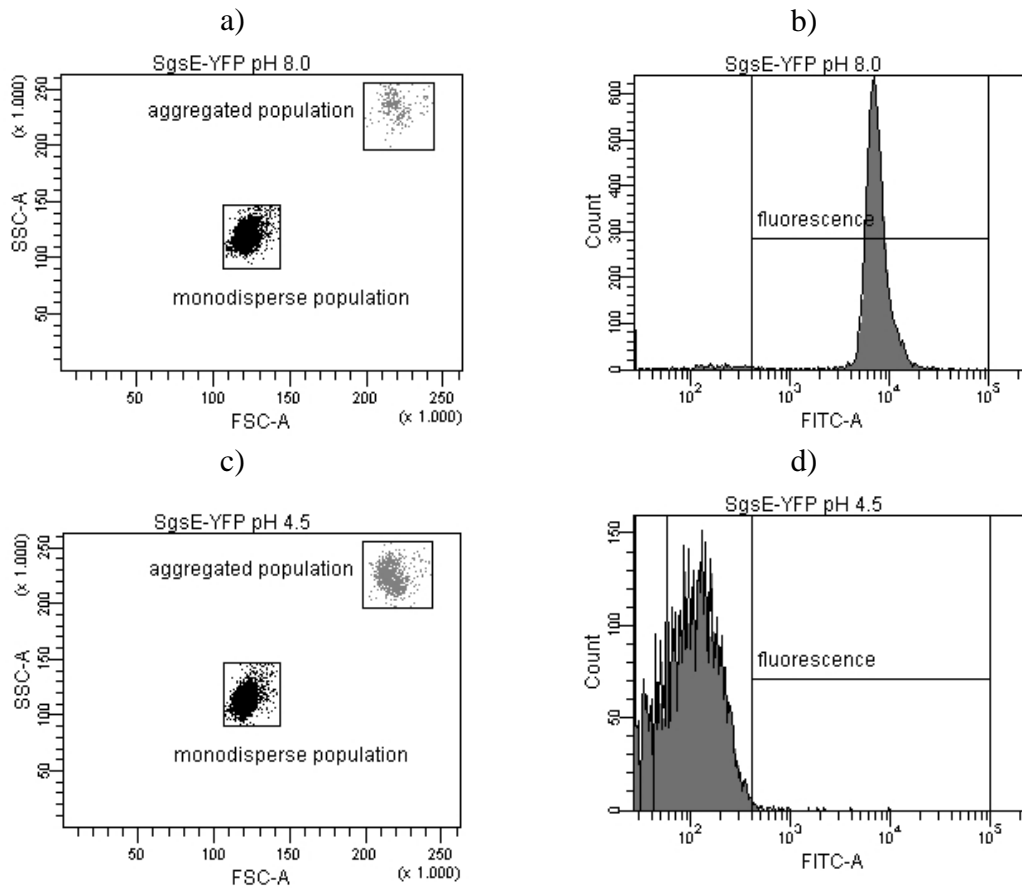


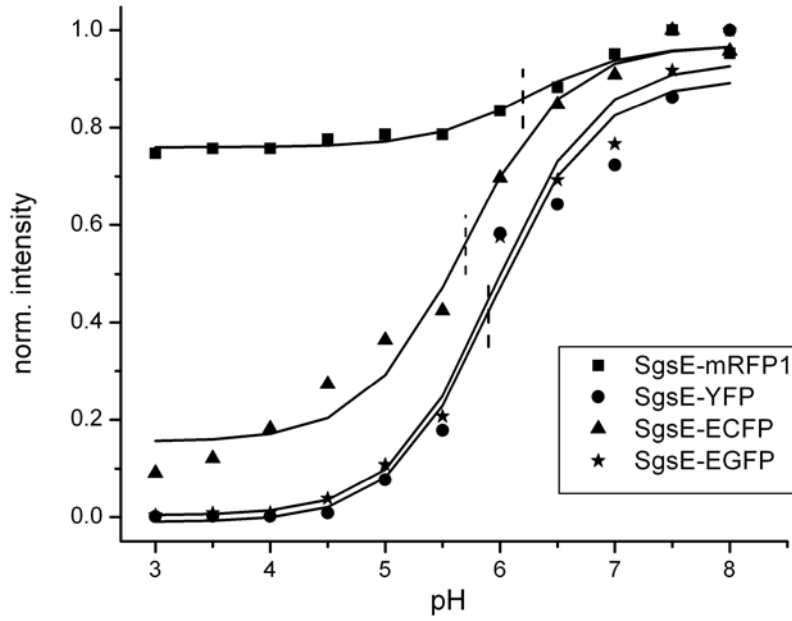
**Figure 4.** Flow cytometry measurements of yellow SgsE biocolloids (3  $\mu\text{m}$ -diameter) as a function of pH. **a)** and **c)** Dot plots of 10,000 collected SgsE-YFP biocolloids in pH 8 and pH 4.5 buffer solutions. The gated black main population indicates monodispersed SgsE-YFP biocolloids while the grey marked population show colloid aggregation. **b)** and **d)** Histogram plots of monodispersed population: number of events versus FITC channel. The histograms were used to evaluate the fluorescence intensity (see Figure 5).

5



10

**Figure 5.** Fluorescence intensity versus pH-values of all four fluorescent S-layer biocolloids. Estimated pKa values are marked as vertical dotted lines; the values and standard free reaction energies  $\Delta G^0$  are listed in Table 2.



1 Manuscript submitted to: Journal of structural biology

2

3

4

5 **Fluorescence energy transfer in the bi-fluorescent S-layer tandem fusion protein ECFP-**  
6 **SgsE-YFP**

7

8

9

10 Birgit Kainz<sup>a</sup>, Kerstin Steiner<sup>a,b</sup>, Uwe B. Sleytr<sup>a</sup>, Dietmar Pum<sup>a</sup>, and José L. Toca-Herrera<sup>c,\*</sup>

11

12

13

14

15 <sup>a</sup>Department of NanoBiotechnology, University of Natural Resources and Applied Life  
16 Sciences (BOKU), Muthgasse 11, 1190 Vienna (Austria)

17

18 <sup>b</sup>Present address: Institute of molecular Biotechnology, Graz University of Technology,  
19 Petersgasse 14, 8010 Graz, Austria

20

21 <sup>c</sup> CICbiomaGUNE, Biosurfaces Unit, Paseo Miramón 182, 20009 San Sebastián (Spain)

22

23

24

25

26

27

28

29 \*Corresponding author:

30 José L. Toca-Herrera (CIC biomaGUNE)

31 Tel.: 0034 943530013

32 E-mail: [jltocaherrera@cicbiomagune.es](mailto:jltocaherrera@cicbiomagune.es)

33

34

35

36

37

38

39

40

1 **Abstract**

2 This work reports for the first time on the fabrication of a bi-functional S-layer tandem fusion  
3 protein which is able to self-assemble on solid supports without losing its functionality.

4 The S-layer protein SgsE of *Geobacillus stearothermophilus* NRS 2004/3a was fused with the  
5 cyan ECFP donor protein at the SgsE N-terminus and with the yellow YFP acceptor protein at  
6 the C-terminus. The fluorescence energy transfer was studied with spectrofluorimetry,  
7 confocal microscopy and flow cytometry, while protein self-assembly (on silicon dioxide  
8 particles) and structural investigations were carried out with atomic force microscopy (AFM).

9 The fluorescence resonance energy transfer efficiency of reassembled SgsE tandem protein  
10 was 20 % which is the same transfer efficiency shown in solution. The calculated relative  
11 molecular distance between the two chromophores is 6.2 nm. Finally, the 1:1 donor and  
12 acceptor stoichiometry within the bi-fluorescent S-layer fusion was used to gain structural  
13 information about the distance between the N and the C-terminus, and the self-assembly  
14 ability of the S-layer fusion permitted the fabrication of bi-fluorescent biocolloids.

15

16

17

18

19

20 **Keywords**

21 S-layer tandem fusion protein, self assembly, fluorescence resonance energy transfer,  
22 biocolloid

23

## 1 **Introduction**

2 One of the key challenges in nanopatterned bio-surface science is the control of the molecular  
3 self-assembling capability of biological systems into higher-order structures [1]. In recent  
4 years much work has been done on the design and fabrication of multifunctional,  
5 nanostructured and biomimetic surfaces [2-6]. In addition to lipids, which self-assemble into  
6 bilayers [7,8], extracellular crystalline surface protein layers (S-layers), obtained from  
7 prokaryotic organisms (bacteria, archaea) can be used as a structural scaffold [9-12].

8 S-layer (glyco)proteins that have been genetically functionalised have the capability to  
9 reassemble into 2D isoporous closed monocrystalline layers. Oblique (p1, p2), square (p4) or  
10 hexagonal (p3, p6) lattices can be formed on different solid supports and on liposomes with a  
11 composition and structure similar to that originally found in bacteria [9, 13].

12 Thus, S-layer proteins have been successfully used as basic building blocks in a biomolecular  
13 construction kit [10,14]. Genetically engineered chimeric S-layer fusion proteins feature  
14 functional moieties fused to the N- or C-terminus (streptavidin, cysteine, enzymes, allergens,  
15 antibodies, and fluorescent proteins), at defined molecular orientation and in a 1:1  
16 stoichiometry [15-20].

17 At the moment, little is known about the tertiary structure of S-layer proteins. Molecular  
18 dynamics simulations have been used to elucidate the structure of the S-layer protein SbsB  
19 from *Geobacillus stearothermophilus* PV72/p2 [21], while crystallisation studies have helped  
20 to gain insight into different parts of the S-layer protein SbsC from *Geobacillus*  
21 *stearothermophilus* ATCC 12980 [22]. Self-assembly studies on solid supports have revealed  
22 the importance of the surface chemistry for the protein layer structure of SbpA from  
23 *Lysinibacillus sphaericus* CCM 2177 as well as for the formation kinetics [23,24].

24 S-layer lattices have already been utilised for the immobilisation and deposition of different  
25 molecules [25-27].

26 The work presented here is the first to describe the generation of a nanopatterned biointerface  
27 system based on S-layers with more than one functionality. The goal of this work was to  
28 incorporate two moieties in one S-layer protein, so that the S-layer protein could act as  
29 scaffold in order to fabricate an interfacial fluorescence resonance energy transfer biosystem.

30 Fluorescence resonance energy transfer (FRET) is a nonradioactive dipole-dipole interaction  
31 that occurs when two fluorophores are located within a few nanometers of each other, and  
32 when the emission spectrum of the donor fluorophore overlaps with the excitation spectrum  
33 of the acceptor fluorophore [28]. FRET-based approaches are playing an increasing role in  
34 biological investigations at the nanometer-scale, at which protein-protein and cell component

1 interactions are characterised [29,30]. In recent studies, much work has been done on the  
2 development of FRET-based biosensors and on the design of the required proteins [31].

3 Some effort has been made to optimise the green fluorescent protein (GFP) family and its  
4 spectral variants for intracellular FRET investigations [32,33]. The GFP protein is composed  
5 of 238 amino acids, is cylindrical in shape (4 nm long, 3 nm in diameter) and the  
6 chromophore is located and protected in the centre of the cylinder [34]. The often used GFP  
7 variants for FRET investigations are the cyan CFP (donor) and the yellow YFP (acceptor)  
8 proteins [35,36]. When FRET occurs, the donor emission decreases while acceptor emission  
9 increases. The transfer efficiency between donor and acceptor can be monitored using  
10 spectrofluorimetry, confocal microscopy [37,38] and flow cytometry [29,39].

11 The big advantage of genetically engineered fluorescent protein-based biosensors are that  
12 they are easy to construct using standard molecular biology with no variation of the desired  
13 stoichiometry. This compares to alternative technologies such as dye-based chemical  
14 modifications to label the protein in which the fluorophore may be at undefined  
15 stoichiometric ratio with respect to the protein.

16

17 In this work the building up of a fluorescence resonance energy transfer system (FRET) with  
18 molecular precision on silica particles is described by using a newly designed bi-fluorescent  
19 S-layer tandem fusion protein. The S-layer protein SgsE of *Geobacillus stearothermophilus*  
20 NRS 2004/3a [40,41] was fused to the cyan ECFP donor protein at the SgsE N-terminus and  
21 to the yellow YFP acceptor protein at the SgsE C-terminus. This bi-functional S-layer tandem  
22 fusion protein was able to self-assemble on solid supports without losing its fluorescent  
23 properties. Protein self-assembly (on silicon dioxide substrates) and structural investigations  
24 were carried out with atomic force microscopy (AFM). The fluorescence energy transfer was  
25 studied with spectrofluorimetry, confocal microscopy and flow cytometry. The energy  
26 transfer efficiency was determined by measuring the ECFP donor quenching coupled with an  
27 increase in the acceptor fluorescence. By calculating the distance between the two  
28 chromophores knowing the 1:1 donor and acceptor stoichiometry within the bi-fluorescent S-  
29 layer fusion, it was possible to gain structural information about the distance between the N  
30 and the C-terminus. This novel S-layer tandem fusion protein represents a new patterning  
31 element for a bio-molecular construction kit with two (interacting) functional moieties.

32

33

## 1 **Materials and Methods**

### 2 *Plasmid construction*

3 The molecular cloning steps were carried out with the sequence of rSgsE<sub>131-903</sub> (C\_SgsE), an  
4 130 amino acid N-terminal truncated form of the S-layer protein SgsE, which will be named  
5 from now as SgsE, incorporating C- and/or N-terminal fluorescent proteins [42].

6 The enhanced cyan fluorescent protein ECFP (F64L, S65T, Y66W, N146I, M153T, V163A)  
7 and the yellow fluorescent protein YFP 10C (S65G, V68L, S72A, T203Y), variants of the  
8 green fluorescent protein GFP, were used as fusion partners [36]. The cloning steps to  
9 produce SgsE-YFP fusion protein with the yellow YFP fused at the C-terminal has been  
10 described in a previous work [16].

11 To construct the fusion protein with the cyan fluorescent protein ECFP fused to the N-  
12 terminus of SgsE or SgsE-YFP, ECFP was PCR (polymerase chain reaction) amplified using  
13 the forward primer pair ECFP\_for(NcoI) (5'  
14 AATCACCATGGTGAGCAAGGGCGAGGAG-3') and the reverse primer ECFP\_rev(NcoI)  
15 (5'AATCACCATGGACTTGTACAGCTCGTCCATG-3'), digested with NcoI and ligated  
16 into the NcoI linearised plasmids pET28a-C\_SgsE(Kpn) and pET28a-C\_SgsE-YFP [16,42].

17 Bacterial strains, general methods and molecular cloning procedures were the same as  
18 previously published [42]. PCR was carried out using Super Yield *Pwo* polymerase (Roche,  
19 Vienna, Austria). Restriction enzymes and T4 DNA ligase were purchased from Invitrogen  
20 (Lofer, Austria). *Escherichia coli* DH5 (Invitrogen, Lofer, Austria) was used for plasmid  
21 propagation, and all other cloning and expression experiments were performed using *E. coli*  
22 BL21 Star (DE3). Protein expression and protein purification were monitored with SDS-  
23 PAGE (SDS-polyacrylamide gels) by visualising the protein bands with Coomassie Blue R-  
24 250 as described elsewhere [42]. Cells were grown at 37°C in Luria-Bertani (LB) medium  
25 supplemented with kanamycin (50 µg/mL) until OD<sub>600</sub> 0.8, and protein expressions were  
26 induced with 1 mM IPTG (Fermentas, St. Leon-Rot, Germany). Cultivations were continued  
27 at 37°C for additional 4 hours in the dark. Isolation of the fusion proteins (SgsE-YFP, ECFP-  
28 SgsE, ECFP-SgsE-YFP) and FPLC-purification (Superdex 200 prep grade XK16 FPLC-  
29 column, 1.6 x 60 cm, GE-Healthcare) were carried out as recently described [16,42]. The  
30 proteins were dialysed (cut-off 12 - 16 kDa, Biomol) against 2 mM EDTA over night at 4°C.  
31 After centrifugation protein concentrations were determined with a NanoDrop  
32 spectrophotometer (ND-1000, Peqlab Biotechnology, Germany) at 280 nm. Physico-chemical  
33 parameters (amino-acid, atomic compositions, and extinction coefficients) were calculated  
34 from the theoretical protein sequence using the Peptide Properties calculator

1 (<http://www.expasy.ch/tools/protparam.html>). The protein solutions were diluted to 1 mg/mL  
2 with Milli-Q water (resistivity: 18.2 MΩ cm<sup>-1</sup>) and stored at 4°C in the dark.

### 3 4 *Atomic force microscopy (AFM)*

5 Silica wafers were rinsed twice with EtOH and Milli-Q water and then dried under nitrogen.  
6 The wafers were incubated with HBSS (Hankø balanced salt solution containing calcium and  
7 magnesium, pH 7.4) assembling solution containing 0.1 mg/ml of fluorescent S-layer fusion  
8 protein for 4 h at room temperature. Coated wafers were rinsed with Milli-Q water and stored  
9 at 4°C in Milli-Q water until use for AFM measurements. AFM measurements of the S-layer  
10 coated silica wafer were carried out in contact mode with a Nanoscope IIIa multimode (Veeco  
11 Instruments, Santa Barbara, CA) with a J-scanner (nominal scan size 130 μm x 130 μm).  
12 Silicon nitride cantilevers with a nominal spring constant of 0.06 Nm<sup>-1</sup> (NP-S, NanoProbes,  
13 Digital Instruments, Santa Barbara, CA) were used. Samples were measured in 100 mM NaCl  
14 solution to avoid electrostatic interactions between tip and sample. The imaging scan rate was  
15 approximately 4 Hz and the applied force during scanning was minimised to prevent the tip  
16 from modifying the sample. The S-layer lattice parameters (base vector lengths and base  
17 angle) were determined based on Fourier analysis using homemade software.

### 18 19 *Coating of microparticles*

20 3μm diameter colloidal SiO<sub>2</sub> microparticles for flow cytometer measurements were purchased  
21 from Fluka (Austria), and 8μm diameter SiO<sub>2</sub> microparticles for confocal microscopy studies  
22 were purchased from Microparticles (Berlin). The SiO<sub>2</sub>-microparticles were coated by mixing  
23 them with HBSS assembling solution containing 0.1 mg/ml of protein. Assembling was  
24 carried out under rotation for 4 hours at room temperature on a Test Type Rotator. To remove  
25 the excess of non-assembled proteins, the fluorescent S-layer biocolloids were centrifuged  
26 (Eppendorf bench centrifuge, 13,000g, room temperature, 15 sec) and washed three times  
27 with Milli-Q water (resistivity: 18.2 MΩ cm<sup>-1</sup>). The S-layer biocolloids were stored in Milli-Q  
28 water at 4°C.

### 29 30 *Steady-state spectrofluorimetry*

31 Steady-state fluorescence measurements with the fluorescent S-layer monomers (0.5 μM) in  
32 PBS solution (phosphate buffered saline solution, pH 7.4) were acquired using a FluoroLog<sup>®</sup>-  
33 3 (Model FL3-22) spectrofluorimeter (Horiba Jobin Yvon) with integration time of 0.1 sec,  
34 and an entrance slit, intermediate slit, and exit slit of 5 nm for excitation and emission

1 monochromators. Measurements were carried out at room temperature in quartz cuvettes with  
2 a path length of 10 mm and a minimum test volume of 2 ml. Spectra were recorded with  
3 FluorEssence™ and analysed using Origin7 software (Origin Lab, Northampton, MA) after  
4 excitation at 435 nm for ECFP and at 514 nm for YFP. The emission intensities obtained at  
5 476 nm (ECFP emission maximum) and 527 nm (YFP emission maximum) were taken for  
6 energy transfer calculations.

7

8 The energy transfer efficiency (FRET) and the relative molecular distance between the two  
9 fluorescent proteins were calculated according to equation 1 [38]:

$$10 \quad E = 1 - \frac{I_{DA}}{I_D} = \frac{1}{\left[1 + \left(\frac{r}{r_0}\right)^6\right]} \quad (1)$$

11 where E is the energy transfer efficiency,  $I_{DA}$  is the fluorescence intensity of the donor ECFP  
12 in presence of the acceptor YFP,  $I_D$  is the fluorescence intensity of the donor ECFP in absence  
13 of the acceptor YFP, r is the distance between the centres of the donor ECFP (D) and the  
14 acceptor YFP (A) chromophores, and  $r_0$  is the Förster distance corresponding to 50% FRET  
15 efficiency (about  $4.92 \pm 0.10$  nm for the ECFP-YFP pair assuming a  $\kappa^2$  value of 2/3 for rapid  
16 random orientation [33]). The variation of the relative orientations of the donor and the  
17 acceptor can lead to different  $\kappa^2$  values ranging from 1 to 4, which can induce an error in the  
18 estimation of (r) of 26% [43].

19

### 20 *Confocal microscopy*

21 Spectral imaging of S-layer coated 8  $\mu\text{m}$  sized  $\text{SiO}_2$ -particles was carried out in PBS buffer  
22 solution (phosphate buffered saline solution, pH 7.4) at room temperature using a Zeiss  
23 LSM510 META (Zeiss, Jena, Germany) laser scanning microscope. Cyan ECFP and yellow  
24 YFP fluorescence emissions were imaged through a BP465-510-nm filter and LP530-nm  
25 emission filter, respectively, after excitation with the 458-nm laser line of an Argon/2 laser. In  
26 addition, the yellow YFP samples were excited with the 514-nm laser line of an Argon/2 laser  
27 and imaged through the LP 530-nm emission filter. Wavelength scans (scanning step size: 10  
28 nm) were performed by exciting the fusion proteins with the 458-nm laser. Images and  
29 wavelength scan data were taken using ZEN software (Zeiss, Jena, Germany) and analysed  
30 with the Zeiss LSM Image Browser software. The energy transfer was determined to be  
31 positive when ECFP intensity decreased in the tandem protein ECFP-SgsE-YFP compared to

1 the intensity of the ECFP-SgsE protein. Energy transfer calculations were carried out in the  
2 same way as described in the fluorimetry section (see equation 1).

### 3 4 *Flow cytometry*

5 Flow cytometry measurements were performed on a CantoII Flow cytometer (BD  
6 Biosciences, San Jose, CA) and analysed using BD FACSDiva 6.0 software (BD  
7 Biosciences). 10,000 events of S-layer coated 3  $\mu\text{m}$ -diameter  $\text{SiO}_2$  particles were measured in  
8 PBS (phosphate buffered saline solution, pH 7.4). The ECFP and FRET signals were  
9 collected with an AmCyan 510/50-nm filter after excitation with the violet 405-nm laser. The  
10 SgsE-YFP emission signal was collected using a FITC 530/30-nm filter after excitation with  
11 the 488-nm laser.

## 12 13 **Results**

14 A new S-layer bi-fluorescent tandem fusion protein ECFP-SgsE-YFP for dual colour and  
15 energy transfer investigations was prepared and is shown schematically in Figure 1.

16 The protein was made by incorporating an N-terminal fused cyan ECFP donor protein and a  
17 C-terminal yellow YFP acceptor protein. In addition, a mono-fluorescent S-layer protein was  
18 engineered by fusing ECFP to the N terminus of the SgsE protein. Yellow and cyan fusion  
19 proteins SgsE-YFP and SgsE-ECFP carrying the fluorescence tag at the C-terminus were  
20 available from previous work [16].

21 The different S-layer fusion proteins (ECFP-SgsE, SgsE-YFP, ECFP-SgsE-YFP) were  
22 heterologously expressed and accumulated as inclusion bodies within the cytoplasm of *E.coli*  
23 BL21 Star (DE3) host cells carrying the respective expression plasmids. Based on the masses  
24 of the template reference SgsE (rSgsE<sub>131-903</sub>, 82.8 kDa), the mass of the different fusion  
25 protein constructs were calculated to be 109.8 kD for ECFP-SgsE and SgsE-YFP and 136.8  
26 kDa for the tandem fusion protein ECFP-SgsE-YFP. This was in accordance with the bands  
27 of a 4-h expression culture on an SDS-PAGE after Coomassie staining as shown in Figure 2.  
28 The higher molecular weight of the single tagged fluorescent SgsE fusion proteins (lane 3 and  
29 lane 4) and the SgsE tandem fusion protein (lane 5) is clearly visible in comparison to the  
30 untagged SgsE protein in lane 2 in Figure 2.

31  
32 The SgsE and the C-terminal fusion protein SgsE-YFP could be expressed in higher yields  
33 (demonstrated by thick bands in lane 1 and lane 2 in Figure 2) than the N-terminal ECFP and  
34 the ECFP-SgsE-YFP proteins (lighter bands in lane 4 and lane 5 in Figure 2). After protein

1 extraction and purification, the chimeric fusion proteins could be used for spectroscopic  
2 investigations and assembling studies.

#### 3 4 *FRET measurement by steady-state spectrofluorimetry*

5 First of all, the spectral overlap of the cyan ECFP-SgsE donor and the yellow SgsE-YFP  
6 acceptor was determined by measuring the excitation and emission spectra of both protein  
7 solutions (pH 7.4) using steady-state spectrofluorimetry. The obtained spectra are shown in  
8 Figure 3a. The shapes and maxima of the curves (ECFP 435/476-nm, YFP 514/527-nm) were  
9 in accordance with previously published data [16]. The spectral overlap region of the cyan  
10 donor emission curve with the yellow acceptor excitation spectrum can be seen in Figure 3a.

11 The first experiment to determine a fluorescence resonance energy transfer (FRET) between  
12 the two moieties of the SgsE tandem fusion protein ECFP-SgsE-YFP was carried out with  
13 protein monomers in PBS solution by monitoring the fluorescence emission over the  
14 wavelength range from 450 nm to 600 nm after excitation at 435 nm.

15 The FRET curve in Figure 3b (solid black line), obtained from ECFP-SgsE-YFP, shows a  
16 decrease in the cyan donor intensity and a significant increase in the yellow acceptor emission  
17 intensity compared to the single tagged reference proteins (ECFP-SgsE: cyan curve, SgsE-  
18 YFP: orange curve) at donor excitation. Measurements of the mono-fluorescent SgsE fusion  
19 proteins were done to determine the part of the donor emission spectrum that overlaps with  
20 the acceptor emission spectrum, and to estimate the fluorescence of the acceptor emission  
21 excited by the donor excitation wavelength. The emission spectrum of the YFP moiety in the  
22 tandem fusion protein after excitation at the YFP maximum (514 nm) is presented in Figure  
23 3b. The shape and the emission maximum (527 nm) remain the same indicating that the  
24 ECFP-SgsE-YFP tandem fusion protein contains two different intact functionalities. The  
25 values for calculating the energy transfer efficiency were obtained from the emission scan  
26 intensities of the donor at 476 nm in Figure 3b. Based on the degree of donor quenching, the  
27 energy transfer efficiency E was 19.6 %, which according to Equation 1 corresponds to a  
28 distance between the two chromophores<sup>1</sup> of (6.2 ±0.1) nm.

29 An increase of the yellow YFP acceptor fluorescence of about 39 % could be determined in  
30 the new designed ECFP-SgsE-YFP tandem fusion protein after excitation at the donor  
31 absorption. No energy transfer was detected in mixtures of cyan and yellow mono-fluorescent  
32 fusion proteins after excitation at 435 nm. Both chromophores emitted fluorescence but no  
33 sign of energy transfer was observed.

---

<sup>1</sup> Calculations were carried with the mean values of  $I_D$  and  $I_{DA}$  obtained from five experiments:  
 $I_D = (8123260 \pm 9924) \cdot 10^6$  and  $I_{DA} = (6526670 \pm 5173) \cdot 10^6$ . The efficiency value was  $E = (19.6 \pm 0.1) \%$

1 *Self-assembly studies on silicon dioxide investigated with AFM*

2 The self-assembly capability of the bi-fluorescent S-layer protein on silicon wafers was  
3 investigated by atomic force microscopy (AFM) in contact mode. The ECFP-SgsE-YFP S-  
4 layer tandem protein reassembled by forming differently sized randomly distributed  
5 polycrystalline patches with S-layer lattices, covering the whole support as shown in Figure  
6 4a. The oblique p2 lattice was found in different crystalline domains. According to the AFM  
7 images, the fused GFP tags<sup>2</sup> seemed to be part of the SgsE p2 lattice. Figure 4b displays the  
8 Fourier transform of the SgsE-structure and a noise filtered image. Fourier analysis provided  
9 the following lattice parameters:  $a=14.0$  nm,  $b=11.6$  nm, and  $\gamma=81^\circ$ . It may therefore be seen  
10 that the self-assembly ability of the S-layer protein is not affected by the fused tags on the C-  
11 and N-terminus. The single tagged fusion proteins assembled in the same way showing  $a =$   
12  $11.2$  nm,  $b = 8.8$  nm, and  $\gamma = 79.1^\circ$  as lattice parameters. Compared to previously obtained  
13 electron microscopy (TEM) and AFM results, the lattice parameters of the bi-fluorescent S-  
14 layer protein are slightly larger than those reported for SgsE fusion proteins and those found  
15 *in vivo* on *Geobacillus stearothermophilus* NRS 2004/3a ( $a=11.6$  nm,  $b=9.4$  nm,  $\gamma=78^\circ$ ) [16,  
16 41,42].

17

18 *Steady-state FRET confocal microscopy*

19 The bi-fluorescent S-layer protein ECFP-SgsE-YFP was used to create a fluorescence energy  
20 transfer system on silica microparticles. These biocolloids were analysed by confocal  
21 microscopy. Figure 5a shows a mixture of cyan ECFP-SgsE and yellow SgsE-YFP  
22 biocolloids, sequentially excited with the 458 nm and 514 nm laser lines to test the crosstalk  
23 of the two fluorophores as well as to determine the maximal fluorescence intensities of both  
24 proteins. There was neither yellow fluorescence from the SgsE-YFP biocolloids using the 530  
25 nm filter after excitation with the 458-nm donor laser-line nor cyan fluorescence in the 530  
26 nm filter for YFP. This filter setup was used for measuring the ECFP-SgsE-YFP biocolloids.  
27 Figure 5b shows that the cyan fluorescence intensity is very weak (compared to the emission  
28 intensity of the cyan biocolloids of Figure 5a) whereas the yellow YFP emission intensity  
29 increases after excitation with the 458 nm laser line. This result indicates that energy transfer  
30 between the two fused fluorescent moieties takes place when bi-fluorescent ECFP-SgsE-YFP  
31 proteins are assembled on silica particles. Wavelength scan experiments were carried out to  
32 quantify the fluorescence intensity and the energy transfer efficiency of the assembled

---

<sup>2</sup> The molecular weight of one GFP protein is 27 kDa

1 proteins on silica microparticles. For that purpose, ECFP-SgsE-YFP as well as ECFP-SgsE  
2 donor and SgsE-YFP acceptor reference spectra were recorded between 470 nm and 600 nm  
3 after excitation with the 458 nm laser line as shown in Figure 5.

4 The energy transfer efficiency<sup>3</sup> was calculated taking into account the decrease in donor  
5 fluorescence intensity in the presence of the acceptor moiety, being again around 20%.  
6 According to Equation 1, this corresponds to a chromophore-chromophore distance of  $(6.2 \pm$   
7  $1.5)$  nm. These results obtained from surface measurements of S-layer biocolloids agree with  
8 the results obtained for the proteins in solution (fluorimetry). Co-assembling of ECFP-SgsE  
9 and SgsE-YFP S-layer fusion proteins on silica microparticles did not result in energy transfer  
10 although both fluorescent chromophores were detected. This means that the donor and  
11 acceptor dyes are only in close proximity when they are tagged to the same protein.

12

### 13 *FRET measurements with flow cytometry*

14 Flow cytometry measurements confirmed the confocal microscopy results showing the  
15 biointerface resonance energy transfer between the cyan ECFP donor and the yellow YFP  
16 acceptor of the bi-fluorescent fusion protein ECFP-SgsE-YFP (Figure 6). For this purpose  
17 only the violet laser setup (405 nm) with the associated AmCyan filter (485-535 nm) was  
18 available. Histogram plots (counts versus intensity) were chosen to illustrate and determine  
19 the mean fluorescence intensities obtained from the AmCyan-channel (510/50nm filter).  
20 Quantitative information of the fluorescence emission was obtained from the gated areas.  
21 Figure 6a presents the histogram plot of the ECFP-SgsE biocolloids and Figure 6b the  
22 histogram of the SgsE-YFP biocolloids. To test the fluorescence emission intensities of the  
23 cyan (435/476 nm) and yellow fluorescent proteins (514/527 nm) in the AmCyan filter,  
24 reference biocolloids were measured. A weak fluorescence signal could be detected for  
25 ECFP-SgsE biocolloids, but no signal was monitored for the SgsE-YFP biocolloids after  
26 excitation at 405 nm. With the ECFP-SgsE-YFP biocolloids a remarkable increase in the  
27 fluorescence intensity could be detected as shown in Figure 6c. This indicates that only an  
28 increase of the yellow acceptor fluorescence and no decrease in the donor emission took  
29 place, therefore no energy transfer efficiency was calculated. In addition the emission signal  
30 of the yellow moiety of the bi-fluorescent protein was measured in the FITC-channel after  
31 excitation with the blue 488-nm laser configuration (Figure 6d). Further experiments

---

<sup>3</sup> In this case, the mean values for  $I_D$  and  $I_{DA}$  obtained from a sample of 20 particles were:  
 $I_D = (93.58333 \pm 5.123)$  and  $I_{DA} = (74.5 \pm 4.06499)$ . The efficiency value was  $E = (20.4 \pm 6.1) \%$

1 demonstrated that there was no fluorescence energy transfer between ECFP-SgsE and SgsE-  
2 YFP after co-assembling mixtures of mono-fluorescent proteins on silica microparticles.

### 4 **Discussion**

5 The aim of this work was to design and characterise a bi-fluorescent S-layer fusion protein, to  
6 investigate its intrinsic self-assembly properties, to test its functionality after recrystallisation,  
7 and to gain information about the protein 3D structure. In order to accomplish this, a  
8 resonance energy transfer (FRET) system on the S-layer protein was genetically engineered  
9 by fusing the ECFP donor protein to the N-terminus and the YFP acceptor protein to the C-  
10 terminus of the SgsE protein. AFM results indicate that the bi-fluorescent fusion protein  
11 forms p2 crystalline lattices on silicon dioxide, which are similar to those formed by mono-  
12 fluorescent SgsE fusion proteins and untagged SgsE proteins.

13 This means that the fusion of two well-defined protein markers, such as YFP and ECFP, to  
14 both ends of the S-layer protein SgsE does not disturb its intrinsic self-assembly behaviour.  
15 However, the obtained lattice parameters, the base vector lengths and base angle ( $a = 14.0$   
16  $\text{nm}$ ,  $b = 11.6 \text{ nm}$ ,  $\gamma = 81^\circ$ ), are larger than for the single tagged proteins ( $a = 11.2 \text{ nm}$ ,  $b = 8.8$   
17  $\text{nm}$ ,  $\gamma = 79.1^\circ$ ), probably due to the increase of mass after fusing a new fluorescent protein.

18 Regarding the topology of the formed biointerfaces, no noticeable difference between the  
19 tandem bi-fluorescent fusion protein, the single tagged fusion protein and the wild-type  
20 protein was detected with atomic force microscopy. These results imply that the two  
21 cylindrically shaped fluorescent proteins (3 nm diameter, 4 nm length [34]) are part of the  
22 measured protein crystal lattice. Thus the two fused fluorescent protein do not behave like  
23 external bodies lying on top of the protein scaffold or pointing outwards with different  
24 degrees of freedom. The localisation of the exact position of the two moieties in the tertiary  
25 structure of the protein after crystal formation is a challenging issue for S-layer (fusion)  
26 proteins in general. Currently, very little is known about this subject, although experiments  
27 carried out with the SbsB S-layer protein have provided some insights about the tertiary  
28 protein structure after crystal formation. For example, insertion mutagenesis screen  
29 investigations revealed a molecular interaction between the N- and C-terminus of the S-layer  
30 protein because of their proximity in the crystal structure [44].

31 The steady-state fluorescence measurements of the bi-fluorescent ECFP-SgsE-YFP fusion  
32 proteins in solution indicate that their spectral properties do not differ from the reference  
33 proteins, which leads to the conclusion that both GFP-proteins are correctly folded within the  
34 S-layer protein.

1 In addition, the results indicate that the FRET efficiency between the donor dye ECFP and the  
2 acceptor dye YFP in solution was about 19.6 %. From previous work it is known that the S-  
3 layer protein solutions contain monomers, dimers, small self-assembly products and also  
4 oligomers which cannot be separated; it is therefore not clear if the calculated distance  
5 between the donor and acceptor chromophore, ( $6.2 \pm 0.1$ ) nm, is intra or inter-molecular,  
6 because ECFP might be able to interact with the nearest neighbour. We also observed that  
7 different ratios of mono-fluorescent SgsE fusion protein mixtures did not lead to energy  
8 transfer in solution (see Table 1). Remarkably, only the bi-fluorescent protein seemed to be  
9 responsible for FRET, a phenomenon which only takes place at distances less than 10 nm and  
10 for permitted relative orientations between the dipoles of the chromophores.

11 We have shown that FRET also occurs after the recrystallisation of bi-fluorescent S-layer  
12 fusion protein on silica particles, with an energy transfer efficiency of about 20%, which  
13 corresponds to a distance between the two chromophores (and therefore between the N- and  
14 C-terminus) of ( $6.2 \pm 1.6$ ) nm. These results are supported by the control measurements  
15 carried out with mixtures of mono-fluorescent cyan and yellow S-layer fusion proteins co-  
16 assembled on silica particles (results included in the additional information). Although the  
17 cyan and yellow proteins were mixed on the particle surface, no sign of FRET could be  
18 observed (see Table 1 for a qualitative description).

19 Since the FRET studies in solution and on biocolloids lead to similar results, we conclude that  
20 the energy transfer takes place within one protein molecule (separated by ca. 6 nm). This is  
21 consistent with the AFM studies which indicate that the two fluorescent moieties must be a  
22 part of the tertiary structure of the bi-fluorescent fusion S-layer protein.

23

## 24 **Conclusion**

25 In this work we have studied a novel bi-fluorescent SgsE S-layer tandem fusion protein which  
26 represents a new self-assembly system for the building of functional nanostructured  
27 biointerfaces. Atomic force microscopy showed that the N- and C-terminally incorporated  
28 fluorescent tags did not change the intrinsic self-assembly behaviour of the S-layer protein.  
29 The bi-fluorescent engineered protein formed crystalline domains on silicon dioxide  
30 substrates with lattice similar to that formed by the S-layer wild-type protein. Steady-state  
31 fluorimetry, confocal microscopy and flow cytometry indicate that both fused fluorescent  
32 proteins are functional, retaining their specific fluorescence properties. Since the cyan  
33 fluorescent protein was fused to the N-terminus and the yellow protein to the C-terminus, the  
34 energy transfer between both chromophores was used to gain information about the

1 interaction between both termini. FRET investigations revealed that the distance between the  
2 donor-acceptor-chromophores within the S-layer protein was about 6.2 nm.  
3 We present here the first bi-functional S-layer fusion protein, which can be used to  
4 functionalise colloidal particles and also to study the structural properties of bacterial protein  
5 layers, particularly the interaction between the N and C-terminus. Finally, the self-assembly  
6 properties of this bi-fluorescent S-layer tandem fusion protein make it suitable to engineer  
7 multi-functional nanopatterned biocoatings for future applications in nanobiotechnology.

8  
9

## 10 **Acknowledgements**

11 This work was supported by the Austrian NanoInitiative under the project SLAYSENS within  
12 the project cluster ISOTEC and by the U.S. Air Force Office of Scientific Research (AFOSR)  
13 Projects FA9550-07-0313 and FA9550-09-1-0342. This work was partially financed by the  
14 Spanish Ministry of Education and Science (Project CTQ-2007-66541). The authors thank S.  
15 Küpcü, J. Friedmann and A. Scheberl for technical support and scientific discussions. C.  
16 Schäffer and P. Messner are acknowledged for providing the SgsE plasmid and scientific  
17 information. K. Melzak is acknowledged for reading the manuscript.

## 1    **References**

- 2
- 3    [1]    D. Papapostolou, S. Howorka, Engineering and exploiting protein assemblies in  
4    synthetic biology, *Mol. Biosyst.* 5 (2009) 723-732.
- 5    [2]    E.K. Sinner, S. Ritz, Y. Wang, J. Dostálek, U. Jonas, W. Knoll, Molecularly controlled  
6    functional architectures, *Materials Today* 13 (2010) 46-55.
- 7    [3]    R. F. Roskamp, A. Brunsen, M. Gianneli, P. Jakubowicz, B. Menges, U. Jonas, G.  
8    Fytas, W. Knoll, Hydrogels: Synthesis, Functionalization and Optical Investigation, *Polymer*  
9    *Preprints* 49 (2008) 1018-1019.
- 10    [4]    K. Godula, M.L. Umbel, D. Rabuka, Z. Botyanszki, C.R. Bertozzi, R. Parthasarathy,  
11    Control of the Molecular Orientation of Membrane-Anchored Biomimetic Glycopolymers, *J.*  
12    *Am. Chem. Soc.* 131 (2009) 10263-10268.
- 13    [5]    W. Knoll, R. Naumann, M. Friedrich, J. W. F. Robertson, M. Losche, F. Heinrich, D.  
14    J. McGillivray, B. Schuster, P. C. Gufler, D. Pum, U. B. Sleytr, Solid supported lipid  
15    membranes: New concepts for the biomimetic functionalization of solid surfaces,  
16    *Biointerphases* 3 (2008) FA125-135.
- 17    [6]    B. Schuster, U. B. Sleytr, Composite S-layer lipid structures, *J. Struct. Biol.* 168  
18    (2009) 207-216.
- 19    [7]    W. Knoll, K. Bender, R. Förch, C. Frank, H. Götz, C. Heibel, T. Jenkins, U. Jonas, A.  
20    Kibrom, R. Kügler, C. Naumann, R. Naumann, J. Rühle, S. Schiller, E.K. Sinner, Polymer-  
21    tethered bimolecular lipid membranes, in: W. P. Meier, W. Knoll (Eds.), *Advances in*  
22    *Polymer Science*, Vol. 224, *Polymer Membranes/Biomembranes*, Springer, Heidelberg, 2010,  
23    pp. 87-112.
- 24    [8]    E. Sackmann, Supported Membranes: Scientific and Practical Applications, *Science*  
25    271 (1996) 43-48.
- 26    [9]    U. B. Sleytr, P. Messner, D. Pum, M. Sára, Crystalline Bacterial Cell Surface Layers  
27    (S Layers): From Supramolecular Cell Structure to Biomimetics and Nanotechnology,  
28    *Angew. Chem. Int. Ed.* 38 (1999) 1034-1054.
- 29    [10]    U. B. Sleytr, M. Sára, D. Pum, B. Schuster, Crystalline Bacterial Cell Surface Layers  
30    (S-layers): A Versatile Self-Assembly System, in: A. Ciferri (Ed.), *Supramolecular Polymers*,  
31    Boca Raton, Florida, 2005, pp.583-612.
- 32    [11]    U. B. Sleytr, M. Sára, D. Pum, B. Schuster, P. Messner, C. Schäffer, Self-assembly  
33    protein systems: microbial S-layers, in: A. Steinbüchel, S.R. Fahnestock (Eds.), *Polyamides*  
34    *and complex proteinaceous materials*, Wiley-VCH, Weinheim, 2002, pp. 285-338.
- 35    [12]    M. Sára, D. Pum, S. Küpcü, P. Messner, U. B. Sleytr, Isolation of two physiologically  
36    induced variant strains of *Bacillus stearothermophilus* NRS 2004/3a and characterization of  
37    their S-layer lattices, *J. Bacteriol.* 176 (1994) 848-860.
- 38    [13]    U. B. Sleytr, Basic and applied S-layer research: an overview, *FEMS Microbiol. Rev.*  
39    20 (1997) 5-12.
- 40    [14]    U. B. Sleytr, E. M. Egelseer, N. Ilk, D. Pum, B. Schuster, S-layers as a Basic Building  
41    Block in a Molecular Construction Kit, *FEBS J.* 274 (2007) 323-334.
- 42    [15]    E. M. Egelseer, N. Ilk, D. Pum, P. Messner, C. Schäffer, B. Schuster, U. B. Sleytr, S-  
43    Layers, Nanobiotechnological Applications, in: M. C. Flickinger (Ed.), *The Encyclopedia of*  
44    *Industrial Biotechnology: Bioprocess, Bioseparation, and Cell Technology*, John Wiley &  
45    Sons, Inc., Hoboken, USA, in press.
- 46    [16]    B. Kainz, K. Steiner, M. Möller, D. Pum, C. Schäffer, U. B. Sleytr, J. L. Toca-Herrera,  
47    Absorption, steady-state, fluorescence lifetime and 2D self-assembly properties of newly  
48    engineered fluorescence S-Layer fusion proteins of *Geobacillus Stearothermophilus* NRS  
49    2004/3a, *Biomacromolecules* 11 (2010) 207-214.

- 1 [17] H. Badelt-Lichtblau, B. Kainz, C. Vollenkle, E. M. Egelseer, U. B. Sleytr, D. Pum, N.  
2 Ilk, Genetic Engineering of the S-Layer Protein SbpA of *Lysinibacillus sphaericus* CCM  
3 2177 for the Generation of Functionalized Nanoarrays, *Bioconjug. Chem.* 20 (2009) 895-903.
- 4 [18] H. Tschiggerl, A. Breitwieser, G. de Roo, T. Verwoerd, C. Schäffer, U. B. Sleytr,  
5 Exploitation of the S-layer self-assembly system for site directed immobilization of enzymes  
6 demonstrated for an extremophilic laminarinase from *Pyrococcus furiosus*, *J. Biotechnol.* 133  
7 (2008) 403-411.
- 8 [19] N. Ilk, S. Küpcü, G. Moncayo, S. Klimt, R. C. Ecker, R. Hofer-Warbinek, E. M.  
9 Egelseer, U. B. Sleytr, M. Sára, A functional chimaeric S-layer-enhanced green fluorescent  
10 protein to follow the uptake of S-layer-coated liposomes into eukaryotic cells, *Biochem. J.*  
11 379 (2004) 441-448.
- 12 [20] D. Moll, C. Huber, B. Schlegel, D. Pum, U. B. Sleytr, M. Sára, S-layer-streptavidin  
13 fusion proteins as template for nanopatterned molecular arrays, *Proc. Natl. Acad. Sci. USA* 99  
14 (2002) 14646-14651.
- 15 [21] C. Horejs, D. Pum, U. B. Sleytr, R. Tscheliessnig, Structure prediction of an S-layer  
16 protein by the mean force method, *J. Chem. Phys.* 128 (2008) 065106.
- 17 [22] T. Pavkov, E. M. Egelseer, M. Tesarz, D. I. Svergun, U. B. Sleytr, W. Keller, The  
18 structure and binding behavior of the bacterial cell surface layer protein SbsC, *Structure* 16  
19 (2008) 1226-1237.
- 20 [23] S. Moreno-Flores, A. Kasry, H.-J. Butt, Ch. Vavilala, M. Schmittl, D. Pum, U. B.  
21 Sleytr, J. L. Toca-Herrera, From native to non-native two-dimensional protein lattices via  
22 underlying hydrophilic/hydrophobic nanoprotusions, *Angew. Chem. Int. ed.* 120  
23 (2008) 4707-4710.
- 24 [24] A. Eleta Lopez, S. Moreno Flores, D. Pum, U.B. Sleytr and J.L. Toca-Herrera, Surface  
25 dependence of nanocrystal protein formation, *Small* 6 (2010) 396-403.
- 26 [25] U. B. Sleytr, D. Pum, B. Schuster, M. Sára, Molecular nanotechnology and  
27 nanobiotechnology with two-dimensional protein crystals (S-layers), In: M. Rosoff (Ed.),  
28 *Nano-Surface Chemistry*, Marcel Dekker, New York, 2001, pp. 333-389.
- 29 [26] W. Shenton, D. Pum, U.B. Sleytr, S. Mann, Synthesis of cadmium sulphide  
30 superlattices using self-assembled bacterial S-layers, *Nature* 389 (1997) 585-587.
- 31 [27] S. R. Scheicher, B. Kainz, S. Kostler, M. Suppan, A. Bizzarri, D. Pum, U. B. Sleytr,  
32 V. Ribitsch, Optical oxygen sensors based on Pt(II) porphyrin dye immobilized on S-layer  
33 protein matrices, *Biosens. Bioelectron.* 25 (2009) 797-802.
- 34 [28] J. R. Lakowicz, *Principles of Fluorescence Spectroscopy*, third ed., Springer, 2006, pp.  
35 443-475.
- 36 [29] A. W. Nguyen, P. S. Daugherty, Evolutionary optimization of fluorescent proteins for  
37 intracellular FRET, *Nat. Biotechnol.* 23 (2005) 355-360.
- 38 [30] E. Galperin, V. V. Verkhusha, A. Sorkin, Three-chromophore FRET microscopy to  
39 analyze multiprotein interactions in living cells, *Nat. Methods* 1 (2004) 209-17.
- 40 [31] A. Ibraheem, R. E. Campbell, Designs and applications of fluorescent protein-based  
41 biosensors, *Curr. Opin. Chem. Biol.* 14 (2010) 30-36.
- 42 [32] B. A. Pollok, R. Heim, Using GFP in FRET-based applications, *Trends Cell Biol.* 9  
43 (1999) 57-60.
- 44 [33] G. H. Patterson, D. W. Piston, B. G. Barisas, Förster Distances between Green  
45 Fluorescent Protein Pairs, *Anal. Biochem.* 284 (2000) 438-440.
- 46 [34] S. S. Patnaik, S. Trohalaki, R. Pachter, Molecular modeling of green fluorescent  
47 protein: Structural effects of chromophore deprotonation, *Biopolymers* 75 (2004) 441-452.
- 48 [35] M. A. Rizzo, G. H. Springer, B. Granada, D. W. Piston, An improved cyan fluorescent  
49 protein variant useful for FRET, *Nat. Biotechnol.* 22 (2004) 445-449.
- 50 [36] R. Y. Tsien, The green fluorescent protein, *Annu. Rev. Biochem.* 67 (1998) 509-544.

1 [37] H. Wallrabe, A. Periasamy, Imaging protein molecules using FRET and FLIM  
2 microscopy, *Curr. Opin. Biotechnol.* 16 (2005) 19-27.

3 [38] G. W. Gordon, G. Berry, X. H. Liang, B. Levine, B. Herman, Quantitative  
4 Fluorescence Resonance Energy Transfer Measurements Using Fluorescence Microscopy,  
5 *Biophys. J.* 74 (1998) 2702-2713.

6 [39] L. He, T. D. Bradrick, T. S. Karpova, X. Wu, M. H. Fox, R. Fischer, J. G. McNally, J.  
7 R. Knutson, A. C. Grammer, P. E. Lipsky, Flow cytometric measurement of fluorescence  
8 (Förster) resonance energy transfer from cyan fluorescent protein to yellow fluorescent  
9 protein using single-laser excitation at 458 nm, *Cytometry A* 53 (2003) 39-54.

10 [40] U. B. Sleytr, R. Plohberger, The dynamic process of assembly of two-dimensional  
11 arrays of macromolecules on bacterial cell walls, in: W. Baumeister, W. Vogell (Eds.),  
12 *Electron microscopy at molecular dimensions.*, Berlin, Heidelberg, New York: Springer-  
13 Verlag, Heidelberg, 1980, pp. 36-47.

14 [41] P. Messner, D. Pum, U.B. Sleytr, Characterization of the ultrastructure and the self-  
15 assembly of the surface layer of *Bacillus stearothermophilus* strain NRS 2004/3a, *J.*  
16 *Ultrastruct. Mol. Struct. Res.* 97 (1986) 73-88.

17 [42] C. Schäffer, R. Novotny, S. Küpcü, S. Zayni, A. Scheberl, J. Friedmann, U. B. Sleytr,  
18 P. Messner, Novel biocatalysts based on S-layer self-assembly of *Geobacillus*  
19 *stearothermophilus* NRS 2004/3a: a nanobiotechnological approach, *Small* 3 (2007) 1549-  
20 1559.

21 [43] I. N. Serdyuk, N. R. Zaccai and J. Zaccai, *Methods in Molecular Biophysics, Structure,*  
22 *Dynamics, Function*, Cambridge University Press, 2007, pp. 672.

23 [44] H. Kinns, H. Badelt-Lichtblau, E. M. Egelseer, U. B. Sleytr, S. Howorka, Identifying  
24 assembly-inhibiting and assembly-tolerant sites in the SbsB S-layer protein from *Geobacillus*  
25 *stearothermophilus*, *J. Mol. Biol.* 395 (2010) 742-754.

26  
27  
28

1 **Figure captions**

2  
3 **Figure 1.** Left: Schematic representation of the S-layer fusion protein technology. Middle:  
4 Creation of S-layer proteins with fluorescent moieties on the N- and/or C-terminus of the S-  
5 layer protein SgsE. Right: intrinsic self-assembling capability of the SgsE S-layer protein,  
6 which forms a crystalline lattice of p2 symmetry. The marked grey area shows one unit cell  
7 consisting of two monomeric proteins.

8  
9 **Figure 2.** SDS-PAGE patterns of SDS extracts of biomass samples (the *E.coli* BL21 Star  
10 (DE3) host cells carrying the respective expressed fluorescent fusion proteins) after  
11 Coomassie staining (left). The bands associated with the S-layer proteins are indicated by  
12 boxes and arrows. The lines are as follows, lane 1: All Blue Standard (Roche); lane 2:  
13 expressed SgsE (82.795 kDa); lane 3: expressed SgsE-YFP (109.833 kDa); lane 4: expressed  
14 ECFP-SgsE (109.769 kDa); lane 5: expressed ECFP-SgsE-YFP (136.808 kDa).

15  
16 **Figure 3.** Fluorescence spectra of the protein solutions (0.5  $\mu$ M) in PBS solution (pH 7.4). A)  
17 Determination of the spectral overlap region between the cyan ECFP-SgsE donor emission  
18 (em) and the yellow SgsE-YFP excitation (ex) spectra. Fluorescence spectra of ECFP-SgsE  
19 (ex/em 435/476 nm) and SgsE-YFP (ex/em 514/527 nm). B) Fluorescence resonance energy  
20 transfer (FRET) emission spectrum (solid black curve) of ECFP-SgsE-YFP. Note the donor  
21 emission spectrum ECFP-SgsE and the SgsE-YFP emission spectrum after excitation at 435  
22 nm. The YFP emission spectrum of ECFP-SgsE-YFP after excitation at 514 nm (acceptor  
23 excitation) is shown in the yellow curve. The black arrows indicate the decrease in the ECFP-  
24 donor emission intensity and the increase in the YFP-acceptor emission intensity in the FRET  
25 measurement.

26  
27 **Figure 4.** AFM deflection images of assembled ECFP-SgsE-YFP on silicon dioxide.  
28 Measurements were carried out in contact mode in aqueous solution. The oblique p2 protein  
29 lattice ( $a=14\text{nm}$ ,  $b=11.6\text{nm}$ ,  $\gamma=81^\circ$ ) can be seen in different areas. Image A shows that the  
30 whole surface is covered with nanostructured domains of assembled S-layer fusion proteins.  
31 Figure B is a zoom of Figure A: the nanostructure of one crystalline domain can be observed.  
32 The inset on the right top corner in image B shows the Fourier transform of the p2  
33 nanostructure and the inset at lower represents the filtered image reconstruction of the ECFP-  
34 SgsE-YFP tandem fusion protein.

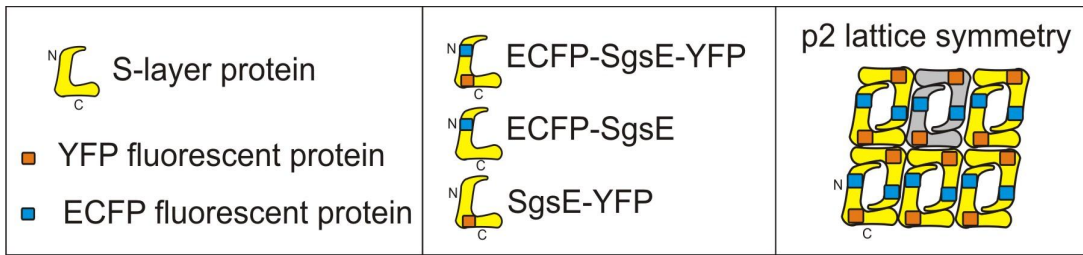
35  
36 **Figure 5.** Confocal microscopy investigations. A) An overlay of cyan ECFP-SgsE biocolloids  
37 and yellow SgsE-YFP biocolloids sequentially excited and monitored overlay. B) Tandem  
38 fusion protein ECFP-SgsE-YFP biocolloids: the cyan donor moiety (left) and yellow acceptor  
39 moiety (right) after excitation with the 456-nm laser line. C) Wavelength scan measurement  
40 of ECFP-SgsE and SgsE-YFP reference biocolloids and the ECFP-SgsE-YFP tandem fusion  
41 protein biocolloids after excitation with the 458-nm laser line. Arrows indicate the decrease in  
42 the donor and the increase in the acceptor fluorescence emission intensity. (Scan steps: 11 nm,  
43 Bar: 20  $\mu$ m)

44  
45 **Figure 6.** Flow cytometer histograms (number of events versus AmCyan or FITC channel  
46 signal) showing ECFP, YFP and FRET signals on the surface of S-layer coated biocolloids (3  
47  $\mu$ m diameter). Histograms showing a weak AmCyan-signal for ECFP-SgsE biocolloids (A),  
48 no signal for SgsE-YFP biocolloids (B) and an increase in the AmCyan-signal of ECFP-SgsE-  
49 YFP FRET biocolloids (C) after excitation with the 405-nm laser. In (D) only the yellow part  
50 of the tandem fusion protein ECFP-SgsE-YFP is measured in the FITC channel after  
51 excitation with the 488-nm laser. The mean values refer to the gated area.

1 **Figure 1**

2

3



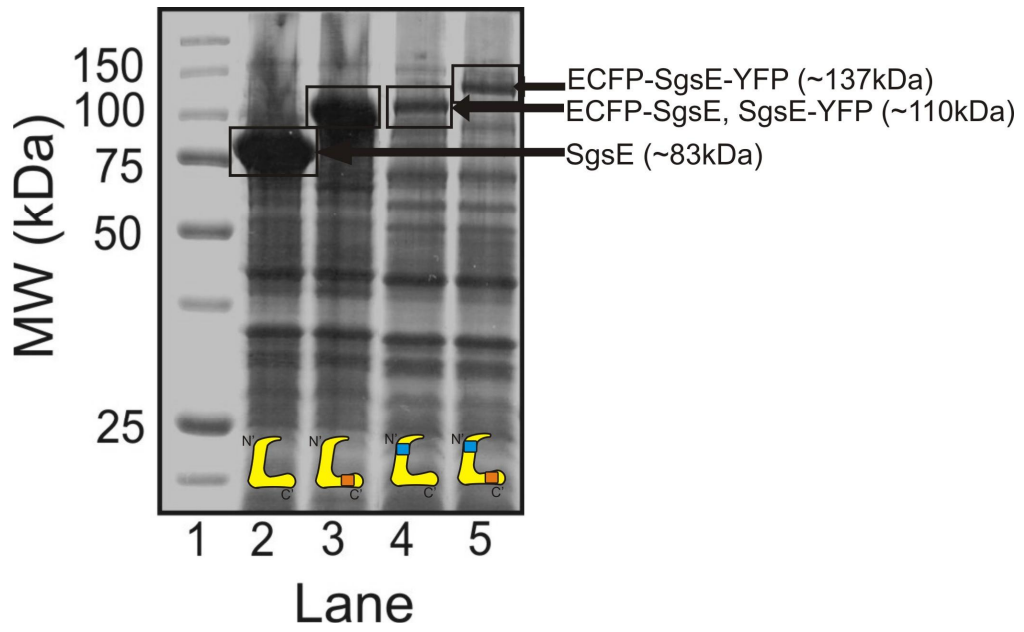
4

1 **Figure 2**

2

3

4

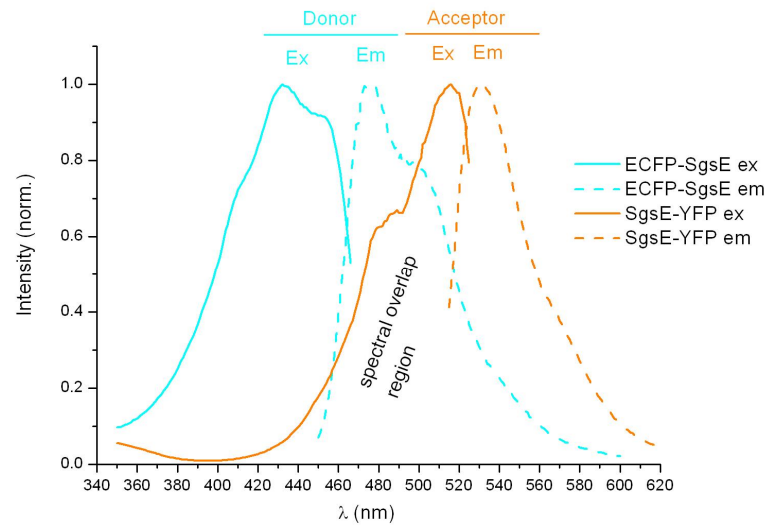


1 **Figure 3**

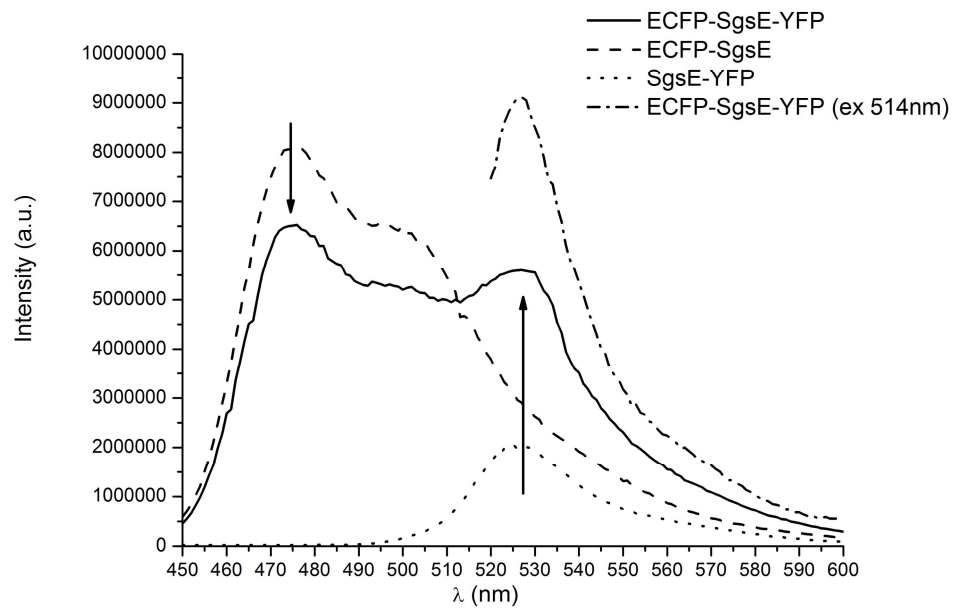
2

3

A)



B)



4

5

6

7

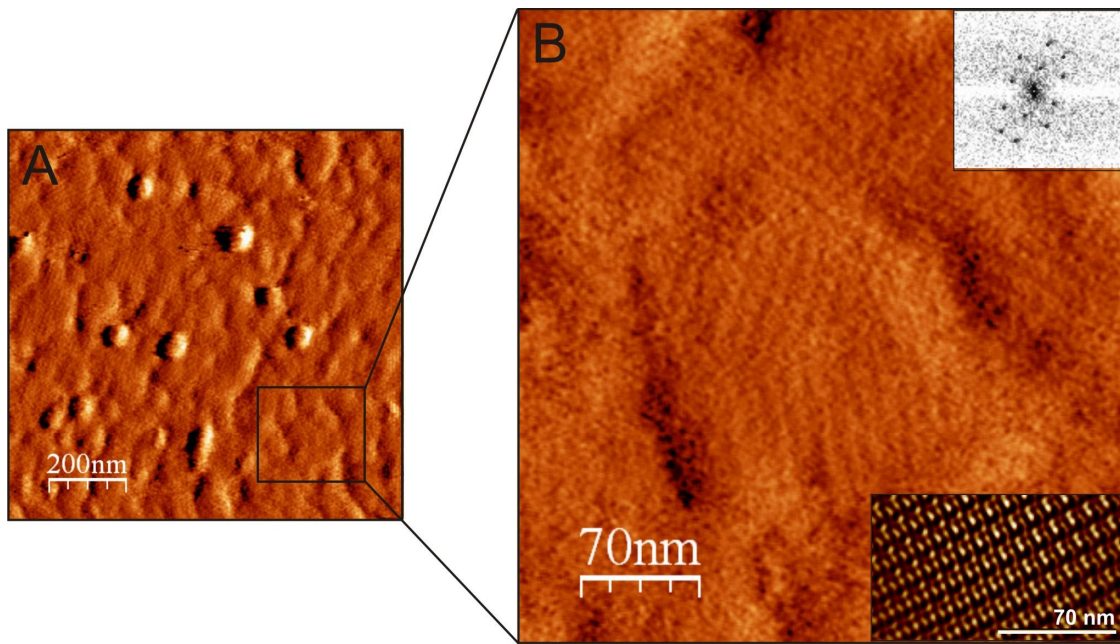
8

9

1 **Figure 4**

2

3



4

5

6

7

8

9

10

11

12

13

14

15

16

17

18

19

20

21

22

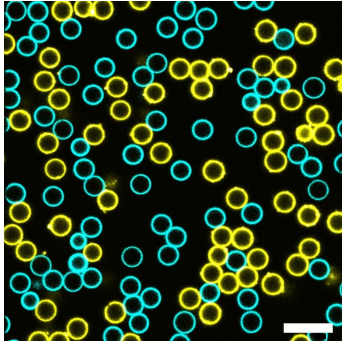
23

1 **Figure 5**

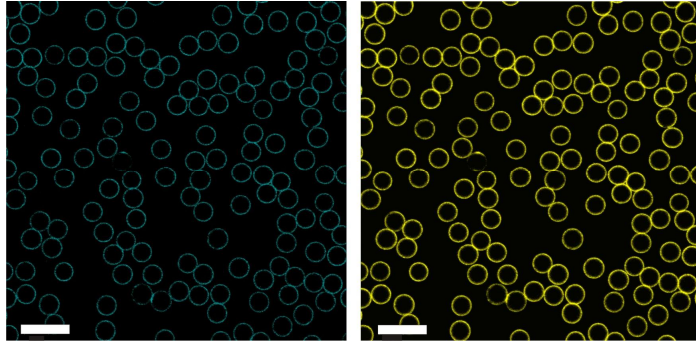
2

3

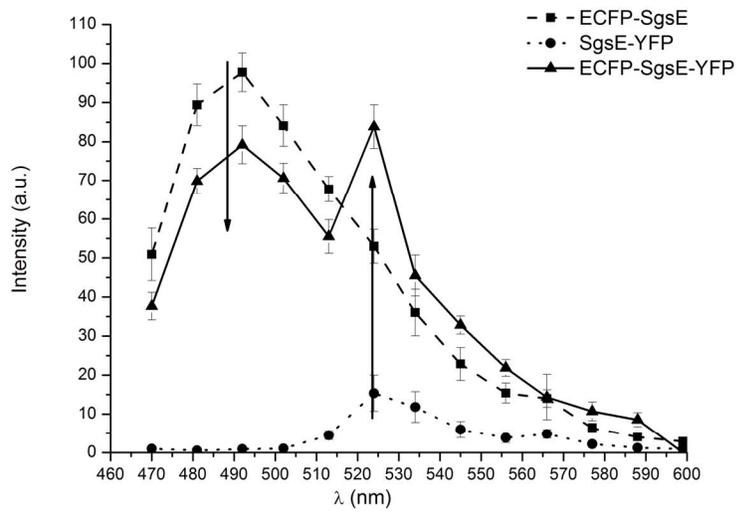
A)



B)



C)



4

5

6

7

8

9

10

11

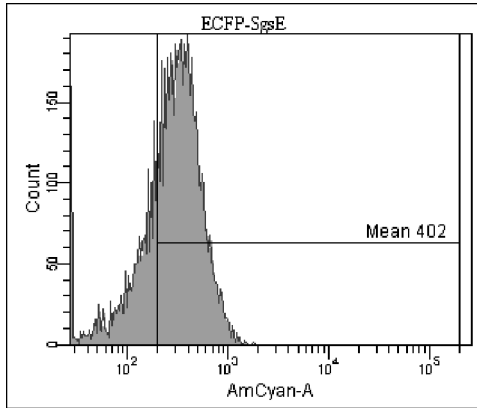
12

13

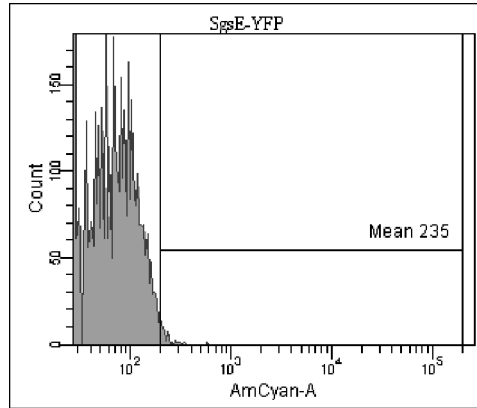
1 **Figure 6**

2  
3

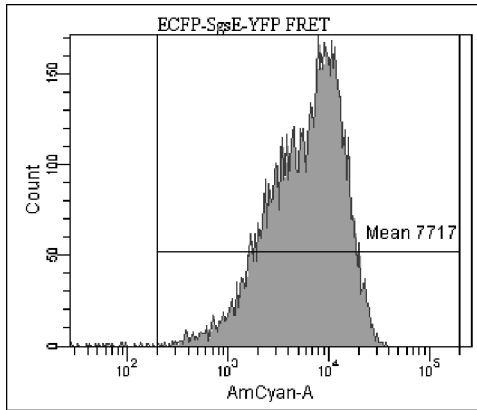
A)



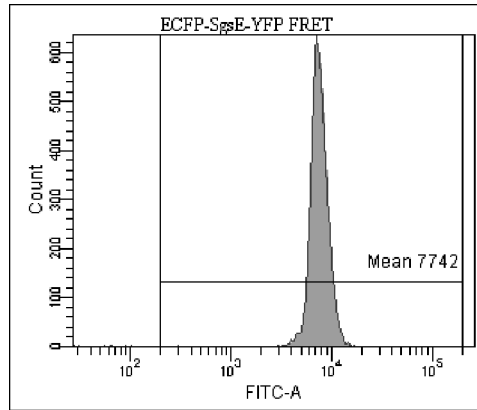
B)



C)



D)



4  
5

1 **Table 1:** Fluorescence resonance energy transfer (FRET) results of mono-fluorescent SgsE  
2 fusion protein mixtures in solution and used for coating of silica microparticles compared  
3 with the bi-fluorescent SgsE fusion protein. Note that (1+1, 1+2, etc.) represent the used  
4 molar mixtures (1, 2 and 3 are multiples of the protein concentration 0.5  $\mu$ M).  
5  
6  
7

Fluorescent S-layer fusion proteins	FRET	
	Solution	Biocolloids
ECFP-SgsE + SgsE-YFP (1+1, 1+2, 1+3, 2+1)	No	No
SgsE-ECFP + SgsE-YFP (1+1, 1+2, 1+3 2+1)	No	No
ECFP-SgsE-YFP	Yes	Yes

8  
9  
10  
11

## Additional Information of the manuscript “Study of the fluorescent energy transfer in the bi-fluorescent S-layer tandem fusio nprotein ECFP-SgsE-YFP” by Birgit Kainz et al.

### *Transmission electron microscopy*

Isolated SgsE S-layer subunits have the intrinsic capability to form and self-assembly products (sheets, cylinders) in recrystallisation buffer solution.

Figure 1 shows an electron micrograph taken using a JEOL JEM-2100F (Model EM-20014) transmission electron microscope. Hydrophilized carbon-coated pioloform supported 300-mesh copper grids were incubated with SgsE-protein suspension. Adsorbed SgsE self-assemblies were chemically fixed with 0.5% glutaraldehyde in 0.1 K-dydrogen phosphate buffer (pH 7.2) for 10 min and negatively stained with 1.0% uranyl acetate within 1 min. The S-layer lattice parameters (base vector lengths and base angle) were investigated using a homemade software based on Fourier analysis. More information can be found in reference [16].

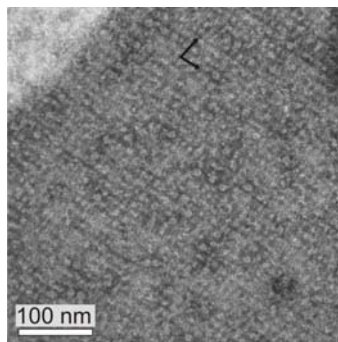


Figure 1: Transmission Electron microscopy image showing the typical p2 lattice symmetry of (truncated) SgsE. The lattice parameters are:  $a=10.5\text{nm}$ ,  $b=13.1\text{nm}$  and  $\gamma=79^\circ$ . Note the black arrows showing the base lattice vectors.

### *Making fluorescent S-layerfusion proteins*

Figure 1. Scheme describing the construction of the ECFP-SgsE-YFP and ECFP-SgsE fusion protein: (a) ECFP was PCR (polymerase chain reaction) amplified and digested with NcoI and (b) ligated into the NcoI linearised plasmids pET28a-SgsE and pET28a-SgsE-YFP to create recombinant plasmids (pET28a-ECFP-SgsE, pET28a-ECFP-SgsE-YFP). *E. coli* DH5 $\alpha$  was used for plasmid propagation and (c) *E.coli* B121 Star was used for heterologous expression of the fusion proteins. (d) After isolation, FPLC-purification and dialyses against 2mM EDTA the fluorescent S-layer fusion protein solutions were used for fluorescent measurements in solution. (e) coating of silicon wafer and silica particles (structure analyses with AFM). The fluorescence measurements with the S-layer coated biocolloids were performed with flow cytometry and confocal microscopy.

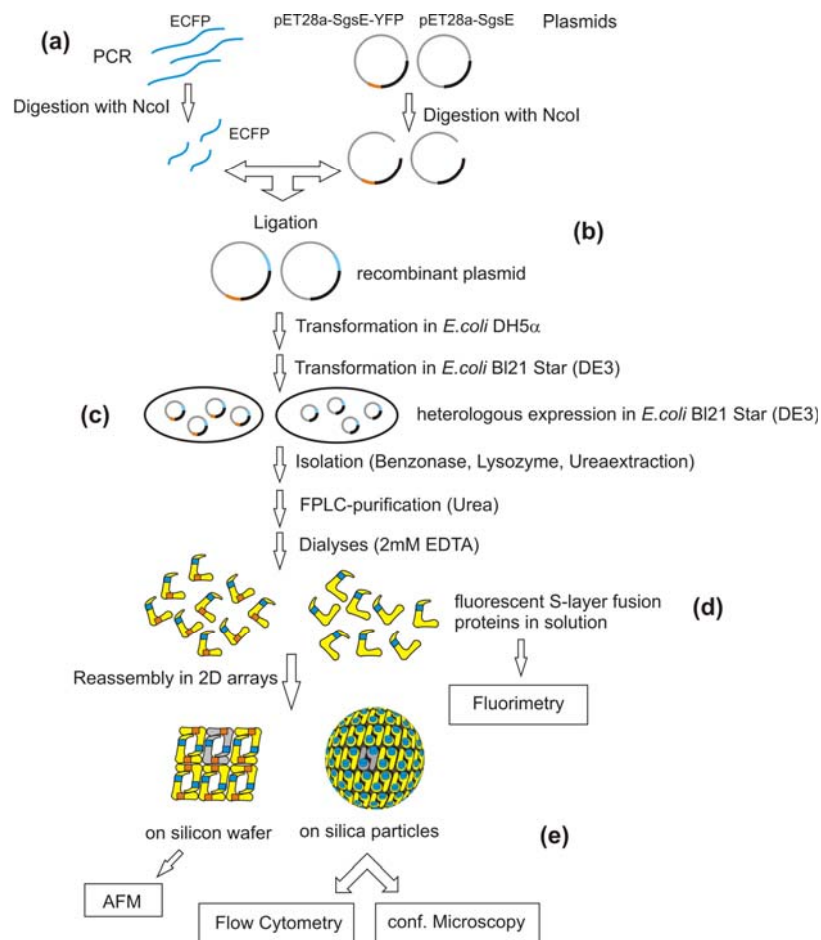


Figure 2. Scheme describing the construction of the ECFP-SgsE-YFP and ECFP-SgsE fusion protein: (a) ECFP was PCR (polymerase chain reaction) amplified and digested with NcoI and (b) ligated into the NcoI linearised plasmids pET28a-SgsE and pET28a-SgsE-YFP to create recombinant plasmids (pET28a-ECFP-SgsE, pET28a-ECFP-SgsE-YFP). *E. coli* DH5 $\alpha$  was used for plasmid propagation and (c) *E. coli* B121 Star was used for heterologous expression of the fusion proteins. (d) After isolation, FPLC-purification and dialyses against 2mM EDTA the fluorescent S-layer fusion protein solutions were used for fluorescent measurements in solution. (e) coating of silicon wafer and silica particles (structure analyses with AFM). The fluorescence measurements with the S-layer coated biocolloids were performed with flow cytometry and confocal microscopy.

### *Energy transfer measurements with mixtures of single tagged fluorescent SgsE fusion proteins*

The transfer rate between donors and acceptors should be linear for homogenous and dilute systems. The reason is the so-called Foerster's sphere of influence. The probability that an acceptor lies inside the Foerster's sphere is higher. A linear dependence was not found for the used concentrations. It was found that when the concentration of the acceptor YFP protein was higher than the donor concentration we could not distinguish between co-excitation of the donor with acceptor excitation and energy transfer.

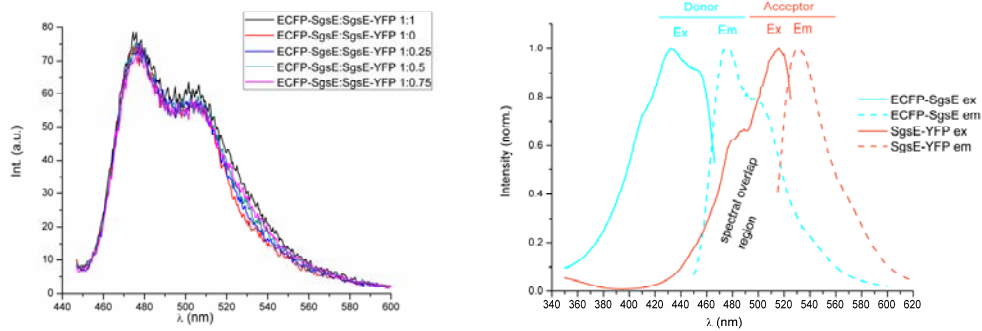


Figure 3. Left: Fluorescence resonance energy transfer measurements with mixtures of single tagged fluorescent SgsE fusion proteins (emission spectra after excitation at 435 nm). There is no decrease in donor fluorescence or increase in acceptor fluorescence. Right: Excitation (Ex) and emission (Em) spectra of the cyan donor protein ECFP-SgsE and the yellow acceptor protein SgsE-YFP. The bimodal excitation spectrum has its maximum at 435 nm and at around 440 nm, the broad emission spectrum of the ECFP protein has its maximum at 476 nm with a shoulder at around 500 nm. The bimodal excitation spectrum of YFP has its maximum at 514 nm and the second peak at around 485 nm, the maximum of the emission spectrum is at 527 nm. The emission spectrum of the donor protein ECFP-SgsE overlaps with the excitation spectrum of the acceptor protein SgsE-YFP. The spectral overlap region is clearly visible in the figure and therefore this two proteins can be used for energy transfer investigations. The numbers refer to molar ratio (based on multiples of the used protein concentration: 0.5 micro molar).

### Flow cytometry measurements

A set of blank experiments were carried out with the flow cytometer.

First of all, uncoated silica particles were measured with the AmCyan-A filter channel (after excitation with the 405-nm laser) and the FITC-A filter channel (after excitation with the 488-nm filter). No fluorescent was detected.

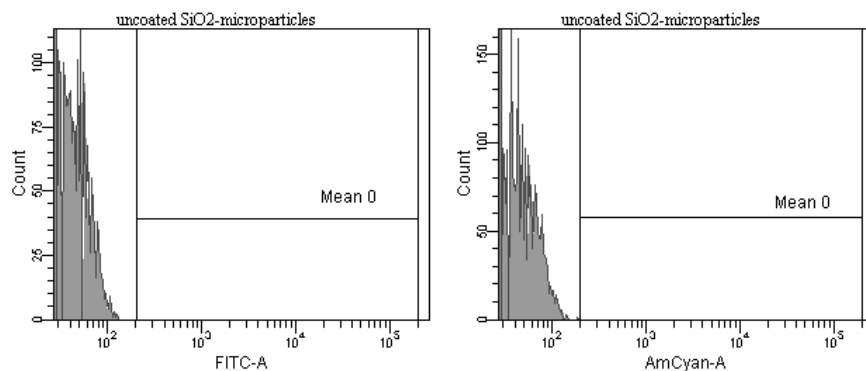


Figure 4. Flow cytometry performed on uncoated silica particles. The filters used were for AmCyan-A and FITC-A.

Figure 5 shows the behaviour of silica particles coated with the bi-fluorescent S-layer fusion protein ECFP-SgsE-YFP in comparison with particles covered with monofluorescent SgsE-YFP and ECFP-SgsE.

A weak signal of the ECFP-SgsE reference biocolloids and a larger signal of the ECFP-SgsE-YFP biocolloids using the AmCyan-A filter could be measured. However, no signal was detected for the SgsE-YFP biocolloids, which might imply that the fluorescence intensity increase for the AmCyan filter might come from the energy transfer.

In addition it was observed that ECFP-SgsE-YFP biocolloids also emitted fluorescence after excitation with the 488-nm laser line, Flow cytometry measurements show that energy transfer take places within the bi-fluorescent fusion S-layer protein.

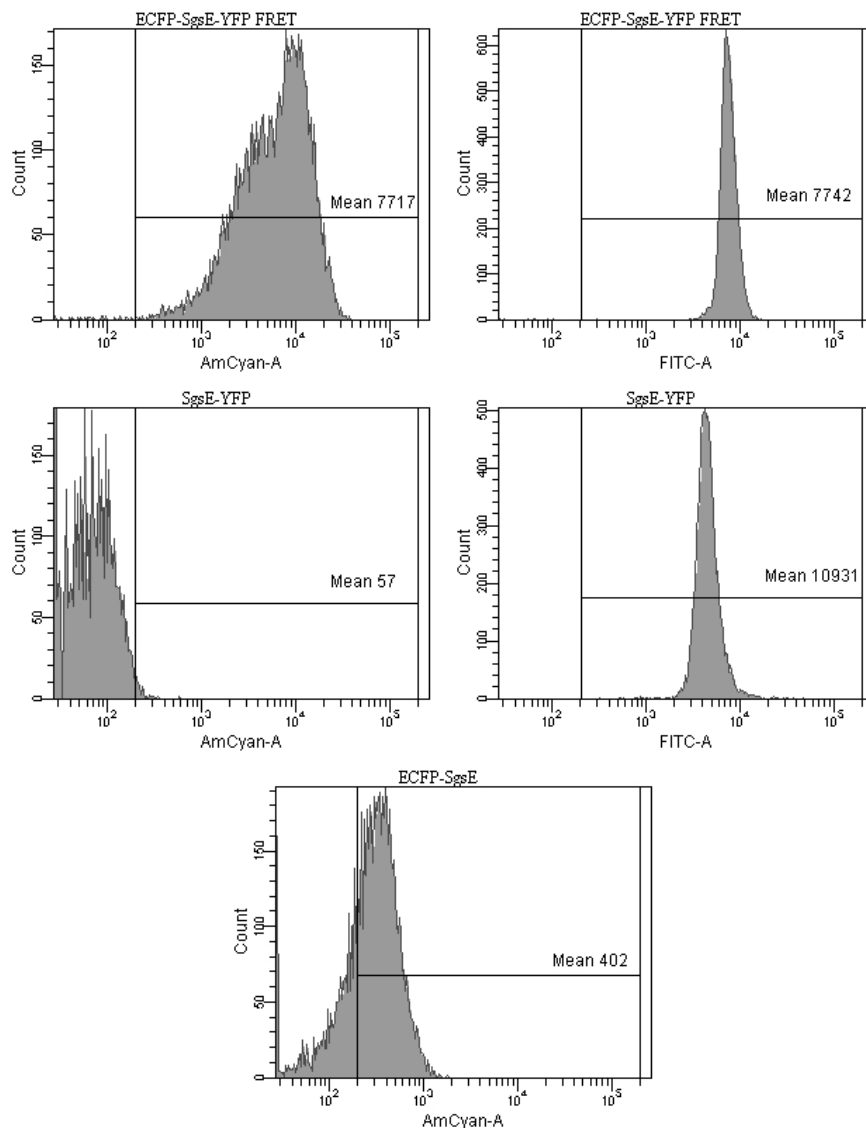


Figure 4. Flow cytometry performed on coated silica particles. The filters used were AmCyan-A and FITC-A. Note that the colloids were coated with a bi-fluorescent S-layer protein (ECFP-SgsE-YFP) and single fusion S-layer proteins (SgsE-YFP and ECFP-SgsE independently)

Figure 5 show flow cytometry measurements carried out on mixtures of single-tagged S-layer fluorescent proteins. The silica particles were covered with different molar ratios (donor/acceptor 1:1, and donor/acceptor: 1:0.5) of ECFP-SgsE and SgsE-YFP protein solutions respectively (protein concentration: 0.5  $\mu\text{M}$ ).

The fluorescence emission of both fluorescent proteins randomly distributed on the particle surface was measured. Neither yellow nor cyan patches on the particle surface could be detected. A molar ratio of 1:1 emitted more fluorescence than the 1:0.5 ratio in the FITC-A channel. The AmCyan-A filter channel provided a slightly higher signal for the 1:0.5 (donor/acceptor) mixture, probably coming from the higher amount of ECFP-SgsE proteins on the particles. The results show no evidence of energy transfer between particles coated with single-tagged fusion proteins.

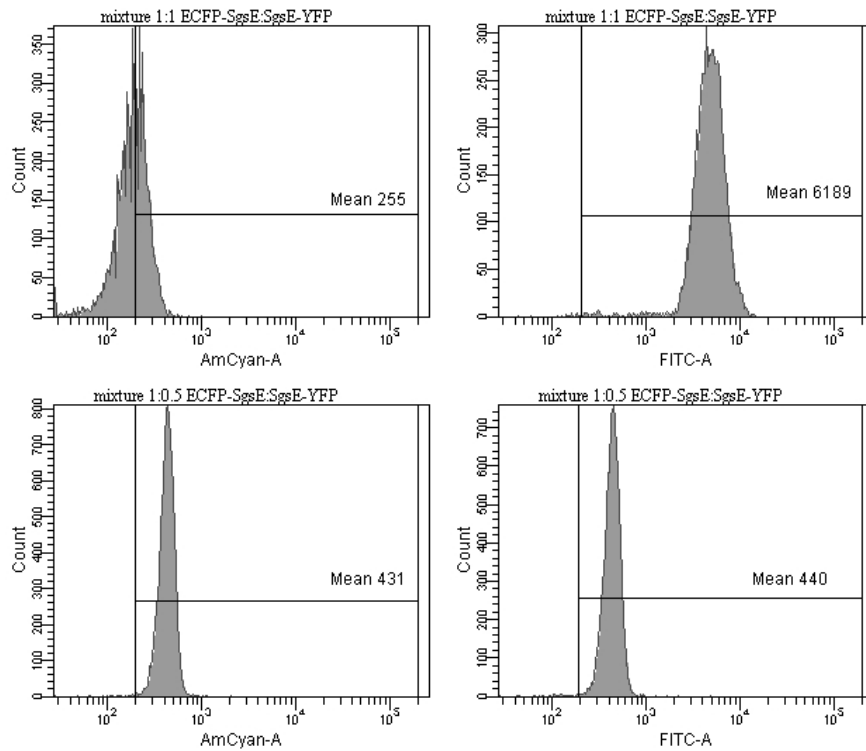


Figure 5. Flow cytometry performed on coated silica particles. The particles were exposed to different protein concentrations (expressed as molar ratio). The filters used were AmCyan-A and FITC-A.

### *Confocal microscopy measurements*

Figure 6 and figure 7 show confocal micrographs of silica particles coated with monofluorescent S-layer fusion proteins. These pictures complement the confocal results reported in the manuscript.

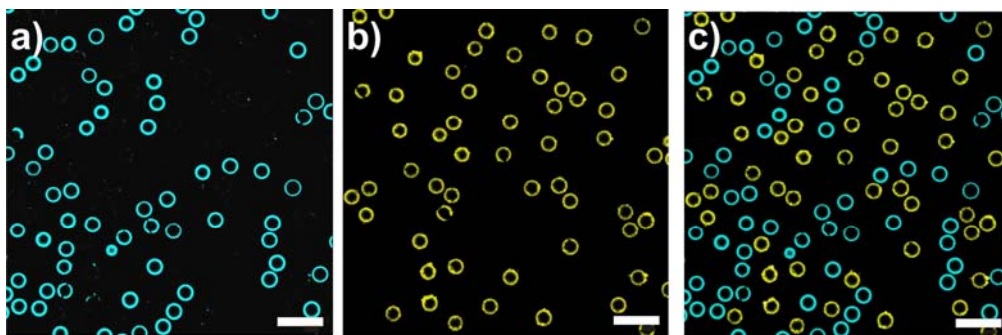


Figure 6. Coated 3 $\mu$ m silica particles, bar=10 $\mu$ m. a) Cyan ECFP-SgsE and yellow SgsE-YFP coated silica particles excited with the Argon/2 laser (458-nm) and imaged through a BP465-510-nm filter and LP530-nm emission filter. b) yellow SgsE-YFP coated silica particles excited with the 514-nm laser line of an Argon/2 laser and imaged through the LP 530-nm emission filter. c) overlay of a)+b)

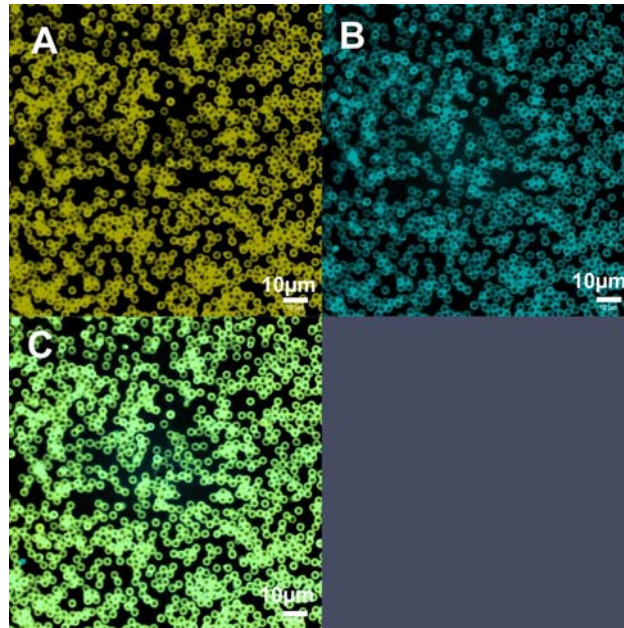


Figure 7. Silica particles (3  $\mu\text{m}$ ) coated with a mixture of ECFP-SgsE and SgsE-YFP. For the coating of the particles an equimolar concentration of ECFP-SgsE:SgsE-YFP protein solution was used. Separated excitation and emission images of (A) SgsE-YFP (514-nm laser for excitation and imaged through a LP 530-nm emission filter), (B) ECFP-SgsE (458-nm laser for excitation and imaged through a BP465-510 nm emission filter) and (C) the overlay of both filter setups.

DOI: 10.1002/sml.200701215

# Recombinant Glycans on an S-Layer Self-Assembly Protein: A New Dimension for Nanopatterned Biomaterials

Kerstin Steiner, Angelika Hanreich, Birgit Kainz, Paul G. Hitchen, Anne Dell, Paul Messner, and Christina Schäffer\*

**C**rucial biological phenomena are mediated through carbohydrates that are displayed in a defined manner and interact with molecular scale precision. We lay the groundwork for the integration of recombinant carbohydrates into a “biomolecular construction kit” for the design of new biomaterials, by utilizing the self-assembly system of the crystalline cell surface (S)-layer protein SgsE of *Geobacillus stearothermophilus* NRS 2004/3a. SgsE is a naturally O-glycosylated protein, with intrinsic properties that allow it to function as a nanopatterned matrix for the periodic display of glycans. By using a combined carbohydrate/protein engineering approach, two types of S-layer neoglycoproteins are produced in *Escherichia coli*. Based on the identification of a suitable periplasmic targeting system for the SgsE self-assembly protein as a cellular prerequisite for protein glycosylation, and on engineering of one of the natural protein O-glycosylation sites into a target for N-glycosylation, the heptasaccharide from the AcrA protein of *Campylobacter jejuni* and the O7 polysaccharide of *E. coli* are co- or post-translationally transferred to the S-layer protein by the action of the oligosaccharyltransferase PglB. The degree of glycosylation of the S-layer neoglycoproteins after purification from the periplasmic fraction reaches completeness. Electron microscopy reveals that recombinant glycosylation is fully compatible with the S-layer protein self-assembly system. Tailor-made (“functional”) nanopatterned, self-assembling neoglycoproteins may open up new strategies for influencing and controlling complex biological systems with potential applications in the areas of biomimetics, drug targeting, vaccine design, or diagnostics.

## Keywords:

- biomimetics
- composites
- protein engineering
- self-assembly
- S-layers

[\*] Prof. C. Schäffer, Dr. K. Steiner,<sup>[+]</sup> A. Hanreich, B. Kainz, Prof. P. Messner  
University of Natural Resources and Applied Life Sciences  
Center for NanoBiotechnology  
Gregor-Mendel-Strasse 33, A-1180 Wien (Austria)  
E-mail: christina.schaeffer@boku.ac.at

Dr. P. G. Hitchen, Prof. A. Dell  
Division of Molecular Biosciences, Faculty of Life Sciences  
Imperial College London, London SW7 2AZ (UK)

[+] Present address: Centre for Biomolecular Sciences  
University of St. Andrews, St. Andrews (UK)

## 1. Introduction

Molecular self-assembly systems that exploit the manufactory precision of biological systems are prime candidates for use in nanobiotechnology. Crystalline-cell surface layers (S-layers) of prokaryotic organisms are a very potent self-assembly system, which can be used in bottom-up processes as a patterning element for a “biomolecular construction kit”.<sup>[1–5]</sup> The unique property of isolated S-layer protein subunits (monomers) to reassemble into two-dimensional (2D) crystals that are identical to those found on intact bacterial cells, either

in suspension, on diverse solid supports, on liposomes, or on various interfaces, opens a wide range of S-layer-based applications.<sup>[6–9]</sup> In previous studies, it has been demonstrated that several functional domains introduced into S-layer proteins at distinct positions by genetic engineering do not interfere with the intrinsic self-assembly property of the S-layer system, while simultaneously fully retaining their specific biological properties.<sup>[2,4,10]</sup>

A novel line of development is directed toward the integration of carbohydrate compounds (glycans) into this biomolecular construction kit through co- or post-translational fusion of the carbohydrates to the self-assembly S-layer protein matrix, leading to the production of self-assembled S-layer neoglycoproteins.<sup>[11]</sup> Considering that glycans are ubiquitous biomolecules, which, in many cases, are key to protein function,<sup>[12–14]</sup> it is evident that glycans are useful means for addressing various questions in the fields of basic and applied research, relating to the areas of biomimetics, drug targeting, vaccine design,<sup>[15]</sup> or diagnostics.<sup>[16,17]</sup> Vital cellular functions that are regulated or influenced by glycans include, for instance, recognition, signaling, trafficking, biological half life, and adhesion events; several immunological phenomena are also enabled and enhanced through glycan “signals” on proteins. Thus, engineering of tailor-made (“functional”) glycoproteins (neoglycoproteins) will decisively change our capability to influence and control complex biological systems. In this context, high-density, periodic, and controllable display of glycans, which through random chemical coupling reactions of glycans to various supports cannot be fully accomplished, will play a pivotal role. For this demand, the S-layer protein self-assembly system offers an attractive solution.

In this study, the S-layer protein SgsE from *Geobacillus stearothermophilus* NRS 2004/3a (GenBank accession number AF328862) is exploited as a matrix for the high-density display of glycans in a nanometer-scaled, periodic, way using a combined carbohydrate/protein engineering approach. SgsE is a 903-amino acid protein, which includes a 30-amino acid signal peptide aligned by an entropy-driven process into a 2D crystalline array<sup>[8]</sup> with oblique (p2) symmetry exhibiting nanometer-scaled periodicity (lattice parameters:  $a = 11.6$  nm,  $b = 9.4$  nm,  $\gamma \approx 78^\circ$ ).<sup>[18,19]</sup> SgsE was chosen for proof of concept because it is naturally O-glycosylated with long-chain poly-L-rhamnans linked via a  $\beta$ -D-galactose residue to the amino acids threonine<sub>590</sub>, threonine<sub>620</sub>, and serine<sub>794</sub> of the S-layer protein.<sup>[19,20]</sup> The protein-inherent glycosylation sites are predicted to form a loop structure that is spatially accessible to the glycosylation machinery of the bacterium. Thus, these sites offer ideal targets for engineering of specific glycosylation sequences that would be recognized by heterologous oligosaccharyl:protein transferases, as required for S-layer neoglycoprotein design.

Glycans are generally synthesized in a complex, template-independent way that has let them escape (nano)biotechnological applications so far. Our understanding of the molecular details of the protein glycosylation process and the availability of the biosynthesis machineries for several glycans in the form of chromosomal gene clusters are prerequisites for the production of S-layer neoglycoproteins in bacterial hosts.<sup>[11]</sup> Recent demonstrations of the functional transfer of protein

glycosylation pathways into the experimental model organism *Escherichia coli* at the genetic level opens new avenues for carbohydrate engineering of S-layer proteins.<sup>[21,22]</sup> Based on the availability of molecular tools, the Pgl protein N-glycosylation system from *Campylobacter jejuni*<sup>[23]</sup> and the *E. coli* O7 antigen biosynthesis system<sup>[24]</sup> were used for the design of SgsE-neoglycoproteins. The *C. jejuni* Pgl enzymes synthesize a heptasaccharide with the structure D-GalNAc- $\alpha$ 1,4-D-GalNAc- $\alpha$ 1,4-(D-Glc- $\beta$ 1,3)-D-GalNAc- $\alpha$ 1,4-D-GalNAc- $\alpha$ 1,3-D-Bac, where Bac is 2,4-diacetamido-2,4,6-trideoxy-D-Glc,<sup>[25]</sup> involving the lipid carrier undecaprenylpyrophosphate.<sup>[26]</sup> The heptasaccharide is transferred by the PglB oligosaccharyl:protein transferase to asparagine residues present in the target protein consensus sequence D-X-N-Z-S/T (where X and Z are any amino acid except proline).<sup>[27,28]</sup> Using *E. coli* as a host, it was shown that PglB has relaxed substrate specificity, transferring several O-antigen polysaccharides, carrying a 2-acetamido modification at the reducing-end sugar of the glycan, to distinct protein glycosylation sites.<sup>[22]</sup> Among the glycans tested in the course of this previous study was also the *E. coli* O7 antigen with the repeating unit structure [3-D-VioNAc- $\beta$ 1,2-(L-Rha- $\alpha$ 1,3)-D-Man- $\alpha$ 1,4-D-Gal- $\alpha$ 1,3-D-GlcNAc- $\alpha$ 1-]<sub>n</sub>, where VioNAc is 2-acetamido-2,6-dideoxy-D-Glc. In Gram-negative bacteria, the oligosaccharyl:protein transferase is proposed to act in the periplasm<sup>[21]</sup> in a mechanism, which is, in contrast to eukaryotes, independent of the protein translocation machinery, and is able to glycosylate folded and unfolded proteins.<sup>[29]</sup>

The aim of this study is the transfer of the *C. jejuni* heptasaccharide and the *E. coli* O7 polysaccharide onto the SgsE S-layer protein of *G. stearothermophilus* NRS 2004/3a, and the successful expression of the S-layer neoglycoproteins in *E. coli*. For proof of concept we specifically deal with: i) the establishment of a periplasmic targeting system for the S-layer protein as a prerequisite for S-layer neoglycoprotein production in *E. coli*,<sup>[30]</sup> ii) engineering of an N-glycosylation site in the naturally O-glycosylated S-layer protein to serve as a potential target for the PglB oligosaccharyl:protein transferase to act on, iii) the unequivocal proof of the neoglycoprotein nature of the engineered products, and, most importantly, iv) the demonstration of the self-assembly capability of the produced nanostructured composites.

## 2. Results and Discussion

### 2.1. Periplasmic Targeting of SgsE

The export of SgsE to the periplasm of *E. coli* is a prerequisite for the biosynthesis of S-layer neoglycoproteins, because in Gram-negative bacteria the final step of protein glycosylation takes place in the periplasm. Currently, there is nothing known about the mode of translocation used by the S-layer protein SgsE to travel from the cytoplasm across the cytoplasmic membrane of its native host, which is *G. stearothermophilus* NRS 2004/3a, to reach the cell surface as its final destination.

At the point of the conceptualization of this study it was clear from recombinant SgsE production in heterologous organisms

such as *E. coli* or *Lactococcus lactis*<sup>[31]</sup> that the intrinsic force to promote S-layer protein self-assembly was so strong that the cytoplasm of these organisms was fully packed with assembled protein. This, however, is undesired for recombinant S-layer protein glycosylation. Thus the suitability of different signal peptides to export SgsE from the cytoplasm, where it is synthesized, to the periplasm was investigated, including signal peptides from different Gram-negative organisms, which generally mediate the export of either unfolded proteins (Sec-secretory pathway) or folded proteins (twin arginine translocation (TAT) secretory pathway). More specifically, the signal sequence of pectate lyase B (ssPelB) from *Erwinia carotovora*, the maltose-binding protein (MBP) of *E. coli* including its signal peptide, which both mediates protein export via the Sec-secretory pathway, as well as the signal peptide TorA (ssTorA) of the trimethylamine N-oxide (TMAO) reductase from *E. coli*, which supports the TAT-secretory pathway, were translationally fused to the N-terminus of the S-layer protein. In the course of this study, two distinct forms of SgsE were compared with regard to their suitability as a protein target for recombinant glycosylation. These are the forms A\_SgsE, corresponding to the mature S-layer protein devoid of its native signal peptide (A\_SgsE<sub>31–903</sub>), and the truncated protein G\_SgsE, corresponding to a 330-amino acid N-terminal truncation (G\_SgsE<sub>331–903</sub>). Either form of SgsE has been shown to possess an excellent self-assembly capability.<sup>[2]</sup> G\_SgsE was included in this study because it can be imagined that, due to its smaller size compared to the mature protein, its export to the periplasm will be facilitated. In another neoglycoprotein production experiment, ssPelB and ssTorA were successfully used for the transfer of the N-glycosylation target protein AcrA of *C. jejuni* to the periplasm of *E. coli*, demonstrating that bacterial N-glycosylation can occur independently of the protein translocation machinery.<sup>[21,29]</sup> Concerning periplasmic targeting of S-layer proteins in general, MBP has been reported to export the S-layer protein SbsA of *G. stearothermophilus* PV/72 to the periplasm of *E. coli*.<sup>[32]</sup>

The different S-layer fusion proteins were expressed in *E. coli* BL21 Star (DE3) carrying the respective expression plasmids. Based on the masses of A\_SgsE and G\_SgsE of 93.7 and 61.0 kDa, respectively, the masses of the different fusion proteins were calculated to be 95.9 and 63.2 kDa for the ssPelB constructs, 139.2 and 106.5 kDa for the MBP constructs, and 98.4 and 65.7 kDa for the ssTor constructs. This was in accordance with the sodium dodecylsulfate–polyacrylamide electrophoresis (SDS–PAGE) evidence (Figure 1, lanes 3–8). Using ssPelB and ssTor, both A\_SgsE and G\_SgsE could be expressed in high yield, whereas the fusion with MBP resulted in lower protein yield, with the A\_SgsE form being detectable only by Western blotting using anti-SgsE antibody (not shown). To investigate if the native signal peptide of SgsE could mediate export of the S-layer protein into the periplasm of *E. coli*, full length SgsE including its signal peptide was introduced into the expression vector pET28a and produced in *E. coli* BL21 Star (DE3). According to SDS–PAGE analysis, the S-layer protein possessed the expected mass of 96.6 kDa and was produced in high yield (Figure 1, lane 2).

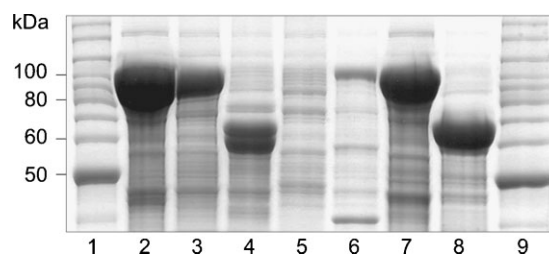


**Figure 1.** Periplasmic targeting of the S-layer protein SgsE according to SDS–PAGE analysis (10% gel) after Coomassie Blue staining. Lane 1: Bench-mark ladder (Invitrogen); lane 2: SP-SgsE; lane 3: ssPelB–A\_SgsE; lane 4: ssPelB–G\_SgsE; lane 5: MBP–A\_SgsE; lane 6: MBP–G\_SgsE; lane 7: ssTor–A\_SgsE; lane 8: ssTor–G\_SgsE; lane 9: Bench-mark ladder.

The subcellular localization of the S-layer protein was investigated by electron microscopy after immunogold-labeling (anti-SgsE antibody) of thin-sectioned cells of *E. coli* BL21 Star (DE3) expression cultures. To compare the export efficiency mediated via the different signal peptides, gold particles present in the cytoplasmic and in the periplasmic compartment were counted from electron micrographs. Averaging the values obtained from five cells, each from separate labeling experiments, the approximate periplasm to cytoplasm ratio is 0.3:1 for the ssTor constructs, 1:1 for full-length SgsE possessing its native signal peptide, 2:1 for the ssPelB constructs, and 3:1 for the MBP constructs. The periplasmic-to-cytoplasmic ratio was invariant for different cell sizes. Interestingly, no significant difference in the export efficiency between A\_SgsE and G\_SgsE was observed, indicating that S-layer protein length does not affect S-layer protein translocation through the cytoplasmic membrane. Thus, SgsE can be targeted to the periplasm by the PelB- and the MBP-signal peptides as well as by its native signal peptide, but not with ssTorA. This indicates that SgsE is exported in an unfolded state via the Sec-secretory pathway. As the native signal peptide was also recognized by the export machinery of *E. coli*, we assume also that in the *in vivo* background of *G. stearothermophilus* NRS 2004/3a the export of SgsE follows the Sec-pathway. This has already been described for the S-layer proteins of other Gram-positive organisms such as *Clostridium difficile*<sup>[33]</sup> and *Corynebacterium glutamicum*.<sup>[34]</sup>

For the following S-layer neoglycoprotein production, the signal peptide of PelB was chosen for periplasmic expression of SgsE, because it was the best compromise between export efficiency and product yield (Figure 2). In addition, ssPelB is a small peptide of only 22 amino acids, which should be cleaved off *in vivo* after the export of the protein to the periplasm and, importantly, the ssPelB–SgsE fusion proteins were shown to fully maintain the self-assembly capability of the native S-layer protein (this study, not shown).

## 2.2. Design of an SgsE Neoglycoprotein Carrying a *C. jejuni* Heptasaccharide

For the first time, an S-layer neoglycoprotein has been designed, comprising the S-layer protein SgsE from *G. stearothermophilus* NRS 2004/3a, including the PelB signal peptide for periplasmic targeting, and the heptasaccharide

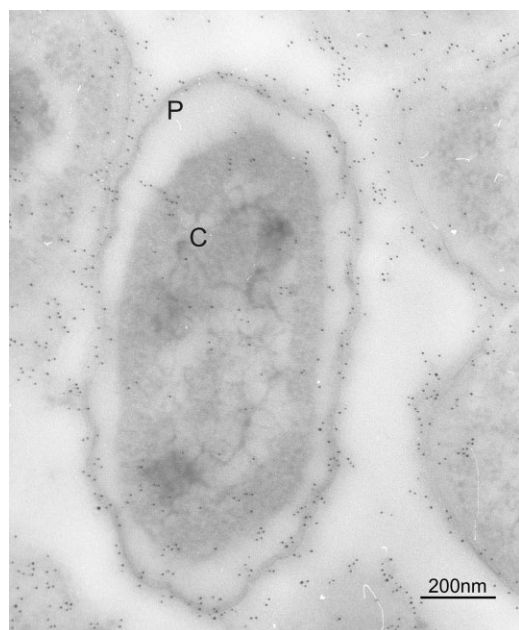


**Figure 2.** Transmission electron micrograph of an ultrathin, cross-sectioned and immunogold-labeled cell of *E. coli* BL21 Star (DE3) expressing the S-layer protein SgsE, to which the PelB signal peptide has been fused (ssPelB–A\_SgsE). The presence of the high number of gold particles in the periplasmic space indicates the efficiency of this export mechanism for the S-layer protein. P, periplasmic space; C, cytoplasm.

Glc(GalNAc)<sub>5</sub>Bac of *C. jejuni*. For this purpose, the plasmid pACYCpgl harboring the complete pgl gene cluster of *C. jejuni* that is responsible for heptasaccharide biosynthesis and its transfer to the protein was transformed into *E. coli* BL21 Star (DE3).<sup>[21]</sup> As a positive control, to confirm that the glycosylation machinery of *C. jejuni* functions under the chosen conditions, the plasmid pEC(AcrA-per), expressing periplasmic soluble AcrA of *C. jejuni* with the PelB signal peptide and a C-terminal hexahistidine tag, was transferred to electrocompetent *E. coli* BL21 Star (DE3) cells containing pACYCpgl.<sup>[29]</sup> Analysis of the expression product by Western immunoblotting, using a heptasaccharide specific antibody (anti-pgl antibody), confirmed glycosylation of AcrA (Figure 3, lane 8).

In *C. jejuni*, Glc(GalNAc)<sub>5</sub>Bac is naturally linked to distinct *N*-glycosylation sites of the protein AcrA,<sup>[21]</sup> while the S-layer protein SgsE possesses *O*-glycosidically linked glycan chains. Inspection of the S-layer protein sequence revealed the presence of one putative *N*-glycosylation site at position N<sub>879</sub> (DVNQT; the glycosylated asparagine residue is underlined), conforming with the amino acid sequence requirement of the oligosaccharyl:protein transferase PglB of *C. jejuni*, which is the key enzyme for protein *N*-glycosylation.<sup>[22,28,35]</sup> Thus, in a first glycosylation approach, the potential of PglB to glycosylate native SgsE with its endogenous heptasaccharide Glc(GalNAc)<sub>5</sub>Bac substrate in *E. coli* was investigated by expression of ssPelB–A\_SgsE from plasmid pET22b–A\_SgsE in *E. coli* BL21 Star (DE3) harboring pACYCpgl.<sup>[21]</sup> However, no glycosylated protein was visible on a Western immunoblot, implying that the putative *N*-glycosylation site of

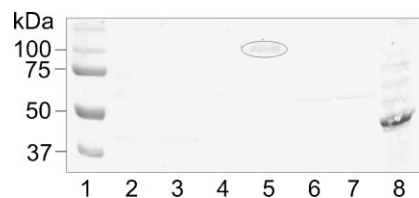


**Figure 3.** Engineering of *N*-glycosylation sites on the S-layer protein SgsE as determined by recombinant glycosylation with the *C. jejuni* heptasaccharide (pgl) and Western immunoblot detection using a glycan-specific antibody. Lane 1: Precision Plus All Blue Protein Standard (BioRad); lane 2: A\_SgsE\_S,T5-pgl; lane 3: A\_SgsE\_S,T12-pgl; lane 4: A\_SgsE\_T5-pgl; lane 5: A\_SgsE\_T12-pgl; lane 6: A\_SgsE\_S5-pgl; lane 7: A\_SgsE\_S12-pgl; lane 8: glycosylated AcrA protein (control). Successful neoglycoprotein production is marked by a circle.

SgsE at position N<sub>879</sub> was not recognized by PglB (not shown). The same negative result was obtained when testing a second putative *N*-glycosylation site (dNNVS; the mutated amino acid is underlined) located at the rather C-terminal position of SgsE (amino acid N<sub>893</sub>), which was created by site-directed mutagenesis of G<sub>891</sub>D using a mutant primer (with pET22b–A\_SgsE\_G<sub>891</sub>D being the respective expression plasmid). Another set of *N*-glycosylation experiments utilized the *N*-glycosylation consensus sequence DFNRS of the glycoprotein AcrA of *C. jejuni*, or the longer sequence ASKDFNRSKALFS, instead of SgsE inherent sequences. Initially, either sequence was translationally fused to the N-terminus of the truncated S-layer protein G\_SgsE, based on the assumption that the N-terminus of SgsE would be spatially accessible for the PglB enzyme. This is because the N-terminus is proposed to mediate anchoring of the S-layer protein to the cell wall in *G. stearothermophilus* NRS 2004/3a, implying its spatial exposure to the environment. However, when introducing the respective fusion proteins encoded by pET22b–DFNRS\_G\_SgsE and pET22b–long\_G\_SgsE into *E. coli* BL21 Star (pACYCpgl), again no S-layer neoglycoprotein production occurred (not shown). Finally, the endogenous *O*-glycosylation sites of SgsE were engineered to become *N*-glycosylation target sequences. By this strategy, the amino acid sequence adjacent to the naturally *O*-glycosylated amino acids Thr<sub>620</sub> or Ser<sub>794</sub> of SgsE, or both of them, was replaced by the *N*-glycosylation consensus sequence DFNRS or ASKDFNRS–KALFS, respectively. For this purpose, an intermediate form of SgsE lacking the sequence between amino acids L<sub>610</sub> and E<sub>804</sub> was constructed, with the corresponding nucleotide sequence having an artificial KpnI restriction site introduced between the amino acids at the position 611 and 612. After introducing the respective *N*-glycosylation sequence, while simultaneously deleting part of sgsE by the use of megaprimers for polymerase chain reaction (PCR) and subsequent ligation into the intermediate sgsE form provided through plasmid pET22b–A\_SgsE\_inter, the sequence DFNRS replaced K<sub>618</sub>TTSD<sub>622</sub> (pET22b–A\_SgsE\_T5) or L<sub>792</sub>TSAD<sub>796</sub> (pET22b–A\_SgsE\_S5), or both of them (pET22b–A\_SgsE\_S,T5), and the sequence ASKDFNRSKALFS replaced A<sub>615</sub>DLKTTSDNFKLY<sub>627</sub> (pET22b–A\_SgsE\_T12), or T<sub>789</sub>ATLTSADVIRVD<sub>901</sub> (pET22b–A\_SgsE\_S12), or both of them (pET22b–A\_SgsE\_S,T12). Due to the cloning procedure, all chimeric S-layer proteins contained

a C-terminal hexahistidine tag, which was used for determination of the molecular mass of the constructs in Western blot analysis. The signals obtained with anti-His-antibody at approximately 96 kDa were in accordance with the expected masses (not shown).

S-layer neoglycoprotein production was induced by isopropyl- $\beta$ -thiogalactopyranoside (IPTG) in *E. coli* BL21 Star (pACYCpgl) harboring the different expression plasmids coding for the modified S-layer proteins. According to the Western immunoblot evidence using anti-pgl antibody (Figure 3, lanes 2–7), after an expression period of 20 h, the best *N*-glycosylation result was obtained with the S-layer protein in which the endogenous Thr<sub>620</sub>-*O*-glycosylation site had been replaced by the extended *C. jejuni* *N*-glycosylation sequence ASKDFNRSKALFS (Fig. 3, lane 5). After prolonged development of the Western blot, weak bands were also visible for the S-layer protein forms, where this site had been replaced by DFNRS or in which the Thr<sub>620</sub> and Ser<sub>794</sub> sites had been simultaneously replaced by the *N*-glycosylation target sequence (data not shown). Unexpectedly, no glycosylation signal was obtained when using the S-layer protein forms in which the Ser<sub>794</sub> glycosylation site had been replaced by the *N*-glycosylation target sequence (Fig. 3, lanes 6 and 7). The same results were obtained for the modified forms of G<sub>SgsE</sub> for which, due to the higher expression level, a higher probability of glycosylation could have been expected (data not shown). This indicates that the consensus sequence alone is not sufficient for *N*-glycosylation, but the spatial environment is also important.<sup>[29,36]</sup> For the bacterial *N*-glycosylation system it is proposed that the glycosylation sites are located in flexible parts of folded proteins.<sup>[29]</sup> Rangarajan and coworkers<sup>[36]</sup> elucidated the structure of PEB3, a glycosylated adhesin from *C. jejuni*, and showed that the glycosylation site is located within a surface-exposed loop joining two structural elements. While the tertiary structure of SgsE is unknown, secondary structure prediction using PSIPREDView<sup>[37]</sup> revealed that Thr<sub>620</sub> and Ser<sub>794</sub> are located in a loop between two protein strands, thereby fulfilling the general requirement for bacterial glycosylation. Considering the negative result when using the engineered Ser<sub>794</sub> *N*-glycosylation target sequence, it is interesting to note that the pI value of the native amino acid sequence surrounding Ser<sub>794</sub> of 4.2 (T<sub>789</sub>ATLTSAD-VIRVDFS<sub>903</sub>) is markedly different from that of the introduced ASKDFNRSKALFS *N*-glycosylation sequence (pI = 10.0; A<sub>789</sub>SKDFNRSKALFS<sub>903</sub>). In contrast, for the engineered consensus sequence around the Thr<sub>620</sub> site that was recognized by the heterologous PglB enzyme, there was only a slight difference in pI values between the native (pI = 8.4; K<sub>611</sub>AVGADLKTSDNFKLY<sub>627</sub>) and the engineered (pI = 9.9; G<sub>611</sub>TVGASKDFNRSKALFS<sub>627</sub>) S-layer protein.

These results indicate that the requirements for protein glycosylation in heterologous systems are complex. Thus, the availability of a well-characterized naturally glycosylated S-layer protein such as SgsE from *G. stearothermophilus* NRS 2004/3a is very valuable for engineering of tailor-made glycosylation target sequences that will be recognized by oligosaccharyltransferases from diverse glycosylation systems to produce self-assembly S-layer neoglycoproteins.

### 2.3. Purification of the SgsE Neoglycoprotein Carrying the *C. jejuni* Heptasaccharide

The SgsE neoglycoprotein carrying the *C. jejuni* heptasaccharide (named A<sub>SgsE\_T12</sub>-pgl) was isolated according to a standard S-layer purification protocol that had been adjusted to the periplasmic location of the S-layer neoglycoprotein, and subsequently purified by gel-filtration chromatography on a Superdex 200 prep grade column using 6 M urea as eluent. The purification process was monitored by SDS-PAGE and Western blot analyses using anti-SgsE and anti-pgl antibodies (Figure 4). It was clearly visible that the S-layer neoglycoprotein could be enriched upon purification, resulting in a final yield of 13.4 mg L<sup>-1</sup> of expression culture. In intact cells of an *E. coli* BL21 Star (pACYCpgl, pET22b-A<sub>SgsE\_T12</sub>) expression culture (Figure 4, lane 2) the amount of S-layer neoglycoprotein seems to be low, whereas the protein band in the periplasmic fraction and in the subsequently separated fractions of the dialysate and the soluble material are similarly strong, upon Coomassie staining as well as upon development with both anti-SgsE and anti-pgl antibodies (Figure 4, lanes 3–5). This result indicates on the one hand that the A<sub>SgsE\_T12</sub> target sequence is not fully exported to the periplasm, but on the other hand it also clearly shows that the exported S-layer protein is almost fully

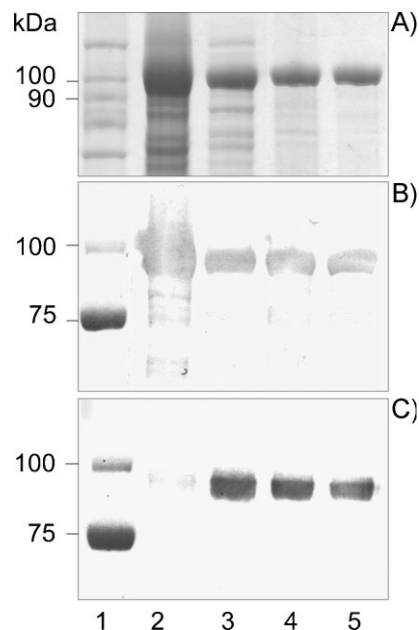


**Figure 4.** Monitoring of the purification procedure of A<sub>SgsE\_T12</sub>-pgl carrying the *C. jejuni* heptasaccharide. SDS-PAGE after A) Coomassie staining and Western immunoblot analysis using antibodies raised against B) the S-layer protein SgsE or C) the *C. jejuni* heptasaccharide. Lane 1: A) Bench-mark ladder (Invitrogen); B), C): Precision Plus All Blue Protein Standard; lane 2: intact cells of *E. coli* BL21 Star (DE3) expressing the S-layer neoglycoprotein; lane 3: periplasmic fraction; lane 4: dialysate; lane 5: soluble fraction. It is evident that the S-layer neoglycoprotein is enriched in the periplasm of *E. coli* BL21 Star (DE3) cells; according to Western blot analyses the glycosylation degree of this fraction reaches completeness.

glycosylated. To verify that periplasmic targeting was mediated by ssPelB, the purified S-layer neoglycoprotein was subjected to N-terminal sequencing. Unexpectedly, the mature S-layer neoglycoprotein revealed the sequence AQPA, corresponding to the four C-terminal amino acids of the signal peptide, which means that the PelB signal peptide was only partially cleaved off upon export of the protein to the periplasm. This finding, however, has no consequence for the functionality of the established S-layer neoglycoprotein production system.

#### 2.4. MS Analysis of the SgsE Neoglycoprotein Carrying a *C. jejuni* Heptasaccharide

Mass spectrometry was performed in order to confirm that the complete Glc(GalNAc)<sub>5</sub>Bac *N*-glycan had been transferred onto the *N*-glycosylation site of A\_SgsE\_T12. Purified A\_SgsE\_T12-pgl neoglycoprotein was digested with trypsin and the resulting peptides were analyzed by nanoliquid-chromatography (nano-LC) matrix-assisted laser-desorption ionization-time of flight (MALDI-TOF)/TOF mass spectrometry (MS). The resulting MS and MS/MS data were analyzed for the predicted A\_SgsE\_T12-pgl tryptic glycopeptide. A signal observed in the MS with a mass-to-charge ratio (*m/z*) of 1956.9<sup>1+</sup> was identified as having the correct mass for the modified peptide (data not shown). Analysis of the resulting product ion spectrum (Figure 5) clearly shows a series of singly charged fragment ions consistent with glycosidic cleavage products from the tryptic peptide DFNR modified with a heptasaccharide glycan moiety, with sufficient information to assign the sequence and branching pattern as observed for the *C. jejuni* *N*-glycan (Fig. 5, inset).<sup>[21]</sup>

#### 2.5. Self-Assembly of SgsE Neoglycoprotein Carrying the *C. jejuni* Heptasaccharide

After the glycoprotein nature of the A\_SgsE\_T12-pgl neoglycoprotein was confirmed, self-assembly of the recombinant construct was investigated. Following a protocol elaborated in the course of a recent study,<sup>[2]</sup> self-assembly of the monomeric S-layer neoglycoprotein as obtained after purification was triggered upon removal of the chaotropic agent, by dialysis against distilled water. Self-assembly was investigated by electron microscopy using negatively stained preparations. An electron micrograph of the negatively stained A\_SgsE\_T12-pgl neoglycoprotein is shown in Figure 6. Due to the low signal-to-noise ratio only one base vector pair is revealed. Since only second order reflections were unambiguously detectable, no reconstruction of the ultrastructure of this neoglycoprotein meshwork was possible at high resolution. The length of the base vectors, however, compared well with previous results of negatively stained native S-layer glycoprotein from *G. stearotherophilus* NRS

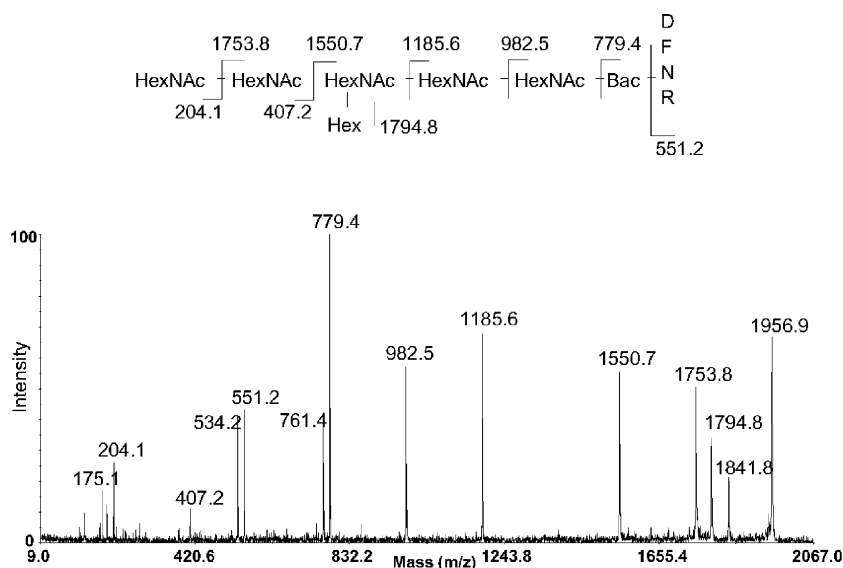


**Figure 5.** MALDI TOF/TOF product ion spectrum of  $[M + H]^{1+}$  *m/z* 1956.9 derived from the tryptic digest of the S-layer neoglycoprotein A\_SgsE\_T12 carrying the *C. jejuni* heptasaccharide. The fragment pattern for the glycan is shown inset.

2004/3a<sup>[18]</sup> as well as with the lattice parameters of self-assembled rSgsE protein ( $a = 11.6$  nm,  $b = 9.4$  nm,  $\gamma \approx 78^\circ$ ).<sup>[2]</sup> Comparing that material with the S-layer neoglycoprotein produced in the course of the present study, a slightly changed staining behavior of the latter was observed on the micrographs, with the lattice of the neoglycoprotein apparently blurred to some extent. Despite this fact, in self-assembled A\_SgsE\_T12-pgl the SgsE S-layer protein matrix itself kept its crystallinity. Thus, recombinant SgsE S-layer protein glycosylation is fully compatible with the intrinsic self-assembly property of the protein matrix.

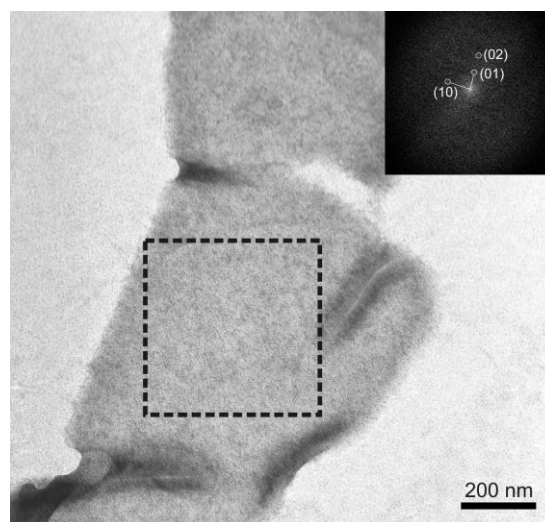


**Figure 6.** Electron micrograph of self-assembled S-layer neoglycoprotein A\_SgsE\_T12 carrying the *C. jejuni* heptasaccharide after negative staining. The inset is the Fourier spectrum of the marked area. The spectrum shows more than one reciprocal lattice. Due to the low signal-to-noise ratio only one base vector pair is shown.

Due to the lack of a suitable microscopic method for visualization of the periodic, nanometer-scale, naturally outwardly-orientated display of heptasaccharides on a self-assembled A\_SgsE-T12-pgl *neoglycoprotein* monolayer, which is conferred to this new nanostructured composite by the S-layer protein portion, we used a combined electron microscopy–modeling approach. In this approach, a negatively stained preparation of the S-layer protein self-assembled in solution served as a base for image reconstruction, and space-filling models of the Glc(GalNAc)<sub>5</sub>Bac heptasaccharides were positioned onto the subunits of the SgsE nanolattice (Figure 7A). The resulting model is an in-scale visualization of the first self-assembled S-layer *neoglycoprotein* nanolattice. In this nanolattice, each constituting subunit carries one heptasaccharide at the engineered Thr<sub>620</sub> position (Thr<sub>620</sub> was assumed at a surface-exposed, but fictive, position in the model). The periodicity of glycan display results from the base vectors of the SgsE p2 lattice, which are 11.6 and 9.4 nm, respectively. From detailed self-assembly studies of the SgsE matrix and of functionalized SgsE S-layer protein, it can be expected that self-assembly S-layer *neoglycoprotein* nanolattices do not only work in solutions, but that they are also suitable for coating of various planar solid supports, liposomes,<sup>[2]</sup> or even porous structures like membranes.<sup>[38]</sup>

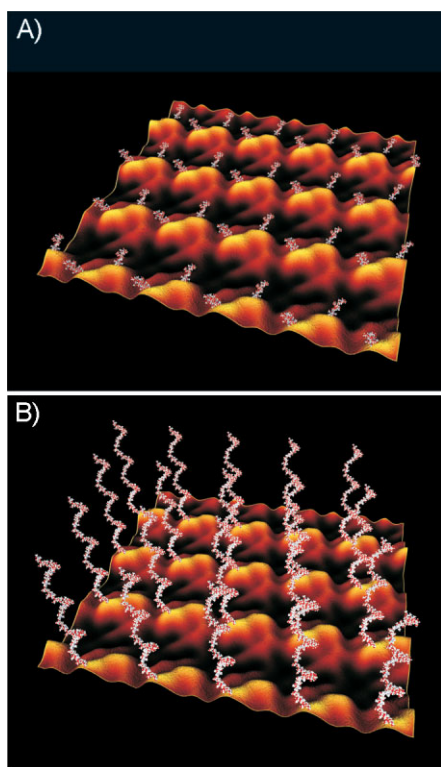


**Figure 7.** Model of a self-assembled SgsE(p2)-*neoglycoprotein* monolayer displaying engineered glycans in a nanometer-scaled, periodic way. Image reconstruction using Cinema 4D is based on a negatively stained preparation of the S-layer protein self-assembled in solution and on the pdb data of the glycans generated with Sweet at <http://www.glycosciences.de/>. The short-chain glycan of *C. jejuni* (A) and the polymerized, long chain *E. coli* O7 antigen (B) that have been used throughout this study were modeled onto the patterning S-layer matrix.

This flexibility offers a wide repertoire of opportunities for integration of glycan-mediated interactions in vitro as well as in vivo systems, as may be relevant to address basic and applied questions both in life and nonlife sciences. A potent example for in vivo carbohydrate engineering with a direct applicational aspect was the construction of a recombinant *E. coli* bacterium that displayed a modified lipopolysaccharide (LPS) mimicking a Shiga toxin receptor on its cell surface.<sup>[39]</sup>

## 2.6. Transfer of *E. coli* O7 Antigen to the Engineered *N*-Glycosylation Site of SgsE

To demonstrate the wider applicability of the engineered SgsE self-assembly matrix for recombinant glycosylation, the O7 antigen from *E. coli* was transferred onto the S-layer protein A\_SgsE-T12. This approach is based on the finding of Feldman and coworkers,<sup>[22,35]</sup> who discovered that the oligosaccharyl:protein transferase PglB of *C. jejuni* is able to transfer glycan chains with different 2-acetamido sugars at the reducing end to the *N*-glycosylation sites of proteins.<sup>[22,29,35]</sup> In our study, we investigated the possibility that PglB can also transfer glycan chains with GlcNAc at the reducing end (as present in O7) onto the engineered Thr<sub>620</sub> *N*-glycosylation site on SgsE.

In this experiment, the *E. coli*-K12 mutant strain CLM24 that lacks the O-antigen ligase and, in addition, does not synthesize O-antigen due to an inactivating insertion in *wbbL*, the gene that encodes a rhamnosyl transferase necessary for the transfer of the second sugar of the O7 antigen, was used as expression host. This strain should favor the PglB-mediated transfer of O-antigen from its carrier to the protein acceptor, because of accumulation of undecaprenylpyrophosphate-linked polysaccharide.<sup>[22]</sup> PglB was expressed under the control of the arabinose-inducible BAD promoter from plasmid pMAF10.<sup>[22]</sup> The two modified S-layer protein forms A\_SgsE-T12 and G\_SgsE-T12 with the PelB signal peptide, the extended *N*-glycosylation site from *C. jejuni* replacing the *O*-glycosylation site T<sub>620</sub> and a C-terminal hexahistidine-tag were cloned from pET22b into pBAD24 vector, which is arabinose inducible. The gene cluster necessary for the synthesis of *E. coli* O7 antigen provided through plasmid pJHCV32<sup>[24]</sup> was introduced in *E. coli* CLM24 together with PglB and A\_SgsE-T12 or G\_SgsE-T12. After induction of protein expression with arabinose over night, the SgsE *neoglycoprotein* was analyzed by Western immunoblotting using anti-SgsE-antibody. In addition to bands at 97.0 and 64.0 kDa, corresponding to nonglycosylated A\_SgsE-T12 and G\_SgsE-T12, respectively, a ladder-like banding pattern in a higher molecular weight range of ≈130–150 kDa for A\_SgsE-T12-O7 and of 75–100 kDa for G\_SgsE-T12-O7 could be detected (Figure 8, lanes 1 and 2). The specific banding pattern of each *neoglycoprotein* displays differences in the degree of polymerization of individual O7 repeating units, which is characteristic of O-antigens.

We have visualized the display of polymerized *E. coli* [VioNAc(Rha)ManGalGlcNAc]<sub>n</sub> O7 antigen via the SgsE self-assembly matrix using the same approach as described above for the *C. jejuni* heptasaccharide (Figure 7B). The recombinant transfer not only of short-chain carbohydrates,

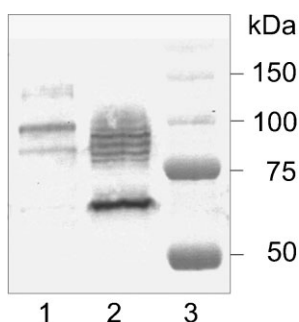


**Figure 8.** Glycosylation of the S-layer protein A\_SgsE\_T12 and G\_SgsE\_T12 with *E. coli* O7 polysaccharide. The S-layer neoglycoprotein was analyzed by SDS-PAGE (10% gel) and transfer of the samples to a PVDF membrane followed by immunodetection with an antibody recognizing SgsE. Lane 1: A\_SgsE\_T12-O7; lane 2: G\_SgsE\_T12-O7. The banding pattern of each neoglycoprotein (at  $\approx 130$ – $150$  and  $\approx 75$ – $100$  kDa, respectively) displays differences in the degree of polymerization of individual O7 repeating units. The prominent band at  $\approx 97$  and  $\approx 64$  kDa, respectively, corresponds to nonglycosylated protein; lane 3: Precision Plus All Blue Protein Standard.

such as the *C. jejuni* heptasaccharide, but also of elongated glycan chains, such as O-antigens, upon maintenance of the self-assembly property of the S-layer protein matrix, is highly relevant for the future conceptualization of functional S-layer neoglycoproteins. It can be imagined that this approach is mimicking the natural situation in *G. stearothersophilus* NRS 2004/3a, where long-chain poly-L-rhamnans are attached to the distinct O-glycosylation sites of the S-layer protein. Benefits of self-assembled S-layer neoglycoproteins carrying elongated functional glycan chains may be expected in the field of disease intervention and prevention. In general, the finding that several human pathogens contain polysaccharides as surface decoration has opened up a rapidly developing area of biomedical research.<sup>[40]</sup> Investigations over the past decade have shown that carbohydrates possess an enormous potential as lead structures for drug discovery, aiming at antagonizing the interaction of the physiological carbohydrate ligands with their receptor proteins.

To demonstrate the principal possibility of control over glycan display density by coassembly of S-layer neoglycoproteins with unmodified SgsE monomers, we show in this model a self-assembled A\_SgsE\_T12-O7 monolayer, in which only every second subunit is carrying the O7 modification, corresponding to a 1:1 mixture of A\_SgsE\_T12 and A\_SgsE\_T12-O7 (Figure 7B). In addition, coassembly of engineered SgsE-based proteins offers also an attractive option for producing multifunctional self-assembly nanolattices.

### 3. Conclusions

Carbohydrates are an important class of biomolecules that are key components for the mediation of crucial cellular phenomena, with density of glycan display and molecular scale precision of interaction being most relevant aspects. Despite the fact that carbohydrates are promising lead components for diverse in vivo as well as in vitro applications, they have

escaped (nano)biotechnological applications so far due to the complexity of their biosynthesis. Using a carbohydrate/protein engineering approach in the experimental host *E. coli*, we aimed at integration of carbohydrates into a nanobiotechnological concept through combination with the established S-layer protein self-assembly system SgsE of *G. stearothersophilus* NRS 2004/3a. First S-layer neoglycoproteins were obtained after engineering of the natural protein O-glycosylation site threonine<sub>620</sub> to become a target for N-glycosylation through insertion of the N-glycosylation consensus sequence of *C. jejuni*, and the subsequent recombinant transfer of a heptasaccharide from *C. jejuni* and of the O7 polysaccharide from *E. coli* onto the S-layer protein by the action of the oligosaccharyltransferase PglB. Due to the intrinsic self-assembly property conferred to these neoglycoproteins by the S-layer matrix, these novel nanostructured composites allow nanometer-scale and periodic display of carbohydrates. It can be assumed that due to the recombinant production process and the utilization of the S-layer self-assembly matrix, this concept is superior to conventional, random chemical carbohydrate immobilization.

Tailor-made (“functional”) nanopatterned, self-assembled neoglycoproteins follow the current trend for exploiting means for organizing biological functions at the nanometer level aiming at the development of novel concepts for life and nonlife sciences.

### 4. Experimental Section

**Bacterial strains, growth conditions, and plasmids:** *G. stearothersophilus* NRS 2004/3a was obtained from the N. R. Smith Collection, US Department of Agriculture (Peoria, IL) and was grown on modified S-VIII medium (1% peptone, 0.5% yeast extract, 0.5% meat extract, 0.13% K<sub>2</sub>HPO<sub>4</sub>, 0.01% MgSO<sub>4</sub>, 0.06% sucrose) at 55 °C. *E. coli* DH5 $\alpha$  (Invitrogen, Lofer, Austria) was used for plasmid propagation. *E. coli* BL21 Star (DE3) and *E. coli* CLM24<sup>[22]</sup> were used for (neoglyco)protein expression. *E. coli* strains were grown at 37 °C in Luria–Bertani (LB) broth supplemented with ampicillin (Amp<sup>r</sup>; 50  $\mu$ g mL<sup>-1</sup>), kanamycin (Km<sup>r</sup>; 50  $\mu$ g mL<sup>-1</sup>), chloramphenicol (Cm<sup>r</sup>; 30  $\mu$ g mL<sup>-1</sup>), trimethoprim (Tnp<sup>r</sup>; 50  $\mu$ g mL<sup>-1</sup>), or tetracycline (Tet<sup>r</sup>; 20  $\mu$ g mL<sup>-1</sup>), when appropriate. Plasmids pACYC184p $gI$ ,<sup>[21]</sup> pJHCV32,<sup>[24]</sup> pEC(AcrAper),<sup>[28]</sup> and pMAF10<sup>[22]</sup> have been described previously. All strains and plasmids are listed in Table 1. Oligonucleotide primers used for PCR amplification are summarized in Table 2.

**General methods:** Genomic DNA of *G. stearothersophilus* NRS 2004/3a was isolated with the Qiagen Genomic-tip 100 kit (Qiagen, Hilden, Germany) according to the manufacturer’s instruction. Restriction enzymes and T4 DNA ligase were purchased from Invitrogen, and calf intestinal alkaline phosphatase was obtained from Roche (Vienna, Austria). The Qiagen MinElute gel extraction kit was used to purify DNA fragments from agarose gels and the Qiagen MinElute reaction cleanup kit was used to purify digested oligonucleotides and plasmids. Plasmid DNA from transformed cells was isolated with the Qiagen plasmid miniprep kit. Agarose gel electrophoresis was performed as

**Table 1.** Strains and plasmids used in this study.

Strain or plasmid	Description	Source
<i>G. stearothermophilus</i> NRS 2004/3a	Wild-type covered by an S-layer	N. R. Smith collection
<i>E. coli</i> DH5 $\alpha$	F <sup>-</sup> $\phi$ 80lacZM15 $\Delta$ (lacZYA-argF) U169recA1 endA1 hsdR17 (r <sub>k</sub> <sup>-</sup> , m <sub>k</sub> <sup>+</sup> ) phoA supE44 thi-1 gyrA96 relA1 $\lambda$ <sup>-</sup>	Invitrogen
<i>E. coli</i> BL21 Star (DE3)	F <sup>-</sup> ompT hsdS <sub>B</sub> (r <sub>B</sub> <sup>-</sup> m <sub>B</sub> <sup>-</sup> ) gal dcm rne131 (DE3)	Invitrogen
<i>E. coli</i> W3110	rph-1 1N(rrnD-rrnE)	M. Valvano [22]
<i>E. coli</i> CLM24	W3110, $\Delta$ waal	
pET28a(+)	<i>E. coli</i> expression vector, IPTG inducible, Km <sup>r</sup>	Novagen
pET22b(+)	<i>E. coli</i> expression vector; Amp <sup>r</sup> , used for introducing an N-terminal PelB signal peptide	Novagen
pMAL-p2x	<i>E. coli</i> expression vector; Amp <sup>r</sup> , used for introducing N-terminally MBP including its signal peptide	NEB
pET28a-ssTor	pET28a(+) containing the signal peptide of TorA from <i>E. coli</i> W3110, Km <sup>r</sup>	This study
pET28a-SgsE	pET28a(+) containing SgsE from <i>G. stearothermophilus</i> NRS 2004/3a including its signal peptide, Km <sup>r</sup>	This study
pET22b-A_SgsE	pET22b(+) containing SgsE from <i>G. stearothermophilus</i> NRS 2004/3a, devoid of its signal peptide (aa 1–30), N-terminal PelB signal peptide; Amp <sup>r</sup>	This study
pET22b-G_SgsE	pET22b(+) containing SgsE from <i>G. stearothermophilus</i> NRS 2004/3a, devoid of the first 300 amino acids of the mature SgsE, N-terminal PelB signal peptide; Amp <sup>r</sup>	This study
pMAL-A_SgsE	pMAL-2px containing SgsE from <i>G. stearothermophilus</i> NRS 2004/3a, devoid of its signal peptide (aa 1–30), N-terminal MBP; Amp <sup>r</sup>	This study
pMAL-G_SgsE	pMAL-2px containing SgsE from <i>G. stearothermophilus</i> NRS 2004/3a, devoid of the first 300 amino acids of the mature SgsE, N-terminal MBP; Amp <sup>r</sup>	This study
pET28a-ssTor_A_SgsE	pET28a-ssTor containing SgsE from <i>G. stearothermophilus</i> NRS 2004/3a, devoid of its signal peptide (aa 1–30), N-terminal TorA signal peptide; Km <sup>r</sup>	This study
pET28a-ssTor_G_SgsE	pET28a-ssTor containing SgsE from <i>G. stearothermophilus</i> NRS 2004/3a, devoid of the first 300 amino acids of the mature SgsE, N-terminal TorA signal peptide; Km <sup>r</sup>	This study
pET22b-A_SgsE_G <sub>891</sub> D	pET22b-A_SgsE with a mutation at position G <sub>891</sub> ; Amp <sup>r</sup>	This study
pET22b-SgsE_inter	pET22b-A_SgsE, devoid of aa L <sub>610</sub> to E <sub>804</sub> , and an additional Kpn site at position 611; C-terminal His <sub>6</sub> tag; Amp <sup>r</sup>	This study
pET22b-A_SgsE_S,T5	pET22b-A_SgsE, the sequence DFNRS replaces K <sub>618</sub> TTSD <sub>622</sub> and L <sub>792</sub> TSAD <sub>796</sub> ; C-terminal His <sub>6</sub> tag; Amp <sup>r</sup>	This study
pET22b-A_SgsE_S,T12	pET22b-A_SgsE, the sequence ASKDFNRSKALFS replaces A <sub>615</sub> DLKTTSDNFKLY <sub>627</sub> and T <sub>789</sub> ATLTSADVIRVD <sub>901</sub> ; C-terminal His <sub>6</sub> tag; Amp <sup>r</sup>	This study
pET22b-A_SgsE_T5	pET22b-A_SgsE, the sequence DFNRS replaces K <sub>618</sub> TTSD <sub>622</sub> ; C-terminal His <sub>6</sub> tag; Amp <sup>r</sup>	This study
pET22b-A_SgsE_T12	pET22b-A_SgsE, the sequence ASKDFNRSKALFS replaces A <sub>615</sub> DLKTTSDNFKLY <sub>627</sub> ; C-terminal His <sub>6</sub> tag; Amp <sup>r</sup>	This study
pET22b-A_SgsE_S5	pET22b-A_SgsE, the sequence DFNRS replaces L <sub>792</sub> TSAD <sub>796</sub> ; C-terminal hexa-His tag; Amp <sup>r</sup>	This study
pET22b-A_SgsE_S12	pET22b-A_SgsE, the sequence ASKDFNRSKALFS replaces T <sub>789</sub> ATLTSADVIRVD <sub>901</sub> ; C-terminal His <sub>6</sub> tag; Amp <sup>r</sup>	This study
pET22b-G_SgsE_S,T5	pET22b-G_SgsE, the sequence DFNRS replaces K <sub>618</sub> TTSD <sub>622</sub> and L <sub>792</sub> TSAD <sub>796</sub> ; C-terminal His <sub>6</sub> tag; Amp <sup>r</sup>	This study
pET22b-G_SgsE_S,T12	pET22b-G_SgsE, the sequence ASKDFNRSKALFS replaces A <sub>615</sub> DLKTTSDNFKLY <sub>627</sub> and T <sub>789</sub> ATLTSADVIRVD <sub>901</sub> ; C-terminal His <sub>6</sub> tag; Amp <sup>r</sup>	This study
pET22b-G_SgsE_T5	pET22b-G_SgsE, the sequence DFNRS replaces K <sub>618</sub> TTSD <sub>622</sub> ; C-terminal His <sub>6</sub> tag; Amp <sup>r</sup>	This study
pET22b-G_SgsE_T12	pET22b-G_SgsE, the sequence ASKDFNRSKALFS replaces A <sub>615</sub> DLKTTSDNFKLY <sub>627</sub> ; C-terminal His <sub>6</sub> tag; Amp <sup>r</sup>	This study
pET22b-G_SgsE_S5	pET22b-G_SgsE, the sequence DFNRS replaces L <sub>792</sub> TSAD <sub>796</sub> ; C-terminal His <sub>6</sub> tag; Amp <sup>r</sup>	This study
pET22b-G_SgsE_S12	pET22b-G_SgsE, the sequence ASKDFNRSKALFS replaces T <sub>789</sub> ATLTSADVIRVD <sub>901</sub> ; C-terminal His <sub>6</sub> tag; Amp <sup>r</sup>	This study
pET22b-DFNRS_G_SgsE	pET22b containing G_SgsE with DFNRS fused to the N-terminus, N-terminal PelB signal peptide; C-terminal His <sub>6</sub> tag; Amp <sup>r</sup>	This study
pET22b-long_G_SgsE	pET22b containing G_SgsE with ASKDFNRSKALFS fused to the N-terminus, N-terminal PelB signal peptide; C-terminal His <sub>6</sub> tag; Amp <sup>r</sup>	This study
pACYCpgl	pACYC184 containing the <i>C. jejuni</i> pgl cluster; Cm <sup>r</sup>	[21]
pEC(AcrA-per)	pEC415, expressing periplasmic soluble AcrA with PelB signal peptide and C-terminal His <sub>6</sub> tag; Amp <sup>r</sup>	[28]
pBAD24	<i>E. coli</i> expression vector, arabinose inducible, Amp <sup>r</sup>	[45]
pBAD24-PelB_A_SgsE_T12	pBAD24, expressing periplasmic A_SgsE_T12 with PelB signal peptide and C-terminal His <sub>6</sub> tag; Amp <sup>r</sup>	This study
pBAD24-PelB_G_SgsE_T12	pBAD24, expressing periplasmic G_SgsE_T12 with PelB signal peptide and C-terminal His <sub>6</sub> tag; Amp <sup>r</sup>	This study
pMAF10	hemagglutinin-tagged PglB cloned in pMLBAD; Tmp <sup>r</sup>	[22]
pJHCV32	Encodes the O7 antigen cluster from <i>E. coli</i> ; Tet <sup>r</sup>	[24]

**Table 2.** Oligonucleotide primers used for PCR amplification reactions.

Primer	Nucleotide sequence (5' → 3')[a]
bsE-K1	TAGGCTCCATGG[ <u>a</u> ]ACAAAAAGAAAGC
sgsE_rev(XhoI)	AATCA <u>CTCGAGG</u> GATACATGTGCGGTACAAGAAAGC
sgsE_rev(XhoI,-Stop)	AATCA <u>CTCGAG</u> TTTTGCTACGTTTACAACAGTAGC
A_sgsE_for(NcoI)	AATCA <u>CCATGG</u> CGGACGTGGCGACGGTCCG
G_sgsE_for(NcoI)	AATCA <u>CCATGg</u> TAAAATTAGTGGTTGATGGCGC
A_sgsE_for(EcoRI)	AATCAGA <u>ATTTCG</u> CAACGGACGTGGCGACGGTCCG
G_sgsE_for(EcoRI)	AATCAGA <u>ATTTCATG</u> TAAAATTAGTGGTTGATGGCGC
sgsE_rev(XbaI)	AATCATCTAGAGGATACATGTGCGGTACAAGAAAGC
ssTorA(NcoI)_for	AATCA <u>CCATGg</u> ACAATAACGATCTCTTTTACG
ssTorA(EcoRI)_rev	AATCAGA <u>ATTCCG</u> CTTGGCGCCGACGTC
sgsE_rev(G <sub>891</sub> D,XhoI,+Stop)	AATCA <u>CTCGAG</u> TTATTTTGTACGTTTACAACAGTAGCAGAAACATTGTTGtCAAC
sgsEteil_rev(KpnI)	AATCAGGTACCAAGTACATTTGTTTCGTCATATACTTATC
sgsEteil_for(KpnI)	AATCAGGTACCGAACCGGTGGCAAATGCGACG
sgsE_T_N-glyk(DFNRS)_for(KpnI)	AATCAGGTACCGTGGCGCAGATTTGGATTTAATCGTTCTAATTTCAAATTATATCTGCCGACAGACGGAAATCG
sgsE_S_N-glyk(DFNRS)_rev(KpnI)	AATCAGGTACCGTGGCGCAGATTTGAAACGATTAAATCGGTCGCTGTGAACGTCGGAGCCACGTTTTCTTTC
sgsE_T_N-glyk(lang)_for(KpnI)	AATCAGGTACCGTGGCGCAAGCAAGGATTTAATCGTTCTAAAGCTCTTTTGTAGTCTGCCGACAGACGGAAATCGAAA TCGG TTGCTTTG
sgsE_S_N-glyk(lang)_rev(KpnI)	AATCAGGTACCACTAAAAGAGCTTTAGAACGATTAAATCCTTGTGCGAACGTCGGAGCCACGTTTTCTTTCATGTATTC
sgsE_T_rev(KpnI)	AATCAGGTACCGTGGCGCAGATTTGAAACGATTAAATCCTTGTGCGAACGTCGGAGCCACGTTTTCTTTCATGTATTC
sgsE_S_for(KpnI)	AATCAGGTACCGTGGCGCAGATTTGAAACGATTAAATCCTTGTGCGAACGTCGGAGCCACGTTTTCTTTCATGTATTC
G_sgsE_for(NcoI, long)	AATCA <u>CCATGG</u> CAAGCAAGGATTTAATCGTTCTAAAGCTCTTTTGTAGTTTAAATTAGTGGTTGATGGCGC
G_sgsE_for(NcoI, DFNRS)	AATCA <u>CCATGG</u> CAAGCAAGGATTTAATCGTTCTAAAGCTCTTTTGTAGTTTAAATTAGTGGTTGATGGCGC
PeIB-SgsE_for(EcoRI)	AATCAGA <u>ATTTCATG</u> AAATACCTGCTGCCGAC
SgsE-His_rev(XbaI)	AATCATCTAGATCAGTGGTGGTGGTGGTGG

[a]Artificial restriction sites are underlined; lowercase letters indicate changes in the chromosomal DNA sequence. The artificial glycosylation sites are marked in bold. The triples corresponding to the initiation and termination codons in the primer sequence are shown in boxes.

described by Sambrook and Russell.<sup>[41]</sup> PCR (Sprint Thermocycler, Hybaid, Ashford, UK) was performed using Super Yield Pwo polymerase (Roche). PCR conditions were optimized for each primer pair and amplification products were purified using the Qiagen MinElute PCR purification kit. *E. coli* transformation was done according to the manufacturer's instructions (Invitrogen). Transformants were screened by in situ-PCR reactions using RedTaq ReadyMix PCR Reaction Mix (Sigma-Aldrich, Vienna, Austria); recombinant clones were analyzed by restriction mapping and confirmed by sequencing (Agowa, Berlin, Germany).

SDS-PAGE and visualization of protein bands with Coomassie Blue R-250 staining reagent was carried out according to references.<sup>[42]</sup> Western immunoblotting using anti-SgsE antibody and anti-pgl-glycan antibody was done as described elsewhere.<sup>[43]</sup> Anti-SgsE antibody was available in our laboratory from previous studies and anti-pgl-glycan antibody was kindly provided by Prof. Markus Aebi (ETH Zurich, Switzerland). N-terminal sequencing of blotted protein bands that have been excised from the polyvinylidene fluoride (PVDF) membrane after visualization with Coomassie Blue R-250 staining reagent was performed by Prof. Herbert Lindner, University of Innsbruck, Austria.

**Construction of plasmids for periplasmic targeting of SgsE:** To identify a suitable system for the export of SgsE into the periplasm of *E. coli*, the S-layer protein was translationally fused to different signal peptides of Gram-negative bacteria directing the protein to the Sec-pathway (i.e., pectate lyase, PelB) signal peptide from *E. carotovora* and MBP including its signal peptide (i.e., periplasmic targeting peptide) from *E. coli*, and to the TAT-responsive ssTor

signal peptide of the *E. coli* TMAO reductase. Depending on the target vector, the sequences encoding rSgsE<sub>31-903</sub>, corresponding to the mature S-layer protein of *G. stearothermophilus* NRS 2004/3a devoid of its signal peptide (named A\_SgsE) and an N-terminally truncated form thereof (rSgsE<sub>331-903</sub>, named G\_SgsE) were amplified by PCR with the primer pairs A\_sgsE\_for(NcoI)/sgsE\_rev(XhoI) or G\_sgsE\_for(NcoI)/sgsE\_rev(XhoI) (for the PelB construct), A\_sgsE\_for(EcoRI)/sgsE\_rev(XbaI) or G\_sgsE\_for(EcoRI)/sgsE\_rev(XbaI) (for the MBP construct), and A\_sgsE\_for(EcoRI)/sgsE\_rev(XhoI) or G\_sgsE\_for(EcoRI)/sgsE\_rev(XhoI) (for the ssTor construct). Amplification products were digested with NcoI/XhoI, EcoRI/XbaI, and EcoRI/XhoI, respectively, and inserted into the dephosphorylated expression vectors pET22b, pMAL-p2x, or pET28a-ssTor. The latter vector was constructed by PCR amplification of the Tor signal peptide from chromosomal DNA of *E. coli* W3110 with the primer pair ssTorA(NcoI)\_for/ssTorA(EcoRI)\_rev, digestion with NcoI/EcoRI and ligation of the fragment into pET28a(+). In addition, SgsE possessing its endogenous signal peptide from *G. stearothermophilus* NRS 2004/3a was cloned. The sequence encoding rSgsE<sub>1-903</sub> of *G. stearothermophilus* NRS 2004/3a was amplified by PCR with the primer pairs sgsE-K1/sgsE\_rev(XhoI) and ligated into vector pET28a(+) using the restriction sites NcoI/XhoI. The resulting plasmids for overexpression of periplasmic rSgsE protein with the different N-terminal signal peptides were named pET22b-A\_SgsE and pET22b-G\_SgsE (PelB constructs), pMAL-A\_SgsE and pMAL-G\_SgsE (MBP constructs), pET28a-ssTor\_A\_SgsE and pET28a-ssTor\_G\_SgsE (ssTor constructs), and pET28a-SgsE (endogenous signal peptide).

**Engineering of *N*-glycosylation sites on *SgsE*:** For the introduction of a distinctive protein *N*-glycosylation consensus sequence from the *C. jejuni* AcrA *N*-glycoprotein replacing the naturally *O*-glycosylation sites of the *S*-layer protein,<sup>[19,20]</sup> a modified *sgsE* gene containing an artificial *KpnI* site at position nt 1830 (corresponding to amino acid position 611), coding for a protein with a PelB signal peptide and lacking the amino acid sequence between L<sub>610</sub> and E<sub>804</sub> was constructed. N- and C-terminal parts of *sgsE* were amplified separately by PCR using the primer pairs A<sub>sgsE\_for(NcoI)/sgsEteil\_rev(KpnI)</sub> and sgsEteil\_for(KpnI)/sgsE\_rev(XhoI), respectively. After digestion with *KpnI*, the two parts were ligated and the resulting product was amplified with the primer pair A<sub>sgsE\_for(NcoI)/sgsE\_rev(XhoI,-Stop)</sub>. The amplification product was digested with *NcoI* and *XhoI* and ligated with vector pET22b, yielding vector pET22b-SgsEinter that additionally equips *SgsE* with a C-terminal hexahistidine tag. Subsequently, either a five or a twelve amino acid sequence containing the *N*-glycosylation consensus sequence DXNZS (DFNRS and ASKDFNRSKALFS, respectively) was introduced into the *sgsE* sequence of *G. stearothermophilus* NRS 2004/3a by PCR amplification reactions using megaprimers. Different combinations of the megaprimers sgsE\_T\_N-glyk(DFNRS)\_for(KpnI), sgsE\_T\_N-glyk(DFNRS)\_rev(KpnI), sgsE\_T\_N-glyk(long)\_for(KpnI), sgsE\_T\_N-glyk(long)\_rev(KpnI), sgsE\_S\_for(KpnI), and sgsE\_T\_rev(KpnI) were used to yield six distinctive amplification products. These products were ligated into the vector pET22b-SgsEinter via the *KpnI* site. The resulting plasmids were named pET22b-A\_SgsE\_T5, pET22b-A\_SgsE\_T12, pET22b-A\_SgsE\_S5, pET22b-A\_SgsE\_S12, pET22b-A\_SgsE\_S,T5, and pET22b-A\_SgsE\_S,T12, respectively, and coded for modified *SgsE* proteins, in which either the natural *O*-glycosylation site Thr<sub>620</sub>, Ser<sub>794</sub>, or both sites were replaced by either DFNRS or ASKDFNRSKALFS. These six plasmids were used as templates to create *G\_SgsE* forms with the same *N*-glycosylation sites by PCR with the primer pair G\_sgsE\_for(NcoI)/sgsE\_rev(XhoI,-Stop) and ligation into pET22b. In another approach for *N*-glycosylation of *SgsE* the sequon DVN<sub>893</sub>VS was created by site-directed mutagenesis of G<sub>891</sub>D using A\_sgsE\_for(NcoI) and the modified reverse primer sgsE\_rev(G<sub>891</sub>D,XhoI,+Stop) for PCR. Cloning into vector pET22b was performed via *NcoI/XhoI* sites and the resulting plasmid was named pET22b-A\_SgsE\_G<sub>891</sub>D. In addition, the DFNRS and ASKDFNRSKALFS *N*-glycosylation sequence were translationally fused to the N-terminus of *SgsE* using the primer pairs G\_sgsE\_for(NcoI, long)/sgsE\_rev(XhoI,-Stop) and G\_sgsE\_for(NcoI, DFNRS)/sgsE\_rev(XhoI,-Stop), and after ligation via *NcoI/XhoI* to pET22b and the resulting plasmids were named pET22b-DFNRS\_G\_SgsE and pET22b-long\_G\_SgsE. All the plasmids described so far are inducible by IPTG (Fermentas, St. Leon-Rot, Germany).

To obtain an expression system for the *S*-layer protein that was inducible with arabinose, the periplasmic *SgsE* forms PelB\_A\_SgsE\_T12 and PelB\_G\_SgsE\_T12 including the C-terminal hexahistidine tag were cloned from pET22b into vector pBAD24, using the primer pair PelB-SgsE\_for(EcoRI)/SgsE-His\_rev(XbaI) for PCR. The corresponding expression plasmids were named pBAD24-PelB\_A\_SgsE\_T12 and pBAD24-PelB\_G\_SgsE\_T12, respectively.

**Production and purification of an *SgsE* neoglycoprotein with a *C. jejuni* glycan:** *E. coli* BL21 Star (DE3) cells containing pACYCpgl

carrying the *C. jejuni* glycosylation apparatus that is constitutively expressed were transformed with a pET22b-based plasmid encoding a periplasmic *SgsE* acceptor protein. As a control, the soluble periplasmic *C. jejuni* protein AcrA expressed from pEC(AcrA\_per)<sup>[28]</sup> was used in combination with pACYCpgl. pEC(AcrA\_per) was kindly provided by Prof. Markus Aebi; pACYCpgl<sup>[21]</sup> was obtained from Prof. Brendan Wren. Cells were grown in 400 mL cultures. At an OD<sub>600</sub> of ≈0.8, IPTG was added to a final concentration of 1 mM and cultivation was continued for additional 20 h. The biomass was collected by centrifugation at 4500 *g*, at 4 °C, for 15 min.

For *S*-layer neoglycoprotein purification, 1 g of biomass (wet weight) was suspended in 10 mL of buffer A (10 mM MgCl<sub>2</sub> in 50 mM Tris/HCl, pH 7.5) containing 500 U of benzonase (Merck, Darmstadt, Germany) and 4 mg of lysozyme (Merck), and incubated for 20 min at 37 °C. The spheroplast fraction was removed by centrifugation at 1620 *g* and the supernatant, containing the periplasmic fraction, was concentrated using Microcon centrifugal filter units (cut-off 50 kDa; Millipore). To the retentate, urea (Fluka, Buchs, Switzerland) was added to a final concentration of 6 M to disintegrate the water-insoluble *S*-layer protein. This extract was loaded onto a Superdex 200 prep grade XK16 FPLC-column (1.6 × 60 cm<sup>2</sup>; GE Healthcare, Uppsala, Sweden). Elution was performed at a flow rate of 1 mL min<sup>-1</sup> using 6 M urea in buffer A. Fractions containing the desired proteins were pooled and dialyzed four times against distilled water, 3 L each (dialysis tubing cut-off 20 kDa; Millipore), to promote self-assembly.

**Production of an *SgsE* neoglycoprotein with *E. coli* O7 glycosylation:** *E. coli* CLM24 cells containing the plasmids pMAF10 (encoding the oligosaccharyl/protein transferase PglB from *C. jejuni*,<sup>[22]</sup> p)HCV32 (encoding *E. coli* O7 antigen<sup>[24]</sup>), and pBAD24-PelB\_A\_SgsE\_T12 or pBAD24-PelB\_G\_SgsE\_T12 (encoding periplasmic *SgsE* forms), were induced by the addition of arabinose to 0.02% (wt vol<sup>-1</sup>). After induction at 37 °C for 5 h, arabinose was added again to ensure protein expression when the carbon source becomes limiting (as arabinose can be metabolized by the cells).

**Electron microscopy:** Periplasmic targeting and self-assembly of *S*-layer neoglycoproteins was investigated by transmission electron microscopy using a Philips model CM 12 electron microscope (Philips, Eindhoven, NL) operated at 80 kV using a 50 μm objective aperture.<sup>[44,45]</sup>

Periplasmic targeting of *SgsE* was investigated after immunogold-labeling of ultrathin sectioned *E. coli* BL21 Star (DE3) cells expressing *SgsE* to which different targeting signals have been fused. Cell pellets from 5 mL expression cultures grown to the late logarithmic growth phase were fixed overnight at 4 °C in 0.1 M sodium cacodylate buffer (pH 7.4) containing 2.5% glutaraldehyde, 2.5% paraformaldehyde, and 2.5 mM CaCl<sub>2</sub>. After a washing step with cacodylate buffer, dehydration was performed by incubating the cells in ethanol solutions of increasing concentrations (70, 80, 90, and 96%). Subsequently, LR-White resin mixed with ethanol (50%) was added to the cell pellet and the sample was agitated for 30 min. The sample was incubated with 200 μL of resin overnight at 4 °C. New resin was added to the cell pellet, and finally the pellet was transferred to a dry gelatine capsule, filled with LR-Whit resin, and polymerized at 55 °C for 24 h. Thin sections were cut with an Ultracut ultramicrotome (Reichert-Jung,

Vienna, Austria) and placed on 200-mesh copper grids coated with picroform and carbon films. For immunolabeling of thin sections the grids were incubated face-down on drops of anti-SgsE antibody raised in rabbit, diluted 1:1000 with a solution containing 15 mM Tris, 150 mM NaCl, 27 mM ethylenediaminetetraacetic acid (EDTA), 2.9% gelatine from cold-water fish skin (Sigma-Aldrich), 1% Top Block (Sigma-Aldrich), and 0.5% Brij 35 (Sigma-Aldrich) for 1 h at room temperature. After one washing step with buffer, the grids were incubated for 1 h with goat-anti-rabbit antibody labeled with 10 nm gold particles (Sigma-Aldrich). The grids were repeatedly rinsed with distilled water and the thin sections were finally stained with 1% uranyl acetate in Tris-buffered saline (TBS, pH 7.5) for 45 s. Self-assembly formation of S-layer neoglycoproteins was examined after negative staining of purified proteins with 1% uranyl acetate in TBS. For image processing, electron microscopy film negatives were digitized at 4000 dpi using a Super Coolscan 4000 ED film scanner (Nikon, Tokyo, Japan). The S-layer lattice parameters (base vector lengths and base angle) were determined in the Fourier spectra using software developed in house (Prof. Dietmar Pum, personal communication).

**Modeling of nanopatterned neoglycoproteins:** Image reconstruction of the SgsE(p2) matrix using Cinema 4D was based on a Fourier transformed transmission electron micrograph of a negatively stained preparation of the S-layer protein self-assembled in solution. Pdb data of the short-chain (Glc(GalNAc)<sub>5</sub>Bac) glycan of *C. jejuni* and the polymerized, long chain *E. coli* O7 antigen [VioNAc(Rha)ManGalGlcNAc]<sub>n</sub> were generated with Sweet at <http://www.glycosciences.de/>. The glycans were positioned onto the S-layer matrix in arbitrarily chosen positions and at arbitrarily chosen angles. For simplification of the model, and to avoid an overlapping of glycans, an O antigen of homogeneous length is shown and only one subunit of the p2 unit cell carries a glycan modification.

**MS analysis:** Purified A\_SgsE\_T12 glycosylated with *C. jejuni* heptasaccharide was separated by SDS-PAGE and stained using Novex colloidal blue reagent (Invitrogen), and the desired protein was excised, lyophilized, and digested with trypsin (E.C.3.4.21.4, Promega, Southampton, UK) overnight, followed by extraction of peptides from the gel pieces. Nano-LC was performed on an Ultimate 3000 using a PepMap 100 75 μm × 15 cm fused silica C18 analytical column (LC Packings, Dionex, Sunnyvale, CA), coupled to a Probot for fraction collection and matrix addition, with 2,5-dihydrobenzoic acid as the matrix. A gradient of 2–60% acetonitrile in 0.1% trifluoroacetic acid was delivered over 60 min at a flow rate of 0.300 nL min<sup>-1</sup>. MALDI TOF/TOF MS was performed using a Applied Biosystems 4800 mass spectrometer (Foster City, CA) in the positive reflectron mode with delayed extraction. MS precursor acquisition was followed by interpretation and data-dependent MS/MS acquisition with the CID on. Data interpretation was configured to select a maximum of 10 precursor ions per fraction with a minimum signal-to-noise ratio of 50.

## Acknowledgements

The authors thank Prof. Markus Aebi from ETH Zurich and Prof. Brendan W. Wren from London School of Hygiene and Tropical

Medicine, University of London, for providing the tools for working with the *C. jejuni* glycosylation system. *E. coli* CLM24 and pJHCV32 were kindly obtained from Dr. Cristina Marolda and Prof. Miguel A. Valvano (University of Western Ontario, London, ON, Canada). We also acknowledge Prof. Dietmar Pum and Markus Gossmann (Center for NanoBiotechnology, University of Natural Resources and Applied Life Sciences, Vienna) for image processing and help with the construction of the S-layer neoglycoprotein model. Financial support came from the Austrian Science Fund, projects P19047-B12 (to C. S.) and P18013-B10 (to P. M.), the Hochschuljubiläumstiftung der Stadt Wien, project H-1809/2006 (to C. S.), the Biotechnology and Biological Sciences Research Council and the Wellcome Trust (to A. D.). A. D. was a Biotechnology and Biological Sciences Research Council Professorial Research Fellow.

- [1] M. Sára, D. Pum, B. Schuster, U. B. Sleytr, *J. Nanosci. Nanotechnol.* **2005**, *5*, 1939.
- [2] C. Schäffer, R. Novotny, S. Küpcü, S. Zayni, A. Scheberl, J. Friedmann, U. B. Sleytr, P. Messner, *Small* **2007**, *3*, 1549.
- [3] U. B. Sleytr, P. Messner, D. Pum, M. Sára, *Angew. Chem. Int. Ed.* **1999**, *38*, 1034.
- [4] U. B. Sleytr, C. Huber, N. Ilk, D. Pum, B. Schuster, E. M. Egelseer, *EMS Microbiol. Lett.* **2007**, *267*, 131.
- [5] U. B. Sleytr, E. M. Egelseer, N. Ilk, D. Pum, B. Schuster, *FEBS J.* **2007**, *274*, 323–334.
- [6] S. Ávall-Jääskeläinen, A. Palva, *FEMS Microbiol. Rev.* **2005**, *29*, 511.
- [7] C. Schäffer, P. Messner, *Glycobiology* **2004**, *14*, 31R.
- [8] U. B. Sleytr, M. Sára, D. Pum, B. Schuster, P. Messner, C. Schäffer, in *Biopolymers*, Vol. 7, (Eds: A. Steinbüchel, S. R. Fahnstock), Wiley-VCH, Weinheim, Germany **2002**, p. 285.
- [9] B. Schuster, D. Pum, M. Sára, U. B. Sleytr, *Mini Rev. Med. Chem.* **2006**, *6*, 909.
- [10] M. Sára, E. M. Egelseer, C. Huber, N. Ilk, M. Pleschberger, D. Pum, U. B. Sleytr, in *Biological and Pharmaceutical Nanomaterials*, (Ed: C. Kumar), Wiley-VCH, Weinheim, Germany **2006**, p. 219.
- [11] P. Messner, K. Steiner, K. Zarschler, C. Schäffer, *Carbohydr. Res.* doi:10.1016/j.carres.2007.12.025.
- [12] R. Apweiler, H. Hermjakob, N. Sharon, *Biochim. Biophys. Acta* **1999**, *1473*, 4.
- [13] R. G. Spiro, *Glycobiology* **2002**, *12*, 43R.
- [14] K. Ohtsubo, J. D. Marth, *Cell* **2006**, *126*, 855.
- [15] C. Jones, *An. Acad. Bras. Cienc.* **2005**, *77*, 293.
- [16] D. M. Ratner, P. H. Seeberger, *Curr. Pharm. Des.* **2007**, *13*, 173.
- [17] J. Stevens, O. Blixt, T. M. Tumpey, J. K. Taubenberger, J. C. Paulson, I. A. Wilson, *Science* **2006**, *312*, 404.
- [18] P. Messner, D. Pum, U. B. Sleytr, *J. Ultrastruct. Mol. Struct. Res.* **1986**, *97*, 73.
- [19] C. Schäffer, T. Wugeditsch, H. Kählig, A. Scheberl, S. Zayni, P. Messner, *J. Biol. Chem.* **2002**, *277*, 6230.
- [20] K. Steiner, G. Pohlentz, K. Dreisewerd, S. Berkenkamp, P. Messner, J. Peter-Katalinić, C. Schäffer, *J. Bacteriol.* **2006**, *188*, 7914.
- [21] M. Wacker, D. Linton, P. G. Hitchen, M. Nita-Lazar, S. M. Haslam, S. J. North, M. Panico, H. R. Morris, A. Dell, B. W. Wren, M. Aebi, *Science* **2002**, *298*, 1790.
- [22] M. F. Feldman, M. Wacker, M. Hernandez, P. G. Hitchen, C. L. Marolda, M. Kowarik, H. R. Morris, A. Dell, M. A. Valvano, M. Aebi, *Proc. Natl. Acad. Sci. USA* **2005**, *102*, 3016.
- [23] C. Szymanski, R. Yao, C. P. Ewing, T. J. Trust, P. Guerry, *Mol. Microbiol.* **1999**, *32*, 1022.

- [24] C. L. Marolda, M. F. Feldman, M. A. Valvano, *Microbiology* **1999**, *145*, 2485.
- [25] N. M. Young, J. R. Brisson, J. Kelly, D. C. Watson, L. Tessier, P. H. Lanthier, H. C. Jarrell, N. Cadotte, F. St. Michael, E. Aberg, C. M. Szymanski, *J. Biol. Chem.* **2002**, *277*, 42530.
- [26] D. Linton, N. Dorrell, P. G. Hitchen, S. Amber, A. V. Karlyshev, H. R. Morris, A. Dell, M. A. Valvano, M. Aebi, B. W. Wren, *Mol. Microbiol.* **2005**, *55*, 1695.
- [27] M. Nita-Lazar, M. Wacker, B. Schegg, S. Amber, M. Aebi, *Glycobiology* **2005**, *15*, 361.
- [28] M. Kowarik, N. M. Young, S. Numao, B. L. Schulz, I. Hug, N. Callewaert, D. C. Mills, D. C. Watson, M. Hernandez, J. F. Kelly, M. Wacker, M. Aebi, *EMBO J.* **2006**, *25*, 1957.
- [29] M. Kowarik, S. Numao, M. F. Feldman, B. L. Schulz, N. Callewaert, E. Kiermaier, I. Catrein, M. Aebi, *Science* **2006**, *314*, 1148.
- [30] S. Cristobal, J. W. De Gier, H. Nielsen, G. von Heijne, *EMBO J.* **1999**, *18*, 2982.
- [31] R. Novotny, A. Scheberl, M. Giry-Laterriere, P. Messner, C. Schäffer, *FEMS Microbiol. Lett.* **2005**, *242*, 27.
- [32] E. Riedmann, J. M. Kyd, A. M. Smith, S. Gomez-Gallego, K. Jalava, A. W. Cripps, W. Lubitz, *FEMS Immunol. Med. Microbiol.* **2003**, *37*, 185.
- [33] K. Mukherjee, S. Karlsson, L. G. Burman, T. Akerlund, *Microbiology* **2002**, *148*, 2245.
- [34] C. Houssin, D. T. Nguyen, G. Leblon, N. Bayan, *FEMS Microbiol. Lett.* **2002**, *217*, 71.
- [35] M. Wacker, M. F. Feldman, N. Callewaert, M. Kowarik, B. R. Clarke, N. L. Pohl, M. Hernandez, E. D. Vines, M. A. Valvano, C. Whitfield, M. Aebi, *Proc. Natl. Acad. Sci. USA* **2006**, *103*, 7088.
- [36] E. S. Rangarajan, S. Bhatia, D. C. Watson, C. Munger, M. Cygler, A. Matte, N. M. Young, *Protein Sci.* **2007**, *16*, 990.
- [37] K. Bryson, L. J. McGuffin, R. L. Marsden, J. J. Ward, J. S. Sodhi, D. T. Jones, *Nucl. Acids Res. (Web Server issue)* **2005**, *33*, W36.
- [38] H. Tschiggerl, A. Breitwieser, G. de Roo, T. Verwoerd, C. Schäffer, U. B. Sleytr, *J. Biotechnol.* **2008**, *133*, 403.
- [39] A. W. Paton, R. Morona, J. C. Paton, *Nat. Methods* **2000**, *6*, 265.
- [40] I. Benz, M. A. Schmidt, *Mol. Microbiol.* **2002**, *45*, 267.
- [41] J. Sambrook, D. W. Russell, *Molecular Cloning: A Laboratory Manual*, 3rd Edn, Cold Spring Harbor Laboratory Press, Cold Spring Harbor, NY **2001**.
- [42] U. K. Laemmli, *Nature* **1970**, *227*, 680.
- [43] K. Steiner, R. Novotny, K. Patel, E. Vinogradov, C. Whitfield, M. A. Valvano, P. Messner, C. Schäffer, *J. Bacteriol.* **2007**, *189*, 2590.
- [44] P. Messner, F. Hollaus, U. B. Sleytr, *Int. J. Syst. Bacteriol.* **1984**, *34*, 202.
- [45] L. M. Guzman, D. Belin, M. J. Carson, J. Beckwith, *J. Bacteriol.* **1995**, *177*, 4121.

Received: December 6, 2007

# Genetic Engineering of the S-Layer Protein SbpA of *Lysinibacillus sphaericus* CCM 2177 for the Generation of Functionalized Nanoarrays<sup>†</sup>

Helga Badelt-Lichtblau,<sup>‡</sup> Birgit Kainz,<sup>‡</sup> Christine Völlenkle,<sup>§</sup> Eva-Maria Egelseer,<sup>‡</sup> Uwe B. Sleytr,<sup>‡</sup> Dietmar Pum,<sup>‡</sup> and Nicola Ilk<sup>\*,‡</sup>

Center for NanoBiotechnology, University of Natural Resources and Applied Life Sciences (BOKU), Vienna, Gregor Mendelstrasse 33, A-1180 Vienna, Austria, and Research Laboratories-Molecular Cardiology, I.R.CCS Policlinico San Donato, Via R. Morandi, 30, 20097 S. Donato M.se (MI), Italy. Received October 16, 2008; Revised Manuscript Received March 30, 2009

The mesophilic organism *Lysinibacillus sphaericus* CCM 2177 produces the surface (S)-layer protein SbpA, which after secretion completely covers the cell surface with a crystalline array exhibiting square lattice symmetry. Because of its excellent *in vitro* recrystallization properties on solid supports, SbpA represents a suitable candidate for genetically engineering to create a versatile self-assembly system for the development of a molecular construction kit for nanobiotechnological applications. The first goal of this study was to investigate the surface location of 3 different C-terminal amino acid positions within the S-layer lattice formed by SbpA. Therefore, three derivatives of SbpA were constructed, in which 90, 173, or 200 C-terminal amino acids were deleted, and the sequence encoding the short affinity tag *Strep*-tag II as well as a single cysteine residue were fused to their C-terminal end. Recrystallization studies of the rSbpA/STII/Cys fusion proteins indicated that C-terminal truncation and functionalization of the S-layer protein did not interfere with the self-assembly capability. Fluorescent labeling demonstrated that the orientation of the crystalline rSbpA<sub>31–1178</sub>/STII/Cys lattice on solid supports was the same, like the orientation of wild-type S-layer protein SbpA on the bacterial cell. In soluble and recrystallized rSbpA/STII/Cys fusion proteins, *Strep*-tag II was used for prescreening of the surface accessibility, whereas the thiol group of the end-standing cysteine residue was exploited for site-directed chemical linkage of differently sized preactivated macromolecules via heterobifunctional cross-linkers. Finally, functionalized two-dimensional S-layer lattices formed by rSbpA<sub>31–1178</sub>/STII/Cys exhibiting highly accessible cysteine residues in a well-defined arrangement on the surface were utilized for the template-assisted patterning of gold nanoparticles.

## INTRODUCTION

Crystalline bacterial cell surface layer (S-layer) proteins form the outermost cell envelope component of prokaryotic organisms. They are composed of identical protein or glycoprotein subunits, which completely cover the cell surface during all stages of bacterial growth and division. Even after isolation from the cell wall, S-layer proteins have the intrinsic tendency to self-assemble into crystalline arrays in suspension or to recrystallize on solid supports, such as silicon wafers, gold chips, silanized glass, or plastic materials, on polyelectrolytic microcapsules, on Langmuir lipid films, on liposomes, and at the air–water interface (1–5). General aspects of the structure of S-layer proteins have been examined quite extensively, such as the ultrastructure of the lattice, and the binding and anchoring of S-layer proteins to the underlying cell envelope through the so-called S-layer-homology (SLH)-domains. Together with the high density and regular arrangement of functional groups in the S-layer lattice, this specific feature opens a broad application potential in biotechnology, molecular nanotechnology, and biomimetics (3). In previous studies, mainly carboxyl groups in the S-layer lattice were exploited for covalent binding of biologically active macromolecules, such as enzymes, antibodies, or ligands for the production of S-layer-based biosensors (3), solid-phase dipstick style immunoassays (6–8), or affinity matrices based on self-assembly products (9). The possibility to change the properties of S-layer proteins by genetic engineering offers new ways for tuning

their functional and structural features as required in nanobiotechnology as well as in material sciences.

The S-layer protein SbpA of *Lysinibacillus sphaericus* CCM 2177 consists of a total of 1,268 amino acids (including a 30-amino-acid-long signal peptide). SbpA self-assembles into a square (p4) lattice structure with a center-to-center spacing of the morphological units of 13.1 nm. The self-assembly process is strongly dependent on the presence of bivalent cations (10). In their absence, SbpA stays in the water-soluble state, which means that the self-assembly process of this S-layer protein is dirigible (11). The N-terminal part of SbpA possesses 3 typical S-layer homologous (SLH) motifs and an additional 58 amino acid-long SLH-like motif that recognizes a distinct type of secondary cell wall polymer (SCWP), consisting of 8 to 9 disaccharide repeating units, as the proper anchoring structure in the rigid cell wall layer (10). These specific interactions can be exploited for an oriented binding of SbpA on solid supports precoated with SCWP to generate monomolecular protein lattices (12).

The gene *sbpA*, encoding this S-layer protein, has been sequenced, cloned, and expressed in *Escherichia coli* HMS174(DE3) (13). Studies on the structure–function relationship of SbpA revealed that deletions of up to 237 C-terminal amino acids do not interfere with the ability to self-assemble into the square lattice structure. However, the deletion of 350 amino acids was linked to a change from square (p4) to oblique (p1) lattice symmetry (14). An N- and C-terminally truncated form was capable of self-assembling into the square (p4) lattice structure with lattice parameters similar to that formed by the full-length SbpA. These findings indicated that the segment between amino acid 203 and 1,031 is responsible for the self-assembly process and for pore formation (14).

<sup>†</sup> This article is dedicated to the memory of Margit Sára.

\* Corresponding author. Tel: + 43-1-47654-2233. Fax: + 43-1-4789-112. E-mail: nicola.ilk@boku.ac.at.

<sup>‡</sup> University of Natural Resources and Applied Life Sciences.

<sup>§</sup> I.R.CCS Policlinico San Donato.

**Table 1. Survey on the Three Genetically Engineered SbpA Derivatives**

SbpA derivative	forward primer <sup>a</sup>	reverse primer <sup>a</sup>	cloning site	number of C-terminally truncated amino acids	C-terminally fusion of	theoretical molecular mass
<b>rSbpA<sub>31–1178</sub>/STII/Cys</b>	<i>sbpA37</i> [5'-CG GAT TCC ATG GCG CAA GTA AAC GAC TAT AAC AAA ATC-3']	<i>sbpAII/3</i> [5'-GGT TTA GTG GTT GCA TCA GCA TCT GGT GGT TGG TCT CAC CCG CAG TTC GAA AAA GGT GGT TGC TAA CTC GAG CGG TC 3']	<i>NcoI XhoI</i>	90	<i>Strep</i> -tag II, cysteine	121,345 Da
<b>rSbpA<sub>31–1095</sub>/STII/Cys</b>	<i>sbpA37</i> [5'-CG GAT TCC ATG GCG CAA GTA AAC GAC TAT AAC AAA ATC-3']	<i>sbpAII/4</i> [5'-GCA GCA ACT ACT GCA TAT TCA GAA GGT GGT TGG TCT CAC CCG CAG TTC GAA AAA GGT GGT GGT TGC TAA CTC GAG CGG TC 3']	<i>NcoI XhoI</i>	173	<i>Strep</i> -tag II, cysteine	113,720 Da
<b>rSbpA<sub>31–1068</sub>/STII/Cys</b>	<i>sbpA37</i> [5'-CG GAT TCC ATG GCG CAA GTA AAC GAC TAT AAC AAA ATC-3']	<i>sbpAII/5</i> [5'-GCA GCA ACT ACT GCA TAT TCA GAA GGT GGT TGG TCT CAC CCG CAG TTC GAA AAA GGT GGT GGT TGC TAA CTC GAG CGG TC 3']	<i>NcoI XhoI</i>	200	<i>Strep</i> -tag II, cysteine	111,241 Da

<sup>a</sup> Cloning sites are in bold text (*NcoI* at the 5'-end and *XhoI* at the 3'-end of the coding sequence); *Strep*-tag II is underlined; and cysteine residue is in italic text and is underlined.

Recent studies have shown that bacterial S-layer proteins can be used for controlled deposition of inorganic material, which can be achieved by using the S-layer lattices as templates for direct precipitation of metals from solution or by binding preformed metallic and semiconductor nanoparticles (15–18). In this context, gold nanoparticles formed on cells and purified S-layer protein of *Bacillus sphaericus* JG-A12 after incubation with Gold(III) solution in the presence of H<sub>2</sub> as reducing agent were characterized by X-ray absorption spectroscopy, UV–vis spectroscopy, and X-ray powder diffraction (19). In another approach, the self-assembly of dendrimer-encapsulated platinum nanoparticles on S-layer proteins from the archaeon *Sulfolobus acidocaldarius* and the gram-positive *Deinococcus radiodurans* was used to create patterned nanoparticle arrays with potential technological applications (20).

In the present study, C-terminal functionalization of the S-layer protein SbpA combined with targeted chemical modification was used to identify amino acids that are located at the surface of the S-layer lattice and therefore accessible for binding of functional molecules or nanoparticles. A C-terminal cysteine residue was introduced with the aim to produce structured crystalline monolayers on solid supports offering free sulfhydryl groups for the activation with various heterobifunctional cross-linkers and covalent attachment of differently sized (macro)molecules. Binding of gold nanoparticles to the surface located cysteine residues should finally lead to the formation of regularly ordered nanoarrays.

## MATERIAL AND METHODS

**Cloning and Expression of the Genes Encoding the S-Layer Fusion Proteins rSbpA<sub>31–1178</sub>/STII/Cys, rSbpA<sub>31–1095</sub>/STII/Cys, and rSbpA<sub>31–1068</sub>/STII/Cys.** For amplification of the genes encoding the C-terminally truncated forms rSbpA<sub>31–1178</sub>,

rSbpA<sub>31–1095</sub> and rSbpA<sub>31–1068</sub>, chromosomal DNA of *Lysinibacillus sphaericus* CCM 2177 was used as a template. Isolation of chromosomal DNA and PCR amplifications were performed as described in ref 21. General procedures for DNA manipulations were carried out as reported in ref 22. The oligonucleotide forward primer *sbpA37* as well as the reverse primers *sbpA II/3*, *sbpA II/4*, and *sbpA II/5* (all listed in Table 1) introduced the cloning sites *NcoI* and *XhoI* at the 5'- and 3'-ends, respectively. In comparison to the wild-type S-layer protein, the reverse primers led to the C-terminal deletion of 90, 173, or 200 amino acids in the respective proteins, as well as to the fusion of *Strep*-tag II and a single cysteine residue to the C-terminal end. Cloning of pET28a (Invitrogen), carrying the genes *sbpA<sub>(93–3534)</sub>/STII/Cys*, *sbpA<sub>(93–3285)</sub>/STII/Cys*, and *sbpA<sub>(93–3204)</sub>/STII/Cys* in *E. coli* TG1 (Stratagene), was done as described in ref 13. For the selection of positive transformants, kanamycin was added at a final concentration of 30 μg/mL. Heterologous expression of the genes *sbpA<sub>(93–3534)</sub>/STII/Cys*, *sbpA<sub>(93–3285)</sub>/STII/Cys*, and *sbpA<sub>(93–3204)</sub>/STII/Cys* in *E. coli* BL21Star (DE3) One Shot (Invitrogen) was performed as described in ref 21. Samples of the *E. coli* BL21(DE3) cultures were taken before and 4 h after the induction of expression. For all three S-layer fusion proteins, preparation of samples for SDS–PAGE analysis was carried out as described by Laemmli (23). Immunoblotting with a polyclonal rabbit antiserum raised against the S-layer protein SbpA of *Ly. sphaericus* CCM 2177 was performed as described previously (24).

**Isolation of the Three S-Layer/STII/Cys Fusion Proteins from the Host Cells and Purification.** Isolation of the three different truncated SbpA fusion proteins carrying *Strep*-tag II and a cysteine residue at the C-terminal end was performed as previously described (21) except that only degassed buffers were

used, and additionally 1,4-dithio-D,L-threitol (DTT, GERBU) in a final concentration of 1 mM was added as reducing agent to all buffers to prevent the formation of disulfide bridges between the C-terminally located cysteine residues. Purification of the fusion proteins by gel permeation chromatography (GPC) using a Superdex 200 column (Pharmacia; Upsala, Sweden) in 2 M guanidine hydrochloride (GHCl) in 50 mM Tris-HCl/150 mM NaCl buffer (pH 7.2) and 1 mM DTT was done as described before (25). Fractions containing rSbpA<sub>31-1178</sub>/STII/Cys, rSbpA<sub>31-1095</sub>/STII/Cys, or rSbpA<sub>31-1068</sub>/STII/Cys were pooled, dialyzed against degassed Milli-Q water containing 1 mM DTT for 18 h at 4 °C, analyzed by SDS-PAGE, lyophilized, and stored at -20 °C.

**Investigation of the Self-Assembly and Recrystallization Properties of rSbpA<sub>31-1178</sub>/STII/Cys, rSbpA<sub>31-1095</sub>/STII/Cys, and rSbpA<sub>31-1068</sub>/STII/Cys by Transmission Electron Microscopy (TEM) and Atomic Force Microscopy (AFM).** To investigate the ability of the three rSbpA/STII/Cys fusion proteins to form self-assembly products in suspension, 2 mg of GPC-purified fusion protein were dissolved in 1 mL of 5 M GHCl in 50 mM Tris-HCl buffer (pH 7.2) with 1 mM DTT and dialyzed against degassed Milli-Q water containing 1 mM DTT and 10 mM CaCl<sub>2</sub> for 18 h at 4 °C. For recrystallization on solid supports, the fusion proteins dissolved as described above were dialyzed against degassed Milli-Q water containing 1 mM DTT. Then, 1 mg of lyophilized peptidoglycan-containing sacculi of *Ly. sphaericus* CCM 2177, prepared according to refs 10 and 13, was added to 1 mL of the solution containing the monomeric S-layer fusion protein. To induce the recrystallization process, 10 mM CaCl<sub>2</sub> was added, and the suspensions were stirred for 18 h at 4 °C.

To investigate the ability of monomeric rSbpA/Cys fusion proteins to recrystallize on poly-L-lysine coated copper grids, the GHCl-extracts were dialyzed against distilled water for 18 h at 4 °C. After centrifugation for 5 min at 16,000g, the clear supernatants containing nonassembled S-layer protein were incubated with poly-L-lysine (Sigma P2636) coated copper grids according to the procedures described in ref 26.

For electron microscopical examination, 30  $\mu$ L of the solution containing self-assembly products or recrystallization products was transferred onto a carbon-coated electron microscope grid, which had been rendered hydrophilic by glow discharge. Negative staining of the samples with 2.5% uranyl acetate was performed as described in ref 26. Electron micrographs were taken with a Philips CM 12 transmission electron microscope (Philips Eindhoven, The Netherlands) operated at 80 kV in low-dose mode.

AFM measurements of rSbpA/STII/Cys fusion proteins recrystallized on silicon wafers were performed on a Digital Instruments Nanoscope IIIa (Santa Barbara, CA) with a J-scanner (nominal 130- $\mu$ m scan size). Silicon wafers (100, p-type, boron-doped, resistivity 25–45  $\Omega$  cm; MEMC, Italy) were cut into pieces of 1  $\times$  1 cm and precleaned as previously described in ref 27. The rSbpA/STII/Cys fusion proteins (0.1 mg/mL in recrystallization buffer: 0.5 mM Tris/HCl, pH 9, 10 mM CaCl<sub>2</sub>) were recrystallized on the silicon wafers as reported in ref 16. The scanning was carried out in contact mode under fluid (100 mM NaCl, pH 7.5). For imaging, standard 200- $\mu$ m-long oxide-sharpened silicon nitride cantilevers (NanoProbes, Digital Instruments, INC) with a nominal spring constant of 0.06 N/m were used. The scan speed was approximately 6 Hz, and the applied force was kept minimized during scanning to prevent the tip from modifying the sample surface.

**Immunoblotting for Detection of the C-Terminally Fused *Strep*-tag II and Surface Accessibility Screens by Immuno Dot Assays.** For immunoblotting, monomeric fusion proteins were subjected to SDS-PAGE and transferred to a nitrocel-

lulose membrane by semidry-blotting as described previously (24). For detection of *Strep*-tag II, membranes were incubated with a monoclonal mouse anti-*Strep*-tag II antibody (IBA) diluted 1:350 in 2% Blocking Reagent GE in 0.1 M TBS (Tris-buffered saline) for 2 h at room temperature. After several washing steps and incubation with antimouse IgG-alkaline phosphatase (ALP) conjugate (Sigma), diluted 1:5,000 in 2% Blocking Reagent GE in 0.1 M TBS, for 1 h at room temperature, detection was accomplished by treatment with 5-bromo-4-chloro-3-indolyl phosphate and nitroblue tetrazolium chloride (BCIP/NBT, Roche).

To investigate the surface accessibility of *Strep*-tag II within the S-layer lattice, the three different SbpA fusion proteins were recrystallized on peptidoglycan-containing sacculi of *Ly. sphaericus* CCM 2177. Recrystallization products were dried onto a nitrocellulose membrane, and immuno dot assay using monoclonal mouse anti-*Strep*-tag II antibody and antimouse IgG-ALP conjugate was performed as described in ref 28.

**Chemical Modification of the Cysteine Residues in Monomeric rSbpA<sub>31-1178</sub>/STII/Cys Fusion Protein by Linkage of Differently Sized Preactivated Macromolecules.** A monomeric solution of rSbpA<sub>31-1178</sub>/STII/Cys was produced by dissolving 1 mg of S-layer fusion protein in 1 mL of 5 M GHCl in 50 mM Tris/HCl buffer (pH 7.2) with 1 mM DTT and dialyzing against degassed Milli-Q water containing 1 mM DTT. After removal of DTT by PD10 desalting columns, the protein solution was mixed with a 2-fold molar excess of methoxypoly(ethylene glycol)maleimide (m-PEG-mal, Nektar therapeutics) with a size of 5 or 20 kDa, respectively, overlaid with nitrogen and incubated overnight at 4 °C.

For modification of the cysteine residues with differently sized macromolecules via a heterobifunctional cross-linker, solutions containing monomers of rSbpA<sub>31-1178</sub>/STII/Cys were mixed in a molar ratio of 1:2 with Protein A (Sigma), carbonic anhydrase (Sigma), or the major birch pollen allergen (rBet v1), which was preactivated with *m*-maleimido-benzoyl-*N*-hydroxysulfosuccinimide ester (Sulfo-MBS, Pierce). For that purpose, 2 mg of Protein A, carbonic anhydrase, or Bet v1 was dissolved in conjugation buffer, PBS (0.1 M, pH 7.2), and Sulfo-MBS, prepared according to the manufacturer's recommendations, was added in a 10-fold molar excess. The mixture was incubated for 2 h at 4 °C. The excess unbound cross-linker was removed by using desalting columns (PD10, GE Healthcare) equilibrated with the conjugation buffer. Chemical modification was checked by SDS-PAGE analysis (gel shift assay).

**Investigation of the Recrystallization Properties of the SbpA<sub>31-1178</sub>/STII/Cys/Carbonic Anhydrase Conjugates by TEM and Detection of the Enzyme on the Surface of the S-Layer Lattice.** For recrystallization, conjugates between carbonic anhydrase and rSbpA<sub>31-1178</sub>/STII/Cys (1 mg/mL in recrystallization buffer: 0.5 mM Tris/HCl, pH 9, and 10 mM CaCl<sub>2</sub>) were mixed with 1 mg of peptidoglycan-containing sacculi of *Ly. sphaericus* CCM 2177, and the solution was stirred at 4 °C overnight. The formation of recrystallization products was checked after negative staining by TEM. For detection of the preactivated carbonic anhydrase bound to the cysteine residues on the S-layer lattice, immuno dot assays were carried out. For this, recrystallization products were washed three times with Milli-Q water, and 10  $\mu$ L of the sample solution was dried on a nitrocellulose membrane. The membrane was blocked with 2% Blocking Reagent GE (Applichem Biomedica) in 0.1 M TBS overnight at 4 °C followed by incubation with rabbit anticarbonic anhydrase antibody (Sigma), diluted 1:5,000 in 2% Blocking Reagent GE in 0.1 M TBS, for 2 h at room temperature. After several washing steps and incubation of the membrane with antirabbit IgG-ALP conjugate (Sigma), diluted

1:5,000 in 2% Blocking Reagent GE in 0.1 M TBS, for 1 h at room temperature, detection was accomplished by treatment with BCIP/NBT.

**Binding of a Fluorescent Thiol-Reactive Dye to Crystalline Monolayers Formed by rSbpA<sub>31-1178</sub>/STII/Cys.** For site-specific-labeling, rSbpA<sub>31-1178</sub>/STII/Cys was recrystallized overnight under rotation in recrystallization buffer (0.5 mM Tris/HCl, 10 mM CaCl<sub>2</sub>, pH 9) on microparticles, which were based on silicon dioxide (SiO<sub>2</sub>) in aqueous solution (3 μm SiO<sub>2</sub>-particles; Fluka). Subsequently, the particles were incubated with 7-diethylamino-3-(4'-maleimidylphenyl)-4-methylcoumarin (CPM; Invitrogen) for 30 min at room temperature. The thiol-reactive coumarin, CPM is very weakly fluorescent until reacted with the thiol-group of the cysteine residue producing a conjugate with excitation and emission maxima of ~384/470 nm. The covered particles were washed three times with Milli-Q water and analyzed by using a fluorescence microscope (Nikon Eclipse TE 2000-S) with the filter DAPI. Wild-type S-layer protein SbpA recrystallized on SiO<sub>2</sub>-particles as well as SiO<sub>2</sub>-particles without S-layer protein, used as blanks, were measured under the same conditions. For measurement of excitation and emission spectra of the samples (protein concentration 0.1 mg/mL), the luminescence spectrometer LS 55 (PerkinElmer, Shelton CT, U.S.A.) was used. Fluorescence spectroscopy of the protein samples was carried out by wavelength scan with a scan speed of 500 nm/min in a quartz cuvette (1 cm). The band-pass for both the excitation and emission monochromators was 5 nm. Emission spectra were recorded at a fixed wavelength of the excitation maximum and excitation spectra at a fixed wavelength of the emission maximum. For the measurement of the emission and excitation spectra, 2 mL of 50 mM Tris/HCl buffer (pH 8) was mixed with 50 μL of SiO<sub>2</sub>-particles covered with rSbpA<sub>31-1178</sub>/STII/Cys or 10 μL of rSbpA<sub>31-1178</sub>/STII/Cys solution (protein concentration 1 mg/mL) and stirred in a quartz cuvette with a magnetic stirring shaft. After 360 s, 100 μL of 2 mM fluorophore was added, and 1800 s later excitation and emission were measured. For reference studies, the sole fluorophore, soluble rSbpA<sub>31-1178</sub>/STII/Cys without dye, soluble wild-type SbpA incubated with the dye, wild-type SbpA recrystallized on microparticles incubated with the fluorophore, and SiO<sub>2</sub>-particles alone or incubated with the fluorophore were analyzed.

**Chemical Modification of the Cysteine Residues of Recrystallized rSbpA<sub>31-1178</sub>/STII/Cys with Carbonic Anhydrase via a Heterobifunctional Cross-Linker.** Preactivation of carbonic anhydrase with Sulfo-MBS was carried out as described above. Recrystallization products consisting of rSbpA<sub>31-1178</sub>/STII/Cys recrystallized on peptidoglycan-containing sacculi of *Ly. sphæricus* CCM 2177 were incubated with preactivated carbonic anhydrase for 2 h at 4 °C. To remove unbound preactivated carbonic anhydrase the recrystallization products were washed with Milli-Q water three times. For detection of the preactivated carbonic anhydrase bound to the cysteine residues on the S-layer lattice, immuno dot assays using rabbit anticarbonic anhydrase antibody (Sigma) and antirabbit IgG-ALP conjugate (Sigma) were carried out as described above.

**Binding of Colloidal Gold Nanoparticles to Monolayers Formed by rSbpA<sub>31-1178</sub>/STII/Cys on Peptidoglycan-Containing Sacculi of *Ly. sphæricus* CCM 2177.** Recrystallization products consisting of rSbpA<sub>31-1178</sub>/STII/Cys fusion protein recrystallized on peptidoglycan-containing sacculi of *Ly. sphæricus* CCM 2177 as well as self-assembly products of the fusion protein were incubated with 75 μL of colloidal gold (5 nm, HAuCl<sub>4</sub> in Tris/HCl, pH 7.2, Sigma) at room temperature for 20 min and then centrifuged for 10 min at 13,400 rpm. The procedure was repeated 2 times, then the pellet was washed three times with Milli-Q water and resuspended in 15 μL of

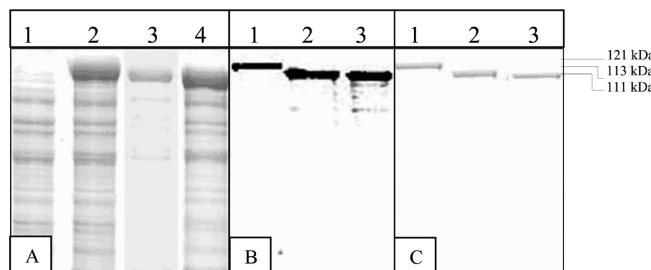


**Figure 1.** (A) SDS-PAGE analysis of SDS-extracted whole cells of *E. coli* BL21star(DE3) harboring plasmid pET28a/sbpA<sub>(93-3534)</sub>/STII/Cys before the induction of expression (lane 1); *E. coli* BL21star(DE3) harboring plasmid pET28a/sbpA<sub>(93-3534)</sub>/STII/Cys (lane 2); *E. coli* BL21star(DE3) harboring plasmid pET28a/sbpA<sub>(93-3285)</sub>/STII/Cys (lane 3), *E. coli* BL21star(DE3) harboring plasmid pET28a/sbpA<sub>(93-3204)</sub>/STII/Cys (lane 4), respectively, 4 h after the induction of expression. (B) Immunoblot analysis of rSbpA<sub>31-1178</sub>/STII/Cys (lane 1), rSbpA<sub>31-1095</sub>/STII/Cys (lane 2), and rSbpA<sub>31-1068</sub>/STII/Cys (lane 3) using a polyclonal rabbit antiserum raised against the S-layer protein SbpA of *Ly. sphæricus* CCM 2177. (C) GPC-purified fusion protein rSbpA<sub>31-1178</sub>/STII/Cys (lane 1), rSbpA<sub>31-1095</sub>/STII/Cys (lane 2), and rSbpA<sub>31-1068</sub>/STII/Cys (lane 3).

Milli-Q water, and unstained samples were investigated by TEM. As a control, the same procedure was carried out with (a) self-assembly products formed by wild-type SbpA and (b) recrystallization products prepared with wild-type SbpA recrystallized on peptidoglycan-containing sacculi of *Ly. sphæricus* CCM 2177.

**Image Processing.** Electron microscopical images were recorded on 35 mm negative film (Kodak Fine Grain 5302, Eastman Kodak, Rochester, NY) and subsequently digitized with a Nikon Film Scanner (Model Super Cool Scan 4000 ED; Nikon Tokyo, Japan) at a resolution of 4000 dpi. Estimates of the lattice vectors of the gold nanoparticle superlattice were determined from digital diffraction patterns after Fourier transform of the image data. An accurate lattice fit, where gold nanoparticles at interlattice positions were also sorted out, was performed by using cross-correlation averaging (CCA) (29). Cross-correlation is a matched filtering image processing technique allowing reliable and almost fully automatic image averaging for near-periodic structures. First of all, a reference motif is cross-correlated with the image in order to indicate similar regions in the image. A superposition of small regions centered on each cross-correlation peak position lead to an improvement of the signal-to-noise ratio. Vectors pointing from positions on a least-squares fitted lattice toward actually found positions yield a graphical representation of the displacement field (29). The lattice parameters (two base vectors and a vector offset) were determined by minimizing the squared deviation between nanoparticle positions found in the course of CCA and ideal lattice sites. The root-mean-square deviation (r.m.s.) is a convenient measure of the degree of order in the superlattice of gold nanoparticles. Image processing software was developed in house.

## RESULTS

**Cloning and Expression of the Genes Encoding the Three S-Layer Fusion Proteins rSbpA<sub>31-1178</sub>/STII/Cys, rSbpA<sub>31-1095</sub>/STII/Cys, and rSbpA<sub>31-1068</sub>/STII/Cys.** PCR products were ligated into the pET28a vector, cloned in *E. coli* TG1, and then established in *E. coli* BL21(DE3) for expression. Biomass samples were harvested before and at 4 h after induction of expression and subjected to SDS-PAGE analysis. In comparison to noninduced *E. coli* BL21(DE3) cells (Figure 1A, lane 1), in samples from *E. coli* BL21(DE3) cultures induced to express the genes encoding rSbpA<sub>31-1178</sub>/STII/Cys, rSbpA<sub>31-1095</sub>/STII/Cys, and rSbpA<sub>31-1068</sub>/STII/Cys, additional high molecular mass protein bands were observed on SDS-gels (Figure 1A,

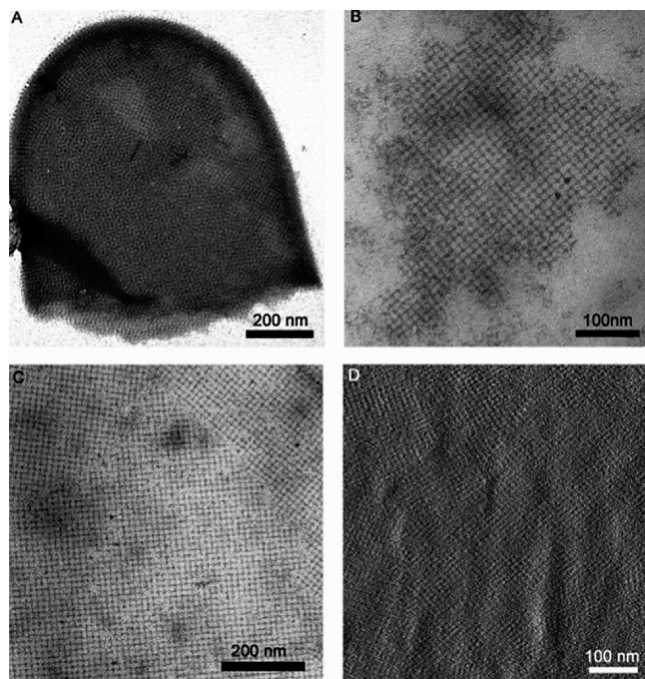


**Figure 2.** Electron micrograph of negatively stained preparations demonstrating the formation of the square S-layer lattice by the fusion protein rSbpA<sub>31-1178</sub>STII/Cys on peptidoglycan-containing sacculi of *Ly. sphaericus* CCM 2177 (A); of rSbpA<sub>31-1178</sub>STII/Cys self-assembly products in suspension (B); rSbpA<sub>31-1178</sub>STII/Cys recrystallized into a closed monolayer consisting of numerous randomly oriented patches on poly-L-lysine coated EM-grids (C); and AFM image of rSbpA<sub>31-1178</sub>STII/Cys recrystallized into a closed crystalline monolayer on a silicon chip (D).

lanes 2, 3, and 4). These additional protein bands had apparent molecular masses of 121,000 Da, 114,000 Da, and 111,000 Da, respectively, which corresponded to the theoretical molecular masses estimated for the three fusion proteins of 121,345 Da, 113,720 Da, and 111,241 Da, respectively. Immunoblotting using the polyclonal rabbit antiserum raised against the S-layer protein SbpA of *Ly. sphaericus* CCM 2177 revealed a strong cross-reaction with each of the three additional protein bands (Figure 1B, lanes 1, 2, and 3).

**Isolation of the Three rSbpA/STII/Cys Proteins from the Host Cells and Purification and Investigation of the Recrystallization Properties.** As derived from SDS-PAGE analysis of samples collected during the isolation procedure, all three fusion proteins had accumulated in the insoluble fraction of the lysed *E. coli* BL21(DE3) cells (data not shown). After purification by GPC, single protein bands with an apparent molecular mass of 121,000 Da, 114,000 Da, or 111,000 Da, respectively, were detected on SDS-gels (Figure 1C, lanes 1, 2, and 3). Recrystallization on peptidoglycan-containing sacculi of *Ly. sphaericus* CCM 2177 was induced by the addition of 10 mM CaCl<sub>2</sub> to monomeric solutions of the rSbpA fusion proteins. To avoid potential dimer formation caused by the C-terminally fused cysteine residue, which would disturb the recrystallization process, 1 mM DTT was added to the recrystallization buffer. As shown by transmission electron microscopy for the derivative rSbpA<sub>31-1178</sub>STII/Cys (Figure 2A), all three rSbpA derivatives recognized peptidoglycan-containing sacculi of *Ly. sphaericus* CCM 2177 as binding sites and recrystallized into the square lattice structure with a center-to-center spacing of the morphological units of 13.1 nm, which is typical for the S-layer protein SbpA. In this approach, the specific recognition mechanism between the N-terminal SLH-domain of the S-layer protein and the SCWP in the peptidoglycan-containing sacculi was used for oriented binding of the fusion proteins on the solid support. As shown by negative staining for rSbpA<sub>31-1178</sub>STII/Cys, all three

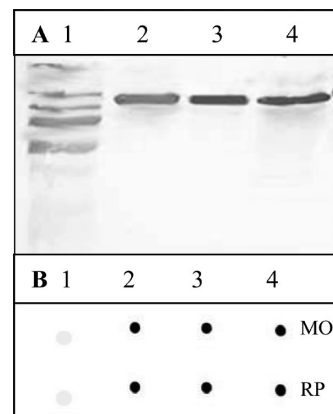


**Figure 3.** (A) Immunoblot analysis of rSbpA<sub>31-1178</sub>STII/Cys (lane 2), rSbpA<sub>31-1095</sub>STII/Cys (lane 3), and rSbpA<sub>31-1068</sub>STII/Cys (lane 4) using monoclonal mouse anti-Strep-tag II antibody. Lane 1, bench mark ladder (All blue). (B) Immunodot assay indicating the accessibility of the C-terminal Strep-tag II of rSbpA<sub>31-1178</sub>STII/Cys (lane 2), rSbpA<sub>31-1095</sub>STII/Cys (lane 3), and rSbpA<sub>31-1068</sub>STII/Cys (lane 4) in a monomeric state (MO) or recrystallized on peptidoglycan-containing sacculi of *Ly. sphaericus* CCM 2177 (RP). In lane 1, corresponding samples prepared with wild-type SbpA showed no cross-reaction with the monoclonal mouse antibody raised against STII.

rSbpA/STII/Cys fusion proteins were able to reassemble in suspension into flat double layer sheets with a maximum size of 2  $\mu$ m, clearly exhibiting the square lattice structure (Figure 2B). These results demonstrated that neither the C-terminal deletions nor the fusion of the *Strep*-tag II and the single cysteine residue interfered with the recrystallization and the cell wall binding properties of the S-layer protein. As shown for rSbpA<sub>31-1178</sub>STII/Cys in Figure 2C, all three rSbpA/STII/Cys fusion proteins were capable of recrystallizing into closed crystalline monolayers consisting of numerous randomly oriented patches on poly-L-lysine coated EM-grids. Additionally, AFM analysis of the three rSbpA/STII/Cys fusion proteins recrystallized on silicon chips clearly demonstrated the formation of closed monolayers displaying the square lattice structure (shown in Figure 2D for rSbpA<sub>31-1178</sub>STII/Cys). Comparison of the recrystallization behavior of the three differently truncated fusion proteins revealed that the derivative rSbpA<sub>31-1178</sub>STII/Cys was able to recrystallize into closed crystalline monolayers showing a good long-range order on solid supports (Figure 2A–D), whereas rSbpA<sub>31-1095</sub>STII/Cys and rSbpA<sub>31-1068</sub>STII/Cys showed a more patch-like recrystallization pattern (data not shown).

**Investigation of the Accessibility of *Strep*-tag II in Water-Soluble and Recrystallized rSbpA/STII/Cys Fusion Proteins.** The presence of *Strep*-tag II at the C-terminus of all three rSbpA/STII/Cys fusion proteins was confirmed by immunoblotting with a monoclonal mouse antibody raised against *Strep*-tag II. All three fusion proteins showed significant cross-reactions with the anti-*Strep*-tag II antibody (Figure 3A, lanes 2–4). Immunodot assays of the three fusion proteins in a water-soluble state as well as those recrystallized on peptidoglycan-containing sacculi showed a good accessibility of *Strep*-tag II on the surface of the S-layer lattice (Figure 3B). These findings indicated that the accessibility of the *Strep*-tag II was not reduced in recrystallized S-layer fusion proteins. However, equal color-intensity of the dots indicated that minor differences in accessibility of the differently truncated C-termini of the three derivatives cannot be estimated with this method. Wild-type SbpA recrystallized on peptidoglycan-containing sacculi of *Ly. sphaericus* CCM 2177, used as a control, showed no reaction with the antibody against *Strep*-tag II (Figure 3B, lane 1).

**Targeted Chemical Modification of the Cysteine Residue of Monomeric rSbpA<sub>31-1178</sub>STII/Cys with Differently Sized Preactivated Macromolecules.** To assess the surface accessibility of the cysteine residue at the C-terminal end of folded monomers

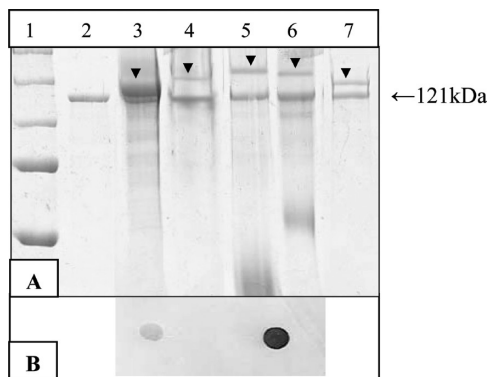


**Figure 4.** (A) Examination of the surface accessibility of the C-terminal cysteine residue of monomeric rSbpA<sub>31-1178</sub>/STII/Cys fusion protein by targeted chemical modification with differently sized macromolecules. Bench mark ladder (All blue, Biorad laboratories, Hercules, CA) (lane 1); GPC-purified rSbpA<sub>31-1178</sub>/STII/Cys (lane 2); rSbpA<sub>31-1178</sub>/STII/Cys chemically modified with sulphydryl-specific PEG-maleimide 5 kDa (lane 3) and 20 kDa (lane 4) as well as rSbpA<sub>31-1178</sub>/STII/Cys modified with protein A ( $M_r = 42$  kDa) (lane 5), carbonic anhydrase ( $M_r = 29$  kDa) (lane 6), or rBet v1 ( $M_r = 17$  kDa) (lane 7) preactivated with the heterobifunctional cross-linker Sulfo-MBS. The positions of modified (upshifted) bands are indicated by arrows. (B) Immuno dot assay using rabbit anticarbonic anhydrase antibody indicating the presence of carbonic anhydrase on the surface of the monolayer formed by recrystallization of rSbpA<sub>31-1178</sub>/STII/Cys-Sulfo-MBS-carbonic anhydrase conjugate on peptidoglycan-containing sacculi of *Ly. sphaericus* CCM 2177 (right dot). Left dot: recrystallization products consisting of wild-type SbpA recrystallized on PGS of *Ly. sphaericus* CCM 2177 showed no signal.

of rSbpA<sub>31-1178</sub>/STII/Cys in solution (Figure 4A, lane 2), sulphydryl-specific PEG-maleimide modification was performed. The modification with m-PEG-mal, size 5 and 20 kDa, resulted in an increase of the molecular mass of the protein visible as a gel shift on SDS-PAGE corresponding to the molecular mass of the respective m-PEG-maleimide (Figure 4A, lanes 3 and 4). By the addition of DTT, the upshift of the rSbpA<sub>31-1178</sub>/STII/Cys-PEG conjugate could be reversed (data not shown), which indicated that the cysteine residues of the mutant were specifically PEGylated.

Consistently, chemical modification of the cysteine residues of monomeric SbpA<sub>31-1178</sub>/STII/Cys fusion protein with the differently sized macromolecules Protein A, ( $M_r$  42 kDa), carbonic anhydrase ( $M_r$  29 kDa), or rBet v1 ( $M_r$  17 kDa) via the heterobifunctional cross-linker Sulfo-MBS, resulted in an increase of the molecular mass as calculated for the sum of the theoretical masses of the truncated S-layer protein plus the respective macromolecules (Figure 4A, lanes 5, 6, and 7). The modification pattern of the mutant indicated the presence and accessibility of the cysteine residues in the monomeric fusion protein. Although during all stages of the experiment DTT was added, and the solutions and buffers were degassed, the monomeric mutant could not be completely modified, which indicated that maybe irreversible oxidation of the sulphydryl groups of some of the cysteine residues has occurred. Increase of the molar ratio between rSbpA<sub>31-1178</sub>/STII/Cys and the respective preactivated macromolecule (from 1:2 to 1:10) did not result in an increase in the modification rate.

**Investigation of the Recrystallization Properties of rSbpA<sub>31-1178</sub>/STII/Cys Conjugated with Carbonic Anhydrase via a Heterobifunctional Cross-Linker by TEM and Detection of the Enzyme on the Surface of the S-Layer Lattice.** Electron microscopy of the recrystallization products showed that modification of the S-layer fusion protein with the preactivated carbonic anhydrase did not interfere with its recrystallization properties (data not shown). Immuno dot blots of recrystallization products with an antibody raised against carbonic

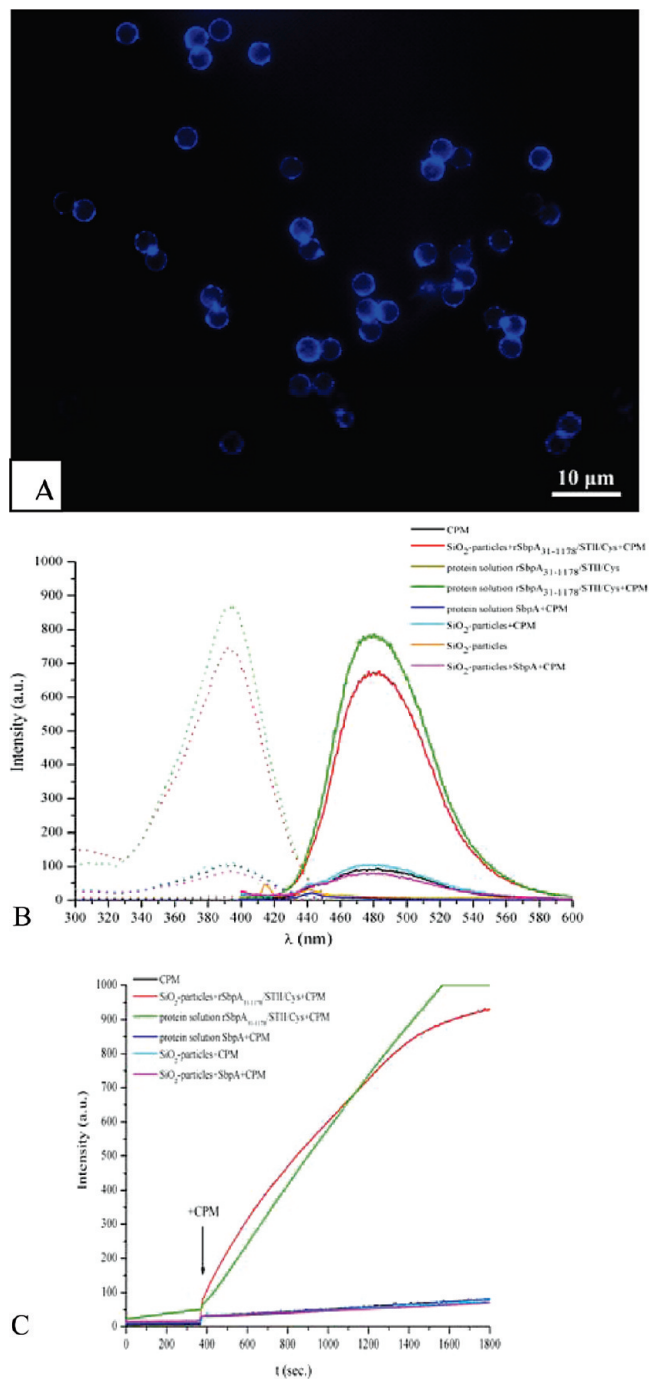


**Figure 5.** (A) Fluorescent micrograph of rSbpA<sub>31-1178</sub>/STII/Cys recrystallized as a monolayer on SiO<sub>2</sub>-microparticles and incubated with CPM indicating surface exposure of the C-terminally fused cysteine residue. (B) Fluorescent excitation and emission spectrum of the fusion protein rSbpA<sub>31-1178</sub>/STII/Cys-CPM conjugate in solution or recrystallized on SiO<sub>2</sub>-particles showing an excitation peak at 388 nm and an emission peak of 480 nm, which was in good accordance with the values (384 nm/470 nm) reported for the dye. As expected, the thiol-reactive coumarin, CPM alone, was very weakly fluorescent without reaction with a thiol group. Soluble rSbpA<sub>31-1178</sub>/STII/Cys without dye, soluble wild-type SbpA incubated with the dye, wild-type SbpA recrystallized on microparticles incubated with the fluorophore, and the SiO<sub>2</sub>-particles alone or incubated with the fluorophore, used as references, did not show a significant fluorescence intensity. (C) A time dependent increase of fluorescence was recorded for rSbpA<sub>31-1178</sub>/STII/Cys-CPM conjugates in solution or recrystallized on SiO<sub>2</sub>-particles, whereas soluble wild-type SbpA or SbpA recrystallized on SiO<sub>2</sub>-particles as well as SiO<sub>2</sub>-particles (all incubated with the dye for 30 min), used as a control for nonspecific interactions with CPM, reached no significant value.

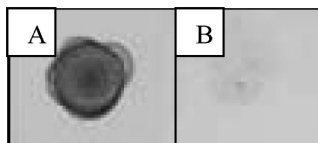


**Figure 6.** Immuno dot assay using rabbit anticarbonic anhydrase antibody demonstrating that carbonic anhydrase preactivated with the heterobifunctional cross-linker Sulfo-MBS could be successfully bound to rSbpA<sub>31–1178</sub>/STII/Cys recrystallized on peptidoglycan-containing sacculi of *Ly. sphaericus* CCM 2177 (A). Wild-type SbpA recrystallized on peptidoglycan-containing sacculi of *Ly. sphaericus* CCM 2177, used as a control, showed no reaction with the antibody against carbonic anhydrase (B).

anhydrase, performed to confirm the presence of the carbonic anhydrase on the surface of the S-layers lattices, showed a clear signal (Figure 4B, right). Wild-type SbpA recrystallized on peptidoglycan-containing sacculi of *Ly. sphaericus* CCM 2177, used as a control, showed no reaction with the antibody against carbonic anhydrase (Figure 4B, left).

**Fluorescent Labeling of the C-Terminal Cysteine Residue of Recrystallized rSbpA<sub>31–1178</sub>/STII/Cys.** To investigate the spatial accessibility of the C-terminal cysteine residue within the fusion protein lattice, rSbpA<sub>31–1178</sub>/STII/Cys was recrystallized on SiO<sub>2</sub>-particles and incubated with methylcoumarin (CPM), known as a thiol-reactive dye, which is only fluorescent if the binding between the thiol-group and the dye proceeds. As derived from former studies performed by using rSbpA (10, 13), because of the specific physicochemical properties of its N-terminal part, the S-layer fusion protein was expected to recrystallize with its inner surface on the SiO<sub>2</sub>-particles, thereby leaving the C-terminally fused cysteine residue exposed to the ambient environment. As shown by fluorescence microscopy, an oriented binding of rSbpA<sub>31–1178</sub>/STII/Cys on SiO<sub>2</sub>-particles could be demonstrated by obtaining a significant fluorescence signal after labeling the cysteine residues with methylcoumarin (Figure 5A). This led to the conclusion that the cysteine residues are located on the surface of the crystalline monolayer formed by rSbpA<sub>31–1178</sub>/STII/Cys on SiO<sub>2</sub>-particles and are accessible for modification with CPM. Compared to these data, wild-type protein SbpA recrystallized on SiO<sub>2</sub>-particles or SiO<sub>2</sub>-particles alone, used as blanks, showed no fluorescence signal (data not shown). Determination of the excitation and emission spectra of the rSbpA<sub>31–1178</sub>/STII/Cys-CPM conjugates in solution or recrystallized on SiO<sub>2</sub>-particles revealed an excitation peak at 388 nm and an emission peak at 480 nm (Figure 5B), which was in accordance with the reported values of  $E_x/E_m$  (nm) 384/

470 for the dye. As described by the manufacturer, the thiol-reactive coumarin, CPM alone was very weakly fluorescent without reaction with a thiol group (Figure 5B). Soluble rSbpA<sub>31–1178</sub>/STII/Cys without dye, soluble wild-type SbpA incubated with the dye, wild-type SbpA recrystallized on microparticles incubated with the fluorophore, and the SiO<sub>2</sub>-particles alone or incubated with the fluorophore, used as references, did not show a significant fluorescence intensity (Figure 5B). A time dependent increase of fluorescence was recorded for rSbpA<sub>31–1178</sub>/STII/Cys-CPM conjugates in solution or recrystallized on SiO<sub>2</sub>-particles (Figure 5C), whereas soluble wild-type SbpA or SbpA recrystallized on SiO<sub>2</sub>-particles as well as SiO<sub>2</sub>-particles (all incubated with the dye for 30 min), used as a control for nonspecific interactions with CPM, reached no significant value (Figure 5C).

**Chemical Modification of the Cysteine Residues of Recrystallized rSbpA<sub>31–1178</sub>/STII/Cys.** By performing immuno dot assays, it could also be shown that preactivated carbonic anhydrase could be successfully bound to rSbpA<sub>31–1178</sub>/STII/Cys, which was recrystallized on peptidoglycan-containing sacculi of *Ly. sphaericus* CCM 2177 (Figure 6A). This result clearly indicated that the C-terminal cysteine residue at amino acid position 1,178 is surface exposed and accessible also in the recrystallized fusion protein rSbpA<sub>31–1178</sub>/STII/Cys. Wild-type SbpA recrystallized on peptidoglycan-containing sacculi of *Ly. sphaericus* CCM 2177, used as a control, showed no reaction with the antibody against carbonic anhydrase (Figure 6B).

**Formation of Gold Nanoparticle Arrays on Crystalline Monolayers Formed by rSbpA<sub>31–1178</sub>/STII/Cys and Image Processing.** Cysteine residues located on the surface of the S-layer lattice formed by rSbpA<sub>31–1178</sub>/STII/Cys on peptidoglycan-containing sacculi of *Ly. sphaericus* CCM 2177 were used for covalent binding of gold nanoparticles with a diameter of 5 nm. A TEM image of the resulting regularly arranged gold nanoparticle array is shown in Figure 7A. Similar results could be obtained when self-assembly products formed by rSbpA<sub>31–1178</sub>/STII/Cys were used as binding templates for a well-organized arrangement of gold nanoparticles (Figure 7B). The superlattice of the gold nanoparticles resembled the underlying square symmetry of the S-layer lattice formed by the fusion protein where every S-layer subunit carries one cysteine residue, and four subunits form one morphological unit. Base vector lengths were ~13.5 nm. An accurate lattice fit was obtained by cross-correlation averaging (CCA) where approximately 90% of the found nanoparticles in the image could be assigned to lattice

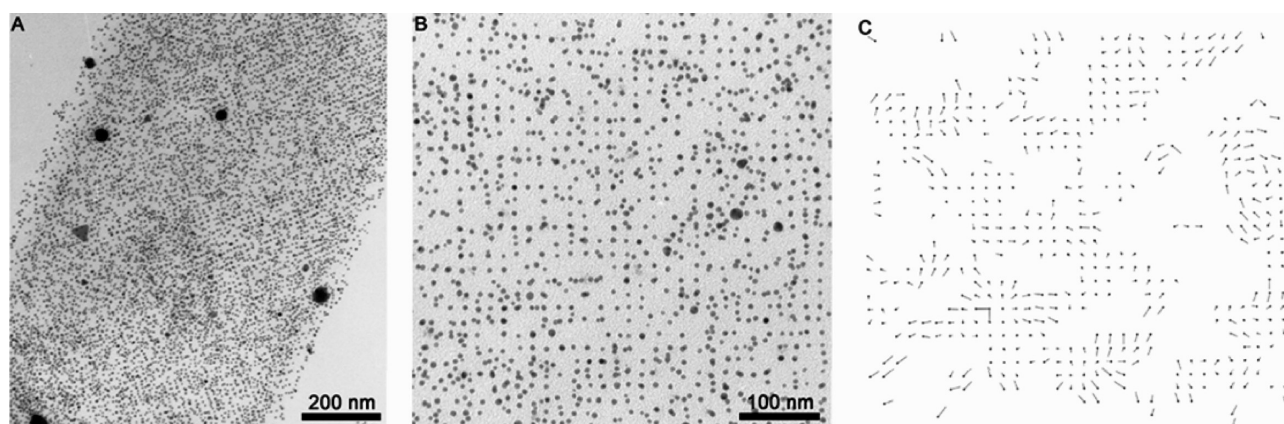


**Figure 7.** TEM micrograph of gold nanoparticles covalently bound to (A) recrystallization products consisting of rSbpA<sub>31–1178</sub>/STII/Cys fusion protein recrystallized on peptidoglycan-containing sacculi of *Ly. sphaericus* CCM 2177 and (B) double-layered self-assembly products formed in suspension by rSbpA<sub>31–1178</sub>/STII/Cys. (C) Cross-correlation averaging (CCA) of B. Bold dots mark positions at the nearest points on a least-squares fitted lattice. Small lines emanating from them indicate the direction and displacement (magnified 5 times) to the actually found positions, thus mapping the displacement field.

points (Figure 7C). The averaged root-mean-square deviation was found to be  $\sim 6\%$  of the base vector lengths ( $\sim 0.8$  nm).

If recrystallization products consisting of wild-type SbpA recrystallized on PGS of *Ly. sphaericus* CCM 2177 were used, no binding of gold nanoparticles could be detected (data not shown). When double-layered self-assembly products formed by wild-type SbpA were used, gold nanoparticles were only found at incomplete regions of the double layer where the inner face of the S-layer lattice was accessible (data not shown). These findings led to the conclusion that the formation of regularly arranged gold nanoparticles on rSbpA<sub>31–1178</sub>/STII/Cys monolayers is the result of specific binding of the nanoparticles to the sulfhydryl groups of the cysteine residues exposed on the outer face of the S-layer lattice.

## DISCUSSION

In recent years, on the basis of the work on binding preactivated macromolecules, it has been demonstrated that metal and semiconducting nanoparticles can be bound in regular arrangements to native S-layer protein lattices by noncovalent bonds (e.g., electrostatic interactions) or by covalent bonds after EDC activation (15–17). An alternative strategy for exploiting S-layer lattices as patterning elements for producing regularly ordered nanoparticle arrays in a much more controlled and specific way relates to genetically engineered S-layer proteins incorporating binding peptide domains.

The aim of the present study was to identify amino acid residues that are located on the surface of the S-layer lattice formed by the S-layer protein SbpA of *Ly. sphaericus* CCM 2177, which should serve as binding sites for functional macromolecules or for metal nanoparticles. Preliminary studies on the structure–function relationship of SbpA revealed that the N-terminal part of SbpA functions as a cell wall binding domain and that the truncated form rSbpA<sub>31–1068</sub>, devoid of 200 C-terminal amino acids, was more surface accessible compared to the C-terminus of the full-length rSbpA<sub>31–1268</sub> (13). These results and the fact that various SbpA fusion proteins exhibit C-terminally fused functional domains (e.g., streptavidin (30), birch pollen allergen (13, 31), camel antibodies (12, 32), enhanced green fluorescent protein (25), and extremophilic enzymes (33)) on the surface of the S-layer lattice revealed that the SbpA-C-terminus must be exposed on the outer face of the S-layer lattice. Therefore, in the present study, for performing a refined surface accessibility screen in the domain between amino acid position 1,068 and 1,268, three different C-terminally truncated forms of SbpA carrying the short affinity tag *Strep-tag* II and a single cysteine residue at the C-terminal end were cloned and heterologously expressed in *E. coli*. Considering that the S-layer protein completely covers the cell surface of *Ly. sphaericus* CCM 2177 and that an aqueous environment is required for the diffusion of nutrients and metabolic degradation products, it can be expected that hydrophilic amino acid residues are exposed on the surface of the S-layer lattice. Therefore, three different hydrophilic amino acid residues within the C-terminally domain of SbpA were chosen as sites for the functionalization with STII and the cysteine residue. As S-layers usually do not possess sulfur-containing amino acids, the insertion of a single cysteine residue into the S-layer protein sequence is particularly attractive since the whole sulfur chemistry can be applied to covalently attach functional entities via the introduced cysteine residue. As reported in ref 34, a single cysteine residue has been inserted at various amino acid positions along the self-assembling domain of the S-layer proteins SbsB of *Geobacillus stearothermophilus* PV72/p2. In accordance with results from this study demonstrating that the replacement of selected amino acids by cysteine residues did not dramatically alter the structure of the S-layer protein SbsB (34), in the present work, electron

microscopical examination revealed that all three rSbpA/STII/Cys fusion proteins retained their self-assembling and recrystallization ability. Recrystallization studies performed by TEM and AFM revealed that the SbpA derivative rSbpA<sub>31–1178</sub>/STII/Cys (devoid of 90 C-terminal amino acids) turned out to be the best candidate for further modification experiments because of its ability to recrystallize into closed crystalline monolayers showing a long-range order on solid supports. This feature represents a prerequisite of regular nanoarrays used as templates for the organized arrangement of nanoparticles.

To conclude, one of the aims of current nanobiotechnological research is the bioinspired synthesis of nanostructured materials with novel mechanical or electrical properties. In the present study, for the first time, a natural self-assembly system based on a genetically engineered bacterial surface-layer protein was used for the bottom up fabrication of regularly arranged gold nanoparticles.

## ACKNOWLEDGMENT

This work was supported by the FP6 EC-STREP project NASSAP 13523, by the Austrian Science Fund (FWF) Project P18510-B12 as well as by the US Air Force Office of Scientific Research (AFOSR) projects F49620-03-1-0222, FA9550-06-1-0208, and FA9550-07-0313. We thank Jacqueline Friedmann for performing the AFM studies and Manfred Tesarz for excellent technical support.

## LITERATURE CITED

- (1) Küpcü, S., Sara, M., and Sleytr, U. B. (1995) Liposomes coated with crystalline bacterial cells surface protein (S-layer) as immobilization structures for macromolecules. *Biochim. Biophys. Acta* 1235, 263–269.
- (2) Moreno-Flores, S., Kasry, A., Butt, H. J., Vavilala, C., Schmittl, M., Pum, D., Sleytr, U. B., and Toca-Herrera, J. L. (2008) From native to non-native two-dimensional protein lattices through underlying hydrophilic/hydrophobic nanoprotusions. *Angew. Chem., Int. Ed.* 47, 4707–4710.
- (3) Sleytr, U. B., Messner, P., Pum, D., and Sára, M. (1999) Crystalline bacterial cell surface layers (S-layers): from supramolecular cell structure to biomimetics and nanotechnology. *Angew. Chem., Int. Ed.* 38, 1034–1054.
- (4) Sleytr, U. B., Sára, M., Pum, D., Schuster, B., Messner, P., and Schäffer, C. (2003) Self Assembly Protein Systems: Microbial S-Layers, in *Biopolymers* (Steinbüchel, A., and Fahnstrock, S., Eds.) pp 285–338, Wiley-VCH, Weinheim, Germany.
- (5) Toca-Herrera, J. L., Krastev, R., Bosio, V., Küpcü, S., Pum, D., Fery, A., Sára, M., and Sleytr, U. B. (2005) Recrystallization of bacterial S-layers on flat polyelectrolyte surfaces and hollow polyelectrolyte capsules. *Small* 1, 339–348.
- (6) Breitwieser, A., Kupcu, S., Howorka, S., Weigert, S., Langer, C., Hoffmann-Sommergruber, K., Scheiner, O., Sleytr, U. B., and Sára, M. (1996) 2-D protein crystals as an immobilization matrix for producing reaction zones in dipstick-style immunoassays. *Biotechniques* 21, 918–925.
- (7) Breitwieser, A., Mader, C., Schocher, I., Hoffmann-Sommergruber, K., Aberer, W., Scheiner, O., Sleytr, U. B., and Sára, M. (1998) A novel dipstick developed for rapid Bet v 1-specific IgE detection: recombinant allergen immobilized via a monoclonal antibody to crystalline bacterial cell-surface layers. *Allergy* 53, 786–93.
- (8) Sleytr, U. B., and Sára, M. (1997) Bacterial and archaeal S-layer proteins: structure-function relationships and their biotechnological applications. *Trends Biotechnol.* 15, 20–6.
- (9) Weiner, C., Sára, M., and Sleytr, U. B. (1994) Novel protein A affinity matrix prepared from two-dimensional protein crystals. *Biotechnol. Bioeng.* 43, 321–330.
- (10) Ilk, N., Kosma, P., Puchberger, M., Egelseer, E. M., Mayer, H. F., Sleytr, U. B., and Sára, M. (1999) Structural and functional analyses of the secondary cell wall polymer of *Bacillus sphaeri-*

- cus CCM 2177 that serves as an S-layer-specific anchor. *J. Bacteriol.* **181**, 7643–6.
- (11) Sára, M., Pum, D., Huber, C., Ilk, N., Pleschberger, M., and Sleytr, U. (2006) Nanoscale Patterning of S-Layer Proteins As a Natural Self-Assembly System, in *Biological and Pharmaceutical Nanomaterials. Nanotechnologies for the Life Sciences* (Kumar, C., Ed.) pp 219–252, Wiley-VCH, Weinheim, Germany.
- (12) Pleschberger, M., Neubauer, A., Egelseer, E. M., Weigert, S., Lindner, B., Sleytr, U. B., Muyldermans, S., and Sara, M. (2003) Generation of a functional monomolecular protein lattice consisting of an s-layer fusion protein comprising the variable domain of a camel heavy chain antibody. *Bioconjugate Chem.* **14**, 440–8.
- (13) Ilk, N., Völlenklee, C., Egelseer, E. M., Breitwieser, A., Sleytr, U. B., and Sára, M. (2002) Molecular characterization of the S-layer gene, *sbpA*, of *Bacillus sphaericus* CCM 2177 and production of a functional S-layer fusion protein with the ability to recrystallize in a defined orientation while presenting the fused allergen. *Appl. Environ. Microbiol.* **68**, 3251–60.
- (14) Huber, C., Ilk, N., Rünzler, D., Egelseer, E. M., Weigert, S., Sleytr, U. B., and Sára, M. (2005) The three S-layer-like homology motifs of the S-layer protein SbpA of *Bacillus sphaericus* CCM 2177 are not sufficient for binding to the pyruvylated secondary cell wall polymer. *Mol. Microbiol.* **55**, 197–205.
- (15) Bergkvist, M., Mark, S. S., Yang, X., Angert, E. R., and Batt, C. A. (2004) Bionanofabrication of ordered nanoparticle arrays: effect of particle properties and adsorption conditions. *J. Phys. Chem. B* **108**, 8241–8248.
- (16) Györfvay, E., Schroedter, A., Talapin, D. V., Weller, H., Pum, D., and Sleytr, U. B. (2004) Formation of nanoparticle arrays on S-layer protein lattices. *J. Nanosci. Nanotechnol.* **4**, 115–120.
- (17) Hall, S. R., Shenton, W., Engelhardt, H., and Mann, S. (2001) Site-specific organization of gold nanoparticles by biomolecular templating. *Chem. Phys. Phys. Chem.* **3**, 184–186.
- (18) Mark, S. S., Bergkvist, M., Yang, X., Teixeira, L. M., Bhatnagar, P., Angert, E. R., and Batt, C. A. (2006) Bionanofabrication of metallic and semiconductor nanoparticle arrays using S-layer protein lattices with different lateral spacings and geometries. *Langmuir* **22**, 3763–74.
- (19) Merroun, M., Rossberg, A., Hennig, C., Scheinost, A. C., and Selenska-Pobell, S. (2007) Spectroscopic characterization of gold nanoparticles formed by cells and purified S-layer protein of *Bacillus sphaericus* JG-A12. *Mater. Sci. Eng. C* **27**, 188–192.
- (20) Mark, S. S., Bergkvist, M., Yang, X., Angert, E. R., and Batt, C. A. (2006) Self-assembly of dendrimer-encapsulated nanoparticle arrays using 2-D microbial S-layer protein biotemplates. *Biomacromolecules* **7**, 1884–1897.
- (21) Jarosch, M., Egelseer, E. M., Mattanovich, D., Sleytr, U. B., and Sára, M. (2000) S-layer gene *sbsC* of *Bacillus stearothermophilus* ATCC 12980: molecular characterization and heterologous expression in *Escherichia coli*. *Microbiology* **146** (Pt 2), 273–281.
- (22) Sambrook, J. F. E. F., and Maniatis, T. (1989) *Molecular Cloning: A Laboratory Manual*, 2nd ed., Cold Spring Harbour Laboratory Press, Plainview, NY.
- (23) Laemmli, U. K. (1970) Cleavage of structural proteins during the assembly of the head of bacteriophage T4. *Nature* **227**, 680–685.
- (24) Egelseer, E. M., Schocher, I., Sleytr, U. B., and Sára, M. (1996) Evidence that an N-terminal S-layer protein fragment triggers the release of a cell-associated high-molecular-weight amylase in *Bacillus stearothermophilus* ATCC 12980. *J. Bacteriol.* **178**, 5602–5609.
- (25) Ilk, N., Küpcü, S., Moncayo, G., Klimt, S., Ecker, R. C., Hofer-Warbinek, R., Egelseer, E. M., Sleytr, U. B., and Sára, M. (2004) A functional chimaeric S-layer-enhanced green fluorescent protein to follow the uptake of S-layer-coated liposomes into eukaryotic cells. *Biochem. J.* **379**, 441–448.
- (26) Pum, D., Sára, M., and Sleytr, U. B. (1989) Structure, surface charge, and self-assembly of the S-layer lattice from *Bacillus coagulans* E38–66. *J. Bacteriol.* **171**, 5296–5303.
- (27) Györfvay, E. S., Stein, O., Pum, D., and Sleytr, U. B. (2003) Self-assembly and recrystallization of bacterial S-layer proteins at silicon supports imaged in real time by atomic force microscopy. *J. Microsc. (Oxford, U. K.)* **212**, 300–306.
- (28) Völlenklee, C., Weigert, S., Ilk, N., Egelseer, E., Weber, V., Loth, F., Falkenhagen, D., Sleytr, U. B., and Sára, M. (2004) Construction of a functional S-layer fusion protein comprising an immunoglobulin G-binding domain for development of specific adsorbents for extracorporeal blood purification. *Appl. Environ. Microbiol.* **70**, 1514–1521; highlight in *Nat. Rev. Microbiol.* **2**(5), 353.
- (29) Saxton, W. O., and Baumeister, W. (1982) The correlation averaging of a regularly arranged bacterial cell envelope protein. *J. Microsc.* **127**, 127–138.
- (30) Moll, D., Huber, C., Schlegel, B., Pum, D., Sleytr, U. B., and Sára, M. (2002) S-layer-streptavidin fusion proteins as template for nanopatterned molecular arrays. *Proc. Natl. Acad. Sci. U.S.A.* **99**, 14646–14651.
- (31) Breitwieser, A., Egelseer, E. M., Moll, D., Ilk, N., Hotzy, C., Bohle, B., Ebner, C., Sleytr, U. B., and Sára, M. (2002) A recombinant bacterial cell surface (S-layer)-major birch pollen allergen-fusion protein (rSbsC/Bet v1) maintains the ability to self-assemble into regularly structured monomolecular lattices and the functionality of the allergen. *Protein Eng.* **15**, 243–249.
- (32) Pleschberger, M., Saerens, D., Weigert, S., Sleytr, U. B., Muyldermans, S., Sára, M., and Egelseer, E. M. (2004) An S-layer heavy chain camel antibody fusion protein for generation of a nanopatterned sensing layer to detect the prostate-specific antigen by surface plasmon resonance technology. *Bioconjug Chem* **15**, 664–671.
- (33) Tschiggerl, H., Breitwieser, A., de Roo, G., Verwoerd, T., Schaffer, C., and Sleytr, U. B. (2008) Exploitation of the S-layer self-assembly system for site directed immobilization of enzymes demonstrated for an extremophilic laminarinase from *Pyrococcus furiosus*. *J. Biotechnol.* **133**, 403–411.
- (34) Howorka, S., Sára, M., Wang, Y., Kuen, B., Sleytr, U. B., Lubitz, W., and Bayley, H. (2000) Surface-accessible residues in the monomeric and assembled forms of a bacterial surface layer protein. *J. Biol. Chem.* **275**, 37876–37886.

BC800445R



## Optical oxygen sensors based on Pt(II) porphyrin dye immobilized on S-layer protein matrices

Sylvia R. Scheicher<sup>a,\*</sup>, Birgit Kainz<sup>b</sup>, Stefan Köstler<sup>a,c</sup>, Michael Suppan<sup>c</sup>,  
Alessandro Bizzarri<sup>c</sup>, Dietmar Pum<sup>b</sup>, Uwe B. Sleytr<sup>b</sup>, Volker Ribitsch<sup>a,c</sup>

<sup>a</sup> Karl Franzens University Graz, Institute of Chemistry, Heinrichstrasse 28, A-8010 Graz, Austria

<sup>b</sup> University of Natural Resources and Applied Life Sciences, Department of Nanobiotechnology, Gregor Mendel-Straße 33, A-1180 Vienna, Austria

<sup>c</sup> Joanneum Research, Institute of Chemical Process Development and Control, Steyrergasse 17, A-8010 Graz, Austria

### ARTICLE INFO

#### Article history:

Received 19 June 2009

Received in revised form 6 August 2009

Accepted 20 August 2009

Available online 27 August 2009

#### Keywords:

S-layer protein

Fiber optic sensor

Oxygen sensor

Phase modulation fluorimetry

Immobilization matrix

### ABSTRACT

This paper describes the development of planar and fiber optic oxygen sensors utilizing surface layer (S-layer) proteins as immobilization matrix for oxygen sensitive dyes. S-layer proteins have the intrinsic capability to reassemble into two-dimensional arrays in suspension and at interfaces. Due to their crystalline character the distribution of functional groups, such as carboxylic groups, is repeated with the periodicity of the lattice and thus allows the reproducible and geometrically distinct binding of functional molecules. For the development of oxygen sensors an oxygen sensitive Pt(II) porphyrin dye was covalently bound to the S-layer matrix. Measurement of the oxygen concentration was performed by phase modulation fluorimetry. Setups comprising low cost optoelectronic components like LEDs and silicon photodiodes were constructed. For both sensor setups (planar and fiber optic) variations in the oxygen concentrations resulted in distinct and reproducible changes in luminescence lifetime and intensity. The luminescence quenching efficiency of these sensors was found to be 1.5–1.9 (expressed as the ratio of signal under nitrogen and air) which compares well to other sensor systems using luminophores embedded in polymer matrices. These results demonstrated the application potential of S-layers as immobilization matrices in the development of (bio-)sensors.

© 2009 Elsevier B.V. All rights reserved.

### 1. Introduction

Continuous measurement of parameters like pH, CO<sub>2</sub> and especially oxygen concentration in blood, tissue and other biological fluids is of major interest in different medical applications such as physiological and respiratory studies (Jiang et al., 2008) as well as in critical care units (Cajlakovic et al., 2009). There is a continuous need and interest to develop more sensitive and improved sensors, especially with respect to biocompatibility of the used materials and prevention of biofouling of the sensor surfaces. The immobilization of functional components like biomolecules and fluorophores on solid supports is still a main task in the development of optical biosensors. Different surface functionalization methods have been developed for covalent binding of e.g. fluorophores to sensor surfaces. Examples are the formation of self-assembled monolayers (e.g. silanes on glass and silica, or thiols on gold) or the formation of reactive surface groups by plasma or UV-irradiation on polymers (Chaki and Vijayamohan,

2002; Zammattéo et al., 2000; Soper et al., 2005). Although these methods have successfully been used for covalent attachment of fluorophores or other functional molecules, each of them only works on a specific substrate material and they do not possess any kind of lateral order or nanostructure within the functional layers. A possibility for a more universal platform to immobilize functional molecules, also showing a well-defined nanostructure and organization, would be to apply self-assembled monolayers of S-layer proteins.

A broad range of bacteria and archaea show crystalline cell surface layers (S-layers) as the outermost cell envelope component (Sleytr and Beveridge, 1999; Sleytr et al., 2007a,b). S-layers are monomolecular arrays composed of a single protein or glycoprotein species ( $M_w$  40–200 kDa) and exhibit either oblique (p1, p2), square (p4) or hexagonal (p3, p6) lattice symmetry with unit cell dimensions in the range of 3–30 nm and thicknesses of 5–10 nm. Depending on the lattice symmetry one morphological unit (=unit cell) consists of one, two, three, four or six identical S-layer proteins. S-layers represent highly porous protein lattices (30–70% porosity) with pores of uniform size and morphology in the 2–8 nm range. Functional groups (e.g. carboxyl groups, amino or hydroxyl groups) or genetically incorporated functional domains (e.g. strep-

\* Corresponding author. Tel.: +43 316 380 5447; fax: +43 316 380 9850.

E-mail address: [syl.scheicher@uni-graz.at](mailto:syl.scheicher@uni-graz.at) (S.R. Scheicher).

tavidin sites for biotin binding, fused with the self-assembling part of the protein) are repeated with the periodicity of the S-layer lattice and are thus responsible for the formation of regular arrays of bound functional molecules or nanoparticles (Messner et al., 1986; Gyorvary et al., 2004). Binding may take place either by electrostatic or covalent interactions. One of the most fascinating properties of isolated S-layer proteins is their capability to form free floating self-assembly products in suspension (e.g. flat sheets, cylinders), to recrystallize into extended monomolecular layers on solid supports, at the air–water interface, and on lipid films and to cover liposomes and nanocapsules completely (Sleytr and Beveridge, 1999; Sleytr et al., 2007a,b). The formation of self-assembled arrays is only determined by the amino acid sequence of the polypeptide chains and consequently the tertiary structure of the S-layer protein species. Furthermore, it could be shown that such S-layer coatings can impart pronounced anti-fouling properties and low unspecific binding to the coated surfaces (Messner et al., 1984). Due to their unique properties S-layer proteins are versatile materials already explored for different kinds of applications like in the fabrication of ultrafiltration membranes (Sara and Sleytr, 1987), in vaccine development (Ford and Thune, 1992) or specific adsorbent materials (Vollenkle et al., 2004). The binding properties of S-layers have also been used in the development of dipstick format immunoassays by binding of antibodies (Breitwieser et al., 1996; Weigert and Sara, 1996) and in enzyme based optical and electrochemical biosensors by immobilization of glucoseoxidase (Neubauer et al., 1996; Neubauer et al., 1993).

Recently, we also could show binding of luminescent metalloporphyrin dyes to S-layer proteins and changing luminescence properties in presence and absence of oxygen (Kostler et al., 2007). The phosphorescence of such Pt(II) porphyrins is known to be efficiently quenched by molecular oxygen, leading to a strong decrease in luminescence lifetime and intensity. These changes in luminescence signals can be used for optical sensing of oxygen (Papkovsky, 1995; Papkovsky and O'riordan, 2005; Wolfbeis, 1991).

In this work we show the development of luminescence lifetime based oxygen sensors applying planar substrates and optical fibers coated with functionalized S-layers as active sensor element. The goal is to show the construction of optical sensors based on low cost optoelectronic components (like LEDs) by using biocompatible, non-fouling S-layer coatings as immobilization matrix for the fluorescent dye.

## 2. Materials and methods

### 2.1. Materials and reagents

The luminophore Pt(II)-meso-mono(4-aminophenyl)-triphenyl-porphyrin (Pt-TPP-NH<sub>2</sub>) was obtained from Frontier Scientific Porphyrin Products. Glutaraldehyde, *N*-(3-dimethylaminopropyl)-*N'*-ethylcarbodiimide (EDC), acetone, guanidine chloride, ethylenediaminetetraacetic acid (EDTA), ethanol<sub>abs</sub> (EtOH), sodium chloride (NaCl), 2-Amino-2-(hydroxymethyl)-1,3-propanediol hydrochloride (Tris-HCl), calcium chloride (CaCl<sub>2</sub>) and dimethyl sulfoxide (DMSO) were from Aldrich. All chemicals were used without further purification.

### 2.2. Sensor substrates

Microscope glass slides from Menzel-Glaeser were used as substrates for the planar oxygen sensor setup. The glass slides with an original size of 25 mm × 60 mm × 0.8 mm were cut using a glass cutter and cleaned by washing twice with ethanol and doubly distilled water.

For the fiber optic sensor setup BHF 48-400 0.48 NA Hard Polymer Clad Multimode Fiber from Thorlabs GmbH with a numerical aperture (NA) of 0.48 were used as substrates. The silica core is 400 μm in diameter and it is surrounded by a 15 μm thick hard polymer cladding, followed by a 150 μm thick Tefzel<sup>®</sup> jacket. The jacket was removed using a fiber stripping tool, the cladding was removed by treating the fiber with acetone, leaving a 5–10 mm bare optical fiber core. Fiber tips were tapered by the tube etching method (Stockle et al., 1999) in 40% hydrofluoric acid and characterized by light microscopy. They were cleaned with ethanol and doubly distilled water like the glass slides.

### 2.3. S-layer protein isolation

The bacterial cell surface layer proteins (S-layer) SbpA, used in this study, were isolated from *Lysinibacillus sphaericus* CCM2177. Growth in continuous culture (30 °C), cell-wall preparation, and extraction of SbpA with guanidine chloride (5 M), and further dialyzed against 2 mM EDTA, were carried out as described previously (Sleytr et al., 1986). After centrifuging (60 min, 10 °C, 30,000 rpm) the protein concentration of the disassembled S-layer subunits was determined at 280 nm and adjusted with Milli-Q water to 1 mg/ml. The SbpA protein solution was stored at 4 °C without addition of preservatives.

### 2.4. Recrystallization of S-layer proteins on sensor substrates

For the recrystallization of SbpA on glass, cleaned substrates were immersed in a protein solution containing 0.1 mg/mL SbpA protein monomers in 0.5 mM Tris-HCl buffer (pH 9) with 10 mM CaCl<sub>2</sub> overnight. The glass substrates with recrystallized protein were washed and stored at 4 °C in Milli-Q water before starting the experiments.

SbpA protein recrystallization experiments on tapered optical fibers were carried out in mini glass flasks (2 mL volume). The cleaned optical fibers were immersed and kept overnight in a protein solution composed of 0.1 mg/mL SbpA protein monomers, 0.5 mM Tris-HCl buffer (pH 9), and 10 mM CaCl<sub>2</sub>. Fibers with recrystallized protein were washed and stored at 4 °C in Milli-Q water before starting the experiments.

The layers were characterized by atomic force microscopy (AFM) in order to confirm the formation of regular, ordered protein patterns. AFM measurements were performed in contact mode using a Nanoscope IIIa multimode (Veeco Instruments, Santa Barbara, CA). 200 μm long oxide-sharpened silicon nitride (Si<sub>3</sub>N<sub>4</sub>) cantilevers with a nominal spring constant of 0.06 N m<sup>-1</sup> (NP-S, Nanoprobes, Digital Instruments, Santa Barbara, CA) were used as tips. The surface topography of the reassembled SbpA S-layer proteins was measured in 100 mM NaCl-solution at room temperature as described above (Gyorvary et al., 2004).

### 2.5. Functionalization of S-layer proteins

S-layer proteins amino groups were crosslinked by incubation in 0.5% glutaraldehyde solution for 15 min at room temperature.

For covalent binding of Pt(II)-TPP-NH<sub>2</sub>, the carboxylic groups of S-layer proteins were activated using the water soluble carbodiimide, *N*-(3-dimethylaminopropyl)-*N'*-ethylcarbodiimide (EDC). By the activation of the carboxylic groups a rather unstable intermediate of *O*-acrylisourea is formed, allowing the covalent binding to the amino group of the dye. The protein layer was incubated for one hour in 15 mg/mL EDC at pH 4.75. After rinsing with doubly distilled water, the protein layer was subsequently incubated in Pt(II)-TPP-NH<sub>2</sub> solution at a concentration of 0.1 mg/mL in DMSO for at least 2 h, leading to covalent binding of the luminophore to

the protein layer. After this incubation step the samples were again rinsed with DMSO and doubly distilled water.

Native and functionalized S-layer samples were stored in doubly distilled water at 4 °C.

## 2.6. Oxygen sensing

For sensing dissolved oxygen, gas equilibrated distilled water was used as medium.

During oxygen measurements the medium was equilibrated with gas mixtures of nitrogen and oxygen (0, 2.1, 4.2, 8.7 mg/L oxygen) using a mass flow controller (Bronkhorst, The Netherlands) and controlled with a paramagnetic gas purity analyzer (Servomex, UK). The temperature of the medium was kept at 25 °C. For measurements with the planar oxygen sensor setup, the medium was equilibrated for 30 min to a final concentration of 0 mg/L oxygen and for 15 min to 2.1, 4.2, and 8.7 mg/L oxygen each. For the fiber optic oxygen sensor setup the medium was equilibrated for 5 min with 0, 2.1, 4.2, 8.7 mg/L oxygen each. Nitrogen N<sub>2</sub> 5.0 and oxygen O<sub>2</sub> 5.0 from Air Liquide (Austria) were used as gas source.

For the planar sensor setup a LED (LED405-03 V) with an emission maximum of 405 nm from Roitner Lasertechnik was used. Modulation of the excitation light source was carried out at a frequency of 4500 Hz with a pulse/function generator (HP8116A, Hewlett Packard). A scheme of the planar sensor setup is shown in Fig. 1. A BG12 filter from Linos was fixed in front of the LED. The LED was fixed in a 45° angle to the flow cell. The flow cell containing the sensor slide was thermostatted at 25 °C. A combination of a RG61 filter (Unaxis) and a LEE 135 filter (Lee) was placed between the flow cell and the PMT. Detection was performed using a Photomultiplier (PMT) H5702-50 from Hamamatsu connected to a Lock-In Amplifier (SR830, Stanford Research) and an oscilloscope (54831D MSO, Agilent).

In the fiber optic setup, excitation was accomplished using a LED (LED NSPES90S, Nichia) with an emission maximum of 510 nm. Modulation of the excitation light at a frequency of 4500 Hz was controlled by a Vector Board V03 (SN 2003-G001) (Trettnak et al., 1996). For scheme of the fiber optic setup see Fig. 2. A BG39 filter (Linos) was fixed in front of the LED and a DC-Red filter (Linos) was fixed in a 45° angle to the LED. The fiber with the sensor tip was connected to the setup with an SMA-to-fiber connector. In front of the Si-photodiode (S62386-SK, Hamamatsu), which was

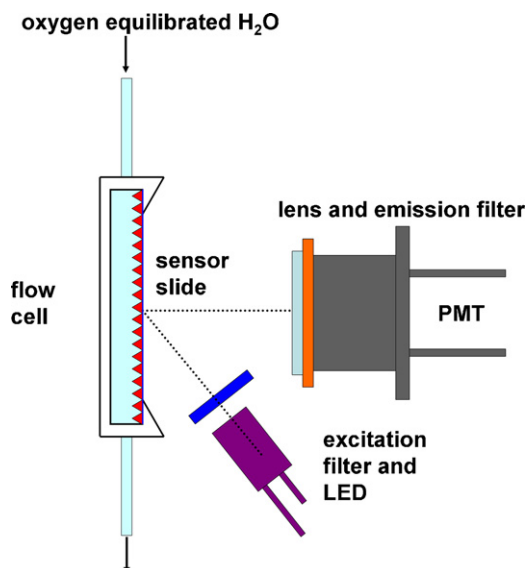


Fig. 1. Scheme of the planar oxygen sensor setup.

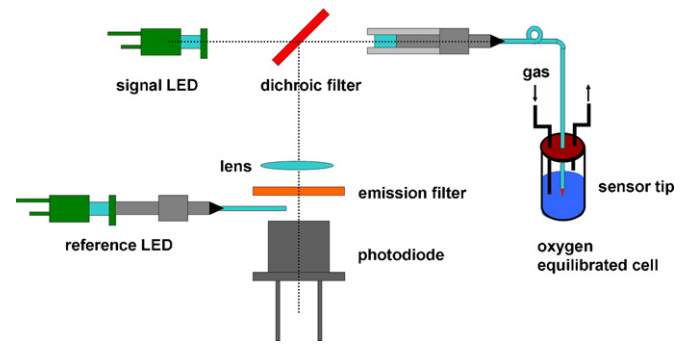


Fig. 2. Scheme of the fiber optic oxygen sensor setup.

used for detection, two filters, RG61 (Unaxis) and Lee135 (Lee) were arranged. A second LED (NSPES90S, Nichia) was used as reference LED in order to eliminate influences on the signal not caused by the analyte (e.g. phase shift of the detection circuitry, drifting of electronic components and detectors with time and temperature, ...).

## 3. Results and discussion

### 3.1. Functionalization of S-layer protein

The S-layer lattice of SbpA used in this study shows square symmetry with a center-to-center spacing of 13.1 nm. The area occupied by one morphological unit is 171.61 nm<sup>2</sup> (Ilk et al., 2002). Recrystallization on the two different substrates, glass slide and tapered optical fiber tips, was confirmed by AFM. Sensor substrates were densely covered by a well ordered, regular pattern of recrystallized S-layer protein SbpA. A scanning force microscopical image of S-layer patterns on the silica core of a declad and tapered optical fiber is shown in Fig. 3.

In order to increase the mechanical stability of the S-layer, the proteins were crosslinked by reaction of glutaraldehyde with the amino groups. After the crosslinking reaction, the protein layer displays free carboxylic groups for further modification. The carboxylic groups had to be activated in order to allow for covalent immobilization of amino-functionalized fluorophores and formation of amide linkages under mild conditions in aqueous media. Activation by the water soluble carbodiimide EDC, one of the most common methods for bioconjugation and protein functionalization, was chosen (Hermanson, 2008). EDC reacts with the free carboxylic acid groups of the protein layer to the rather unstable intermediate O-acrylisourea which allows binding to the amino group of the dye.

Subsequently, the amino functionalized Pt(II)-tetraphenylporphyrine derivative (Pt-TPP-NH<sub>2</sub>) was bound to the activated car-

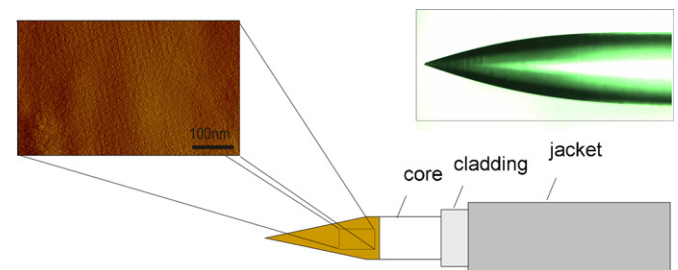
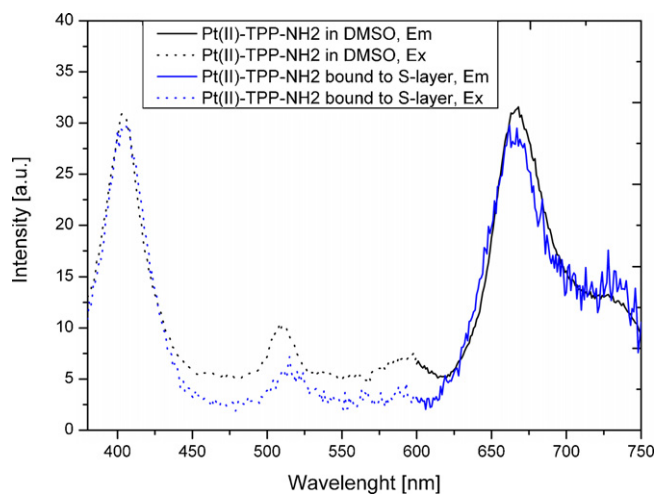


Fig. 3. Scheme of a declad and tapered fiber tip, scanning force microscopic image of S-layer monolayer of protein SbpA from *B. sphaericus* recrystallized into square lattice symmetry on the silica core of the tapered fiber tip (deflection mode, z range = 2 nm) and light microscopic image a tapered fiber tip.



**Fig. 4.** Luminescence emission and excitation spectra of Pt-TPP-NH<sub>2</sub> dye in solution (black) and bound to SbpA S-layer membrane (blue), ( $\lambda_{EX}$  405 nm,  $\lambda_{EM}$  655 nm) (for interpretation of the references to color in this figure legend, the reader is referred to the web version of the article).

boxylic groups. Luminescence excitation and emission spectra of Pt(II)TPP-NH<sub>2</sub> immobilized on the S-layers are shown in Fig. 4. The spectra confirm the successful covalent binding of the dye to the protein layer and that the spectral properties were preserved after immobilization. Excitation maxima at 405 and 510 nm and an emission maximum at 665 nm were found for both, the Pt(II)TPP-NH<sub>2</sub> bound to the protein layer and in aqueous solution.

### 3.2. Oxygen sensing

The well known effect of efficient quenching of Pt(II) metalloporphyrin phosphorescence by molecular oxygen in solution and polymer matrices (Papkovsky, 1995) has also been observed for Pt(II) porphyrins immobilized to S-layer coated surfaces (Kostler et al., 2007). The dependence of luminescence intensity and lifetime of metalloporphyrin complexes on oxygen concentration can be applied in optical sensor systems to determine oxygen concentrations. However, intensity signals are in general strongly influenced by fluctuations in the opto-electronic system (drifts of the light source or photodetector) and leaching or photobleaching of the dye. Lifetime based signals are almost independent of intensity fluctuations of the excitation light and the influence of photobleaching can be dramatically reduced, so most of these interferences can be overcome by measuring the luminescence lifetime (Lakowicz, 2006).

One possibility for luminescence lifetime based measurement in sensors is the so called phase-measurement technique (Trettnak et al., 1996). In this technique the excitation light source is modulated at a certain frequency and the phase shift between excitation light and emitted light is measured. The phase shift can be correlated with the luminescence lifetime via Eq. (1):

$$\tan \Phi = 2\pi\tau f \quad (1)$$

Eq. (1): where  $\Phi$  is the phase shift,  $f$  is the modulation frequency and  $\tau$  is the luminescence lifetime.

S-layers functionalized with metalloporphyrin dyes on planar glass substrates as well as on optical fibers were applied for luminescence lifetime based oxygen sensing systems.

The glass slides coated with dye functionalized S-layers were applied for oxygen sensing in the planar sensor setup. A schematic drawing of the sensor setup can be seen in Fig. 1. Modulation of the excitation light at a frequency of 4.5 kHz allowed for simultaneous luminescence intensity and lifetime based sensing by

analyzing the emission amplitude and phase shift. Oxygen sensing was performed by purging the flow cell with doubly distilled water equilibrated with gas mixtures of different oxygen concentrations (0, 2.1, 4.2, 8.7 mg/L). The phase shifts between the excitation and the luminescence emission and the change in amplitude have been measured cyclically at given oxygen concentrations. An example of such a sensing curve showing the response to different dissolved oxygen concentrations from 0–8.7 mg/L is shown in Fig. 5. Both, amplitude and phase shift decreased with increasing oxygen concentration and the sensor response was found to be fully reversible.

A so called Stern–Volmer plot of the sensor response is shown in Fig. 5. The data could not be fitted with the simple Stern–Volmer equation because they showed a highly nonlinear relationship. Therefore the so called false light model, which is often used to describe the quenching behavior of sensors employing luminophores dissolved in polymeric matrices, was applied to fit the measurement data. This model extends the Stern–Volmer equation with an additional so called false light parameter (Hartmann and Trettnak, 1996), and is described in Eq. (2).

$$\Phi = \Phi_0 \left[ \frac{f_0}{1 + KpO_2} + 1 - f_0 \right] \quad (2)$$

Eq. (2): where  $\Phi$  is the phase shift measured at a certain oxygen concentration  $pO_2$ ,  $\Phi_0$  the phase shift in absence of oxygen,  $K$  is the quenching parameter and  $f_0$  is the false light parameter.

The quenching behavior of the S-layer based oxygen sensor was well fitted by this equation with a coefficient of determination ( $R^2$ ) of 0.99956 (see Fig. 5). This good agreement with the false light model suggests a similar behavior of the S-layer based oxygen sensor and common oxygen sensors based on luminophores immobilized in a polymer matrix. The strong deviation from linearity can for the most part be ascribed to residual excitation light reaching the detector.

The response time  $t_{90}$  (time taken to reach 90% of the steady state signal) for the planar setup measured from 0 mg/L oxygen to 8.7 mg/L oxygen was 3.5 min. The resolution of the sensor system, calculated by the following equation (Eq. (3)), was determined to 0.12 mg/L for air saturated medium and 0.01 mg/L for oxygen free medium.

$$\Delta pO_2 = \frac{|K_{sv}\Phi_0 f_0|}{[K_{sv}\Phi + K_{sv}\Phi_0(f_0 - 1)]^2} 2\sigma_\theta \quad (3)$$

Eq. (3): where  $pO_2$  is the oxygen concentration,  $K_{sv}$  is the Stern–Volmer constant,  $\Phi_0$  the phase shift in absence of oxygen,  $\Phi$  is the phase shift measured at a certain oxygen concentration,  $f_0$  is the false light parameter and  $\sigma_\theta$  is the standard deviation of the phase shift.

In a subsequent development step, a fiber optic sensor system was built using a functionalized S-layer coating. Fiber optic sensor setups offer several well known and quite obvious advantages like flexibility, localized measurement, and miniaturization capability. Additionally, in the case of thin monomolecular fluorescent films, optical fibers allow for improved excitation and collection of fluorescence. If the surface of a declad optical fiber core is coated with a luminophore functionalized S-layer, excitation occurs due to the evanescent field at the fiber surface. This evanescent field excitation minimizes background fluorescence and influence of the sample media. The luminescence emitted from the functionalized S-layer coating efficiently couples back into the fiber core and can be detected at the distal end of the fiber.

For fiber optic sensing of dissolved oxygen, a setup was constructed consisting of an oxygen equilibrated cell, LED light source, reference LED, photodiode and optical filters (see Fig. 2). In contrast to the planar oxygen sensor setup the cell was not rinsed with doubly distilled water, but the doubly distilled water inside the cell was directly equilibrated with different known oxygen concentrations

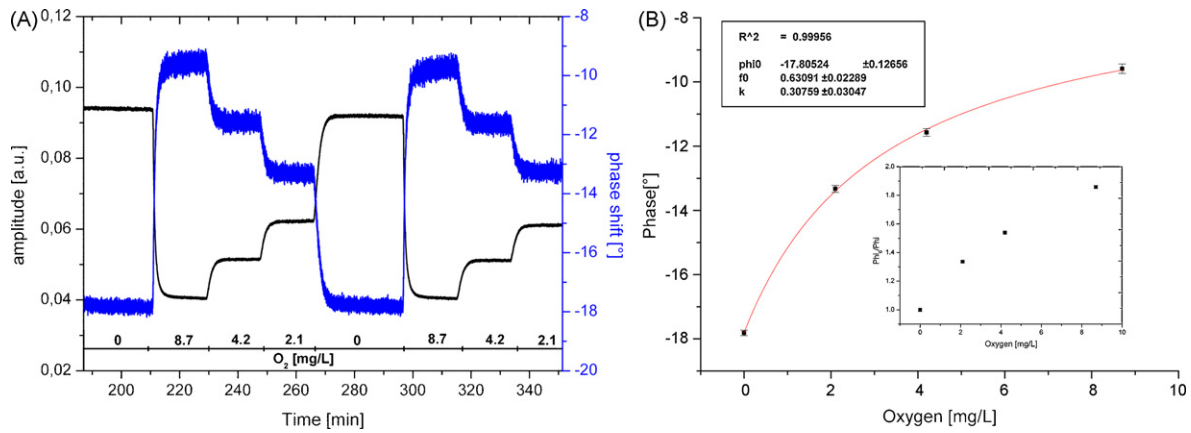


**Fig. 5.** (A) Response curve of S-layer based sensor slide to four different oxygen concentrations (0, 8.7, 4.2, 2.1 mg/L) in water at 25 °C (black: amplitude, blue: phase shift) (B) response curve of sensor slide (black marks, error bars represent standard deviations, relative standard deviations are in the range of 0.2% for oxygen free medium to 0.6% for air saturated medium) and best fit characterization (solid line,  $R^2 = 0.99956$ ) obtained from false light model (Eq. (2)), inset shows Stern–Volmer Plot (for interpretation of the references to color in this figure legend, the reader is referred to the web version of the article).

via gas pipes. For measurement of different oxygen concentrations, tapered optical fibers coated with S-layer proteins and functionalized with Pt(II)-TPP-NH<sub>2</sub> were fixed in the cell. Again modulation of the excitation light at a frequency of 4.5 kHz allows simultaneous intensity and lifetime based sensing analyzing the emission amplitude and phase shift.

Fig. 6 shows a typical example of oxygen sensing with the fiber optic oxygen sensor setup. Amplitude and phase shift decreased with increasing oxygen concentration. Analysis of the response curve showed that there is a clear response to given oxygen concentrations (0, 2.1, 4.2, 8.7 mg/L), both in amplitude change and in phase shift, respectively.

The response of the fiber optic oxygen sensor system was also fitted with the false light model and showed a  $R^2$  0.99914 (see Fig. 6). The response time  $t_{90}$  for the fiber optic setup from 0 to 2.1 mg/L was 1.4 min. The resolution of the fiber optic sensor system, calculated by the Eq. (3), was determined to 0.16 mg/L for air saturated medium and 0.01 mg/L for oxygen free medium.

The quenching efficiency (expressed as the ratio of signal under nitrogen and air) was 1.9 and 1.5 in the planar and the fiber optic setup, respectively, underlining the very good response of the sensor systems to oxygen. The typical quenching efficiencies of other optical oxygen sensor systems like platinum porphyrins or ruthenium chelates incorporated into polymers like polystyrene,

ethylcellulose or silicones are also in the range of 1.8–2.4 (Wolfbeis, 2005). Platinum porphyrins covalently bound to proteins or antibodies in homogeneous solution show a quenching efficiency between 1.5 and 12 (De Haas et al., 1997) which correlates very well to the quenching efficiencies determined in this study.

The difference in response time between the planar and the fiber optic setup is most probably due to two different reasons – first, the response time for the planar setup was measured between 0 and 8.7 mg/L and for the fiber optic sensor between 0 to 2.1 mg/L. Second, in the planar setup the measurement cell was rinsed with doubly distilled water which was pumped in a closed loop and equilibrated with oxygen in a separate vessel. In the fiber optic setup, the doubly distilled water was directly equilibrated with oxygen in the measurement cell, which leads to a faster change in oxygen concentration. Furthermore, the volume of doubly distilled water was smaller than in the planar setup, so equilibration could take place faster.

The different absolute phase shift values in the two sensor setups can be explained by the different detection systems. In the planar setup, a photo multiplier tube was used for detection and direct measurement without reference was performed. In the fiber optic setup, a reference LED was used. The phase shift from the reference LED was subtracted from the signal phase shift. The resulting phase shift is shown in Fig. 6.

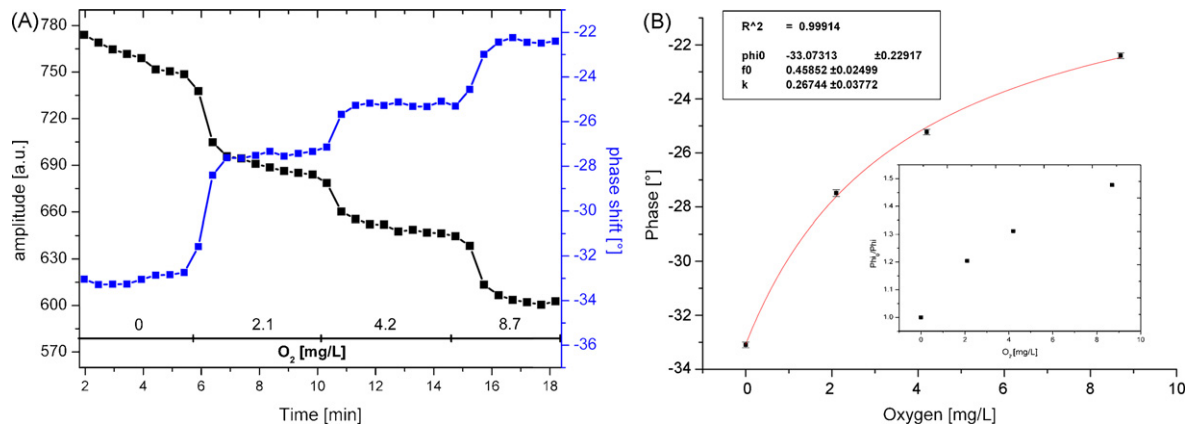


**Fig. 6.** (A) Response curve of S-layer based fiber tip sensor to four different oxygen concentrations (0, 2.1, 4.2, 8.7 mg/L) in water at 25 °C (black: amplitude, blue: phase shift) (B) response curve of sensor slide (black marks, error bars represent standard deviations, relative standard deviations are in the range of 0.3% for oxygen free medium to 0.5% for air saturated medium) and best fit characterization (solid line,  $R^2 = 0.99914$ ) obtained from false light model (Eq. (2)), inset shows Stern–Volmer Plot (for interpretation of the references to color in this figure legend, the reader is referred to the web version of the article).

In the planar oxygen sensor setup a photomultiplier tube for detection was necessary due to the low concentration of fluorophores. As there is only a monolayer of the protein matrix on which the fluorophore was immobilized, statistically there is one binding site every square-nanometer, leading to this low concentration of fluorophores (Weigert and Sara, 1995). In contrast to the planar setup, in the fiber optic setup a less sensitive, cheap Si-photodiode could be used as detector. The difference in detection sensitivity between the planar and fiber optic setup can be explained by efficient evanescent field excitation and the anisotropic emission of fluorophores directly on the dielectric waveguide surfaces. Fluorophores which are in close proximity to the interface between two dielectric media (like glass and water) emit a large portion of the radiation into the higher refractive index substrate (Enderlein et al., 1999; Ruckstuhl et al., 2003). In the fiber optic setup a large portion of the emission coupled back into the fiber core is guided to the detector, whereas in the case of the planar sensor setup only the minor part which is emitted perpendicular to the substrate at the water side is available for detection. Nevertheless, high light intensities at the fiber surface led to considerable photobleaching of the fluorophore. Fig. 6 shows the response of the fiber optic sensor to different oxygen concentrations during one measurement cycle. Within this cycle there is already a drift in amplitude due to bleaching. Measurements of luminescence lifetime or phase shift are less affected by photobleaching and are therefore preferentially used in this kind of sensors. To improve the fiber optic setup, best compromise between excitation intensity, signal intensity and bleaching has to be found.

#### 4. Conclusion

The principle of using S-layer proteins as matrix for covalent immobilization of fluorophores and construction of optical sensors was demonstrated with an example of a luminescence lifetime based oxygen sensor. S-layer proteins were shown to be capable of forming monolayer coatings on optical fiber surfaces allowing evanescent field fluorescence excitation of the bound fluorophores. Even for these monolayer coatings a phase fluorimetric oxygen sensor setup employing low cost optoelectronic components like LEDs and silicon photodiodes could be demonstrated.

The use of S-layer proteins is an interesting alternative to more conventional immobilization methods (such as silane or thiol monolayers) used for the construction of biosensors. In contrast to other immobilization methods, S-layer proteins such as SbpA used in this study, form well ordered, nanostructured, and dense layers on a broad range of surfaces used for optical sensors (e.g. glass, silicon, gold, many polymers and polyelectrolyte layers) (Handrea et al., 2003; Toca-Herrera et al., 2005). Furthermore, it is known that S-layer coatings are characterized by very good biocompatibility and pronounced non-fouling properties (Messner et al., 1984) what probably makes them especially valuable for sensing applications in complex biological fluids or implantable sensors.

The general principle for the construction of optical sensors by immobilization of fluorophores on monomolecular S-layer protein coatings can be applied to the sensing of several different analytes by immobilization of different dyes and/or receptors.

#### Acknowledgements

Financial support by the Austrian Nanoinitiative under the project SLAYSSENS within the project cluster ISOTEC is gratefully acknowledged.

#### References

- Breitwieser, A., Kupcu, S., Howorka, S., Weigert, S., Langer, C., Hoffmann-Sommergruber, K., Scheiner, O., Sleytr, U.B., Sara, M., 1996. *Biotechnology* 21, 918–925.
- Cajlakovic, M., Bizzarri, A., Suppan, M., Konrad, C., Ribitsch, V., 2009. *Sens. Actuators B Chem.* 139, 181–186.
- Chaki, N.K., Vijayamohan, K., 2002. *Biosens. Bioelectron.* 17, 1–12.
- De Haas, R.R., Van Gijlswijk, R.P., Van Der Tol, E.B., Zijlmans, H.J., Bakker-Schut, T., Bonnet, J., Verwoerd, N.P., Tanke, H.J., 1997. *J. Histochem. Cytochem.* 45, 1279–1292.
- Enderlein, J., Ruckstuhl, T., Seeger, S., 1999. *Appl. Optics* 38, 724–732.
- Ford, L.A., Thune, R.L., 1992. *Biomed. Lett.* 47, 355–362.
- Gyrovary, E., Schroedter, A., Talapin, D.V., Weller, H., Pum, D., Sleytr, U.B., 2004. *J. Nanosci. Nanotechnol.* 4, 115–120.
- Handrea, M., Sahre, M., Neubauer, A., Sleytr, U.B., Kautek, W., 2003. *Bioelectrochemistry* 61, 1–8.
- Hartmann, P., Trettnak, W., 1996. *Anal. Chem.* 68, 2615–2620.
- Hermanson, G.T., 2008. *Bioconjugate Techniques*, Second ed. Academic Press, Rockford.
- Ilk, N., Vollenkle, C., Egelseer, E.M., Breitwieser, A., Sleytr, U.B., Sara, M., 2002. *Appl. Environ. Microbiol.* 68, 3251–3260.
- Jiang, J.J., Gao, L., Zhong, W., Meng, S., Yong, B., Song, Y.L., Wang, X.D., Bai, C.X., 2008. *Respir. Physiol. Neurobiol.* 161, 160–166.
- Kostler, S., Konrad, C., Suppan, M., Bizzarri, A., Scheicher, S., Ribitsch, V., Kainz, B., Pum, D., Sleytr, U.B., 2007. *IEEE Sensors* 28–31 October 2007, pp. 600–603.
- Lakowicz, J.R., 2006. *Principles of Fluorescence Spectroscopy*, Third ed. Springer Science and Business Media, Baltimore.
- Messner, P., Hollaus, F., Sleytr, U.B., 1984. *Int. J. Syst. Bacteriol.* 34, 202–210.
- Messner, P., Pum, D., Sara, M., Stetter, K., Sleytr, U.B., 1986. *Ultrastructure of the cell envelope of the archaeobacteria Thermoproteus tenax and Thermoproteus neutrophilus*. *J. Bacteriol.* 166, 1046–1054.
- Neubauer, A., Pum, D., Sleytr, U.B., 1993. *Anal. Lett.* 26, 1347–1360.
- Neubauer, A., Pum, D., Sleytr, U.B., Klimant, I., Wolfbeis, O.S., 1996. *Biosens. Bioelectron.* 11, 317–325.
- Papkovsky, D.B., 1995. *Sens. Actuators B Chem.* 29, 213–218.
- Papkovsky, D.B., O'riordan, T.C., 2005. *J. Fluoresc.* 15, 569–584.
- Ruckstuhl, T., Rankl, M., Seeger, S., 2003. *Biosens. Bioelectron.* 18, 1193–1199.
- Sara, M., Sleytr, U.B., 1987. *J. Membr. Sci.* 33, 27–49.
- Sleytr, U.B., Beveridge, T.J., 1999. *Trends Microbiol.* 7, 253–260.
- Sleytr, U.B., Egelseer, E.M., Ilk, N., Pum, D., Schuster, B., 2007a. *FEBS J.* 274, 323–334.
- Sleytr, U.B., Huber, C., Ilk, N., Pum, D., Schuster, B., Egelseer, E.M., 2007b. *FEMS Microbiol. Lett.* 267, 131–144.
- Sleytr, U.B., Sara, M., Kupcu, Z., Messner, P., 1986. *Arch. Microbiol.* 146, 19–24.
- Soper, S.A., Hashimoto, M., Situma, C., Murphy, M.C., Mccarley, R.L., Cheng, Y.-W., Barany, F., 2005. *Methods* 37, 103–113.
- Stockle, R., Fokas, C., Deckert, V., Zenobi, R., Sick, B., Hecht, B., Wild, U.P., 1999. *Appl. Phys. Lett.* 75, 160–162.
- Toca-Herrera, J.L., Krastev, R., Bosio, V., Kupcu, S., Pum, D., Fery, A., Sara, M., Sleytr, U.B., 2005. *Small* 1, 339–348.
- Trettnak, W., Kolle, C., Reininger, F., Dolezal, C., O'leary, P., 1996. *Sens. Actuators B Chem.* 36, 506–512.
- Vollenkle, C., Weigert, S., Ilk, N., Egelseer, E., Weber, V., Loth, F., Falkenhagen, D., Sleytr, U.B., Sara, M., 2004. *Appl. Environ. Microbiol.* 70, 1514–1521.
- Weigert, S., Sara, M., 1995. *J. Membr. Sci.* 106, 147–159.
- Weigert, S., Sara, M., 1996. *J. Membr. Sci.* 121, 185–196.
- Wolfbeis, O.S., 1991. *Fiber Optic Chemical Sensors and Biosensors*, first ed. CRC Press.
- Wolfbeis, O.S., 2005. *J. Mater. Chem.* 15, 2657–2669.
- Zammatteo, N., Jeanmart, L., Hamels, S., Courtois, S., Louette, P., Hevesi, L., Remacle, J., 2000. *Anal. Biochem.* 280, 143–150.



Contents lists available at ScienceDirect

Carbohydrate Research

journal homepage: [www.elsevier.com/locate/carres](http://www.elsevier.com/locate/carres)

## Cell surface display of chimeric glycoproteins via the S-layer of *Paenibacillus alvei*

Kristof Zarschler <sup>†</sup>, Bettina Janesch, Birgit Kainz, Robin Ristl, Paul Messner <sup>\*</sup>, Christina Schäffer <sup>\*</sup>

Department für NanoBiotechnologie, Vienna Institute of BioTechnology, Universität für Bodenkultur Wien, Muthgasse 11, A-1190 Vienna, Austria

### ARTICLE INFO

#### Article history:

Received 18 December 2009  
Received in revised form 1 April 2010  
Accepted 11 April 2010  
Available online xxx

#### Keywords:

Cell surface display  
S-layer  
Nanopatterning  
Secondary cell wall polymer biosynthesis  
*Paenibacillus alvei*

### ABSTRACT

The Gram-positive, mesophilic bacterium *Paenibacillus alvei* CCM 2051<sup>T</sup> possesses a two-dimensional crystalline protein surface layer (S-layer) with oblique lattice symmetry composed of a single type of O-glycoprotein species. Herein, we describe a strategy for nanopatterned in vivo cell surface co-display of peptide and glycan epitopes based on this S-layer glycoprotein self-assembly system. The open reading frame of the corresponding structural gene *spaA* codes for a protein of 983 amino acids, including a signal peptide of 24 amino acids. The mature S-layer protein has a theoretical molecular mass of 105.95 kDa and a calculated pI of 5.83. It contains three S-layer homology domains at the N-terminus that are involved in anchoring of the glycoprotein via a non-classical, pyruvylated secondary cell wall polymer to the peptidoglycan layer of the cell wall. For this polymer, several putative biosynthesis enzymes were identified upstream of the *spaA* gene. For in vivo cell surface display, the hexahistidine tag and the enhanced green fluorescent protein, respectively, were translationally fused to the C-terminus of SpaA. Immunoblot analysis, immunofluorescence staining, and fluorescence microscopy revealed that the fused epitopes were efficiently expressed and successfully displayed via the S-layer glycoprotein matrix on the surface of *P. alvei* CCM 2051<sup>T</sup> cells. In contrast, exclusively non-glycosylated chimeric SpaA proteins were displayed, when the S-layer of the glycosylation-deficient *wsfP* mutant was used as a display matrix.

© 2010 Elsevier Ltd. All rights reserved.

### 1. Introduction

The presentation of heterologous proteins or peptide epitopes on various cell surfaces by genetic engineering has become an intensely used strategy for a wide range of biotechnological applications, including live vaccine development and delivery,<sup>1</sup> antibody production,<sup>2</sup> peptide library screening,<sup>3</sup> whole-cell biocatalysis,<sup>4</sup> and bioremediation.<sup>5,6</sup> So far, numerous display systems have been studied for both bacteria and yeast.<sup>7–12</sup>

Outer membrane proteins, lipoproteins, autotransporters, ice nucleation proteins, flagellae, and fimbriae are the most common anchoring motifs of Gram-negative surface display systems, whereas for Gram-positive bacteria, staphylococcal protein A and different S-layer proteins, such as RsaA of *Caulobacter crescentus* and EA1/Sap of *Bacillus anthracis* have been utilized.<sup>9,13–19</sup> S-Layers, in general, are among the most frequently observed outermost cell surface structures of bacteria. They are composed of individual protein or glycoprotein species, which have the unique feature of self-assembling into a closed two-dimensional crystalline array

with nanometer-scaled periodicity. Thus, this matrix is ideally suited for cell surface display approaches, where strict control over position and orientation of functional epitopes or molecules is desired.<sup>20</sup> For *C. crescentus*, the insertion of a protein G IgG-binding domain into certain sites of full length S-layer protein RsaA resulted in functional, immunoreactive surface display at very high density.<sup>21</sup> For *B. anthracis*, targeting of active levansucrase of *Bacillus subtilis* and immunogenic tetanus toxin fragment C of *Clostridium tetani* to the cell surface was achieved by translational fusion of the target proteins to the three S-layer homology (SLH) domains of EA1 and Sap, respectively.<sup>15,17</sup>

Amino- and carboxy-terminal SLH domains of an approximately 55 amino acid-long sequence motif, each, have been identified in several S-layer proteins, in many cell wall-bound exoenzymes, and in outer membrane proteins.<sup>22</sup> Although the overall sequence similarity of SLH domains is rather low, a highly conserved TRAE motif has been identified to play a key role for the binding function of SLH domains.<sup>23</sup> In the case of S-layer (glyco)proteins, it has been shown that these anchoring modules do not directly bind to peptidoglycan, but to a non-classical secondary cell wall polymer (SCWP)<sup>24–28</sup> carrying either pyruvate or carboxyl group-containing modifications. In *B. anthracis* and *Thermus thermophilus*, pyruvylation of SCWPs was shown to be dependent on the presence and activity of the polysaccharide pyruvyltransferase CsaB.<sup>24,26</sup> Further, in different *Bacillus* strains, a perfect correlation between the

<sup>\*</sup> Corresponding authors. Tel.: +43 1 47654x2203; fax: +43 1 4789112 (C.S.).

E-mail addresses: [paul.messner@boku.ac.at](mailto:paul.messner@boku.ac.at) (P. Messner), [christina.schaeffer@boku.ac.at](mailto:christina.schaeffer@boku.ac.at) (C. Schäffer).

<sup>†</sup> Present address: Institute of Genetics, General Genetics, Technische Universität Dresden, Zellescher Weg 20b, D-01217 Dresden, Germany.

occurrence of CsaB homologues and the presence of SLH domains exists, leading to the conclusion that the interaction between pyruvylated SCWP and SLH domains is widespread in bacteria and has been conserved during evolution.<sup>24,26</sup>

In the present study, we lay the groundwork for the development of a peptide/protein and glycan cell surface co-display system based on the glycosylated S-layer protein SpaA of *Paenibacillus alvei* CCM 2051<sup>T</sup>. This is a very timely approach, since, due to the complexity of their biosynthesis, glycans have escaped cell surface display approaches, so far. *P. alvei* CCM 2051<sup>T</sup> is a mesophilic, Gram-positive bacterium that is covered with an oblique S-layer nanolattice. The S-layer proteins are naturally O-glycosylated, exposing long-chain saccharides with the structure [ $\alpha$ -D-Galp-(1 $\rightarrow$ 3)- $\beta$ -D-Galp-(1 $\rightarrow$ 4)- $\beta$ -D-ManpNAc-(1 $\rightarrow$ )<sub>n ~ 23</sub>]-[GroA-2 $\rightarrow$ OPO<sub>2</sub> $\rightarrow$ 4- $\beta$ -D-ManpNAc-(1 $\rightarrow$ 4)]-[3]- $\alpha$ -L-Rhap-(1 $\rightarrow$ )<sub>n = 3</sub>]- $\beta$ -D-Galp-(1 $\rightarrow$ O)-Tyr to the environment.<sup>29</sup> This glyco-nanolattice is anchored to the bacterial cell wall via a pyruvate-containing SCWP with the structure [(Pyr4,6)- $\beta$ -D-ManpNAc-(1 $\rightarrow$ 4)- $\beta$ -D-GlcpNAc-(1 $\rightarrow$ 3)]<sub>n ~ 11</sub>-(Pyr4,6)- $\beta$ -D-ManpNAc-(1 $\rightarrow$ 4)- $\alpha$ -D-GlcpNAc-(1 $\rightarrow$ ). These pyruvate-containing and, hence, overall anionic glycan chains are linked via phosphate-containing groups to muramic acid residues of the peptidoglycan layer.<sup>30</sup>

We describe herein (i) the identification of the *spaA* gene coding for the S-layer protein of *P. alvei* CCM 2051<sup>T</sup>, (ii) its utilization as an in vivo surface co-display system, and (iii) the identification of several open reading frames in the upstream region of *spaA* coding for enzymes putatively involved in the biosynthesis of the native cell wall anchor of the S-layer nanolattice, which is the pyruvylated SCWP.

For proof of concept, full-length SpaA was expressed with a carboxy-terminal hexahistidine tag and with enhanced green fluorescent protein as a fusion partner, respectively. Either chimeric protein was shown to be displayed on the cell surface and glycosylated by the native glycosylation machinery of *P. alvei* CCM 2051<sup>T</sup>. To our knowledge, this is the first report on the co-display of a fused functional epitope and an O-glycosidically linked glycan on a bacterial cell surface in a nanolattice-like fashion. This strategy is opening up new avenues for controlled high-density co-display of protein- and carbohydrate-mediated biological functions with defined orientation and with nanometer-scaled precision. This approach ideally mimics, especially for the glycan-mediated functions, the naturally occurring clustering effect. When the S-layer glycosylation-deficient *wsfP* mutant was used for cell surface display, exclusively non-glycosylated chimeric SpaA proteins were obtained.<sup>31</sup>

## 2. Results

### 2.1. General description of the organism

The cell surface of the type culture strain *P. alvei* CCM 2051<sup>T</sup> (ATCC 6344; DSM 29) is completely covered with an oblique S-layer lattice composed of identical O-glycoprotein species. Various aspects of its crystalline S-layer including ultrastructural characterization,<sup>32,33</sup> glycosylation analysis,<sup>29,33</sup> and glycan biosynthesis<sup>34</sup> have been investigated in the past. In SDS-PAGE, the S-layer glycoprotein is separated into three bands with apparent molecular masses of approximately 105, 160, and 240 kDa, respectively. The two high molecular mass bands give a positive PAS staining reaction, corresponding to mono- and di-glycosylated S-layer proteins.<sup>31</sup>

### 2.2. Isolation and molecular characterization of *spaA*

After chemical deglycosylation of the S-layer glycoprotein, Edman degradation revealed the N-terminus of the mature protein to have the amino acid sequence ADAAKTTQEK. Based on this information, the degenerate oligonucleotide primer proof\_wSpa-

for was designed by in silico reverse translation. Identification of the entire *spaA* gene was accomplished using a gene walking approach, starting with the primer specific for the N-terminus of *spaA*. The sequence was deposited at GenBank under the accession number FJ751775. The *spaA* gene revealed one ORF extending 2952 nt, encoding a putative protein of 983 amino acids with a calculated molecular mass of 108.55 kDa. The ORF starts with an ATG at nucleotide position 1, preceded by a typical ribosomal binding site (Shine-Delgarno sequence) 19 nt upstream of the start codon and a putative promoter region comprising a -10 sequence (TTGTATAAT) located 232 nt upstream of the translation start and a putative -35 sequence (TTTACG) starting 252 nt in front of the start codon. 7 nt downstream of the TAA stop codon, a putative  $\rho$ -independent transcriptional termination signal was identified. The terminator consists of a palindromic stem loop sequence of 39 nt with a perfect stem of 13 nt. The average G+C content of the whole *spaA* gene was calculated to be 38.6%.

### 2.3. Description of the S-layer protein SpaA

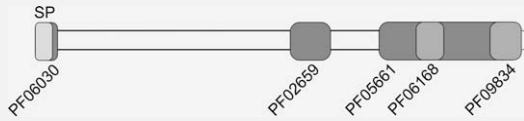
The amino acid sequence ADAAKTTQEK obtained by amino-terminal sequencing of chemically deglycosylated, mature SpaA was identified at positions 25–34 of the *spaA* gene product, indicating that the first 24 amino acids of SpaA constitute a signal sequence, which is cleaved at the Gly-Ala motif during biosynthetic protein processing. The overall amino acid composition of mature SpaA is within the typical data reported for S-layer proteins of Gram-positive bacteria,<sup>35</sup> exhibiting a high content of hydrophobic and acidic amino acids and lacking cysteine. Mature SpaA has a calculated theoretical molecular mass of 105.95 kDa and a pI of 5.83. A conserved motif search revealed the presence of three SLH domains (PF00395) at the amino-terminal region of the S-layer protein; these comprise the amino acid stretches aa 25–65, aa 82–129, and aa 140–181, respectively (Table 1). The comparison of the three SLH domains with the SLH domain profile is depicted in Figure 1.

A homology search using the BLASTP program showed that the amino acid sequence of SpaA shows moderate identities with other surface exposed proteins of different *Bacillaceae*. A phylogenetic tree was constructed by pairwise alignment of SpaA with the first 100 proteins of this BLAST search (Fig. 2). The rooted tree shows that SpaA is closely related to S-layer domain proteins of *Paenibacillus* sp. JDR-2 and *Geobacillus* sp. Y412MC10 as well as to an S-layer domain-containing protein of *Paenibacillus* sp. oral taxon 786 strain D14. A rather distant relationship could be observed between SpaA and several cell surface proteins of different clostridia. The global identity and similarity values of SpaA compared with other well-characterized S-layer proteins are summarized in Table 2. Considering these data, it is obvious that regions of high homology are neither present in the N-termini, responsible for binding of the S-layer protein to the cell wall, nor in the residual amino acid sequence. This corroborates the general concept of low primary sequence similarity of S-layer proteins, even of those of phylogenetically closely related bacteria.<sup>36</sup>

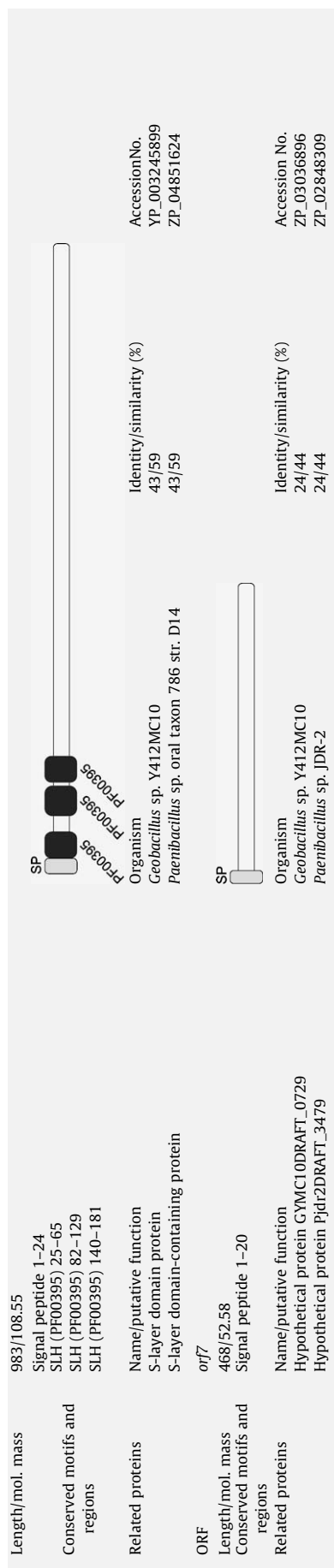
### 2.4. Description of the SCWP biosynthesis locus

Upstream and downstream of the *spaA* gene, several genes were identified, which are most likely involved in the SCWP biosynthesis of *P. alvei* CCM 2051<sup>T</sup> (Fig. 3). By in silico analysis using the *Escherichia coli*  $\sigma^{70}$  promoter consensus sequence, putative promoter sites located upstream of *orf1*, *tagO*, *slhA*, *spaA*, and *orf7* were recognized. In addition to the  $\rho$ -independent bacterial terminator downstream of *spaA*, a single terminator was identified downstream of the *slhA* gene. The prediction of transcription units for the complete ~14-kb DNA fragment resulted in a polycistronic

**Table 1**  
 Predicted gene products encoded by the SCWP biosynthesis locus of *P. alvei* CCM 2051<sup>T</sup> and S-layer protein structural gene *spaA* together with database homologies

ORF	<i>orf1</i>			
Length/mol. mass	657/73.18			
Conserved motifs and regions	Signal peptide 1–23 DUF916 (PF06030) 1–30 DUF204 (PF02659) 341–395 DUF808 (PF05661) 460–641 DUF981 (PF06168) 521–558 DUF2061 (PF09834) 608–650			
Related proteins	Name/putative function Hypothetical protein GYMC10DRAFT_1551 Hypothetical protein Pjdr2DRAFT_3486	Organism <i>Geobacillus</i> sp. Y412MC10 <i>Paenibacillus</i> sp. JDR-2	Identity/similarity (%) 52/72 48/66	Accession No. ZP_03037718 ZP_02848379
ORF	<i>csaB</i>			
Length/mol. mass	396/43.59			
Conserved motifs and regions	PS_pyruv_trans (PF04230) 7–357			
Related proteins	Name/putative function Polysaccharide pyruvyl transferase CsaB protein	Organism <i>Geobacillus</i> sp. Y412MC10 <i>Bacillus anthracis</i> strain Ames	Identity/similarity (%) 49/64 37/56	Accession No. ZP_03037717 NP_843396
ORF	<i>tagA</i>			
Length/mol. mass	252/28.69			
Conserved motifs and regions	Glyco_tran_WecB (PF03808) 60–231			
Related proteins	Name/putative function Glycosyl transferase, WecB/TagA/CpsF family N-Acetylglucosaminylidiphosphoundecaprenol N-acetyl-β-D-mannosaminyltransferase	Organism <i>Paenibacillus</i> sp. JDR-2 <i>Bacillus cereus</i> ATCC 14579	Identity/similarity (%) 62/79 45/65	Accession No. ZP_02848377 NP_835080
ORF	<i>tagO</i>			
Length/mol. mass	377/40.47			
Conserved motifs and regions	Signal peptide 1–33 Glycos_transf_4 (PF00953) 84–247			
Related proteins	Name/putative function TagO protein Undecaprenyl-phosphate N-acetylglucosaminyl 1-phosphate transferase	Organism <i>Bacillus megaterium</i> DSM319 <i>Lysinibacillus sphaericus</i> C3–41	Identity/similarity (%) 53/72 52/72	Accession No. CAL44583 YP_001696879
ORF	<i>slhA</i>			
Length/mol. mass	1335/148.46			
Conserved motifs and regions	Signal peptide 1–31 Galactose-binding domain-like (CBM6) 91–200 Big_3 (PF07523) 493–513 SLH (PF00395) 1125–1169 SLH (PF00395) 1198–1242 SLH (PF00395) 1267–1319			
Related proteins	Name/putative function S-layer domain protein Hypothetical protein BBR47_54190	Organism <i>Paenibacillus</i> sp. JDR-2 <i>Brevibacillus brevis</i> NBRC 100599	Identity/similarity (%) 49/63 46/61	Accession No. ZP_02848374 YP_002774900
ORF	<i>spaA</i>			

(continued on next page)



RNA containing *orf1*, *csaB*, and *tagA* in addition to four separate monocistronic RNAs for *tagO*, *slhA*, *spaA*, and *orf7*. The putative gene products of the SCWP biosynthesis locus have been analyzed by extensive database comparison and are discussed in the order of their appearance within the analyzed region.

#### 2.4.1. *orf1*

The gene product of *orf1* contains eight potential transmembrane domains at its carboxy-terminal part and several domains of unknown functions (DUFs) also found in putative bacterial cell surface and hypothetical transmembrane proteins. The signal peptide of 23 amino acids is followed by a 340 amino acid-containing loop potentially facing the cell exterior. The Conserved Domain Finder (National Center for Biotechnology Information) found a weak similarity to the sublancin ABC transporter SunT of *B. subtilis* 168, suggesting that this protein might act as an exporter<sup>37</sup> like CsaA in the biosynthesis of other pyruvylated SCWPs.<sup>24,26</sup>

#### 2.4.2. *csaB*

Throughout the whole gene *csaB* is highly homologous to genes coding for pyruvyltransferases (CsaB) in various *Bacillus* strains, with the translation product containing a polysaccharide pyruvyltransferase domain. In *B. anthracis* and *T. thermophilus*, CsaB is involved in the addition of pyruvyl groups to the SCWP, a frequently necessary reaction for anchoring of cell wall associated proteins containing SLH domains.<sup>24–27</sup> The presence of a pyruvate-containing SCWP in *P. alvei* CCM 2051<sup>T</sup> suggests that CsaB is responsible for SCWP-pyruvylation in this organism.<sup>30</sup>

#### 2.4.3. *tagA* and *tagO*

The deduced 252- and 377-amino acid proteins encoded by *tagA* and *tagO* reveal high similarity to the glycosyltransferases TagA and TagO of different *Bacillaceae*, respectively. In *B. subtilis*, both enzymes are involved in the biosynthesis of teichoic acids, where TagO couples *N*-acetylglucosamine (GlcNAc) to the membrane-embedded lipid undecaprenylpyrophosphate and TagA catalyzes the addition of *N*-acetylmannosamine (ManNAc) to produce the lipid-linked GlcNAc-ManNAc disaccharide.<sup>38,39</sup> Since a ManNAc-GlcNAc backbone disaccharide motif is found in the SCWP of *P. alvei* CCM 2051<sup>T</sup>, it is conceivable that both enzymes are involved in the biosynthesis of this cell wall polysaccharide.<sup>29,38</sup>

#### 2.4.4. *slhA*

The *slhA* gene product contains three carboxy-terminal SLH domains and is similar to SLH domain-containing proteins of various Gram-positive bacteria. In the central part of the putative protein, a bacterial Ig-like domain found in a variety of bacterial surface proteins is identified.<sup>40</sup> A galactose-binding domain (CBM6) typical for proteins binding to specific ligands, such as cell-surface-attached carbohydrate substrates, was detected in the amino-terminal part. This observation leads to the suggestion that SlhA might be a cell surface-anchored exoenzyme or a receptor.

#### 2.4.5. *orf7*

No homology was found for this incomplete ORF or its putative protein product.

### 2.5. Expression and display of chimeric SpaA constructs on the cell surface

The expression of the hexahistidine tagged S-layer protein SpaA\_6HIS and the chimeric fusion protein SpaA\_EGFP in *P. alvei* CCM 2051<sup>T</sup> wild-type and in *wsfP*::LLtrB mutant cells, respectively, was performed constitutively from the vector pEXALV and confirmed by immunoblot analysis of whole-cell lysates using anti-His-tag and anti-GFP antibody, respectively (Fig. 4A and B).



**Figure 1.** Comparison of the three SLH domains of SpaA with the S-layer homology (SLH) domain profile (PROSITE No.: PS51272). The amino-terminal region starting with the first amino acid of the mature protein (aa 25) is aligned with the PROSITE sequence logo. The total height of an amino acid position depends on the degree of conservation in the corresponding multiple sequence alignment and the height of each letter is proportional to the observed frequency of the particular amino acid.

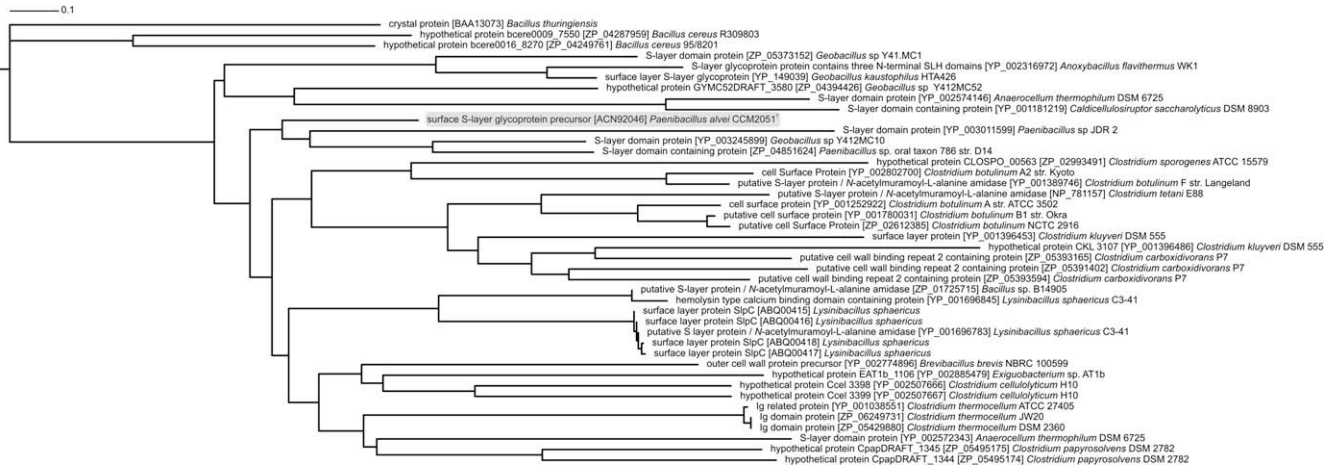


**Figure 2.** Phylogenetic tree of the S-layer protein SpaA of *P. alvei* CCM 2051<sup>T</sup> and its closest relatives. The calculation was done with the Blast Tree View Widget using the Neighbor Joining method.

In either case, three bands, most possibly corresponding to the non-glycosylated, mono-glycosylated, and di-glycosylated forms<sup>31</sup> of SpaA\_6HIS and SpaA\_EGFP were detected when *P. alvei* CCM 2051<sup>T</sup> carrying either pEXALV\_SP\_SpaA\_6HIS or pEXALV\_SP\_SpaA\_EGFP, respectively, was used as an expression host, while no such proteins were detected with *P. alvei* CCM 2051<sup>T</sup> carrying the parental plasmid pEXALV (data not shown). Since the transfer of the completed glycan chain to the S-layer protein is predicted to occur either co-secretionally or on the external face of the cytoplasmic membrane,<sup>41</sup> these results indicate that SpaA\_6HIS and SpaA\_EGFP are correctly expressed and targeted to the cell surface of *P. alvei* CCM 2051<sup>T</sup>. For *P. alvei* CCM 2051<sup>T</sup> *wspP::Li.LtrB* mutant cells, which are, due to the deletion in the initiation enzyme of S-layer glycan biosynthesis, of a glycan-deficient phenotype, only a single band corresponding to non-glycosylated SpaA\_6HIS and SpaA\_EGFP was detected (Fig. 4). Semi-quantitation of the amount of produced recombinant S-layer fusion proteins was performed from Western blots developed with fluorescence-labeled antibodies using the Li-Cor Odyssey Application software. Comparing the expression levels of the recombinant non-glycosylated chimera from *P. alvei* CCM 2051<sup>T</sup> *wspP::Li.LtrB* mutant cells with that of the corresponding chimera produced in glycosylation-competent *P. alvei* CCM 2051<sup>T</sup> cells revealed equal amounts of S-layer fusion proteins, regardless of the glycosylation status. This was inferred from the combined intensities of the non-, mono-, and di-glycosylated bands (Fig. 4A and B, lane 1) being identical to that of the single band originating from the glycosylation-deficient mutant (Fig. 4A and B, lane 2). This indicates that the developed system is well suited for peptide/protein and glycan co-display.

To confirm the surface localization of the chimeric S-layer proteins, immunofluorescence microscopy was used (Fig. 5). For

SpaA\_6HIS, *P. alvei* CCM 2051<sup>T</sup> wild-type cells were probed and fluorescently stained with the penta-His Alexa Fluor 555 conjugate. Cells harboring pEXALV\_SP\_SpaA\_6HIS were brightly fluorescent, indicating that SpaA\_6HIS was successfully displayed on the surface (Fig. 5C). Surface display of SpaA\_EGFP was confirmed by direct fluorescence microscopy (Fig. 5D). *P. alvei* CCM 2051<sup>T</sup> wild-type and *wspP::Li.LtrB* mutant cells (not shown) showed identical results in immunofluorescence microscopy, whereas cells carrying the parental plasmid pEXALV were not stained at all (Fig. 5A and B).

These results show the proper and efficient display of SpaA\_6HIS and SpaA\_EGFP on the cell surface of *P. alvei* CCM 2051<sup>T</sup> simultaneously with the native S-layer glycans while maintaining the S-layer inherent feature of a dynamically closed two-dimensional nanolattice covering the entire bacterium.

### 3. Discussion

Monomolecular isoporous S-layers cover many bacterial cells in the form of nanolattices, that is, two-dimensional crystalline arrays with nanometer-scale periodicity. An intact closed S-layer nanolattice on an average-sized, rod-shaped bacterium consists of ~500,000 monomers making it ideally suited for highly efficient display of a significant number of functional epitopes in defined and precise orientation.<sup>42</sup>

In this report, we describe the identification of the structural gene encoding the S-layer protein SpaA of *P. alvei* CCM 2051<sup>T</sup> and the development of an in vivo surface co-display system using this protein as a cell wall anchor. This was exemplified by the presentation of a heterologous peptide epitope and a functional protein, respectively, in addition to the native S-layer glycan chain (Fig. 6). The strategy is based on the continuous expression of plas-

**Table 2**  
Amino acid sequence comparison between SpaA and different well-characterized S-layer proteins using the EMBOSS Pairwise Alignment Algorithms (Global alignment method, Blosum62 matrix)

Protein	Organism	Accession no.	SLH domains	Analyzed region	Identity%	Similarity%
SbpA	<i>Lysinibacillus sphaericus</i> CCM 2177	AAF22978	33–76	1–1268	18.8	29.1
			92–135	1–200	26.6	38.3
			152–199			
Surface layer protein	<i>Lysinibacillus sphaericus</i> 2362	AAA50256	32–76	1–1176	26.5	39.3
			92–135	1–200	26.7	38.5
			152–199			
SlpC	<i>Lysinibacillus sphaericus</i> C3–41	ABQ00414	32–76	1–1176	26.5	39.3
			92–135	1–200	26.7	38.5
			152–199			
Sap	<i>Bacillus anthracis</i> strain Sterne	YP_027117	33–76	1–814	22.2	34.8
			94–135	1–200	22.6	36.7
			155–197			
EA1	<i>Bacillus anthracis</i> strain Sterne	YP_027118	33–76	1–862	21.8	36.1
			94–136	1–200	23.1	39.1
			156–197			
CTC protein	<i>Bacillus thuringiensis</i> CTC ssp. <i>finitimus</i>	CAA09981	33–76	1–816	20.7	34.0
			94–135	1–200	22.6	37.4
			155–198			
SlpA	<i>Bacillus thuringiensis</i> NRRL 4045 ssp. <i>galleriae</i>	CAB63252	33–76	1–821	22.2	35.3
			94–136	1–200	24.4	36.4
			156–197			
SbsB	<i>Geobacillus stearothermophilus</i> PV72 p2	CAA66724	33–76	1–920	21.8	36.1
			92–133	1–200	21.0	36.1
			150–191			
Middle wall protein precursor	<i>Brevibacillus brevis</i> 47	AAA22760	32–72	1–1053	20.3	31.8
			93–136	1–200	27.1	44.9
			–			
S-Layer protein precursor	<i>Thermoanaerobacter kivui</i>	AAA21930	30–73	1–762	19.2	29.5
			95–137	1–200	27.4	38.4
			–			
P100 protein	<i>Thermus thermophilus</i> HB8	CAA40609	24–67	1–917	21.1	34.2
			–	1–200	27.2	45.6
			–			
SlpA	<i>Clostridium thermocellum</i> NCIB 10682	AAC33404	–	1–1036	23.7	40.4
			94–134	1–200	18.6	29.6
			–			

For analysis of full length proteins, SpaA from aa 1 to 983 was used and for comparison of the amino-terminal parts aa 1–200 were included.

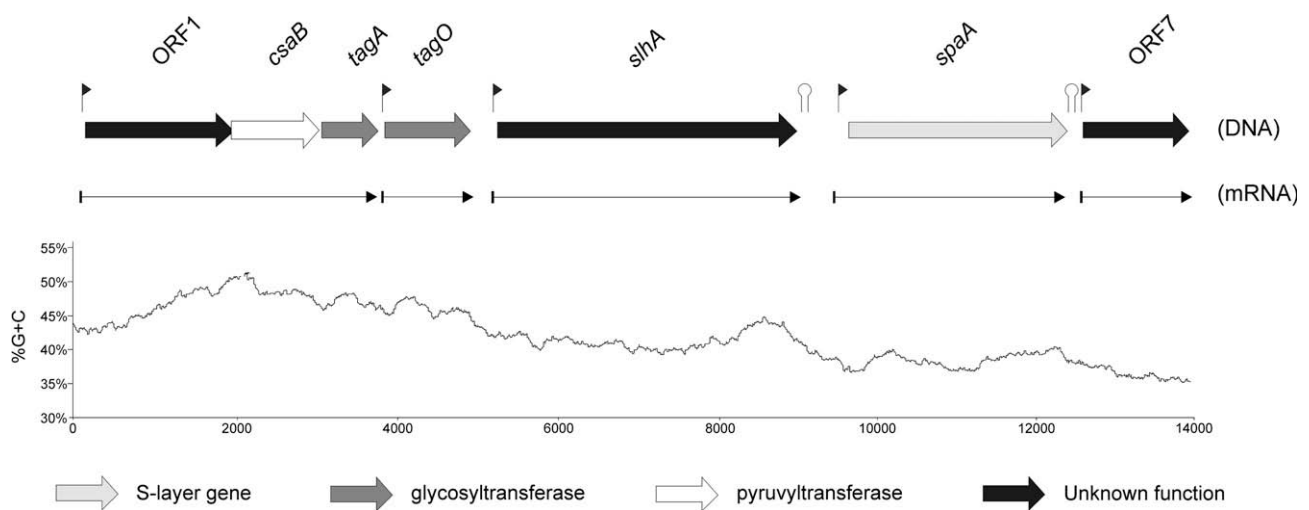


**Figure 3.** Genetic organization of the SCWP biosynthesis locus of *P. alvei* CCM 2051<sup>T</sup>. Predicted open reading frames are indicated by horizontal arrows with the respective gene designations indicated above the arrow. Genes encoding similar functions in SCWP biosynthesis have a similar gray scaling code. Genes coding for proteins with unknown function are indicated in black. Genes highlighted in gray encode putative glycosyltransferases. White indicates the *csaB* gene encoding the pyruvyltransferase. The structural gene *spaA* is highlighted in lightest gray. Putative promoters and terminators are represented as flags and hairpins, respectively. Monocistronic and polycistronic mRNAs are depicted as vertical black arrows. The graphic representation of the G+C percentages is given below the locus map.

mid-encoded S-layer chimera in *P. alvei* CCM 2051<sup>T</sup> using a constitutive promoter and its export, glycosylation as well as surface anchoring, in competition with the wild-type S-layer glycoprotein.

For proof of concept, the hexahistidine tagged S-layer protein SpaA\_6HIS as well as the chimeric fusion protein SpaA\_EGFP was constructed and their cell surface localization was demonstrated by immunofluorescence staining and fluorescence microscopy.

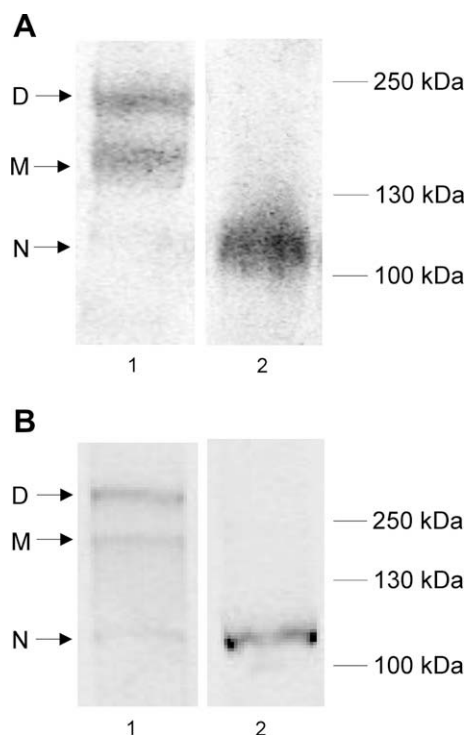


**Figure 4.** Western blot with fluorescence detection of chimeric S-layer proteins. (A) SpaA\_6HIS detected using an anti-His-tag antibody in combination with goat anti-mouse IgG IR Dye 800CW conjugate. (B) Detection of SpaA\_EGFP using an antibody raised against GFP in combination with goat anti-mouse IgG IR Dye 800CW conjugate. The constructs were analyzed by SDS-PAGE (8% gel) and transferred to a PVDF membrane followed by immunoblot detection. Tri-banded appearance corresponds to non-glycosylated (N), mono-glycosylated (M), and di-glycosylated (D)<sup>31</sup> chimeric SpaA proteins produced by *P. alvei* CCM 2051<sup>T</sup> wild-type cells (lanes 1). For *P. alvei* CCM 2051<sup>T</sup> *wsfP*::LL.LtrB mutant cells, sole bands corresponding to non-glycosylated SpaA chimera were detected (lanes 2). Two milligrams of intact cells were loaded per well.

The used *P. alvei* CCM 2051<sup>T</sup> surface display vector pEX-ALV\_SP\_SpaA can be generally utilized for translational fusion of various functional epitopes to the C-terminus of SpaA, their subsequent export and surface presentation. By immunoblot analysis, for both surface-displayed constructs—SpaA\_6HIS and SpaA\_EGFP—a non-glycosylated, mono-glycosylated, and di-glycosylated form resulting from the native S-layer protein O-glycosylation system of wild-type *P. alvei* CCM 2051<sup>T</sup> was detected,

which reflects the native SpaA O-glycosylation pattern. This indicates the suitability of this system for the future in vivo cell surface co-display of engineered, bioactive glycan structures based on the native S-layer glycans, in addition to peptide/protein epitopes. Since the ongoing investigation of the S-layer glycosylation machinery of *P. alvei* CCM 2051<sup>T</sup> revealed some promising insights,<sup>41</sup> this bacterium is a prime candidate for the design and presentation of S-layer neoglycoproteins by means of genetic carbohydrate engineering.<sup>43</sup> Thereby, the S-layer glycosylation deficient mutant strain *wsfP*::LL.LtrB, carrying an insertion in the *wsfP* gene coding for the initiation enzyme of S-layer glycan biosynthesis, provides the possibility of turning on the functional glycosylation of any SpaA chimera, when the activity of WsfP is reconstituted by plasmid-based expression of *wsfP*.<sup>31</sup>

Besides the attachment of a tailor-made, functionalized S-layer protein to the cell envelope, secretion into the medium can also be a desired option for specific purposes, avoiding time- and cost-consuming purification steps. In this context, the anchoring mechanism of the S-layer protein was investigated, starting with the observation of three SLH domains located at the N-terminus of SpaA. The typical, highly conserved TRAE motif could be identified in the first SLH domain (aa 25–65) of SpaA. In the second (aa 82–129) and third (aa 140–181) SLH domain, two different variants of this motif, TVEE and TRAQ, are present. However, these motif variants have also been reported to be functional.<sup>23</sup> Since these SLH domains are known to play a key role in mediating the cell wall binding of various proteins by interacting with SCWPs carrying pyruvate modifications, it was not surprising to identify a pyruvyltransferase encoding gene in the upstream region of *spaA*. Furthermore, with *tagA* and *tagO*, both coding for glycosyltransferases, two additional enzymes obviously involved in SCWP biosynthesis of *P. alvei* CCM 2051<sup>T</sup> were identified. Due to the similarity of TagO to an undecaprenylphosphate *N*-acetylglucosaminyl-1-phosphate transferase, it can be assumed that TagO attaches GlcNAc to the membrane-embedded lipid carrier undecaprenylpyrophosphate at the cytoplasmic side of the membrane. The next step in the biosynthesis pathway would be the addition of ManNAc catalyzed by the *N*-acetylglucosaminyl diphosphoundecaprenol *N*-acetyl- $\beta$ -D-mannosaminyltransferase TagA, to produce the lipid-linked GlcNAc-ManNAc disaccharide. The transfer of the pyruvate modification to ManNAc residue is accomplished by the pyruvyltransferase CsaB. Additional enzymes required for the export and for the formation of the covalent linkage between SCWP and peptidoglycan could not be identified, so far. The prediction of transcription units for the SCWP biosynthesis locus showed that *orf1*, *csaB*, and *tagA* are located on a polycistronic mRNA. This finding

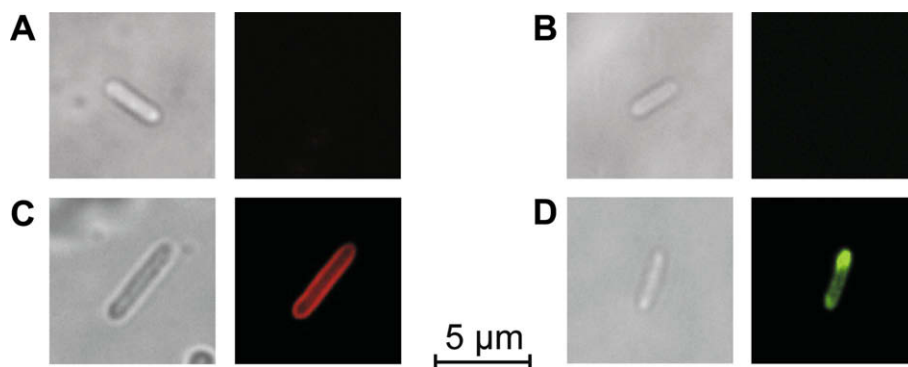


**Figure 5.** Immunofluorescence microscopy of *P. alvei* CCM 2051<sup>T</sup> wild-type cells displaying chimeric S-layer glycoproteins. (A and B) Control *P. alvei* CCM 2051<sup>T</sup> wild-type cells harboring pEXALV. Recombinant *P. alvei* CCM 2051<sup>T</sup> wild-type cells harboring (C) pEXALV\_SP\_SpaA\_6HIS, and (D) pEXALV\_SP\_SpaA\_EGFP. For immunofluorescence staining of surface-located SpaA\_6HIS, cells were probed with the penta-His Alexa Fluor 555 Conjugate (Qiagen). The TRITC and the GFP LP filter blocks were used for detection of Alexa Fluor 555 (A and C) and EGFP (B and D), respectively. Corresponding brightfield images of the same cells are shown in the left. The immunofluorescence images of the *wsfP*::LL.LtrB mutant strain are identical to those observed for wild-type cells and hence not shown.

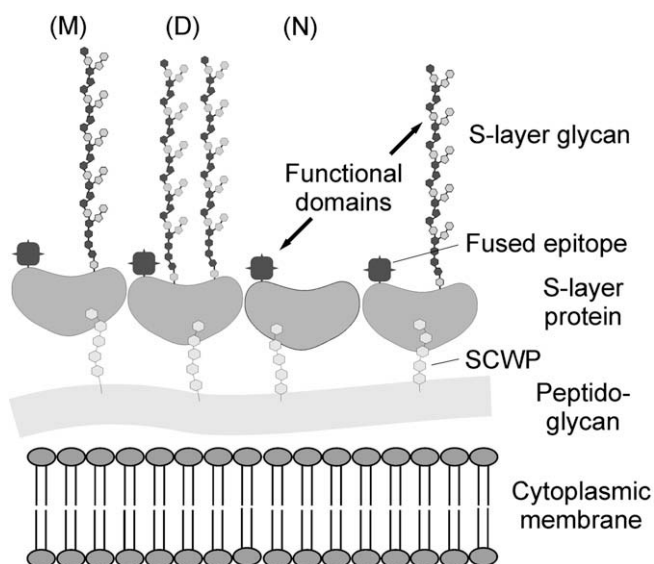


**Figure 6.** Strategy for in vivo cell surface co-display of functional epitopes on *P. alvei* CCM 2051<sup>T</sup> cells. Schematic picture showing the cell wall profile with the peptide/protein epitope and the glycans being presented in nanopatterned fashion to the exterior of the bacterial cell. Non-glycosylated (N), mono-glycosylated (M), and di-glycosylated (D)<sup>31</sup> chimeric SpaA proteins are distributed equally over the cell surface.

is supported by the closed spacing and the absence of a promoter consensus sequence between these three genes. The role of the gene product of *orf1* being part of this polycistronic mRNA remains, due to the lack of reliable sequence similarities, speculative and needs to be further investigated. The encoded protein could be possibly involved in the export of the pyruvylated polymer. *TagO*, *slhA*, and *spaA* are predicted to be transcribed monocistronically. The presence of three SLH domains located at the C-terminus of SlhA argues for its surface exposure and turns this protein into an eligible candidate for co-display of chimeric SpaA- and SlhA proteins interacting with each other or binding a target molecule in two different manners.

In conclusion, we have demonstrated the in vivo cell surface co-display of a heterologous peptide epitope and a functional protein fused to the N-terminus of the S-layer glycoprotein SpaA of *P. alvei* CCM 2051<sup>T</sup> in addition to the S-layer glycans. The developed strategy is the starting point for the future in vivo presentation of different peptides and proteins combined with bioactive glycans, which may have great value in the fields of receptor mimics, vaccine development, or drug delivery.

## 4. Experimental

### 4.1. Bacterial strains and growth conditions

*P. alvei* CCM 2051<sup>T</sup> (Table 3) was obtained from the Czech Collection of Microorganisms (CCM, Brno, Czech Republic) and grown at 37 °C and 200 rpm in Luria–Bertani (LB) broth or on LB agar plates supplemented with 10 µg mL<sup>-1</sup> chloramphenicol (Cm), when appropriate. *E. coli* DH5α (Invitrogen, Lofer, Austria) was grown in LB broth at 37 °C supplemented with 30 µg mL<sup>-1</sup> Cm, when appropriate.

### 4.2. Analytical and general methods

Genomic DNA of *P. alvei* CCM 2051<sup>T</sup> was isolated as described recently.<sup>31</sup> Restriction and cloning enzymes were purchased from Invitrogen. The MinElute gel extraction kit (Qiagen, Vienna, Austria) was used to purify DNA fragments from agarose gels, and the MinElute reaction cleanup kit (Qiagen) was used to purify digested oligonucleotides and plasmids. Plasmid DNA from transformed cells was isolated with the Plasmid Miniprep kit (Qiagen). Agarose gel electrophoresis was performed as described elsewhere.<sup>44</sup> Transformation of *E. coli* DH5α was done according to the manufacturer's protocol (Invitrogen). Transformants were screened by in situ PCR using RedTaq ReadyMix PCR mix (Sigma–Aldrich, Vienna, Austria); recombinant clones were analyzed by restriction mapping and confirmed by sequencing (Agowa, Berlin, Germany). Transformation of *P. alvei* CCM 2051<sup>T</sup> was performed as described recently.<sup>31</sup> SDS–PAGE was carried out according to a standard protocol<sup>45</sup> using a Protean II electrophoresis apparatus (Bio–Rad, Vienna, Austria). Protein bands were visualized with Coomassie Brilliant Blue G250 staining reagent. Western blotting using a Mini Trans-Blot Cell (Bio–Rad) was performed to transfer the proteins to a polyvinylidene difluoride membrane (Bio–Rad). Anti–GFP mouse antibody (Roche, Vienna, Austria) and anti–His–tag mouse antibody (Novagen, Darmstadt, Germany) were used in combination with goat anti–mouse IgG IR Dye 800CW conjugate (Li–Cor, Lincoln, NB, USA) to detect EGFP and hexahistidine epitopes using the Li–Cor Odyssey Infrared Imaging System (Li–Cor). The integrated intensity of detected bands was determined using the Li–Cor Odyssey Application Software 3.0.21. Isolation and purification of S-layer glycoprotein essentially followed published methods.<sup>46</sup> Qiagen's Ni–NTA Spin Kit was used to purify hexahistidine-tagged S-layer glycoprotein under denaturing conditions. Deglycosylation of S-layer glycoprotein and amino-terminal sequencing (Edman degradation) were performed as published previously.<sup>47</sup>

**Table 3**  
Bacterial strains and plasmids used in this study

Strain or plasmid	Genotype and/or relevant characteristics	Source or reference
<i>Strains</i>		
<i>P. alvei</i> CCM 2051 <sup>T</sup>	Wild-type isolate, Km <sup>r</sup>	Czech collection of microorganisms (CCM)
<i>P. alvei</i> CCM 2051 <sup>T</sup> <i>wsfP</i> ::LI.LtrB	S-Layer glycosylation deficient mutant carrying a targetron insertion at the <i>wsfP</i> gene; Km <sup>r</sup>	Ref. 31
<i>Escherichia coli</i> DH5α	F <sup>-</sup> φ80 <i>lacZ</i> Δ <i>M15</i> Δ( <i>lacZYA-argF</i> )U169 <i>deoR recA1 endA1 hsdR17</i> (rK <sup>-</sup> mK <sup>-</sup> ) <i>phoA supE44 thi-1 gyrA96 relA1 λ<sup>-</sup></i>	Invitrogen
<i>Plasmids</i>		
pEXALV	<i>P. alvei</i> expression vector	Ref. 31
pEGFP-N1	Expression vector for mammalian cells encoding a red-shifted variant of wild-type GFP	BD biosciences
pEXALV_SP_SpaA_6HIS	pEXALV carrying the his-tagged <i>spaA</i> gene of <i>P. alvei</i> CCM 2051 <sup>T</sup>	This study
pEXALV_SP_SpaA	pEXALV carrying the <i>spaA</i> gene of <i>P. alvei</i> CCM 2051 <sup>T</sup> lacking the TAA stop codon	This study
pEXALV_SP_SpaA_EGFP	pEXALV carrying a <i>spaA-egfp</i> fusion construct	This study

**Table 4**  
Oligonucleotide primers used for PCR amplification reactions

Oligonucleotide	Sequence (5' → 3') <sup>a</sup>
proof_wSpa_for	GCIGAYGCGICIAARACIACICARG
SP_SpaA_SphI_for	aatca <u>GCATGC</u> CAGAAAAGATTGGCCCTTCTGCTTCCG
SpaA_6HIS_STOP_KpnI_rev	aatca <u>GGTACC</u> ttaatggtgatggtgatggtgCTTACCGGAGTATGTTCCAGGAAGG
SpaA_noSTOP_PstI_rev	aatca <u>CTGCAG</u> CTTACCGGAGTATGTTCCAGGAAGG
EGFP_for_PstI	aatca <u>CTGCAG</u> ATGGTGAGCAAGGGCGAGGAGC
EGFP_rev_KpnI	aatca <u>GGTACC</u> TACTTGACAGCTCGTCCATGCC

<sup>a</sup> Artificial restriction sites are underlined.

### 4.3. PCR and DNA sequencing

PCR (My Cycler™, Bio-Rad) was performed using the Herculanse® II Fusion DNA Polymerase (Stratagene, La Jolla, CA, USA). For each primer pair (Table 4), PCR conditions were optimized, and amplification products were purified using the MinElute PCR purification kit (Qiagen). Primers for PCR and DNA sequencing were purchased from Invitrogen. For sequence determination of the *spaA* gene including upstream and downstream regions, chromosome walking was applied as previously described.<sup>48,49</sup>

### 4.4. Sequence analysis

Nucleotide and protein sequences were analyzed using the BLASTN and BLASTP sequence homology analysis tools (National Center for Biotechnology Information, Bethesda, MD, USA). Open reading frames in the DNA sequence were identified by using the Clone Manager Professional Suite (SECentral, Cary, NC, USA) and the ORF Finder analysis tool (National Center for Biotechnology Information). For the identification of putative protein transmembrane-spanning domains and the presence and location of signal peptide cleavage sites, the TMHMM Server v. 2.0 transmembrane prediction program and the SignalP 3.0 Server (Center for Biological Sequence Analysis, Technical University of Denmark, Lyngby, Denmark) were used, respectively. The G+C content of a certain DNA sequence was determined using the GC Content and GC Skew program (Nano+Bio-Center, University of Kaiserslautern, Germany). For in silico reverse translation the Sequence Manipulation Suite was used.<sup>50</sup> Bacterial promoters, transcriptional terminators, operons, and genes were predicted by the BProm and FindTerm modules of the FGenesB gene prediction program in Molquest software (SoftBerry, Mount Kisco, NY, USA). The presence of conserved motifs in a given protein sequence was analyzed by the Pfam protein families database,<sup>51</sup> the SUPERFAMILY database,<sup>52</sup> and the Conserved Domain Finder of the National Center for Biotechnology Information.<sup>53–55</sup> Physical and chemical parameters for a given protein were calculated using the ProtParam tool.<sup>56</sup> For pairwise alignments of certain protein sequences, the EMBOSS Pairwise Alignment Algorithms were used.<sup>57</sup>

The phylogenetic tree was calculated with the Blast Tree View Widget using the Neighbor Joining method<sup>58</sup> and visualized using iTOL.<sup>59</sup> Sequences with more than 0.85 difference were removed from the treeview.

### 4.5. Construction of the SpaA surface display constructs

The *P. alvei* expression vector pEXALV was used for construction of all SpaA surface display constructs. The carboxy-terminal hexahistidine tag was fused to the coding sequence of *spaA* by PCR using primers SP\_SpaA\_SphI\_for and SpaA\_6HIS\_STOP\_KpnI\_rev, with genomic DNA of *P. alvei* CCM 2051<sup>T</sup> as template. The ~3000-bp PCR product was digested with *SphI* and *KpnI* and ligated into *SphI/KpnI*-linearized and dephosphorylated plasmid

pEXALV. This construct was named pEXALV\_SP\_SpaA\_6HIS. For the construction of an S-layer-EGFP fusion protein, the DNA fragment encoding the *spaA* gene lacking the TAA stop codon was amplified by PCR using primers SP\_SpaA\_SphI\_for and SpaA\_noSTOP\_PstI\_rev with genomic DNA of *P. alvei* CCM 2051<sup>T</sup> as template. The ~3000-bp PCR product was digested with *SphI* and *PstI* and ligated into *SphI/PstI*-linearized and dephosphorylated plasmid pEXALV. This construct was named pEXALV\_SP\_SpaA. The 742-bp *egfp* fragment was amplified by PCR from plasmid pEGFP-N1 using the primers EGFP\_for\_PstI and EGFP\_rev\_KpnI, digested with *PstI* and *KpnI*, and cloned in frame into *PstI/KpnI*-linearized and dephosphorylated plasmid pEXALV\_SP\_SpaA. This construct was named pEXALV\_SP\_SpaA\_EGFP.

### 4.6. Analysis of cell surface display and immunofluorescence staining of SpaA-constructs

The surface accessibility of the displayed hexahistidine-tagged S-layer protein SpaA\_6HIS on intact *P. alvei* cells was analyzed by direct immunofluorescence staining followed by fluorescence microscopy. Briefly, cells transformed with pEXALV\_SP\_SpaA\_6HIS were harvested after expression at an OD<sub>600</sub> ~0.6, resuspended, and washed three times in phosphate-buffered saline (PBS). After resuspension in 200 µL of PBS, 10 µL of penta-His Alexa Fluor 555 conjugate (Qiagen) was added and incubated for 2 h at room temperature on a horizontal shaker. After washing for three times, the cells were resuspended in 500 µL of PBS and analyzed by fluorescence microscopy. To directly assess the functional surface expression of the chimeric S-layer fusion protein SpaA\_EGFP, *P. alvei* cells transformed with pEXALV\_SP\_SpaA\_EGFP were analyzed by fluorescence microscopy. Fluorescence microscope imaging of intact *P. alvei* cells was carried out with a Nikon Eclipse TE2000-S inverted fluorescence microscope with a Hg vapor lamp, a Nikon digital sight DS-Qi1Mc camera, and the NIS-Elements imaging software using the TRITC (540/25 nm for excitation light, 605/55 nm for emission light) filter block for Alexa Fluor 555 and the GFP LP (480/40 nm for excitation light, long pass at 510 nm for emission light) filter block for EGFP.

### Acknowledgments

We thank Andrea Scheberl and Sonja Zayni for excellent technical assistance. Financial support came from the Austrian Science Fund, project P20745-B11 (to P.M.) and projects P19047-B12 and P20605-12 (to C.S.), and the Hochschuljubiläumsstiftung der Stadt Wien, project H-02229-2007 (to K.Z.).

### References

- Georgiou, G.; Stathopoulos, C.; Daugherty, P. S.; Nayak, A. R.; Iverson, B. L.; Curtiss, R., 3rd. *Nat. Biotechnol.* **1997**, *15*, 29–34.
- Miller, K. D.; Pefaur, N. B.; Baird, C. L. *Curr. Protoc. Cytom.* **2008**, *45*, 1–30.
- Daugherty, P. S. *Curr. Opin. Struct. Biol.* **2007**, *17*, 474–480.
- Ishige, T.; Honda, K.; Shimizu, S. *Curr. Opin. Chem. Biol.* **2005**, *9*, 174–180.

5. Wu, C. H.; Mulchandani, A.; Chen, W. *Trends Microbiol.* **2008**, *16*, 181–188.
6. Saleem, M.; Brim, H.; Hussain, S.; Arshad, M.; Leigh, M. B.; Ziaul, H. *Biotechnol. Adv.* **2008**, *26*, 151–161.
7. Samuelson, P.; Gunneriusson, E.; Nygren, P.-Å.; Ståhl, S. J. *Biotechnol.* **2002**, *96*, 129–154.
8. Lee, S. Y.; Choi, J. H.; Xu, Z. *Trends Biotechnol.* **2003**, *21*, 45–52.
9. Wernerus, H.; Ståhl, S. *Biotechnol. Appl. Biochem.* **2004**, *40*, 209–228.
10. Desvaux, M.; Dumas, E.; Chafsey, I.; Hebraud, M. *FEMS Microbiol. Lett.* **2006**, *256*, 1–15.
11. Gai, S. A.; Wittrup, K. D. *Curr. Opin. Struct. Biol.* **2007**, *17*, 467–473.
12. Pepper, L. R.; Cho, Y. K.; Boder, E. T.; Shusta, E. V. *Comb. Chem. High Throughput Screening* **2008**, *11*, 127–134.
13. Bingle, W. H.; Nomellini, J. F.; Smit, J. *Mol. Microbiol.* **1997**, *26*, 277–288.
14. Bingle, W. H.; Nomellini, J. F.; Smit, J. *J. Bacteriol.* **1997**, *179*, 601–611.
15. Mesnage, S.; Tosi-Couture, E.; Fouet, A. *Mol. Microbiol.* **1999**, *31*, 927–936.
16. Mesnage, S.; Tosi-Couture, E.; Mock, M.; Fouet, A. *J. Appl. Microbiol.* **1999**, *87*, 256–260.
17. Mesnage, S.; Weber-Levy, M.; Haustant, M.; Mock, M.; Fouet, A. *Infect. Immun.* **1999**, *67*, 4847–4850.
18. Bingle, W. H.; Nomellini, J. F.; Smit, J. *J. Bacteriol.* **2000**, *182*, 3298–3301.
19. Smit, J. *Structure* **2008**, *16*, 1151–1153.
20. Sleytr, U. B.; Huber, C.; Ilk, N.; Pum, D.; Schuster, B.; Egelseer, E. M. *FEMS Microbiol. Lett.* **2007**, *267*, 131–144.
21. Nomellini, J. F.; Duncan, G.; Dorocicz, I. R.; Smit, J. *Appl. Environ. Microbiol.* **2007**, *73*, 3245–3253.
22. Engelhardt, H.; Peters, J. *J. Struct. Biol.* **1998**, *124*, 276–302.
23. May, A.; Pusztahelyi, T.; Hoffmann, N.; Fischer, R. J.; Bahl, H. *Arch. Microbiol.* **2006**, *185*, 263–269.
24. Mesnage, S.; Fontaine, T.; Mignot, T.; Delepierre, M.; Mock, M.; Fouet, A. *EMBO J.* **2000**, *19*, 4473–4484.
25. Sára, M. *Trends Microbiol.* **2001**, *9*, 47–49. Discussion 49–50.
26. Cava, F.; de Pedro, M. A.; Schwarz, H.; Henne, A.; Berenguer, J. *Mol. Microbiol.* **2004**, *52*, 677–690.
27. Schäffer, C.; Messner, P. *Microbiology* **2005**, *151*, 643–651.
28. Leoff, C.; Choudhury, B.; Saile, E.; Quinn, C. P.; Carlson, R. W.; Kannenberg, E. L. *J. Biol. Chem.* **2008**, *283*, 29812–29821.
29. Messner, P.; Christian, R.; Neuninger, C.; Schulz, G. *J. Bacteriol.* **1995**, *177*, 2188–2193.
30. Schäffer, C.; Müller, N.; Mandal, P. K.; Christian, R.; Zayni, S.; Messner, P. *Glycoconjugate J.* **2000**, *17*, 681–690.
31. Zarschler, K.; Janesch, B.; Zayni, S.; Schäffer, C.; Messner, P. *Appl. Environ. Microbiol.* **2009**, *75*, 3077–3085.
32. Sára, M.; Moser-Thier, K.; Kainz, U.; Sleytr, U. B. *Arch. Microbiol.* **1990**, *153*, 209–214.
33. Altman, E.; Brisson, J.-R.; Messner, P.; Sleytr, U. B. *Biochem. Cell Biol.* **1991**, *69*, 72–78.
34. Hartmann, E.; Messner, P.; Allmeier, G.; König, H. *J. Bacteriol.* **1993**, *175*, 4515–4519.
35. Sleytr, U. B.; Beveridge, T. J. *Trends Microbiol.* **1999**, *7*, 253–260.
36. Messner, P.; Schäffer, C.; Egelseer, E. M.; Sleytr, U. B. In *Prokaryotic Cell Wall Compounds—Structure and Biochemistry*; König, H., Claus, H., Varma, A., Eds.; Springer: Berlin, 2010; pp 53–109.
37. Paik, S. H.; Chakicherla, A.; Hansen, J. N. *J. Biol. Chem.* **1998**, *273*, 23134–23142.
38. Bhavsar, A. P.; Truant, R.; Brown, E. D. *J. Biol. Chem.* **2005**, *280*, 36691–36700.
39. Formstone, A.; Carballido-Lopez, R.; Noiro, P.; Errington, J.; Scheffers, D. J. *J. Bacteriol.* **2008**, *190*, 1812–1821.
40. Pavkov, T.; Egelseer, E. M.; Tesarz, M.; Svergun, D. I.; Sleytr, U. B.; Keller, W. *Structure* **2008**, *16*, 1226–1237.
41. Zarschler, K.; Janesch, B.; Pabst, M.; Altmann, F.; Messner, P.; Schäffer, C. *Glycobiology* **2010**. doi:10.1093/glycob/cwq035.
42. Sleytr, U. B.; Egelseer, E. M.; Ilk, N.; Pum, D.; Schuster, B. *FEBS J.* **2007**, *274*, 323–334.
43. Schäffer, C.; Messner, P. *Biochimie* **2001**, *83*, 591–599.
44. Sambrook, J.; Fritsch, E. F.; Maniatis, T. *Molecular Cloning: A Laboratory Manual*; Cold Spring Harbor Laboratory Press: Cold Spring Harbor, NY, 1989.
45. Laemmli, U. K. *Nature* **1970**, *227*, 680–685.
46. Messner, P.; Sleytr, U. B. In *Bacterial Cell Surface Techniques*; Hancock, I. C., Poxton, I. R., Eds.; John Wiley & Sons: Chichester, 1988; pp 97–104.
47. Schäffer, C.; Wugeditsch, T.; Kählig, H.; Scheberl, A.; Zayni, S.; Messner, P. *J. Biol. Chem.* **2002**, *277*, 6230–6239.
48. Kneidinger, B.; Graninger, M.; Messner, P. *Biotechniques* **2001**, *30*, 248–249.
49. Pilhofer, M.; Bauer, A. P.; Schrällhammer, M.; Richter, L.; Ludwig, W.; Schleifer, K. H.; Petroni, G. *Nucleic Acids Res.* **2007**, *35*, e135.
50. Stothard, P. *Biotechniques* **2000**, *28*, 1102–1104.
51. Finn, R. D.; Tate, J.; Mistry, J.; Coghill, P. C.; Sammut, S. J.; Hotz, H. R.; Ceric, G.; Forslund, K.; Eddy, S. R.; Sonnhammer, E. L.; Bateman, A. *Nucleic Acids Res.* **2008**, *36*, D281–D288.
52. Gough, J.; Karplus, K.; Hughey, R.; Chothia, C. *J. Mol. Biol.* **2001**, *313*, 903–919.
53. Marchler-Bauer, A.; Bryant, S. H. *Nucleic Acids Res.* **2004**, *32*, W327–W331.
54. Marchler-Bauer, A.; Anderson, J. B.; Cherukuri, P. F.; DeWeese-Scott, C.; Geer, L. Y.; Gwadz, M.; He, S.; Hurwitz, D. I.; Jackson, J. D.; Ke, Z.; Lanczycki, C. J.; Liebert, C. A.; Liu, C.; Lu, F.; Marchler, G. H.; Mullokandov, M.; Shoemaker, B. A.; Simonyan, V.; Song, J. S.; Thiessen, P. A.; Yamashita, R. A.; Yin, J. J.; Zhang, D.; Bryant, S. H. *Nucleic Acids Res.* **2005**, *33*, D192–D196.
55. Marchler-Bauer, A.; Anderson, J. B.; Derbyshire, M. K.; DeWeese-Scott, C.; Gonzales, N. R.; Gwadz, M.; Hao, L.; He, S.; Hurwitz, D. I.; Jackson, J. D.; Ke, Z.; Krylov, D.; Lanczycki, C. J.; Liebert, C. A.; Liu, C.; Lu, F.; Lu, S.; Marchler, G. H.; Mullokandov, M.; Song, J. S.; Thanki, N.; Yamashita, R. A.; Yin, J. J.; Zhang, D.; Bryant, S. H. *Nucleic Acids Res.* **2007**, *35*, D237–D240.
56. Gasteiger, E.; Hoogland, C.; Gattiker, A.; Duvaud, S.; Wilkins, M. R.; Appel, R. D.; Bairoch, A. In *The Proteomics Protocols Handbook*; Walker, J. M., Ed.; Humana Press: Totowa, NJ, 2005; pp 571–607.
57. Needleman, S. B.; Wunsch, C. D. *J. Mol. Biol.* **1970**, *48*, 443–453.
58. Saitou, N.; Nei, M. *Mol. Biol. Evol.* **1987**, *4*, 406–425.
59. Letunic, I.; Bork, P. *Bioinformatics* **2007**, *23*, 127–128.